A STUDY OF PASSIVE INTERMODULATION

IN

MULTIFREQUENCY UHF RADIO COMMUNICATION SYSTEMS

by

R.J.C. Bultitude

W.J. Chudobiak

and

B.A. Syrett

P
91
C655
B85
1979

IC

Prepared for The Canadian Government Department of Communications Under Department of Supplies and Services Contract No. 0ST78-00022

August 1979.

A STUDY OF PASSIVE INTERMODULATION

IN

MULTIFREQUENCY UHF RADIO COMMUNICATION SYSTEMS

Industry Canada
Library - Queen

AVR
APR - 2 2013

Industrie Canada
Bibliothèque - Queen

by

R.J.C. Bultitude

W.J. Chudobiak

and

B.A. Syrett

COMMUNICATIONS CANADA
CRC
OCT 21 1986
LIBRARY – BIBLIOTHÈQUE

Prepared for The Canadian Government Department of Communications Under Department of Supplies and Services Contract No. OST78-00022

August 1979.

ACKNOWLEDGEMENTS

The ready and willing help of personnel at The Communications Research Centre during the preformance of work for this contract is gratefully acknowledged.

In particular, gratitude is extended to Mr. R.J. Bonnycastle and Mr. R.F. Hahn of the Space Electronics Croup at CRC for their many helpful suggestions and the effort of Mr. Hahn in conducting the experiments. Special recognition is also extended to the Space Mechanics Group for their help.

COMMUNICATIONS CANADA
C R C
OCT 21 1986
LIBRARY – BIBLIOTHÈQUE

ABSTRACT

This report details an investigation concerning passive intermodulation (PIM) interference generation in UHF (200 - 400 MHz) satellite communication systems. A survey of reported phenomena which can generate PIM is presented. Analytical techniques for the calculation of intermodulation signal powers are reviewed and a novel technique is proposed. A combination of theoretical analysis and experiments with two transmit frequencies is then applied in an investigation concerning the identification of PIM signal sources by power response signatures. A study of the vacuum phenomenon of multipactor breakdown, a known PIM generator, is also reported.

Guidelines to be followed in all stages of design, manufacture, and RF communication system assembly which will result in the minimization of intermodulation signal generation in passive components are given.

TABLE OF CONTENTS

PAGE

PAGE

LIST OF TABLES

LIST OF FIGURES

LIST OF FIGURES (cont'd)

LIST OF FIGURES (cont'd)

LIST OF FIGURES (cont'd)

GLOSSARY OF SYMBOLS

a_i , i = 1,2,....,n	polynomial coefficients
A	generalized transmit signal amplitude
B	magnetic flux density
cw,CW	continuous wave
d	multipactor gap width
e (subscript)	denotes even order
E	electric field
E_1,E_2	amplitude of sinusoidal voltages applied to an IM generator at the frequencies f_1 and f_2 respectively
f_1,f_2	transmit frequencies #1 and #2
f_{IM}	intermodulation product frequency
fd	product of applied signal frequency and multipactor gap width
f_c	cyclotron resonance frequency
FI, I = 1,2,...,8	RF filters #1,...,#8
female/female	RF adapters with female fittings on both ends
h_n	impulse response of order n
H_n	Fourier transform of h_n

GLOSSARY OF SYMBOLS (cont'd)

IM	intermodulation
I_{IM}	intermodulation product current
I_{IML}	intermodulation current carried by a RF system load
I_{IM_N}	Nth order intermodulation product current
I_d	diode current
I_s	reverse saturation current for a semiconductor diode
IMAMP, IMPWR	computer program names
j	complex operator
J_s	surface current density
k	Boltzman's constant: (1.38×10^{-23} J/°K)
K	(1) integer (2) ratio of emission to impact velocity for electrons taking part in the multipactor breakdown process
ℓ	length
LSQPOLY	computer subroutine for fitting a least squares polynomial approximation to discrete data points
L	(1) arbitrary integer (2) inductance
m	(1) arbitrary integer (2) mass of an electron (3) subscript denoting association with transmit frequency f_m

GLOSSARY OF SYMBOLS (cont'd)

male/male	RF adapter with male fittings on both ends
M	designates the number of transmit frequencies
MP	multipactor/multipacting
MPa	Mega-Pascal (metric unit of pressure -- 1MPa = 150 lb/in^2)
MUSAT	Multi-Use UHF Satellite System
n	(1) arbitrary integer (2) multipactor mode index
N	(1) intermodulation product order (2) connector type designation
o (subscript)	denotes odd order
P	arbitrary integer
PIM	passive intermodulation
q	(1) arbitrary integer (2) electronic charge
R_{sh}	shunt resistance
P_T	total transmit power
t	time
T	temperature
TNC	RF connector type designation
v_o	initial electron velocity
v_f	final (impact) electron velocity

GLOSSARY OF SYMBOLS (cont'd)

V_1, V_2	transmitter output voltages at the frequencies f_1 and f_2 respectively
V_T	total transmitter output voltage
W_f	multipacting electron impact energy
$W_{f\ell}$	multipactor electron energy such that $\delta = 1$
x	distance
$x(t)$	independent variable of a transfer characteristic with memory
X	independent variable of a memoryless transfer characteristic
$y(t)$	dependent variable of a transfer characteristic with memory
Y	dependent variable of a memoryless transfer characteristic
α_i , $i = 1,2,\ldots,n$	multiplier for frequency f_i in the combination $f_{IM} = (\pm \alpha_1 f_1 \pm \alpha_2 f_2 \pm \ldots \pm \alpha_n f_n)$
β	f_{IM}/f_1
β_K	contribution to an IM product amplitude from the K th term in the polynomial describing the generating nonlinearity
δ	secondary emission coefficient
Δ	incremental value
ϕ	time phase angle for electrons emitted from a gap wall during multipactor breakdown

GLOSSARY OF SYMBOLS (cont'd)

ϕ_1, ϕ_2	time phase angle of the transmit signals at f_1 and f_2 respectively
μ_0	permeability of free space
μ	material permeability
η	empirically derived constant
$\sigma(T)$	electrical conductivity as a function of temperature
ω_i , $i = 1,2,\ldots,n$	radian frequency corresponding to the frequency f_i

CHAPTER I

INTRODUCTION

1.1 Introduction

The Department of Electronics Engineering at Carleton University, Ottawa, Canada, was commissioned by the Canadian Department of Communications, Communications Research Center (CRC) to conduct theoretical and experimental investigations concerning the generation of passive intermodulation (PIM) interference in high power UHF satellite communication systems. The work was carried out at CRC in cooperation with CRC personnel.

RF interference caused by passive intermodulation or the "rusty bolt" effect is encountered in the operation of multifrequency radio communication systems. Where transmitters and receivers are co-located, microscopic naturally occurring conduction nonlinearities (e.g. in passive RF components, equipment housings, or any other conducting structures exposed to high intensity RF fields at the transmitter output frequencies) can generate intermodulation (IM) signals on frequencies within the receiver bandwidths. Such IM signals can be at significant power levels and cause receiver desensitization as well as interference to desired communications.

In the past, PIM interference has been avoided or minimized by the choice of operating frequencies for co-sited equipments such that the frequencies of all but high* order IM signals fall outside the

---

* For most terrestrial systems, the power of IM signals above fifth order is below receiver sensitivity thresholds.

receiver bandwidths. Due to the increasing congestion of the communications frequency spectrum however, frequency planning can no longer be effected so as to provide sufficient alleviation from the PIM interference problem. In addition, the requirement to communicate over ever increasing distances brought about by space satellite technology necessitates the use of high power transmitters in close proximity and often sharing a common antenna with highly sensitive receivers operating in the same frequency zone. In such systems, even very high order IM product signals can be of sufficient amplitude to severely impair receive channels.

It is clear that modern RF communication systems must be designed so as to avoid potential sources of PIM. This, however, is an extremely difficult task as PIM generators are numerous and the mechanisms of some are not well understood. A number of investigations in the past* have done much to answer some of the questions regarding PIM, but their results are by no means conclusive. There remains therefore a need for further observation of spurious signals generated by passive RF components and basic research concerning naturally occurring nonlinear conduction mechanisms. Coupled with the development of techniques for the prediction of the amplitude of PIM signals generated by particular nonlinearities under different operating conditions, such investigations can lead to the establishment of guidelines for the design of communication systems such that PIM interference can be eliminated.

---

* A bibliography of literature concerning passive intermodulation can be found at the end of this report.

1.2 Study Objectives

This investigation was initiated to provide guidelines for the design of "PIM-free" passive RF components for use in the proposed Canadian Government Multi-Use UHF Satellite (MUSAT) Communication System. This system will operate with uplink frequencies in the 400 MHz range and downlink frequencies between 270 MHz and 300 MHz. It is planned that transmit powers in each of 80 communications channels will be automatically adjustable to maintain the total RF power output from the satellite transponder constant at + 49 dBm regardless of the number of channels in use. Although the satellite design has not been finalized, a common antenna for transmitting and receiving is believed preferable from flight dynamics and antenna deployment considerations. Signal to noise requirements dictate that received signal powers in each operating channel should be a nominal -114 dBm. The maximum permissible power for PIM signals at the receiver input has therefore been specified as -120 dBm, allowing a 6 dB margin for reliability.

To delineate a path along which investigations could proceed, the following seven subobjectives of the study were defined:

(1) The accumulation of reference material and a review of literature concerning passive intermodulation, particularly in satellite communication systems.

(2) Liaison and consultation with other investigators of PIM phenomena.

(3) Experimental investigation of the interference generating potential of commercially available passive RF components.

(4) Experimental evaluation of materials, platings, metallic joints, and hardware mounting schemes to determine the best methods and materials for the manufacture and assembly of PIM free hardware.

(5) The development of techniques for the analytical prediction of the PIM generating potential of particular components and hardware configurations.

(6) Experimental and theoretical investigation of the vacuum phenomenon of multipactor breakdown.

(7) The design of passive RF components for use in the MUSAT system.

1.3 Planning and Organization

Since this investigation was conducted well in advance of the proposed implementation date for the MUSAT system, specific hardware requirements were not known. RF component design and testing therefore took on only minor importance in the study. Major emphasis was placed on the identification and understanding of potential PIM sources in materials which, from considerations other than PIM, qualify for use in the manufacture of system components. This research nature of the

investigation made it practical to study PIM over a wide range of transmit powers and at all IM product orders rather than paying attention only to signals generated in the operating ranges of the MUSAT system. Particular attention was, however, paid to PIM generators peculiar to the space environment. In addition, transmit and receive frequency bands for PIM experiments were chosen to cover those of the satellite transponder. To allow a lesser degree of complication in theoretical analyses and easier interpretation of experimental results, consideration was given to only IM products generated by combinations of two transmit frequencies.

The study was organized to permit the maximum mutual support of theoretical and experimental investigations. Following an initial literature review and preliminary experiments to gain familiarity with CRC equipment* and observe some of the PIM characteristics noted from the literature, a detailed project plan was developed. Highlights of the plan are shown in the flowchart of Fig. 1.1.

The following paragraphs give a broad outline of the work that was to be carried out in connection with the topics in the numbered blocks.

Block A: Preliminary PIM investigations

This work included the initial literature review and limited experiments which provided a basis for detailed project planning.

---

* The CRC PIM measurement facility was purchased and put into use approximately one year prior to the beginning of work for this contract.

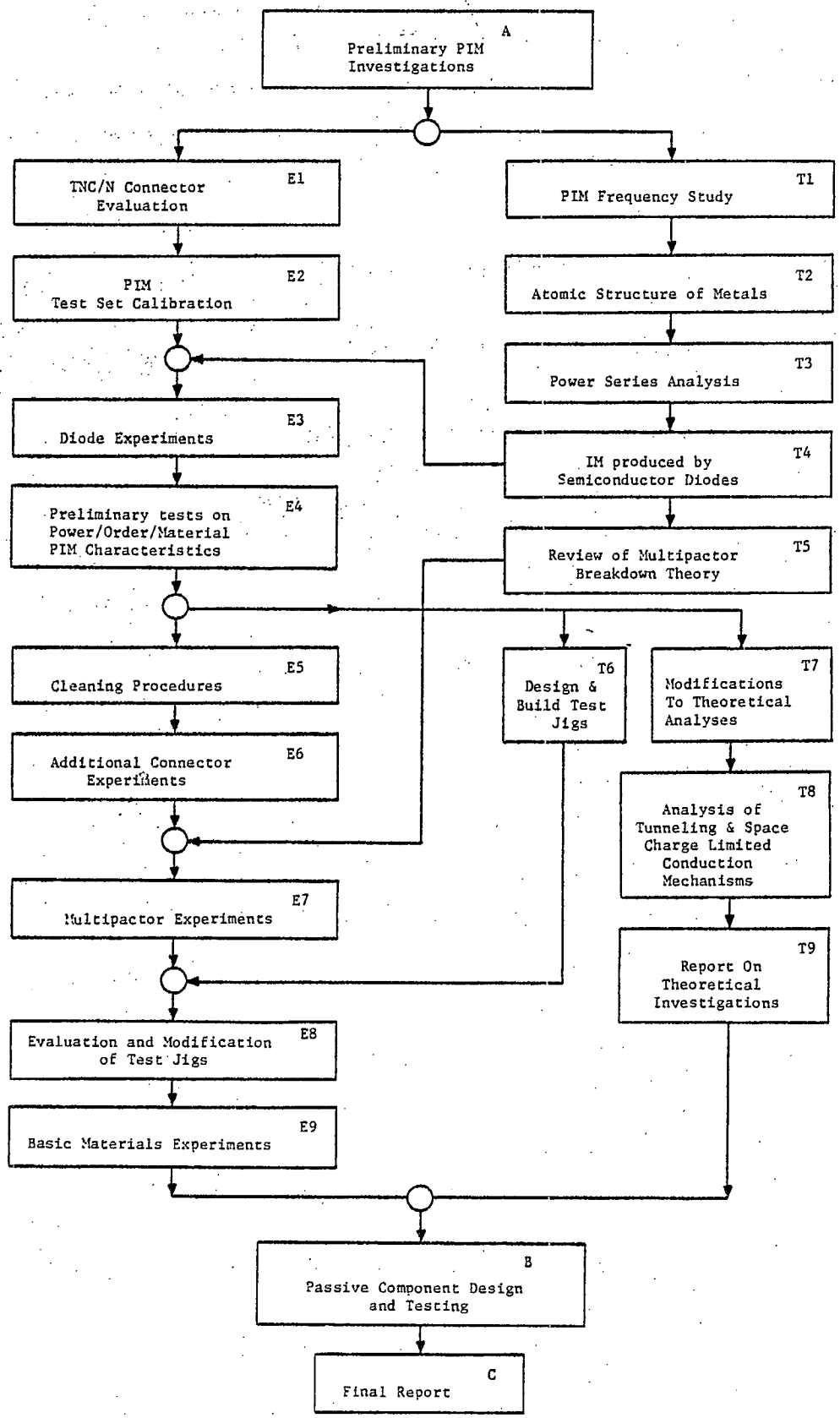

Fig. 1.1 Flow Chart Showing the PIM Study Organization

Block E1: TNC/N Connector Evaluation

As PIM free RF circuit connections are difficult to achieve, many different commercially available connector types were to be evaluated with regard to their PIM generating characteristics. The purpose of the initial evaluation of TNC and N types was to provide the knowledge necessary for planning experiments and the selection of other potentially useful connector families for testing.

Block E2: PIM Test Set Calibration

Early in preliminaty investigations it was recognized that PIM measurement accuracy and repeatability necessary for the verification of theory with experimental results would be difficult to attain. A test set calibration was therefore recommended for the purpose of determining methods for the improvement of measurement capabilities.

Block T1: PIM Frequency Study

The results of this work were to include equations for the quick computation of two tone transmit frequency combinations resulting in particular IM products at frequencies within the test set

receive band. The possibility of different IM products on the same frequency was also to be investigated.

Block T2: Atomic Structure of Metals.

In connection with PIM generated by conduction through metal/metal-oxide/metal interfaces, the atomic structure of various metals was to be studied. The objective was to determine what types of corrosion might be expected at contacts between similar as well as dissimilar metals.

Block T3 and T4

The prediction of PIM signal amplitudes using polynomial representations of nonlinear conduction characteristics was to be studied. As a starting point the amplitude of PIM signals resulting from the application of two transmit signals to the well known nonlinearity of a semiconductor diode were to be calculated. The diode I-V characteristic is similar to that of junctions which can exist between metals and naturally occuring oxides.

Block E3: Diode Experiments

A commercially available semiconductor diode was to be mounted in a test jig for use as the device under test in the measurement facility. Experiments were to be conducted in support of theoretical analysis.

Block E4: Preliminary Tests on Power/Order/Material PIM Characteristics.

Commercially available hardware components of similar construction but different metallic composition were to be used in experiments to determine the power of IM signals resulting from the application of transmit signals of different powers to components manufactured from different materials. Knowledge of these characteristics is important both in the selection of material for the manufacture of PIM free hardware and the identification of PIM sources in functioning RF systems.

Block T5: Review of Multipactor Breakdown Theory.

A source of PIM which is of major significance and is peculiar to RF systems in vacuum is a resonance electrical breakdown mechanism called multipactor breakdown. A review of literature concerning this phenomenon was to be conducted with a view to the suggestion of means for preventing breakdown in MUSAT satellite hardware.

Block T6: Design and Build Test Jigs

To permit experimentation with different conducting materials, surfaces, platings and joining processes, test jigs were to be designed and built so that test samples could be exposed to well defined electromagnetic fields for varied PIM experiments.

Block T7: Modifications to Theoretical Analysis

With the aid of results from the diode and power/order/material experiments, methods for theoretical analysis were to be modified and extended as required.

Block E5: Cleaning Procedures

The effect of dirt, oxidation, tarnish, and other possible conductor surface contamination on PIM generation was to be investigated experimentally. The aim was to develop hardware cleaning and handling procedures for the elimination of contaminants which enhance PIM generation. Such procedures would be used during PIM experiments and satellite assembly.

Block E6: Additional Connector Experiments

Using knowledge gained from TNC/N connector evaluation other connector types were to be tested to ascertain their potential for generating PIM. The construction of each connector type was to be examined to determine peculiarities which could be linked with an increase or decrease in PIM levels.

Block E7: Multipactor Experiments

As a follow up to the multipactor literature review, experiments were to be conducted to determine means for the prevention of multipactor breakdown in satellite hardware.

Block E8: Evaluation and Modification of Test Jigs

This work was to include the measurement of PIM signals generated by empty test jigs and possible jig construction modifications to reduce IM levels to values close to the test set receiver sensitivity threshold.

Block E9: Basic Materials Experiments

To test modified theoretical analyses and gain increased knowledge regarding construction materials, PIM signals generated by different material samples exposed to RF fields in the test jigs were to be measured.

Block T8: Analysis of Tunneling and Space Charge Limited Conduction Mechanisms.

Several reports uncovered during the literature review identified tunneling [1,2] and space charge limited [1] conduction mechanisms at metal/metal-oxide/metal interfaces as possible sources of PIM. Theoretical analysis techniques were to be developed to determine the level of PIM interference that could be generated by these phenomena.

Block T9 : Report on Theoretical Investigations

The results and conclusions from the literature survey and theoretical analysis were to be made available for reference in the design and testing of required passive RF components.

Block B: Passive Component Design and Testing

This work was to include the design and testing of items such as RF connectors, transmission lines, filters, baluns and antennas as specified by MUSAT system designers to ensure the maintenance of PIM interference levels below the specified maximum of -120 dBm.

Block C: Final Report

Preparation and submission of a report covering work performed in fulfillment of the contract.

The study plan proved to be extremely ambitious and as a result of time or equipment limitations, some of the planned work had to be deferred.

Theoretical work included the following:

(1) a thorough review of PIM an multipactor literature and the establishment of an indexed reference library

(2) the planned analysis of different PIM generating frequency combinations

(3) an evaluation of techniques that can be used for the analysis of spurious outputs from nonlinear conduction mechanisms

(4) development of computer programs for use in theoretical analysis

(5) computation of the characteristics of PIM signals generated as a result of the application of two transmit frequencies to a semiconductor diode.

(6) initiation of a study concerning PIM generated by tunneling and space charge limited current conduction mechanisms.

(7) recommendations and planning for the connector evaluation and PIM and multipactor experiments

Experimental work included:

(1) calibration of the measurement facility.

(2) the measurement of passive intermodulation signals generated by a semiconductor diode.

(3) multipactor experiments.

With the exception of theoretical work that was started with regard to tunneling and space charge limited current flow, the topics listed above are discussed in different chapters of this report.

1.4 Report Organization

Chapter II presents a review of literature concerning possible sources of PIM. References are provided and examples are cited which indicate the significance of different PIM generators. In addition sources which are considered to pose the greatest PIM interference threat in the proposed MUSAT system are identified.

Chapter III details four methods of analysis for the calculation of spurious outputs from circuit elements with nonlinear conduction characteristics. These include: trigonometric expansion of terms in a polynomial describing the nonlinear transfer characteristics of the circuit element, a method proposed by Sea [3] for the algebraic manipulation of polynomial terms, Volterra series analysis, and a technique proposed as the result of research for this investigation which is based upon decomposition and spectral analysis of the waveform at the output from a circuit nonlinearity. The limitations of each technique are discussed and information concerning characteristics of IM generation brought to light by the investigation of analysis methods is presented.

The subject of Chapter IV is the measurement of PIM signals. Consecutive sections of the chapter deal with measurement equipment considerations, a description of the CRC test circuit, and experimental methods. Results and conclusions of the preliminary PIM experiments conducted at the beginning of the study are also included.

IM signal power characteristics are studied in Chapter V. First, Sea's method for the algebraic manipulation of polynomial terms is applied using two different polynomial representations of the nonlinear resistance characteristic of a semiconductor diode. IM powers delivered to the load in a RF system model under various transmit signal conditions are calculated. Next, the results from experiments in which a mounted hot carrier diode was inserted as the device under test in the CRC measurement circuit are reported. No attempt is made to match computed and measured IM

signal amplitudes because of modelling inaccuracies and difficulties encountered in the determination of test circuit parameters. Instead measured and computed IM signal power changes in response to drive signal changes are compared, leading to general conclusions regarding drive level/IM signal response characteristics and their use for identifying IM sources in functioning RF systems.

Chapter VI begins with a thorough review of available literature on the subject of multipactor breakdown. The basic breakdown mechanism is explained and different types of multipactor along with their effects on RF circuitry are discussed. Means by which multipactor breakdown might be prevented are suggested next. Finally, experiments to test one of the suggested preventative measures are described, and results are presented.

A summary of the investigation, conclusions, and recommendations fur further research are contained in Chapter VII.

CHAPTER II

SOURCES OF PASSIVE INTERMODULATION

2.1 Introduction

Many types of conduction nonlinearities that can exist in passive components of a radio frequency communication system have been identified in the literature. In order to eliminate these nonlinear effects, it is necessary to understand the fundamental mechanisms by which they generate intermodulation signals, and the components of a system in which they are most likely to exist.

In this chapter, a review of the literature concerning possible sources of PIM is presented. Consecutive sections deal with PIM generation by metal-metal contacts, conductor heating, ferromagnetic materials, semiconductor junctions formed in metal/metal-oxide/metal interfaces, solar panels, multipactor breakdown, and other sources which are thought to be of a lesser significance. In addition, PIM generators are classified with regard to their anticipated relative importance in the MUSAT system.

2.2 PIM Generation at Metal-Metal Contacts

IM products can be generated at metallic junctions across which multiple RF currents flow. Interfaces between similar as well as dissimilar metals can result in the generation of IM products at levels which are dependent upon the contact load, the geometry of the metallic interface, the composition of the metals, and the degree of corrosion at the junction. An overview of reported effects caused by variations in each of these parameters is presented in this section. Semiconductor nonlinearities at corroded contacts are the subject of Section 2.5.

2.2.1 Contact Load

There is general agreement among investigators [1,4,5,6,7,8] that the level of PIM generated at metallic contacts decreases as the result of increased pressure between mating surfaces (load). Reports indicate that the dependence of PIM on contact load is related to RF current density variations in microscopic contact points as load changes.

From intuitive considerations, Von Low [4] analysed the processes that take place when pressure is applied to contact members. He argued that since all metallic surfaces are irregular, initial contact is made at isolated points. With increased load, cold flow occurs as the result of enormous pressures at the contact points, which spread into contact islands. Additional contact points are established simultaneously. As the metallic surfaces are drawn closer together under still greater loads adjacent islands combine and more new contact points form. The total contact surface area is increased as the islands

become larger. The totality of contact island perimeter is decreased, however, thereby decreasing the RF current-carrying area defined by the skin depth at the frequency of operation. In contrast, the formation of new contact points increases the current-carrying area as well as the contact surface area. For low, or intermediate contact loads it is therefore not clear if current density is decreased significantly as a result of increased load. In the case of very large loads, all contact islands eventually combine, causing an overall increase in the current-carrying surface area. This decreases RF current density and results in lower PIM interference levels. Figure 2.1 is an illustrative explanation of the process.

Von Low [4],Bayrak and Benson [6], Cox [5], and Sanli [7] have all reported experimentally observed decreases in PIM level as a result of increases in contact load. Figure 2.2 shows some results of experiments performed by Sanli with two CW microwave (f_1= 2.8 GHz, f_2= 3.2 GHz) carriers applied to a variety of metal-metal contacts.

2.2.2 Contact Surface Geometry and Roughness

A number of experiments have been performed [6,7] in which flat as well as spherically shaped metallic contacts with two frequency microwave excitation were subjected to different loads. Results show that there is only a minor dependence of 3rd and 5th order IM levels on contact geometry. There is some indication, however, that surface (planar) contacts generate the lowest IM levels. Reported data also show that the power of IM signals generated by point contacts decreases most rapidly with slight load increases.

(a) Light Load; Contact established at only a few isolated points.

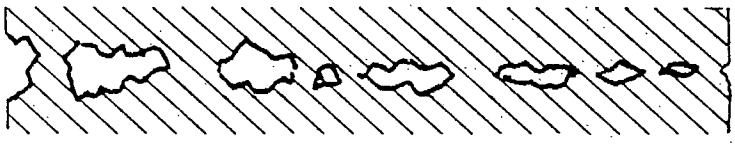

(b) With greater load contact islands form.

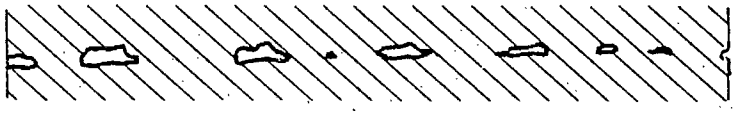

(c) With extremely large loads the contact islands combine and a large contact area is established.

Fig. 2.1. The processes involved when metals are brought into contact.

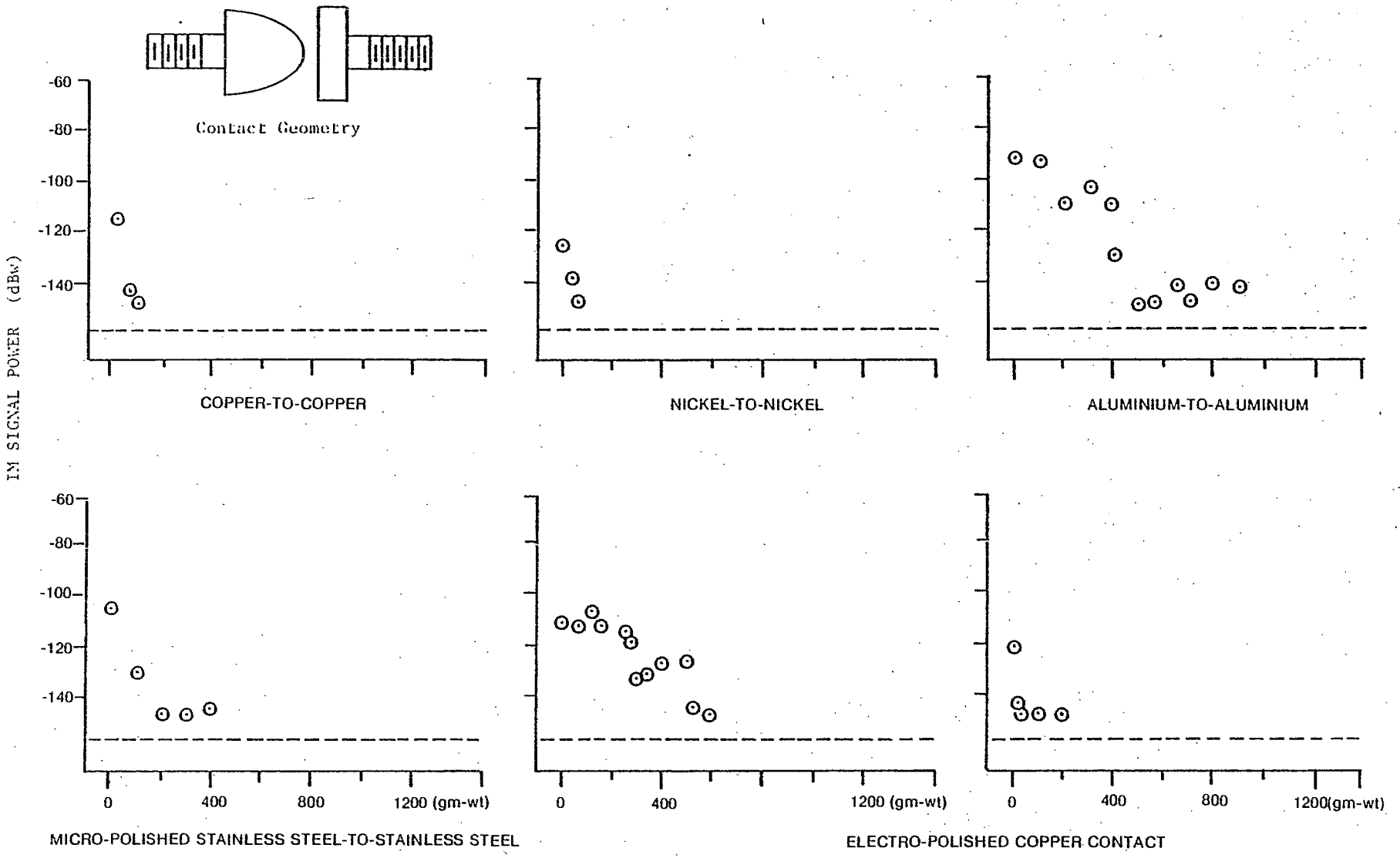

Fig. 2.2 Third order PIM signal power as a function of contact load at 3.6 GHz (from Sanli [7]).

The effect of contact surface roughness on PIM generated at metallic contacts has been investigated by Chapman et al [1] and Martin [8]. According to Chapman, the number and area of point contacts between mating surfaces is a maximum at an undetermined degree of surface roughness. Fewer contact points can be established between metals with rougher surfaces because of severe contact boundary dissimilarities. At the other extreme, rounded knolls on smoother surfaces yield less rapidly under pressure to fit depressions in the mating member. This also results in a decrease of contact area. These considerations suggest that there may be an optimum finish for contacting surfaces which results in minimum PIM generation.

Martin has experimentally observed the effect of surface roughness at aluminum-to-aluminum contacts. Figure 2.3 shows the amplitude of PIM signals generated under equivalent operating conditions, but with three different contact surface finishes. He explained that rough surfaces are more efficient in puncturing oxides at the contact point, thereby enabling a better metal-metal contact, and resulting in the significant reduction of PIM levels shown for the case of the roughest contact surface.

2.2.3 Contacts Between Similar and Dissimilar Metals

The amplitude of PIM signals generated at metallic contacts is dependent upon the type of metals in contact.

Bayrack and Benson [6] have reported the results of a detailed experimental study of IM products generated at contacting interfaces between similar and dissimilar metals under a variety of

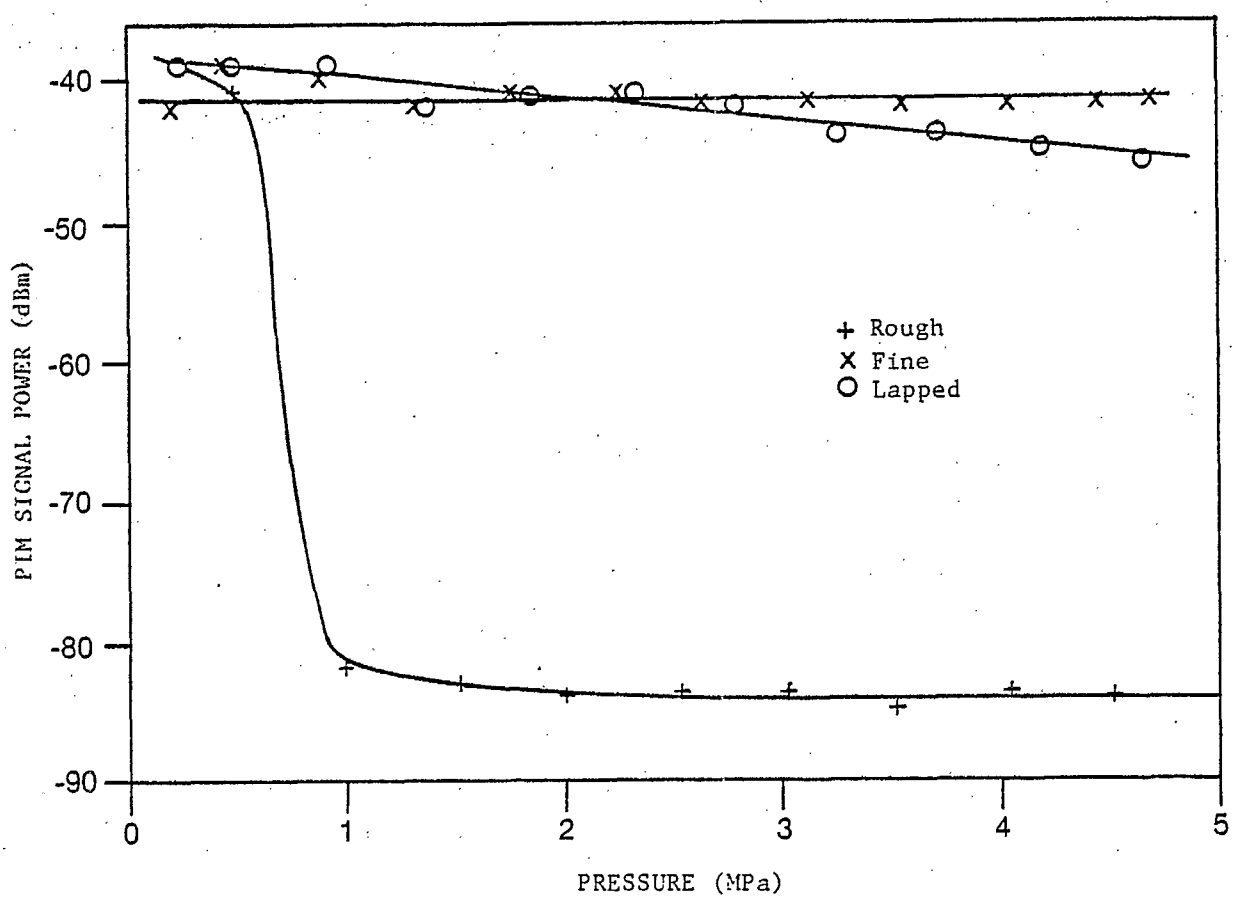

Fig. 2.3. Third order IM signal power as a function of contact pressure for aluminum contacts (from Martin [8]).

conditions. Contact materials of copper, brass, beryllium-copper, nickel, aluminum, stainless steel, and mild steel, as well as electroplated metal contacts of gold, silver, rhodium, copper, and tin on hard brass were used in experiments at 3 GHz. The strongest 3rd and 5th order IM signals were generated by similar and dissimilar contacts with mild steel, aluminum, and stainless steel. Lower IM levels were generated in experiments with copper, brass, beryllium-copper, nickel, and similar and dissimilar electroplated contacts. Dissimilar contacts of mild steel, aluminum, and stainless steel with any other metal generated IM signals of intermediate or high amplitude. Sanli [7] has reported a continuation of this work with similar results.

Martin has also performed experiments with different metallic contacts at HF and UHF. Table 2-1 is taken from his report [8] and shows typical IM levels generated by similar metal contacts under the specified operating conditions. Martin noted that the results presented in the table were not necessarily reproducible as a result of microscopic differences in contact geometry after breaking and re-making contact. Variations were reported to be within ± 5 dB except for aluminum contacts which produced very different IM signal levels after each make/break cycle.

Young [9] reported a number of experimental investigations which show that very strong IM signals can be generated by nonlinear mechanisms in ferromagnetic materials. IM generation by ferromagnetic nonlinearities is the subject of Section 2.4.

TABLE 2-1

PIM Levels (dBm) for Various Similar Metal Junctions at HF and UHF with 2 x 30 watts Fundamental RF Power and 1MPa Contact Load (from Martin [8])

Fundamental Frequencies (MHz)	360, 370	22.47, 25.47
PIM Frequencies (MHz)	350	28.47
Brass	< -86	< -85
Copper	< -86	< -88
Aluminium (99.9%)	-35	-70
Mild Steel	-60	-54
Stainless Steel	-92	-80
Nickel	-82	-61
Silver	< -86	-
Gold	< -95	< -85
Beryllium Copper	< -95	< -84
Oxygen Free Copper	< -95	< -84

2.2.4 Corrosion

It has been reported that, in general, corrosion has a marked effect on the generation of PIM. Bayrack and Benson [6] found that IM levels produced by oxidized contacts were from 5 dB to 25 dB higher than those generated at clean contacts. They also found that scorched or burned contact surfaces lead to increased spurious generation. Coaxial cables tested by Amin and Benson [10] generated much higher IM power levels after being exposed to an oxidizing environment.

In a slight deviation from the subject of contacts, it is interesting to note that corrosion also has an influence on PIM generated and radiated by metal surfaces exposed to multifrequency RF fields. In connection with the study of IM interference generated in a ship-board environment, Betts and Ebenezer [11] corroded mild steel rods to various degrees before testing. They found that 3rd order PIM amplitudes increased by 20 dB as corrosion ranged from non-existent to very severe.

2.3 PIM Generated by Conductor Heating

Due to the finite conductivity [12] of transmission lines and waveguides there is always RF energy loss in a region of volume approximately defined by one skin depth. The cyclic variation of energy in this volume due to RF excitation results in a cyclic variation of conductor temperature. Since the electrical conductivity of metals is a nearly linear function of temperature, this can produce harmonic components of conductivity which modulate the primary input currents and produce conductor currents at IM frequencies.

As a result of finite conductor conductivity, tangential electric fields (E_t) are non-zero. This means that if a transmission line is excited simultaneously by two RF fields at frequencies f_1 and f_2, conductor surface current density is given by:

$$J_s = \sigma(T)\ (E_{t_1} + E_{t_2})\ ,$$

where, $\sigma(T)$ = electrical conductivity as a function of temperature

E_{t_1} & E_{t_2} = the tangential electric fields at f_1 and f_2 respectively.

Equating the corresponding E-M energy equation to the thermal energy equation under appropriate boundary conditions results in an expression which shows that J_s has components at intermodulation frequencies which give rise to IM fields. Further mathematical manipulations show that the power in the IM product fields is inversely proportional to electrical conductivity and depends directly upon the square of the thermal coefficient of conductivity. Also, the

intensity of the IM fields varies along the length of the transmission line. For short distances from the transmitter the field grows as a function of distance squared. At some greater distance, which is a characteristic of the line, the IM field peaks and then is attenuated as are the exciting fields due to dissipation in the conductor.

Sample calculations made by Wilcox and Molmid [13] for 0.141 inch semi-rigid cable show that the IM power reaches its maximum at a distance of 28 meters from the transmitter. For a 3rd order IM frequency of 300 MHz and CW carriers at 30 watts each, the maximum IM power was calculated to be -130 dBm.

Stauss [14] has also made theoretical investigations with regard to conductor heating as a source of PIM. In addition to conductivity changes, local dimensional changes were cited in his report as a possible generator. It was shown, however, that this latter source is insignificant.

In a numerical example Stauss calculated the power of IM signals generated by conductor heating in a very high Q cavity excited by two CW carriers at UHF with a total input to power of 100 watts. These calculations showed that IM powers as high as -142 dBm could be delivered to the load in an assumed circuit model.

From the numerical examples referenced it can be seen that thermally induced variations in electrical conductivity can generate significant PIM under optimum circumstances. This source of PIM is considered, however, to be of only minor importance where transmission lines are short, and circuit Q's are not exceptionally high. From derived equations, Stauss concluded that in the two frequency case thermal IM generation is enhanced in high Q circuits, when transmit carrier

amplitudes are equal, and when carrier frequency separation is small. He advised against the use of conductors with high resistivity, low heat capacity, low thermal conductivity, or a high thermal coefficient of resistivity where multifrequency RF fields can be present. Stauss also assumed a simple relationship between IM power generation and conductor area. From this he concluded that PIM generation increases with conductor surface area. However, the fact that resistance decreases in conductors with larger cross-section (and therefore larger surface area) as does current density, must introduce compensating factors.

2.4 The Generation of Passive Intermodulation in Ferromagnetic Materials

Intermodulation production by ferromagnetic materials has been investigated by Young [9] at the Naval Research Laboratories (NRL) in Washington, D.C. He noted that many of the newer commercially available RF connectors are being manufactured from stainless steel type 303, a low permeability ferromagnetic alloy. He observed also that brass stock connectors are being plated with nickel instead of the previously used silver in order to cut production costs. To determine the magnitude of IM generation by new hardware containing ferromagnetic materials (iron, nickel, cobalt, and their alloys), a large number of commercially available connectors were tested at NRL in a specially built low PIM test set. Various experiments proved that connectors and adapters manufactured from ferromagnetic materials generate significantly (35 - 45 dB) stronger 3rd order IM signals than their silver plated brass counterparts under identical operating conditions. Figure 2.4 shows a set of measured 3rd order IM power curves taken from the referenced report.

In one experiment, a commercially available RF double jack type N precision adapter with a stainless steel body and outer conductor and beryllium-copper inner components was placed in the PIM test set and generated IM levels were measured. An identical connector body was machined from brass, and fitted with the beryllium-copper inner conductor parts from the original adapter. PIM levels generated by this adapter were 45 dB lower. In another experiment a stainless steel adapter was plated with gold to in excess of 5 skin depths at 300 MHz.

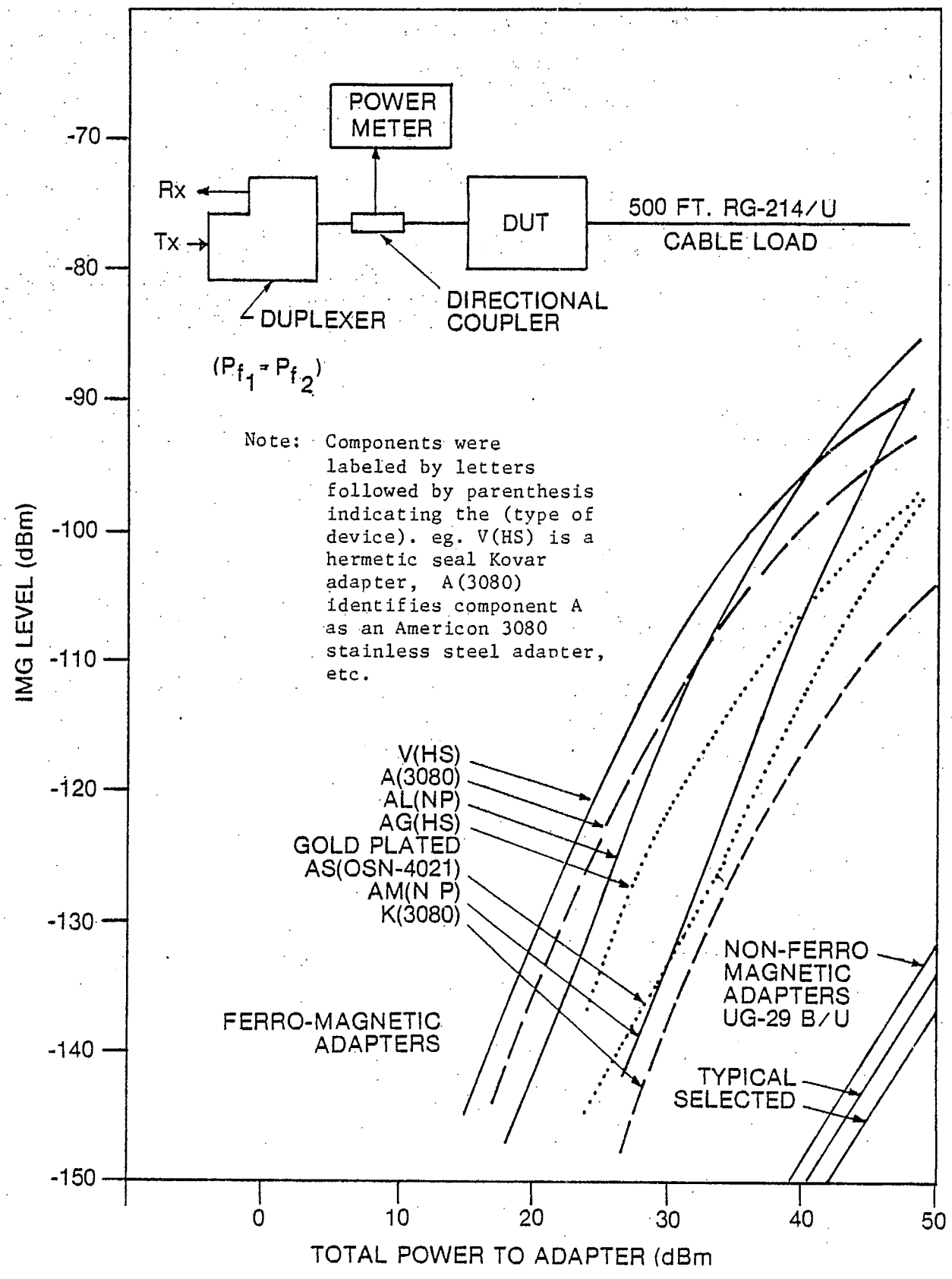

Fig. 2.4. Variations in the power of IM signals generated by commercially available passive RF components as a function of total transmit power, (from Young [9])

This resulted in the reduction of IM levels by 15 dB. Even with this reduction, the IM level was still 30 dB higher than IM products generated by comparable silver-plated adapters. This is surprising since the totality of RF current should have been confined to the gold plated surface area. Experiments were also conducted with nickel plated and hermetically sealed RF components. It was found that the nickel plated devices generated IM signals of almost the same strength as stainless steel components. Adapters with Kovar-glass hermetic seals also generated very strong PIM.

It was speculated by Young that the PIM generating mechanism in ferromagnetic materials is the nonlinear dependence of permeability upon current. Experiments were conducted using external magnetic fields to change material permeabilities during PIM measurements. It was found that components in a degaussed state (high incremental permeability) generated much stronger IM signals than components near magnetic saturation which have a low incremental permeability dependence upon current.

To simulate Young's connector experiments and further identify ferromagnetic generating mechanisms, Bailey and Ehrlich [53] conducted experiments at NRL on another test set using much lower transmit powers (Young's experiments used +45 dBm total RF transmit power). In these tests, plated copper conductors were supported in test jigs so they could be exposed to various magnetic fields while PIM powers were measured. IM characteristics were found to be similar to those reported by Young.

Bailey and Ehrlich postulated that the response of PIM levels to different magnetic field orientations and the decrease in levels as the point of saturation is approached is related to magnetic domain wall displacement and domain rotation. On the assumption that the domain wall motion is responsible for PIM generation in ferromagnetic materials, two possible generating mechanisms were cited. These were: nonlinear intra-domain wall excitations, and domain wall vibrations. In the latter case it was explained that IM signals could arise as a result of the absorption of energy by the oscillating wall, and subsequent re-emission of energy at the fundamental as well as intermodulation frequencies. A mathematical treatment based upon the theory of domain wall vibrations led to a general correlation of measured IM power characteristics with variations in domain structure. A qualitative explanation of IM signal/magnetic field variations was given. Royal and Cushner [13] have also suggested that magnetic domain excitation is a possible source for PIM generation.

In theoretical work by Stauss [14], also at NRL, three sources of IM generation in ferromagnetic materials were suggested, and describing equations were developed. Stauss first expanded previous work [13] on PIM produced by conductor heating, and noted that in the case of ferromagnetic materials, conduction loss is a function of permeability. Calculations indicated that the higher, permeability-dependent resistivity values and low thermal conductivity of some ferromagnetic materials result in the possibility of the production of IM signals at significant power levels by thermally induced conductivity changes.

An exemplifying calculation of the power of PIM signals generated by conductor heating in a 10 cm long section of coaxial cable was made. It was assumed that two equal amplitude UHF CW carriers excited the cable with a total RF power of 100 watts. For a copper inner conductor (outer conductor PIM generation was assumed negligible due to much lower current density), the 3rd order IM power delivered to a matched load in an assumed circuit model was calculated to be -242 dBm. Under equivalent conditions, but with a nickel conductor, the IM power delivered to the load was calculated to be -162 dBm and -186 dBm for average conductor permeabilities of 500 μ_o and 100 μ_o respectively.

Stauss also investigated magneto-resistance as a possible source of PIM. Due to this effect, the resistivity of a conductor is altered by externally applied magnetic fields, or by the conduction of current. Harmonic variations of resistivity due to RF excitation can modulate the primary currents and produce currents at IM frequencies. For the 10 cm long piece of coax with 100 watts RF input, the PIM due to magneto-resistance effects was calculated to be -71 dBm for μ = 500 μ_o and -114 dBm for μ = 100 μ_o. Stauss noted from references that experimentally the change in resistivity with magnetic field is quite linear for a material near magnetic saturation. This would lead to a reduction of PIM with the application of higher magnetic fields, as observed by Young.

The variation of permeability in a changing magnetic field was another possible generating mechanism considered by Stauss. Equations were derived relating IM current density to RF power input and used to compute a ratio of IM power generated by permeability variations to IM generated by the magneto-resistance nonlinearity. For small externally applied magnetic fields and an iron conductor (the permeability of nickel is almost the same as that of iron), use of the derived ratio showed that the variable μ mechanism could produce PIM levels approximately 40 dB higher.

In summary, both theoretical and experimental investigations have shown that ferromagnetic materials are sources of strong IM interference. All investigators have stressed the necessity to completely eliminate such materials from multifrequency RF systems.

2.5 Passive Intermodulation Generated by Current Flow Through Semiconductor Junctions Formed at Metal/Metal-Oxide/Metal Interfaces

A number of reports [1,2,4,5,6,8,15,16] have shown experimental evidence that corrosion at metallic contacts leads to an increase in the production of PIM. In reports produced by Chapman and Darlington [1], Higa [2] and Bond et al [16], conduction mechanisms in metal oxides that could lead to PIM generation have been investigated.

Most metallic surfaces [1] form oxide coatings several angstroms thick under normal environmental conditions. If one considers microscopic surface irregularities, a cross sectional view of the mating of two metallic surfaces can be envisioned as shown in Fig. 2.5. If sufficient contact load were applied, jagged points on the surfaces would completely puncture the oxide and form filamental contact bridges [1,17]. In other regions along the interface, only partial puncture would occur, leaving a very thin insulating oxide layer between metals. In the surrounding areas oxides of various thickness would exist as well as some voids.

If only partial puncture of the oxide has occurred and the remaining oxide between the conductors is sufficiently thin, (< 50 Å) as compared with the DeBroglie wavelength for an electron [2], tunneling can take place. This conduction mechanism is extremely nonlinear and could be a major source of PIM.

Another nonlinear conduction mechanism that can exist where the oxide layer between conductors is between 10 and 100 Angstroms thick [1] is that of space charge limited current flow. Normally, current flow through insulating oxides is prevented due to the lack of free carriers

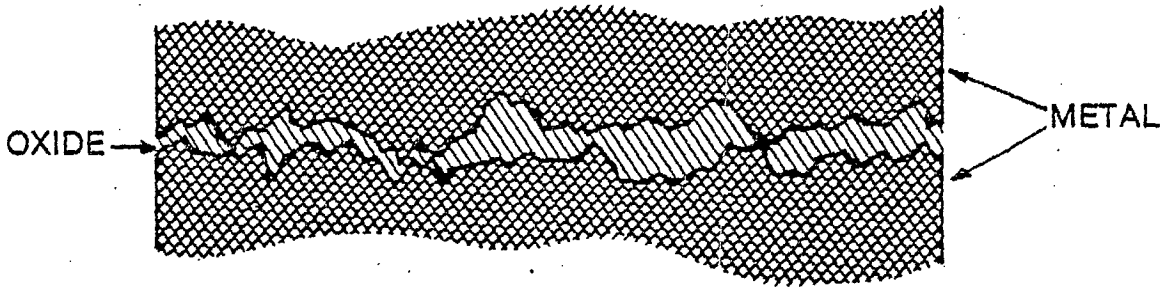

Fig. 2.5. Cross-sectional view of a metal-metal contact, (from Chapman and Darlington [1]).

for conduction. In very thin oxide layers sandwiched between metals, however, [18] the possibility of electron injection must be considered. When a potential is applied across a metal/metal-oxide/metal sandwich electrons can be injected from the cathode into the oxide. These electrons populate the normally empty conduction band and current is permitted to flow. Since the electrons were injected, there are no equalizing holes in the valence band of the oxide in which a space charge is established with the highest electron density near the cathode.

The electric field in the oxide is inversely proportional to the charge density. The field is therefore reduced near the cathode and acts to limit the injected current which is referred to as being one carrier space charge limited. The I-V transfer characteristic for the phenomenon is symmetrical about zero voltage, and is of the form shown in Fig. 2.6. PIM would result if multifrequency excitation were applied where such nonlinearities exist.

The random scattering of tunneling and space charge limited conduction mechanisms at a metallic interface would result in very unstable PIM power levels as signals generated by a number of such elements add with different phase relationships. Complexities of this situation would be compounded, for example, in the case of coaxial cables with braided outer conductors, where many semiconductor-like junctions could exist at corroded inter-braidwire contacts.

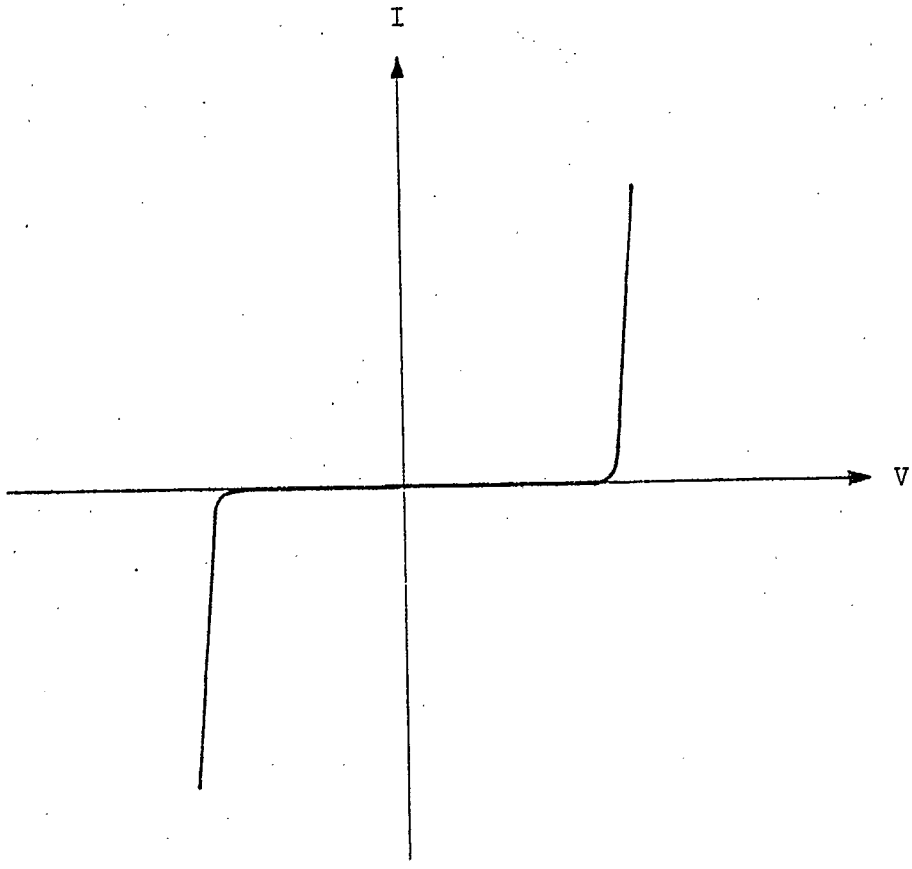

Fig. 2.6. Typical space charge limited conduction characteristic.

2.6 Solar Panels

Arrays of solar cells are used on modern communication satellites to charge batteries which supply energy to on-board electrical equipment. Solar cells are semiconductor devices and have nonlinear I-V characteristics. There is therefore concern that solar panels exposed to RF fields radiated from transmit antennas could generate and radiate PIM interference.

Young [19,20] has experimentally investigated the possibility of IM generation in solar panels. Reported experiments were qualitative and did not involve the measurement of actual IM signals generated by solar cells exposed to multifrequency RF fields at UHF. Instead, a 915 MHz electromagnetic interference detection system was used to determine if harmonics of a single radiated transmit frequency could be generated and radiated by solar panels. A highly selective receiver was tuned to monitor any second and third harmonics of the transmit frequency that were emitted from the direction of the solar arrays. Tests were made with different solar panel configurations and isolated solar cells in short and open circuit conditions and when illuminated or in darkness.

Conclusions were that typical solar cells by themselves would not generate significant PIM interference. It was noted, however, that IM signals could be generated in interconnections between cells and their mechanical attachments to the solar panels. Steering diodes used to prevent the cells from shorting the batteries during periods of darkness, and to minimize circulating currents were also identified as potential sources of strong IM signals.

2.7 Passive Intermodulation Generated by Multipactor Breakdown

Multipactor breakdown is a phenomenon associated with the existence of RF voltages across a gap between dielectric or conducting surfaces in vacuum. It is a resonance effect in which electrons emitted from one surface are accelerated across the gap during one half cycle of the RF voltage and, if their energy is sufficient, release secondary electrons on impact with the opposite gap wall. The resulting chain of electron emissions due to additional accelerations and impacts leads to electrical breakdown which is nonlinearly dependent upon the level of RF excitation. If breakdown takes place in the presence of multifrequency RF fields, strong PIM signals are generated.

The results of experiments performed by Hahn at CRC before work began for this contract show the degree to which PIM generation is enhanced when multipactor breakdown occurs. An open circuited sample of a UHF antenna balun was mounted in a test jig and two frequency RF excitation was applied in air, and under vacuum conditions. The onset of multipactor in the vacuum test was monitored by means of an electron collector plate mounted at the end of the balun section as shown in Fig. 2.7. Simultaneously, PIM signals generated in the test circuit were monitored using the CRC PIM test facility*. Figure 2.8 shows the difference between PIM levels generated under normal operating conditions in air, and under conditions of breakdown in vacuum. The figure

---

* The Communications Research Centre (CRC) PIM test facility is described in detail in Chapter IV

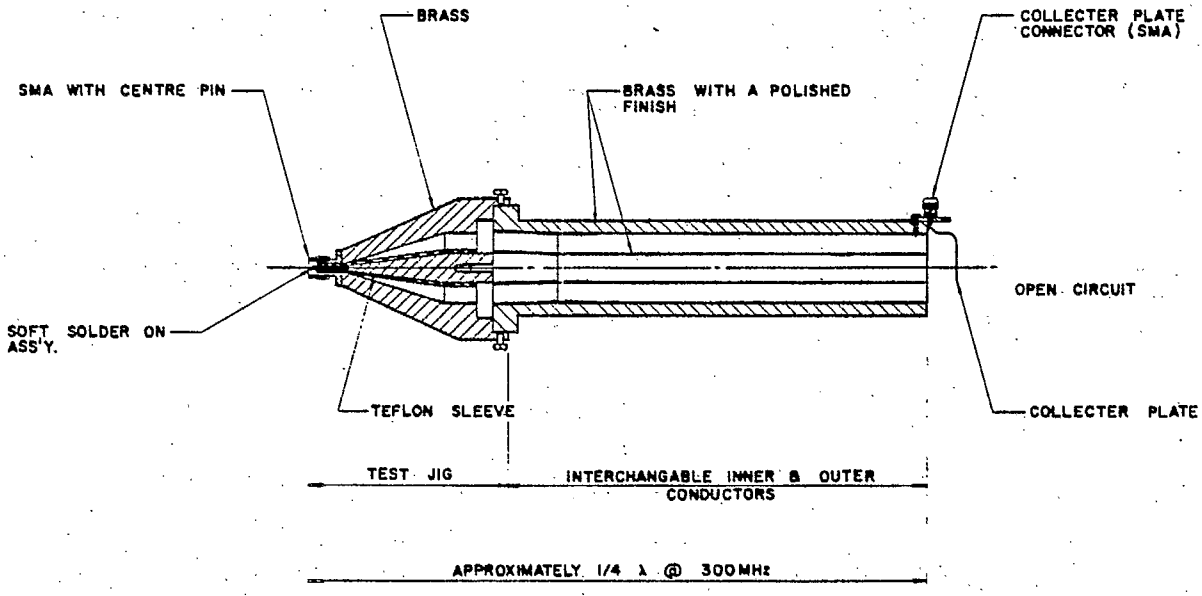

Fig. 2.7. Balun test sample and jig for multipactor experiments.

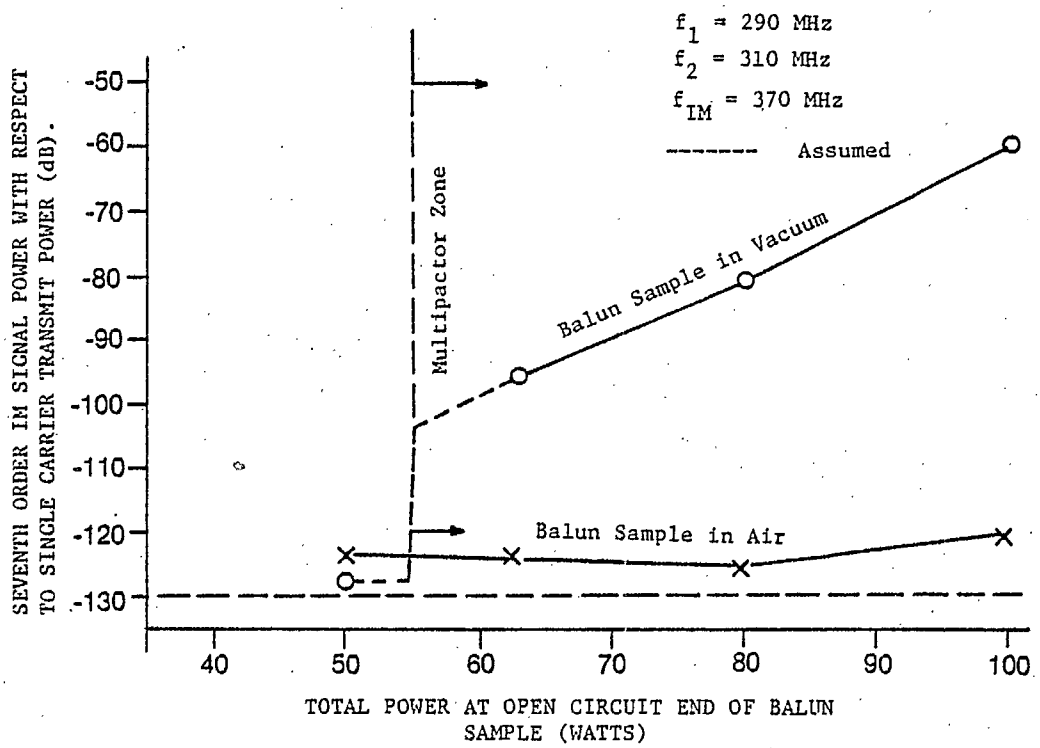

Fig. 2.8. The increase in IM signal generation due to multipactor breakdown.

clearly shows that multipacting cannot be permitted if PIM interference is to be minimized.

Multipactor breakdown and the resulting generation of PIM is the subject of theoretical and experimental work discussed in Chapter VI.

2.8 Other PIM Generators

Theoretical examination of various other phenomena has shown that their nonlinear nature could lead to PIM generation. This section lists several suggested PIM sources, and cites references in which more detailed information can be found. The threat of significant interference due to PIM generated by these mechanisms is considered minimal.

2.8.1 Magneto-Resistance in Nonmagnetic Conductors

As with ferromagnetic materials (section 2.4), the presence of a magnetic field can alter the resistivity of a conductor. If the magnetic field is changing, resultant harmonic variations in resistivity can lead to PIM generation.

In copper [14] the 3rd order IM power resulting from the magneto-resistance effect has been calculated. Powers were found to be 43 to 54 dB down from those generated by conductor heating.

2.8.2 Filament Conduction

If a current [1] is restricted to flow through thin filaments as may be the case in metallic contacts, nonlinearities are known to exist. This effect has an associated "constriction resistance" and "constriction inductance".

IM generation due to filament conduction has not been evaluated numerically. From an intuitive standpoint, however, anticipated characteristics [17] are thought to correlate well with observed 3rd order trends.

2.8.3 Nonlinear Properties of Dielectrics

Variations in dielectric properties may occur in response to electric fields either by heating, or by electrostriction [14]. In good, nonpolar dielectrics, electrostriction is expected to be the principle source of nonlinearity. By this phenomenon, volume changes due to the variation of energy density in a dielectric under RF excitation cause a quadratic dependence of permittivity upon the electric field. The resulting permittivity variations at the fundamental and harmonics of the input frequencies modulate the primary fields, leading to the generation of PIM. Intermodulation powers developed by this mechanism depend inversely upon the square of the bulk modulus of the dielectric.

Along a length of 0.141" semi-rigid (solid teflon dielectric) coaxial cable with two 30 watt equal carrier inputs at UHF, [13] the 3rd order IM power produced due to electrostriction was found to peak at 28 meters from the cable input, and thereafter attenuate with distance. The peak IM power was calculated to be -158 dBm. For shorter lengths of cable, and dielectrics with a higher bulk modulus, this power would be much lower.

2.8.4 Other Low Level Generators

A number of other naturally occurring mechanisms have been suggested as possible contributors to the total passive intermodulation interference in a RF system. These include [1] ionization breakdown, weak plasma effects, water vapor absorption, microdischarge, field emissions from thin projections inside components [13], the nonlinear

character of Lorentz force, [13] and direct resistivity variations as a function of current density. The references cited give explanations of the mechanisms associated with each effect. Conclusions are that their IM contributions are comparatively negligible in components designed for operation at UHF.

2.9 Discussion

The literature review presented in this chapter has revealed mechanisms which have been studied and suggested as possible sources of PIM. Depending upon power, operating environment, and component designs, some sources may be major contributors to PIM in one RF system, while being of only lesser importance in another. For example, conductor heating could produce significant IM noise in high power microwave systems with long waveguide runs. This source would be of little significance, however, in a UHF system operating with moderate powers and using short lengths of coaxial transmission line. Receiver sensitivity is also to be considered when estimating the interference potential of different mechanisms. As sensitivity increases, an increasing number of potential IM sources must be investigated.

A review of the requirements of the UHF system with which this study is associated leads to the following considerations with regard to which sources could be of significance, and require detailed study.

Inter-metallic contacts are a major problem to be tackled in reducing IM noise in most systems. PIM produced at cable and component interconnections can be serious and unstable. It has been reported that PIM [13] generated at properly soldered or welded joints is minimal. Where connections must be made or broken repeatedly, however, these methods cannot be used. PIM can be the result of misalignment or improper tightening, and can increase in magnitude with connector wear. Certainly it would be a major achievement to eliminate or better understand this IM source. Detailed experimental investigations which deal with the effects of such aspects as loading, surface geometry, and metal types have been referenced. It remains now to better explain these effects and to find optimums for each parameter that can be used in component manufacture, and system assembly.

The production of PIM as a result of conductor heating becomes increasingly more important as RF power density increases, conductor properties deteriorate, or transmission line lengths increase. Except in resonant structures or heating elements exposed to multifrequency RF fields, levels of PIM generated by heating are not expected to be of significance in a system of the type under consideration. Sufficient information can be obtained from the references to enable designers to avoid PIM problems arising from this source.

There is much experimental and theoretical evidence that ferromagnetic materials can generate very strong PIM signals. Such evidence makes it clear that the elimination of all ferromagnetic materials from multifrequency RF systems is imperative. Assuming the design of components and systems will follow this guideline, further study of ferromagnetic phenomena is not required.

In relation to the generation problems at connections, the possibility of the formation of semiconductor type junctions is real, and expected to be a major source of PIM. From the references, it is reasonable to conclude that clean surfaces aid in the reduction of generation. The difficulty is in identifying PIM caused by semiconductor nonlinearities, and the location of sources. It is important that more effort be expended in this area.

Multipactor breakdown is a phenomenon, which, like the use of ferromagnetic materials, must be eliminated from proposed systems. Theoretical and experimental work associated with this type of electrical breakdown are important.

Under normal operating conditions, the PIM sources discussed in Section 2.7 are not expected to be troublesome in the MUSAT system.

In summary, it is believed that in the proposed satellite system, PIM generation of significant magnitude can be expected as a result of:

(a) loose or stressed metallic connections,

(b) electron tunneling and semiconductor junctions at metal-oxide/metal interfaces,

(c) multipactor breakdown.

CHAPTER III

ANALYTICAL TECHNIQUES FOR THE THEORETICAL PREDICTION OF INTERMODULATION PRODUCT CHARACTERISTICS

3.1 Introduction

One of the first steps in the elimination or control of passive intermodulation in any system is the prediction of the magnitude of interference that can be generated by each component in the system, and the circumstances under which PIM generation can take place.

Several analytical techniques are described in the literature [3,7,21,22,23,24] which are applicable under various conditions to the calculation of distortion components in the output from a circuit nonlinearity. This chapter shows how three reported techniques can be applied in making IM signal power calculations. In addition, a novel method of analysis which is more suitable for PIM calculations than previously reported methods is proposed. A two frequency sinusoidal input to the PIM generating nonlinearity is assumed in all examples and derivations.

3.2 The Calculation of Intermodulation Product Applitudes by Trigonometric Expansion of Terms in a Power Series.

Intermodulation products are generated* when multiple frequency

---

* It should be noted that IM generation is not a harmonic mixing process. IM signals are generated simultaneously with harmonics and crossmodulation products of each applied frequency. (See appendix A).

signals are applied to a circuit element, the transfer characteristic of which is nonlinear. Figure 3.1 is a representation of such a transfer characteristic having X as the input and Y as the output.

Mathematically, a polynomial of degree (n) depending upon the extent of nonlinearity can be fit to any nonlinear characteristic such that one can write*:

$$Y = a_0 + a_1X + a_2X^2 + a_3X^3 + \ldots + a_nX^n \qquad (3.2\text{-}1)$$

Assume now that it is desired to calculate the amplitude and phase of intermodulation products resulting from the application of two cw signals to a nonlinear circuit element. Assume also that the element nonlinearity is of a low degree so that its I-V transfer characteristic can be represented by (3.2-1) truncated at n = 5 with Y = I, and X = V, so that

$$I = a_0 + a_1V + a_2V^2 + a_3V^3 + a_4V^4 + a_5V^5 \quad . \qquad (3.2\text{-}2)$$

Let the applied signal (V) be the sum of two cosine waves having amplitudes E_1 and E_2 and radian frequencies ω_1 and ω_2,

$$V = E_1 \cos(\omega_1 t + \phi_1) + E_2 \cos(\omega_2 t + \phi_2). \qquad (3.2\text{-}3)$$

Substitution of (3.2-3) in (3.2-2) and trigonometric expansion of the cosine terms results in frequency component generation by each term as shown in Appendix A.

---

* Only polynomials with real coefficients have been considered in this work. Previous reports have shown [25] that the use of only real coefficients introduces little error in PIM calculations.

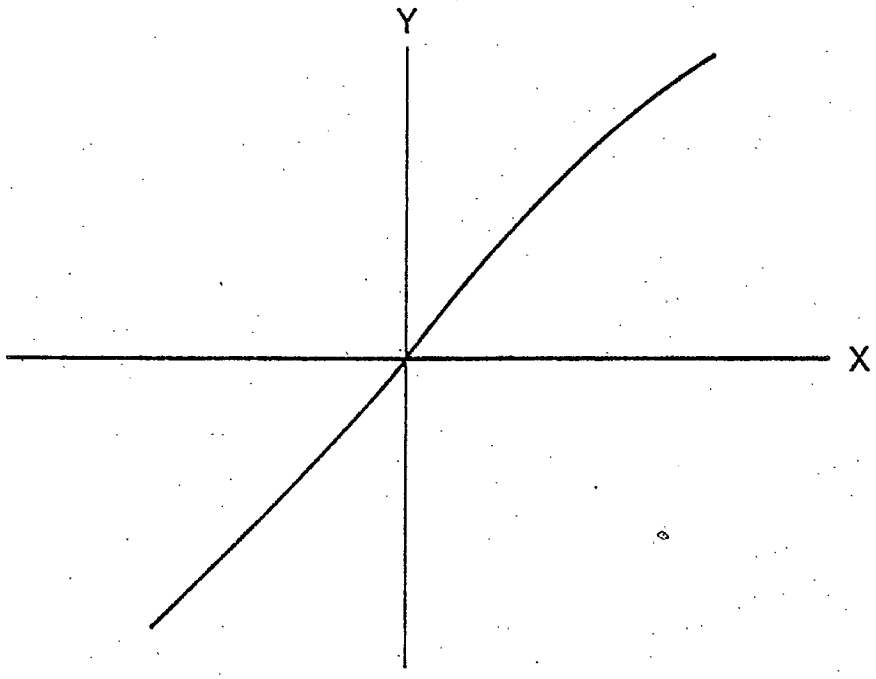

Fig. 3.1. An arbitrary nonlinear transfer characteristic.

Consider first the third-order product $(2f_2 - f_1)$. Amplitude and phase contributions at this frequency from the terms of eqn. 3.2-2 are as shown in Table 3-1. Referring to the table, the desired IM product is:

$$\left[\frac{3}{4}a_3E_1E_2^2 + a_5\left(\frac{5}{4}E_1E_2^4 + \frac{15}{8}E_1^3E_2^2\right)\right] \cos[(2\omega_2 - \omega_1) + 2\phi_2 - \phi_1] \ .$$

Next, consider the 5th order product $(3f_2 - 2f_1)$. Table 3-2 shows the contribution of each term at this frequency.

From Table 3-2, the desired 5th order product is:

$$\frac{5}{8}a_5E_1^2E_2^3 \cos[(3\omega_2 - 2\omega_1)t + 3\phi_2 - 2\phi_1].$$

Three important facts can be noted from Tables 3-1 and 3-2:

(a) Odd order intermodulation components are generated only by odd powered terms of the polynomial describing a nonlinear transfer function.

(b) If the intermodulation order is N, no contribution is made from terms of degree less than N. This means that if Nth order IM products are generated, the generating nonlinearity must be of a degree greater than or equal to N.

TABLE 3-1

Amplitude and Phase Components of the Third Order

IM product at $f_{IM} = (2f_2 - f_1)$

Degree of Term	Contribution to IMP at $f_{IM} = (2f_2 - f_1)$	
	Amplitude	Phase
0	No contribution	No contribution
1	No contribution	No contribution
2	No contribution	No contribution
3	$\frac{3}{4}a_3 E_1 E_2^{\,2}$	$(2\phi_2 - \phi_1)$
4	No contribution	No contribution
5	$a5\left[\frac{5}{4}E_1 E_2^{\,4} + \frac{15}{8}E_1^{\,3}E_2^{\,2}\right]$	$(2\phi_2 - \phi_1)$

TABLE 3-2

Amplitude and Phase Components of the Fifth Order IM product at $f_{IM} = (3f_2 - 2f_1)$

Degree of Term	Contribution to IMP at $f_{IM} = (3f_2 - 2f_1)$	
	Amplitude	Phase
0	No contribution	No contribution
1	No contriution	No contribution
2	No contribution	No contribution
3	No contribution	No contribution
4	No contribution	No contribution
5	$\frac{5}{8}a_5E_1^2E_2^3$	$(3\phi_2 - 2\phi_1)$

(c) Unless* both positive and negative coefficients occur in the describing polynomial, all terms contributing to a given IM product have the same phase. Where coefficients of both signs are included, contributions from some terms will be 180 degrees out of phase. This occurrence can, however, be accounted for by adding the appropriate sign to the amplitude terms. That is, other than by direct subtraction, no phase cancellation of contributions from different terms of the describing polynomial can occur, and transmit signal phases need not be considered in IM calculations when there are only two transmit frequencies.

Sea [3] has proven points (a) and (b) for a describing polynomial of any degree, and made generalizations to include even order products.

As seen by the multiplicity of terms in Appendix A, calculation of intermodulation characteristics by trigonometric expansion of terms in the describing polynomial is laborious, and quickly becomes unmanageable for nonlinearities of higher degree. The need for other methods of computation is evident.

3.3 An Algebraic Equation for Computing the Magnitude and Phase of Intermodulation Products

Sea [3] has derived an equation from which one can calculate the amplitude of any particular component in the spectrum of the output from a nonlinear device the transfer characteristic of which can be described by a power series, and the input to which is the sum of an

---

* When using computer Fourier analysis for computations, one is limited to a finite time interval. In this case, random phases must be assigned to each input signal.

arbitrary number of cosine waves of different frequencies.

Sea's derivation will be repeated here to reinsert steps omitted from Reference 3 and to emphasize some important points. Beginning as in Section 3.2 with the describing polynomial, the output (Y) from a nonlinear device is related to its input (X) by:

$$Y = \sum_{K=0}^{\infty} a_K X^K \tag{3.3-1}$$

Assume again that Y = I, and X = V, where V is the sum of cosine waves:

$$V = \sum_{m=1}^{M} V_m \ , \ V_m = E_m \cos\theta_m \ , \ \theta_m = (\omega_m t + \phi_m) \tag{3.3-2}$$

Substitution in (3.3-1) gives

$$I = \sum_{K=0}^{\infty} a_K \left[\sum_{m=1}^{M} V_m \right]^K \ . \tag{3.3-3}$$

From the multinomial theorem for the expansion of a sum raised to a power, one can write.

$$\left[\sum_{m=1}^{M} V_m \right]^K = \sum_{n_i \ldots n_M} K! \prod_{i=1}^{M} \frac{V_i^{n_i}}{n_i!} \tag{3.3-4}$$

where, $n_1 + n_2 + \ldots + n_M = K$,

$$\sum_{n_i \cdots n_M} = \sum_{n_M = 0}^{K} \sum_{n_{M-1} = 0}^{k_{M-1}} \cdots\cdots \sum_{n_2 = 0}^{k_2} ,$$

$$n_1 = k_1 ,$$

and

$$k_i = K - n_M - n_{M-1} - \cdots\cdots - n_{i+1} .$$

Then, writing $V_i = E_i \cos \theta_i$,

$$\prod_{i=1}^{M} V_i^{n_i} = \left[\prod_{i=1}^{M} E_i^{n_i} \right] \left[\prod_{i=1}^{M} (\cos\theta_i)^{n_i} \right] . \qquad (3.3\text{-}5)$$

Using Eulers' identity:

$$(\cos\theta_i)^{n_i} = \frac{1}{2^{n_i}} (e^{-j\theta_i} + e^{j\theta_i})^{n_i} ,$$

which, by the binomial theorem can be written as

$$\frac{1}{2^{n_i}} (e^{-j\theta_i} + e^{j\theta_i})^{n_i} = \frac{1}{2^{n_i}} \sum_{k_i=0}^{n_i} \frac{n_i! e^{j(2k_i - n_i)\theta_i}}{k_i!(n_i - k_i)!} .$$

Since

$$n_1 + n_2 + \ldots + n_m = K,$$

$$\prod_{i=1}^{M} \frac{1}{2^{n_i}} = \frac{1}{2^K} \quad ,$$

and one can write;

$$\prod_{i=1}^{M} (\cos \theta_i)^{n_i} = \frac{1}{2^K} \prod_{i=1}^{M} \left[\sum_{k_i=0}^{n_i} \frac{n_i!\, e^{j(2k_i - n_i)\theta_i}}{k_i!\,(n_i - k_i)!} \right] \quad . \qquad (3.3\text{-}6)$$

Expansion of the right hand side of this equation gives

$$\prod_{i=1}^{M} (\cos \theta_i)^{n_i} = \frac{1}{2^K} \left[\left(\sum_{k_1=0}^{n_1} \frac{n_1!\, e^{j(2k_1 - n_1)\theta_1}}{k_1!\,(n_1 - k_1)!} \right) \cdot \left(\sum_{k_2=0}^{n_2} n_2! \text{ etc.} \right) \right]$$

Now, since multiplication is commutative, one can rearrange multiplication and summation operations to yield

$$\prod_{i=1}^{M} (\cos \theta_i)^{n_i} = \frac{1}{2^K} \left[\sum_{k_1=0}^{n_1} \cdots \sum_{k_M=0}^{n_M} \left[\prod_{p=1}^{M} \frac{n_p!\, e^{j(2k_p - n_p)\theta_p}}{k_p!\,(n_p - k_p)!} \right] \right]$$

in which substitution of

$$\prod_{i=1}^{M} e^{x_i} = \exp\left[\sum_{i=1}^{M} x_i\right]$$

gives

$$\prod_{i=1}^{M} (\cos\theta_i)^{n_i} = \frac{1}{2^K} \sum_{k_1=0}^{n_1} \cdots \sum_{k_M=0}^{n_M} \left[\prod_{p=1}^{M} \frac{n_p!}{k_p!(n_p-k_p)!}\right] \exp\left[j\sum_{i=1}^{M} (2k_i-n_i)\theta_i\right] . \tag{3.3-7}$$

Equation (3.3-5) can now be written as

$$\prod_{i=1}^{M} V_i^{n_i} = \left[\prod_{i=1}^{M} E_i^{n_i}\right] \left[\frac{1}{2^K} \sum_{k_1=0}^{n_1} \cdots \sum_{k_M=0}^{n_M} \left[\prod_{p=1}^{M} \frac{n_p!}{k_p!(n_p-k_p)!}\right] \exp\left[j\sum_{i=1}^{M} (2k_i-n_i)\theta_i\right]\right] \tag{3.3-8}$$

Putting (3.3-8) in (3.3-4) and (3.3-3) and collection of terms gives

$$I = \sum_{K=0}^{\infty} a_K \left[\sum_{n_1,n_2..n_M} \frac{K!E_1^{n_1}E_2^{n_2}\cdots E_M^{n_M}}{2^K} \left[\sum_{k_1=0}^{n_1} \cdots \sum_{k_M=0}^{n_M} \left[\prod_{p=1}^{M} \frac{1}{k_p!(n_p-k_p)!}\right] \right.\right.$$

$$\left.\left. x \exp\left[j\sum_{i=1}^{M} (2k_i - n_i)\theta_i\right]\right]\right] \tag{3.3-9}$$

Consider the exponential term in (3.3-9). To ascertain the trigonometric form of this term, let M=2, and let $\Gamma_i = (2k_i - n_i)$.

Then,

$$\exp\left[j\sum_{i=1}^{2}(2k_i-n_i)\theta_i\right] = e^{j\Gamma_1\theta_1} \times e^{j\Gamma_2\theta_2}$$

$$= (\cos\Gamma_1\theta_1 + j\sin\Gamma_1\theta_1)(\cos\Gamma_2\theta_2 + j\sin\Gamma_2\theta_2) \qquad (3.3\text{-}10)$$

Expansion of (3.3-10), use of the double angle equations and collection of terms gives

$$\exp\left[j\sum_{i=1}^{2}\Gamma_1\theta_i\right] = \cos(\Gamma_1\theta_1 + \Gamma_2\theta_2) + j\sin(\Gamma_1\theta_1 + \Gamma_2\theta_2)$$

Then in general ,

$$\exp\left[\sum_{i=1}^{M}\Gamma_i\theta_i\right] = \cos(\Gamma_1\theta_1 + \Gamma_2\theta_2 + \ldots + \Gamma_M\theta_M) + j\sin(\Gamma_1\theta_1 + \Gamma_2\theta_2 + \ldots + \Gamma_M\theta_M) \qquad (3.3\text{-}11)$$

Now, an intermodulation product of order N resulting from the application of M signals of different frequencies to a nonlinear circuit element has the angular frequency

$$\omega_{IM} = (\alpha_1\theta_1 + \alpha_2\theta_2 + \ldots + \alpha_M\theta_M) \qquad (3.3\text{-}12)$$

and

$$N = |\alpha_1| + |\alpha_2| + \ldots + |\alpha_M| ,$$

where α_i are integers.

Comparison of (3.3-11) and (3.3-12) shows that any desired IM component can be obtained from (3.3-9) by equating

$$\pm \alpha_i = \Gamma_i = (2k_i - n_i)$$

to get $$k_i = \frac{n_i + \alpha_i}{2} \qquad (3.3\text{-}13\text{-}a)$$

or $$k_i = \frac{n_i - \alpha_i}{2} \; . \qquad (3.3\text{-}13\text{-}b)$$

If $k_i = \frac{n_i + \alpha_i}{2}$, then,

$$\left[\sum_{m=1}^{M} V_m\right]^K = \sum_{n_1,n_2,\ldots n_M} \frac{K!\, E_1^{n_1} \ldots E_M^{n_M}}{2^K} \left[\prod_{p=1}^{M} \frac{1}{\left(\frac{n_p + \alpha_p}{2}\right)! \left(\frac{n_p - \alpha_p}{2}\right)!}\right]$$

$$\times \exp\left[j \sum_{i=1}^{M} \alpha_i \theta_i\right] \; . \qquad (3.3\text{-}14)$$

If $k_i = \frac{n_i - \alpha_i}{2}$, an equation identical to (3.3.-14) is obtained.

Summation of these two equations gives the contribution of the Kth term in the describing polynomial to the chosen IM product as:

$$\beta_K = \sum_{n_1,n_2,\ldots n_M} \frac{K! E_1^{n_1} \ldots E_M^{n_M}}{2^{K-1}} \left[\prod_{p=1}^{M} \frac{1}{\left(\frac{n_p + \alpha_p}{2}\right)! \left(\frac{n_p - \alpha_p}{2}\right)!}\right]$$

$$\times \exp\left[j \sum_{i=1}^{M} \alpha_i \theta_i\right] \; . \qquad (3.3\text{-}15)$$

Now, since both positive and negative coefficients have been accounted for in (3.3-15), α_i can be replaced by $|\alpha_i|$ and to avoid confusion with K, replace k_i by q_i.

Then, $$n_i = 2\, q_i + |\alpha_i| \,, \tag{3.3-16}$$

where q_i is a positive integer.

Equation (3.3-15) now becomes

$$\beta_K = \sum_{q_1,\ldots,q_M} \frac{K!E_1^{2q_1+|\alpha_1|}\cdots\cdots E_M^{2q_M+|\alpha_M|}}{2^{K-1}} \left[\prod_{p=1}^{M} \frac{1}{(q_p+|\alpha_p|)!\,q_p!}\right]$$

$$\times \quad \exp\left[\sum_{i=1}^{M} \alpha_i\theta_i\right] \,. \tag{3.3-17}$$

Recall from (3.3-4) that

$$n_1 + n_2 + \ldots n_M = K$$

Then, using (3.3-16),

$$[(2q_1 + |\alpha_1|) + (2q_2 + |\alpha_2| + \ldots (2q_M + \alpha_M)] \;=\; K$$

and

$$N = |\alpha_1| + |\alpha_2| + \ldots. |\alpha_M|$$

gives

$$(q_1 + q_2 + \ldots. q_M) = \frac{K-N}{2} \tag{3.3-18}$$

From (3.3-18) it is clear that since the q_i are positive integers, K-N must be an even positive integer, or zero. Thus, it is again shown that contributions to the Nth order IM component come only from terms of a degree greater than or equal to N. In addition, only even powered terms contribute if N is even, and only odd powered terms contribute if N is odd. This means that the summation of contributing components omits every second term in the describing polynomial and begins at the Nth term.

i.e. $$I_{IM_N} = a_N\beta_N + a_{N+2}\beta_{N+2} + \ldots = \sum_{L=0}^{\infty} a_{N+2L}\beta_{N+2L}$$

where I_{IM_N} is the intermodulation current of order N. Then using (3.3-17), the exponential term replaced by its trigonometric equivalent, I_{IM_N} can be written as

$$I_{IM_N} = \sum_{L=0}^{\infty} \frac{a_{N+2L}(N+2L)!}{2^{(N+2L-1)}} \sum_{q_1,q_2,\ldots q_M} \left[\prod_{p=1}^{M} \frac{E_p^{2q_p+|\alpha_p|}}{(q_p+|\alpha_p|)!\,q_p!} \right]$$

$$\times \left[\cos(\alpha_1\theta_1+\alpha_2\theta_2+\ldots+\alpha_M\theta_M) + j\sin(\alpha_1\theta_1+\alpha_2\theta_2+\ldots+\alpha_M\theta_M)\right]. \quad (3.3\text{-}19)$$

It should be noted from (3.3-19) that since real and imaginary parts have the same phase, the phases of the input carriers can have no influence on the amplitude of the intermodulation signals.

For generality, refer to equation (3.3-1) in which X is the input to the nonlinear element and Y is the output, where

$$X = \sum_{m=1}^{M} A_M \cos(\omega_m t + \theta_m)$$

Then the intermodulation component of order N at the output is

$$Y_{IM} = \sum_{L=0}^{\infty} \frac{a_{N+2L}\,(N+2L)!}{2^{(N+2L-1)}} \sum_{q_1,\ldots q_M} \prod_{p=1}^{M} \frac{A_p^{2q_p + |\alpha_p|}}{(q_p + |\alpha_p|)!\,q_p!}$$

$$x[\cos(\alpha_1\theta_1 + \ldots + \alpha_M\theta_M) + j \sin(\alpha_1\theta_1 + \ldots + \alpha_M\theta_M)]. \qquad (3.3\text{-}20)$$

where $N = \sum_{i=1}^{M} |\alpha_M| \neq 0$

$$\theta_i = (\omega_i t + \phi_i)$$

$$\sum_{q_1 \ldots q_M} = \sum_{q_M=0}^{L} \sum_{q_{M-1}=0}^{L_{M-1}} \cdots \sum_{q_2=0}^{L_2}$$

$$L_i = L - q_M - q_{M-1} - \ldots - q_{i+1}$$

$$L = q_1 + q_2 + \ldots\ldots\ldots + q_n$$

$$q_1 = L_1$$

A_p = amplitude of transmit signal at ω_p

and $\sum_{i=1}^{M} q_i = L$

The dc component in the output may be calculated by setting all α_i in (3.3-20) equal to zero (N=0) and multiplication by 1/2 since only one set of k_i exists. That is:

$$Y_{dc} = \sum_{L=0}^{\infty} \frac{a_{2L}(2L)!}{2^{(2L)}} \sum_{q_1 \ldots q_M} \prod_{p=1}^{M} \frac{A_p^{2q_p}}{(q_p)!^2} \quad . \tag{3.3-20-a}$$

Equations (3.3-20) are readily adaptable to computer techniques [26] and can be used to compute spectral component amplitudes when an accurate polynomial representation of the transfer characteristic for the IM source is available. This method is used exclusively for IM signal power calculations in Chapter V.

3.4 Calculation of Intermodulation Product Amplitudes Using Volterra Series Analysis

In Sections 3.2 and 3.3, the polynomial

$$Y = \sum_{i=0}^{N} a_i X^i \tag{3.4-1}$$

was used to describe the transfer function of a nonlinear circuit component. If, however, the component exhibits memory, or hysteresis, eqn. (3.4-1) must be replaced by an infinite series of the form

$$y(t) = \sum_{n=1}^{\infty} \int_{-\infty}^{\infty} \cdots \int h_n(\tau_1, \ldots, \tau_n) x(t-\tau_1) \ldots x(t-\tau_n) \, d\tau_1 \ldots d\tau_n \tag{3.4-2}$$

to make the output Y dependent upon past values of the input X . Equation (3.4-2) is a Volterra Functional Series representation of the transfer characteristic of the nonlinear component.

Each term in the Volterra Series may be written as:

$$y_n(t) = \int_{-\infty}^{\infty} \cdots \int h_n(\tau_1,\ldots,\tau_n)x(t-\tau_1)\ldots x(t-\tau_n).d\tau_1\ldots d\tau_n \qquad (3.4\text{-}3)$$

and in particular,

$$y_1(t) = \int_{-\infty}^{\infty} h_1(\tau_1)x(t-\tau_1)d\tau_1 \cdot \qquad (3.4\text{-}4)$$

The kernel of (3.4-4) is recognized to be the impulse response of a linear component. The nth order kernel $h_n(\tau_1\ldots\tau_n)$ can therefore be considered to be the nonlinear impulse response of order n. Its Fourier transform $H_n(f_1,\ldots f_n)$ is then the corresponding transfer function of order n, and

$$H_n(f_1,f_2\ldots f_n) = \int_{-\infty}^{\infty}\cdots\int_{-\infty}^{\infty} h_n(\tau_1,..,\tau_n)$$

$$x \exp -j2\pi(f_1\tau_1+\ldots+f_n\tau_n)\, d\tau_1 d\tau_2 \ldots d\tau_n \qquad (3.4\text{-}5)$$

Conversely,

$$h_n(\tau_1\ldots\tau_n) = \int_{-\infty}^{\infty}\cdots\int_{-\infty}^{\infty} H_n(f_1,f_2,\ldots f_n)$$

$$x \exp\ j2\pi(f_1\tau_1+ \ldots + f_n\tau_n)\, d\tau_1\ldots d\tau_n \cdot \qquad (3.4\text{-}6)$$

Substitution of (3.4-6) in (3.4-3) gives

$$y_n(t) = \int_{-\infty}^{\infty} \cdots \int_{-\infty}^{\infty} H_n(f_1,\ldots,f_n) \prod_{i=1}^{n} X(f_i)\exp(j2\pi f_i t)\, df_i$$

from which the nth order output spectrum can be obtained by taking the Fourier transform of both sides to be

$$Y_n(f) = \int_{-\infty}^{\infty} \cdots \int_{-\infty}^{\infty} H_n(f_1,\ldots,f_n)\, X(f-f_1-\ldots.-f_n) \prod_{i=1}^{n} X(f_i)df_i . \qquad (3.4\text{-}7)$$

The spectrum of the output from the nonlinearity is the sum of the spectra of all nonlinear transfer functions, $Y_n(f)$, or

$$Y(f) = \sum_{n=1}^{\infty} Y_n(f) .$$

The amplitudes of the IM products of concern are the sums of the spectral components of all nonlinear transfer functions at each respective IM frequency.

It should be emphasized that since Volterra series are infinite, there are an infinite number of spectra $Y_n(f)$ which add to give the total spectrum of the output regardless of the degree to which the transfer function is nonlinear. It is possible therefore that the sum of more than N spectra is required to obtain an accurate spectrum for the output from an Nth degree nonlinearity.

The derivation of expressions for the nonlinear transfer functions begins with a circuit model of the component under study. The transfer characteristics of the circuit model elements are expanded in appropriate power series, and a differential equation is written for the circuit model. A variety of techniques [22,27,28,29] can then be used to derive the transfer functions from the differential equation.

This method works well for calculating spectral components in the output from mildly nonlinear devices under small signal conditions. For greater nonlinearities, the number of calculations required to obtain each transfer function increases rapidly. The Volterra series approach therefore becomes impractical, especially when the amplitudes of higher order distortion terms are required.

3.5 The Use of Spectral Analysis for the Computation of Intermodulation Characteristics

Use of the techniques outlined in Sections 3.2 to 3.4 for the calculation of intermodulation product amplitudes is dependent upon the availability of power series or polynomials which accurately describe the nonlinearities of the circuit element being studied. In addition, when there is more than one phenomenon contributing to the total nonlinearity, a circuit model of the component must be developed so that proper addition of intermodulation contributions generated by each mechanism can be effected. There are cases, however, in which it is difficult to develop an accurate circuit model or to obtain a polynomial approximation, or power series expansion for the nonlinear characteristic. This makes it impossible to apply previously described methods.

The influence of all contributing elements to a circuit nonlinearity is reflected in the waveshape of the output from the circuit. This suggests the possibility that intermodulation characteristics can be obtained from the spectrum of the output waveform computed for a circuit model of the component under study. Alternately, the waveshape of the output can be measured on a wideband sampling oscilloscope, and the spectrum computed directly from the measured waveshape.

This eliminates the necessity for a circuit model, making spectral analysis especially suited to the prediction of PIM levels generated by multiple unknown sources.

To illustrate this approach, consider a 5th-degree nonlinearity having a two frequency consinusoidal input as shown in Fig. 3.2.

If one assumes that the input carriers of Fig. 3.2 have equal† amplitudes, then

$$V_{IN} = V(\cos\omega_1 t + \cos\omega_2 t) = 2V \cos\left(\frac{\omega_1+\omega_2}{2}\right)t \cos\left(\frac{\omega_2-\omega_1}{2}\right)t$$

$$\text{Let } \omega_c = \frac{(\omega_1+\omega_2)}{2}, \qquad \omega_e = \frac{(\omega_2-\omega_1)}{2} \tag{3.5-1}$$

$$\text{then, } V_{IN} = 2V \cos\omega_c t \cos\omega_e t$$

Rewriting, the output from the nonlinearity is

$$I = K[2V \cos\omega_c t \times \cos\omega_e t]^5 = 32K^5 \cos^5\omega_c t \cos^5\omega_e t \tag{3.5-2}$$

As seen in Fig. 3.2, the output current wave can be considered to be the product of a distorted cosine wave of unity amplitude and frequency ω_c, and a distorted cosine envelope of frequency ω_e and amplitude

---

† If the carriers are not equal, the output waveform is a distorted carrier with phase and amplitude modulation. The closed form expression for this wave is derived in Appendix B.

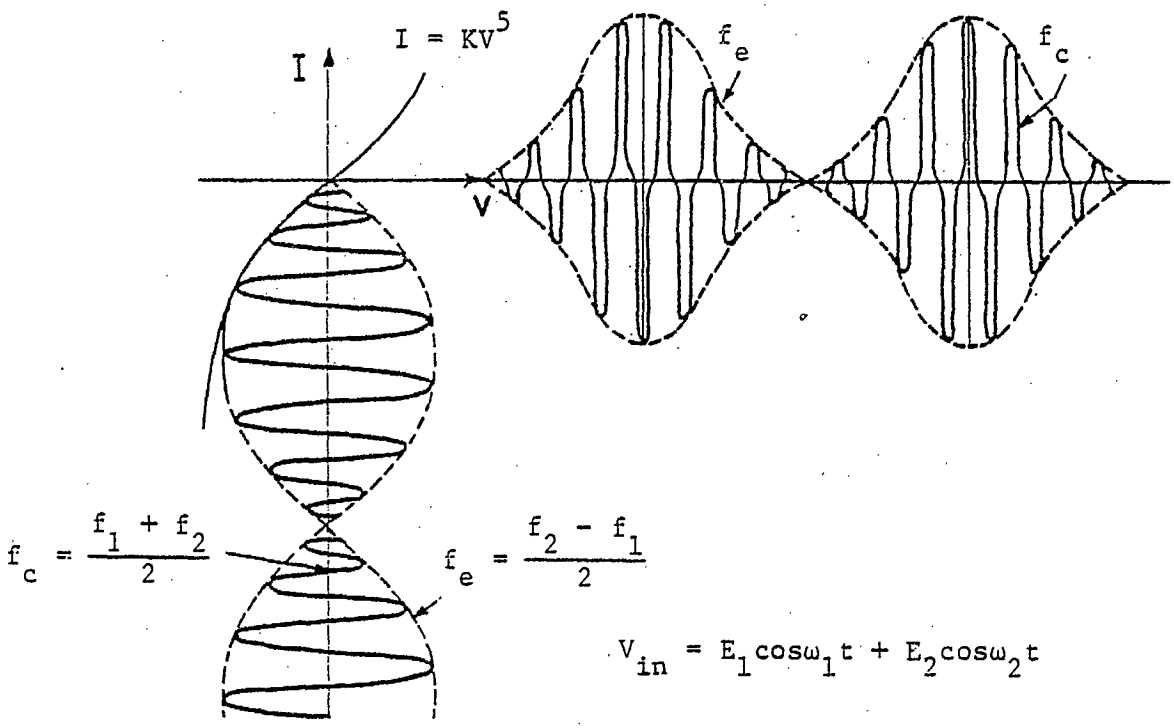

Fig. 3.2. Two frequency cosinusoidal input to a 5th degree nonlinearity and distorted output current waveform.

$32KV^5$. The time and frequency domain representations of these waveforms are shown in Fig. 3.3.

Since the time domain output is the product of the two distorted cosine waves, the spectrum of the output wave is the convolution product of their spectra, and is as shown in Fig. 3.4.

From the figure, the amplitudes of the IM products can be read as follows:

The frequency of the third-order product of concern is $(2f_2-f_1)$. From eqn. (3.5-1),

$$\omega_1 = 2\omega_c - \omega_2$$

$$\omega_2 = 2\omega_e + \omega_1$$

Therefore,

$$\omega_1 = \omega_c - \omega_e$$

and

$$\omega_2 = \omega_c + \omega_e$$

Substitution gives

$$2\omega_2 - \omega_1 = \omega_c + 3\omega_e$$

or

$$2f_2 - f_1 = f_c + 3f_e$$

The amplitude of the spectral component in Fig. 3.4 at this frequency is bA. From Fig. 3.3,

$$b = 5KV^5$$

$$A = 5/16$$

This gives

$$bA = \frac{25}{16}KV^5$$

Conversion from a two-sided to a one-sided spectrum requires doubling this amplitude to give

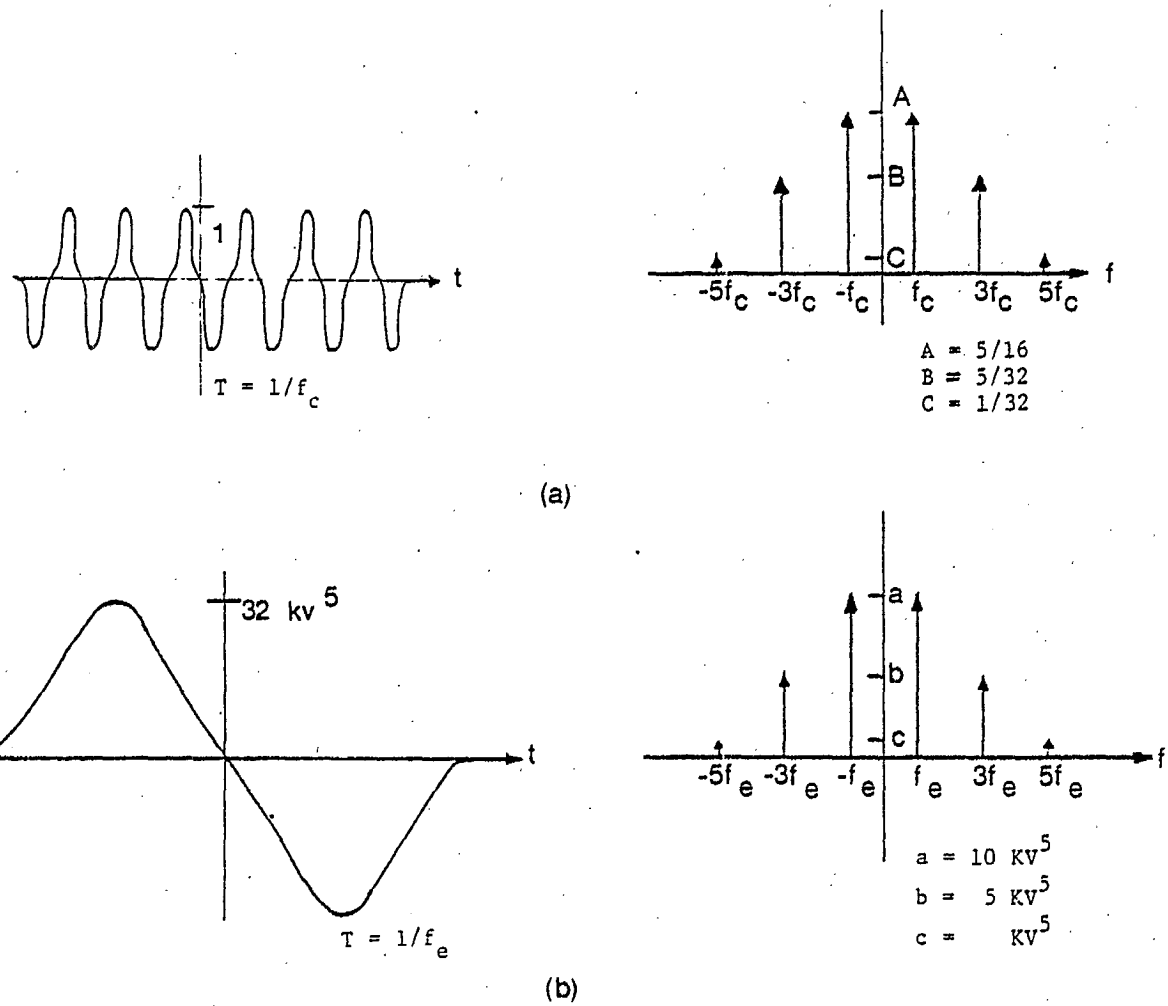

Fig. 3.3. Time and frequency domain representations of: (a) The output carrier wave: (b) The output wave envelope from the 5th degree nonlinearity in Fig. 3.2 with a two frequency consinusoidal input.

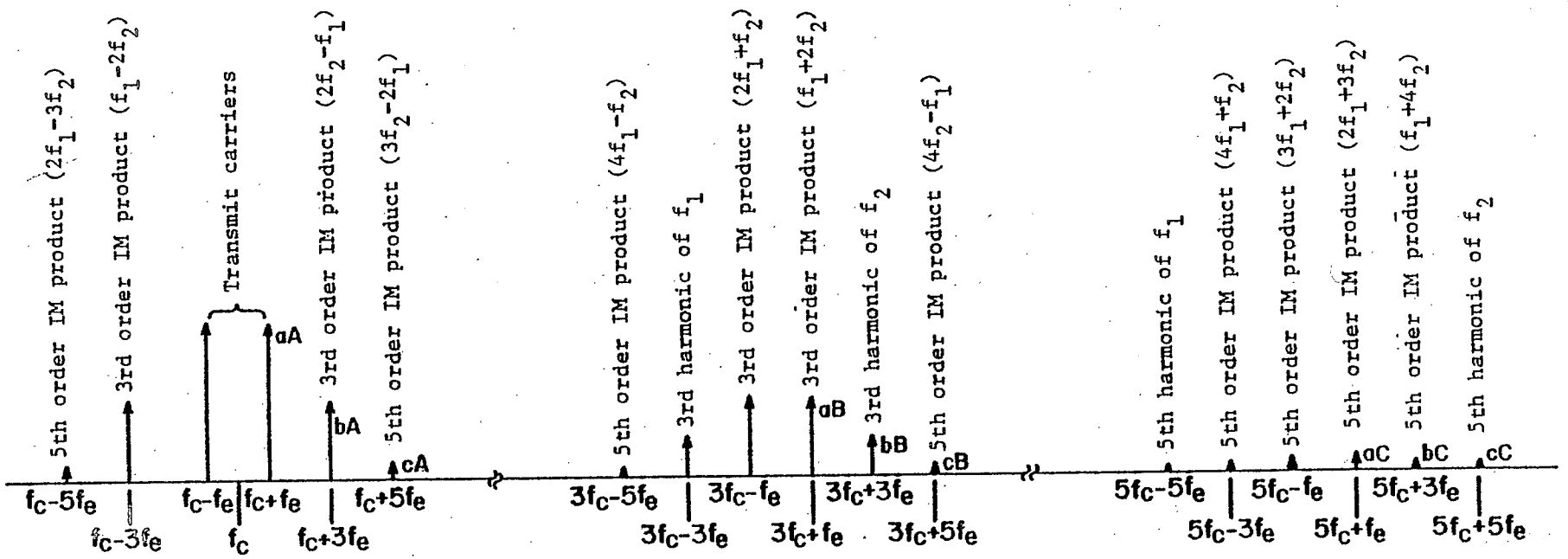

Fig. 3.4. Frequency spectrum of the output from the 5th order nonlinearity in Fig. 3.2 with a two frequency cosinusoidal input.

$$I_{IM_3} = \frac{25}{8} KV^5$$

The frequency of the fifth-order product of concern is

$$(3f_2-2f_1) = f_c + 5f_e$$

From Fig. 3.4, the amplitude of the component at this frequency is cA. From Fig. 3.3,

$$c = KV^5$$

$$A = 5/16$$

this gives

$$cA = \frac{5KV^5}{16}$$

Then converting to one-sided spectra,

$$I_{IM_5} = \frac{5}{8} KV^5$$

These amplitudes are identical to those listed in Appendix A resulting from trigonometric expansion of the fifth-power term in eqn. (3.1-2).

It is interesting to note from Fig. 3.3 that the spectra of the distorted envelope and carrier are identical except for amplitude and frequency scaling. This indicates that another semi-emperical approach may be possible. The spectrum of the output resulting from

a single frequency input near f_c of amplitude 2V could be measured. From this, the spectra of the envelope and carrier could be derived, and the IM signal power calculated as shown.

If the transmit carrier amplitudes are not equal, the input signal has phase, as well as amplitude modulation, making the spectrum of the output difficult to compute analytically. Numerical methods for computing the spectrum should, however, be moderately easy to develop. The proposed technique has not been tested by comparison with measurements due to time limitations placed on the present study.

3.6 Summary

This chapter has described some of the most applicable of reported techniques that can be used for the calculation of distortion components in the output from a nonlinear device.

In addition, a new method of analysis has been proposed which eliminates the requirement for an accurate circuit model and mathematical description of the nonlinear component under study.

It has been shown that all methods are inaccurate or unattractive in certain applications. Consequently, several techniques may have to be used to obtain a reasonable estimate of the passive intermodulation characteristics of a particular component or system.

As a result of exploring different methods of calculating distortion component amplitudes, some important facts about intermodulation have surfaced;

(a) If IM order (N) is even, only even terms in the polynomial describing the generating nonlinearity con-

tribute to the amplitude of the IM signal. Similarly, if N is odd, only odd terms of the polynomial make contributions.

(b) If the IM product is of order N, no contribution is made from terms of degree less than N.

(c) Other than by direct subtraction, no phase cancellation by IM product components generated by different terms of the describing polynomial can occur.

(d) When the sum of carriers having unequal amplitudes is input to a nonlinearity, the resulting intermodulation characteristics differ from the equal carrier case.

CHAPTER IV

PASSIVE INTERMODULATION MEASUREMENTS

4.1 Introduction

The measurement of PIM signal powers is a very difficult task. Many modern multifrequency communications systems operate with receive signal powers in the -100 dBm to -130 dBm range. This means that if required carrier to interference ratios are considered, PIM signals must be below the -140 dBm level to meet system specifications. In the measurement of the power of spurious signals at such low levels major difficulties are encountered in the achievement of measurement accuracy and repeatability.

Since there are varied and unknown sources of PIM it is difficult to design and maintain measurement equipment with internally generated PIM signals that are lower than those generated by devices or systems it is required to test. Factors such as the materials from which test circuit components are manufactured, the test circuit layout, filtering in various sections of the circuit, protection from vibration, and maintenance of constant environmental conditions are all important considerations in the design and construction of a test circuit with a low "residual" PIM level.

The application for which PIM measurements are to be made is also an important equipment consideration. Operating frequencies, impedances and transmitter powers must be chosen to be compatible with the measurement requirements. Important also are experimental methods. Measure-

ments must be made in such a manner as to yield unambiguous results, and problem areas must be identified before experimental procedures are established.

Test equipment and experimental methods are discussed in this chapter. Section 4.2 deals with general equipment considerations and presents a description of the test circuit used for experiments conducted in connection with this PIM investigation. Experimental methods are discussed in Section 4.3. Finally, Section 4.4 describes some preliminary experiments that were conducted at the beginning of the study. Conclusions are drawn from the preliminary experiments with regard to the accuracy and repeatability that can be expected during PIM measurements.

4.2 Measurement Equipment

4.2.1 General Considerations

A. Frequencies

From the literature survey conducted at the beginning of this study, it was noted that similar observations have been reported with regard to PIM generated at HF through to microwave frequencies. Indications are that IM signals are generated by the same sources * in all communications frequency bands. This means that from purely theoretical considerations, the frequency at which PIM experiments are carried out can be dictated by factors such as equipment availability and technical expertise. Practically, however,

* Some experimental investigations [8] have shown that the power of PIM signals generated by a particular IM source increases as transmit frequencies become higher. 30 dB per decade has been cited for the rate of increase between 20 MHz and 5 GHz for aluminum/aluminum contacts.

investigations are normally associated with a study of potential sources of intermodulation in an existing or planned communication system. In such cases receive and transmit bands in the PIM measurement set-up should be close to those of the associated system. This ensures that the same order IM product signals have frequencies in real and test circuit receive bands, that test circuit and communications system component design and manufacturing techniques are similar, and that parts from the actual system can be tested in the measurement facility.

The number of frequencies to be used for PIM measurements is another consideration. If interest is mainly in the study of PIM sources and power response, two transmit frequencies allow easier interpretation of results. In a two frequency system IM signals at a particular frequency are generated by only one combination of transmit frequencies. A single pair of even and odd order IM products can occupy the same frequency, but this situation can be avoided as discussed in Section 4.3. When more than two transmit frequencies are used, IM products of different order and of the same order, but generated by different transmit frequency combinations can occupy the same frequency. In addition to obscuring the "identity" of IM products, this can result in amplitude variations caused by the vector addition of different IM signals. These factors complicate the interpretation of measurement results. For the prediction of IM levels in proposed multifrequency communications systems, however, more than two test frequencies are required to simulate worst case conditions.

B. Power

The power of IM signals produced by passive generators depends upon transmit signal power in a nonlinear manner. If IM power trends are to be investigated in an attempt to characterize particular generators, it is important that experiments be carried out over a wide transmit power range. Experiments conducted over limited power ranges can lead to many different conclusions about IM characteristics which are not generally applicable. Test set transmitter outputs powers should be stable and continuously adjustable so that equal carrier powers or predetermined carrier power ratios at the test position can be obtained. An accurate means for determining the power applied to the device under test is also required. It is imperative when IM testing is associated with a particular communications system that tests be conducted at power levels throughout the operating range of the system.

C. Filter Requirements

A number of filters are required in circuits designed for

PIM Measurements. Transmitter outputs must be individually filtered so that only the desired transmit frequency fundamentals are applied to the device under test. Isolation between transmit channels is also necessary to prevent IM generation in transmitter amplifiers. If there is a requirement to measure a number of different IM product orders in a particular receiver band, small transmit frequency separations are required. Transmitter combiner filters having very steep skirts could therefore be necessary.

A receive band filter is required between the device under test and the receiver. This eliminates the fundamental transmit frequencies from low noise amplifier or receiver mixer circuits where active IM products on identical frequencies to those of passive IM signals could be generated.

The construction of filters as well as other components in multifrequency portions of the circuit must be so as to minimize the "residual" test circuit PIM level.

D. Frequency Stability

PIM test circuit frequency stability requirements depend upon the operating frequency band and the IM product orders of interest. In general, frequency stabilities in all parts of a PIM measurement circuit must be high. Since IM frequencies are combinations of multiples of the transmit frequencies, instabilities at the transmit frequencies could result in large IM frequency variations. In addition to making receiver and spectrum analyser tuning difficult, such instabilities can cause spreading of spectral energy and an artificial reduction in displayed PIM powers [25].

Receiver local oscillator and phase lock reference frequency stabilities should also be high to permit narrow receiver bandwidths in order to maintain low thermal noise levels.

E. Circulators and Dummy Loads

In chapter II, ferromagnetic materials were reported to be strong PIM generators. The use of ferrite devices such as circulators and ferrite phase shifters in multifrequency RF circuitry should be avoided. Connectors, screws, washers and other hardware in all components, test jigs and equipment housings must be made from non-ferromagnetic materials.

Commercially available dummy loads [6,9] often include ferromagnetic materials in their construction and will generate strong IM signals. Such devices can be replaced in test circuits by long lengths of open circuit transmission line. Long transmission lines can also be used as attenuators for the isolation of nonlinear loads or terminations from the test circuit.

F. Transmission Lines and Interconnections Between Circuit Components

The number of connectors in PIM test circuits should be minimized. Where possible, joints should be properly soldered or welded. All joints and connections should be fastened in stationary positions and protected against stress or vibration.

High and unstable PIM signal powers can be generated by multiple interbraidwire contacts in braided cables. All transmission

lines in PIM measurement circuits should therefore be of semi-rigid construction with solid inner conductors.

4.2.2 The Communications Research Center PIM Measurement Facility

Experiments referenced in this report were performed using the measurement facility designed and constructed for the Canadian Department of Communications, Communications Research Center by Sinclair Radio Laboratories Ltd. under Canadian Government Contract DSS 02PD36100-5-2069, Serial Number POL5-0150. The equipment was delivered and put into use approximately one year prior to the beginning of work for this research contract.

A block diagram of the measurement circuit is shown in Fig.4.1. Each of two CW transmit signals is generated by a frequency synthesizer covering the range between 100 and 165 megahertz. The synthesizer frequencies are doubled and each output is fed through a 0 to 120 dB step attenuator to a 200 watt power amplifier usable between 275 MHz and 330 MHz. A Bird in-line power meter monitors each power amplifier output and can be used to measure forward or reflected power.

To ensure the absence of spurious signals at the test port, the power amplifier outputs are passed through tunable narrowband filters, F1 and F2, adjustable over the full 275 to 330 megahertz range of the transmit band. The filter characteristics are such as to maintain a 3rd order residual test set PIM level of -130 dBm at transmit powers of +50 dBm per channel, while permitting a minimum transmit signal separation of 3 MHz. The maximum permissible transmit frequency separation is 55 MHz.

The channel filter outputs are combined and fed to a specially

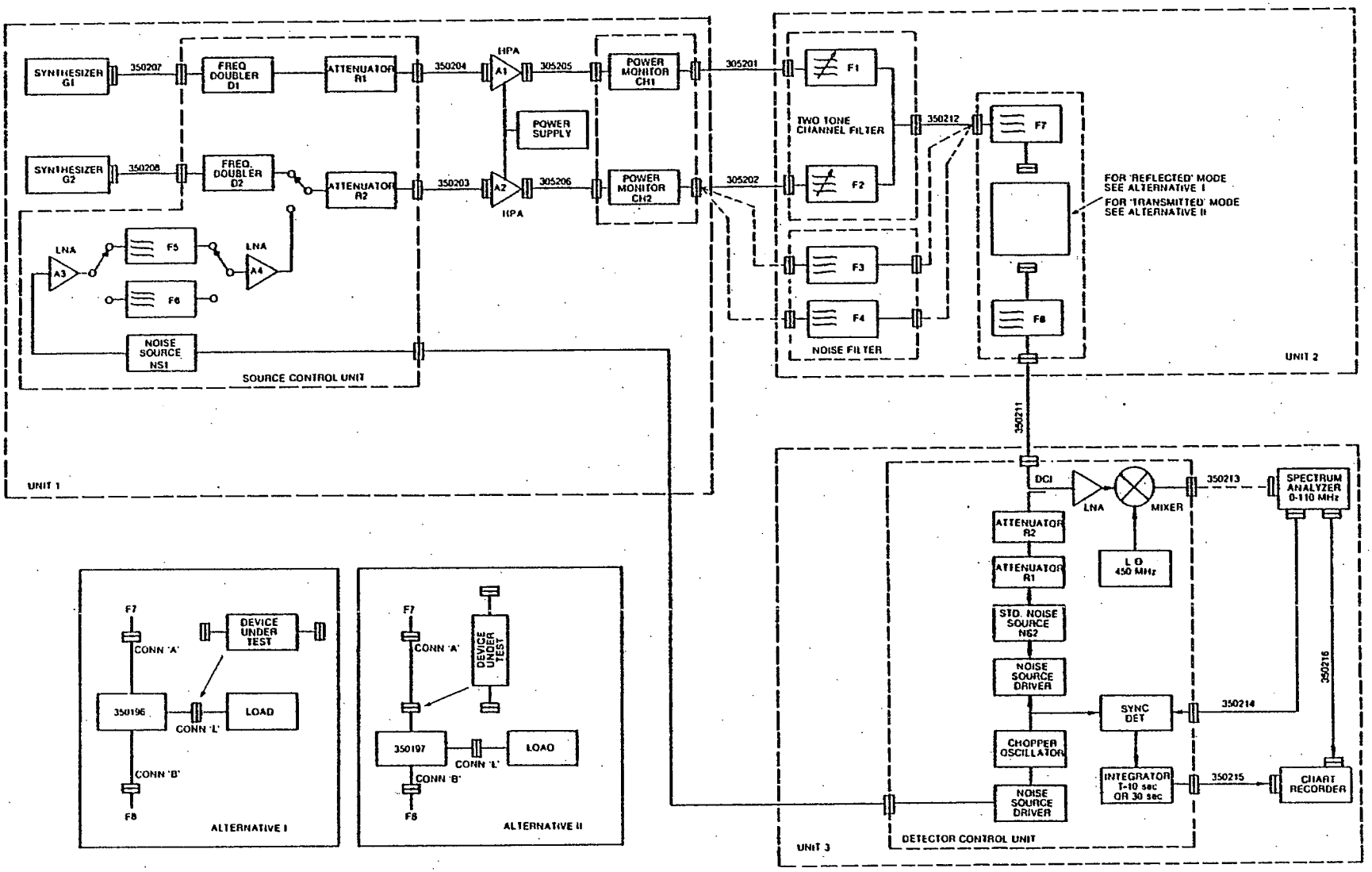

Fig. 4.1. CRC Passive intermodulation measurement facility block diagram, (from manufacturers operating manual).

built, low PIM diplexer (filters F7 and F8), through the device under test, and into an air-cooled load consisting of a transmission line attenuation pad and specially constructed low PIM ceramic termination. The system impedence is 50 ohms.

Reflected IM signals from circuitry following the transmit filter in the frequency range 370 MHz to 406 MHz pass through the diplexer receive filter and 30 feet of low loss transmission line to the receive circuitry.

The receiver subsystem consists of a low noise amplifier which has a gain of 40 dB followed by a frequency converter having a 44 to 80 magahertz output. Spectral component (IM) powers are monitored using a Hewlett Packard spectrum analyser, Model 141T with 8552B and 8553B plug in modules. A Hewlett Packard Model 7183B strip chart recorder is connected to the spectrum analyser output via a selectable time constant noise filter. The noise filter increases display sensitivity to approximately -150 dBm when the longest integration time is used. IM products of different order can be measured by adjusting transmit frequencies so as to produce the desired IM product at a frequency within the 307 MHz to 406 MHz receive band.

In addition to the reflected mode two port measurements described above and used exclusively for experiments referenced in this report, two other measurement options can be selected. PIM generated in one port devices can be measured by removing the dummy load and connecting the one port device at the diplexer output. Transmitted IM products generated in two port components driven from the test facility output and terminated with the dummy load can also be measured.

The generation of PIM signals by more than two transmit frequencies can be simulated by the application of narrowband noise to the device under test.

A photograph of the complete measurement facility can be seen in Fig. 4.2. Prior to the beginning of work for this investigation, the dummy load was removed from the equipment rack and placed on a movable dolly to permit testing of a wider range of hardware configurations.

4.3 Experimental Methods

There are many factors which must be considered during the planning and execution of PIM experiments. Transmit frequencies which result in particular IM components must be determined, the coincidence of even and odd order products on the same frequency must be avoided, displayed IM product signals must be identified and distinguished from RFI, and IM sources in the test circuit must be located and eliminated. Several guidelines which can be applied for the simplification of such problems are discussed in this section.

4.3.1 Selection of Transmit Frequencies for Two Frequency Experiments

The number of transmit frequency combinations that can produce IM products of a particular order becomes larger as consecutively higher orders are considered. When there are only two transmit frequencies, however, only one combination will generate IM products in a fixed bandwidth comparable to that of the receive band in a typical communication system. For equipment compatibility, cosited receivers and transmitters in the same two way communication link normally operate over

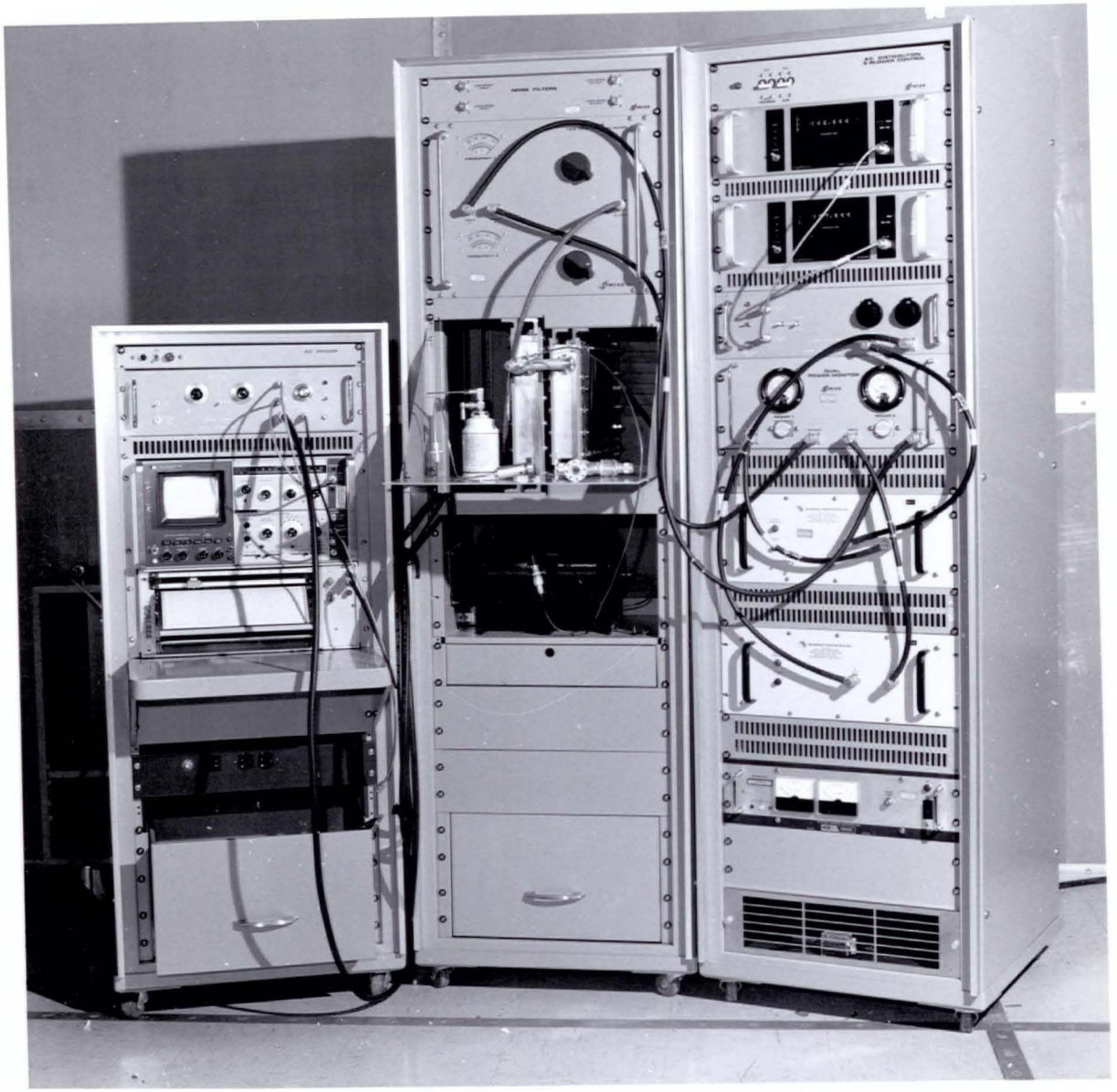

Fig. 4.2 Photograph of the CRC passive inter-modulation measurement facility.

frequency bands within the same (fundamental) zone. This means that frequencies in the higher of the two bands are lower than the second harmonics of the lower band frequencies. Transmit frequency combinations which result in fundamental zone IM signals can be quickly determined from simple algebraic equations derived as outlined below.

In a two frequency system, the relationship between an IM frequency and the transmit frequencies applied to the IM generator can be written as

$$f_{IM} = \pm mf_1 \pm nf_2 \qquad (4.3\text{-}1)$$

where

f_{IM} is the IM frequency

f_1 & f_2 are transmit frequencies

and

n,m are positive integers

order $= |m| + |n|$.

From eqn. 4.3-1 it appears that there are four different IM frequencies corresponding to each pair of integers m and n. If only positive IM frequencies are considered, however, only two combinations remain. These result from the association of opposite algebraic signs with m and n or the association of the positive sign with both integers. Since interest is only in IM products within the fundamental zone the latter combination can be ignored, leaving only cases in which m and n have opposite signs for consideration. For such combinations, integer values must be determined.

If f_1 is chosen to be the lower transmit frequency, f_2 can be related to f_1 by the equation

$$f_2 = f_1 + \Delta f_1, \text{ where } \Delta = \frac{f_2 - f_1}{f_1}$$

Equation 4.3-1 can now be written as

$$f_{IM} = f_1(\pm m \pm n \pm n\Delta).$$

Normalizing with respect to f_1 gives

$$\frac{f_{IM}}{f_1} = \beta = (\pm m \pm n \pm n\Delta).$$

Now, since m and n cannot be associated with the same algebraic sign,

$$\beta = m - n - n\Delta \qquad (4.3\text{-}2)$$

or $$\beta = n - m + n\Delta \qquad (4.3\text{-}3)$$

are the only two cases of interest.

Matrices can be formed by choosing all values of m and n which result in IM products of specific orders and applying (4.3-2) and (4.3-3) using various values for Δ. Calculations quickly show that for typical values of Δ ($1\% \leq \Delta \leq 5\%$) the following general rules apply:

(1) Odd order IM products lie in the fundamental frequency zone ($1 \leq \beta \leq 2$) if m is associated with the negative sign and

$$m_o = (n_o - 1) \tag{4.3-4a}$$

Odd order IM frequencies are then given by

$$f_{IM_o} = f_1(1 + n_o\Delta) \tag{4.3-4b}$$

and

$$\text{order} = (2n_o - 1) \tag{4.3-4c}$$

(2) Even order IM products lie in the fundamental frequency zone if n is associated with the negative sign and

$$m_e = (n_e + 2) \tag{4.3-5a}$$

Even order IM frequencies are then given by

$$f_{IM_e} = f_1(2 - n_e\Delta) \tag{4.3-5b}$$

and

$$\text{order} = (2n_e + 2). \tag{4.3-5c}$$

The coincidence of even and odd order IM products on the same frequency results when

$$f_{IM_e} = f_{IM_o}$$

or

$$f_1(2-n_e\Delta) = f_2(1 + n_o\Delta)$$

from which

$$\Delta = \frac{1}{(n_e + n_o)} \tag{4.3-6}$$

Since n_e and n_o are integers, even and odd order products lie on the same frequency only when $1/\Delta$ is an integer.

The above rules can be used for a number of different calculations

as listed below:

(1) Transmit frequencies required to produce fundamental zone IM products can be determined by

(a) picking values for m and n in accordance with (4.3-4a) or (4.3-5a)

(b) Choosing f_1 and calculating Δ from(4.3-2)or(4.3-3) such that $(1 \leq \beta \leq 2)$

(c) Calculating f_2 from $\Delta = (\frac{f_2 - f_1}{f_1})$

(2) The coincidence of even and odd order IM frequencies can be avoided by ensuring that $1/\Delta$ is not an integer. The orders and frequency of IM product coincidence can be calculated from (4.3-4) and (4.3-5).

(3) The lowest order IM products that fall in a particular fundamental zone frequency band can be determined from equations (4.3-4) and (4.3-5) as follows:

(a) If interest is in the lowest even order IM product that can result in interference in a particular system, f_{IM} can be set equal to the frequency at the upper receive band edge and substituted in (4.3-5b) to calculate n_e when Δ is as large as the transmit band will permit (note that the value of n_e must be rounded up following division). The corresponding order can be calculated from n_e using (4.3-5c).

(b) If interest is in the lowest odd order IM product of concern, f_{IM} can be set equal to the frequency at the lower receive band edge and substituted in (4.3-4b) to permit calculation of n_o, again with Δ at its maximum value and n_o rounded up following division. Order can be calculated from n_o using (4.3-4c).

Similar calculations, with f_{IM} placed at the upper band edge for odd orders and the lower band edge for even orders can be used to calculate the highest IM products in a particular fundamental zone frequency band if Δ is equal to the smallest value permissible. The values calculated for n_e and n_o must be rounded up following division.

4.3.2 A Method for Distinguishing Received IM Signals from Spurious Emissions and Identifying IM Product Orders.

Sometimes it is necessary to increase the bandwidth of the measurement receiver so that several IM products can be detected and displayed simultaneously. With large receiver bandwidths it could become difficult to distinguish between spurious signals and IM products or to identify IM orders. By noting the direction of change in observed signal frequencies as a result of changes in drive frequencies the identity (order and equation) of an IM product can be determined.

Consider the third order IM product at the frequency $f_{IM} = (2f_2 - f_1)$. An increase (Δf) in f_2 will cause f_{IM} increase by 2 Δf, whereas an increase of Δf in f_1 will cause f_{IM} to decrease by Δf. Harmonics and other spurious emissions would not show the same frequency response. Interference from sources external to the PIM measurement set up would be unaffected by transmit frequency changes.

4.3.3 Identification of the Nature of IM Generators

As ferromagnetic materials are known sources of PIM, components and transmission lines in a measurement system are chosen to be of non-ferromagnetic construction. Due to the rising cost of materials, however, some manufacturers are receiving recycled metals from their suppliers. These are apt to contain ferromagnetic materials. In addition, processes used in the manufacturing of components can leave filings and chips from tools embedded in the finished pieces. Consequently, hardware can be marked as "pure brass" and "pure copper" or "non-magnetic" and still contain small pieces of ferromagnetic material. Fig. 4.3 shows scanning electron microscope and xray photographs of a cross section of the inner conductor from a "pure copper" coaxial cable purchased for use as a dummy load. The embedded iron sliver is clearly shown in the photographs, and would generate PIM in a multi-frequency system.

The presence of ferromagnetic nonlinearities in a measurement set up can be detected with the use of magnetic fields [9]. Any PIM amplitude changes as the result of magnetic field intensity changes would identify a ferromagnetic source.

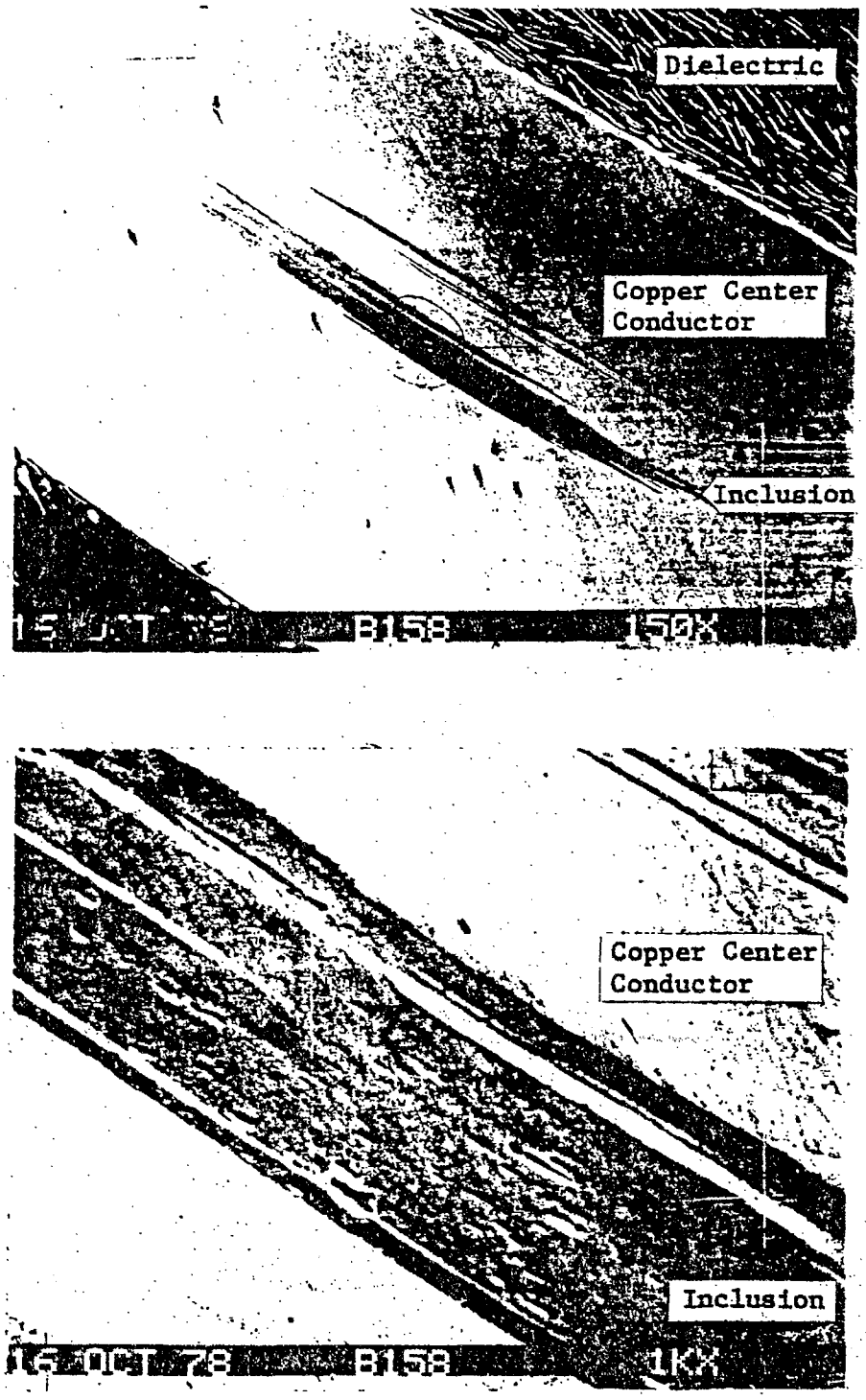

Fig. 4.3(a) Scanning electron microscope photographs of a cross-section of the center conductor in 0.141" semi-rigid coaxial cable: (i) inclusion shown as dark area in center of photograph, magnification = 150X, (ii) magnification = 1000X.

(i)

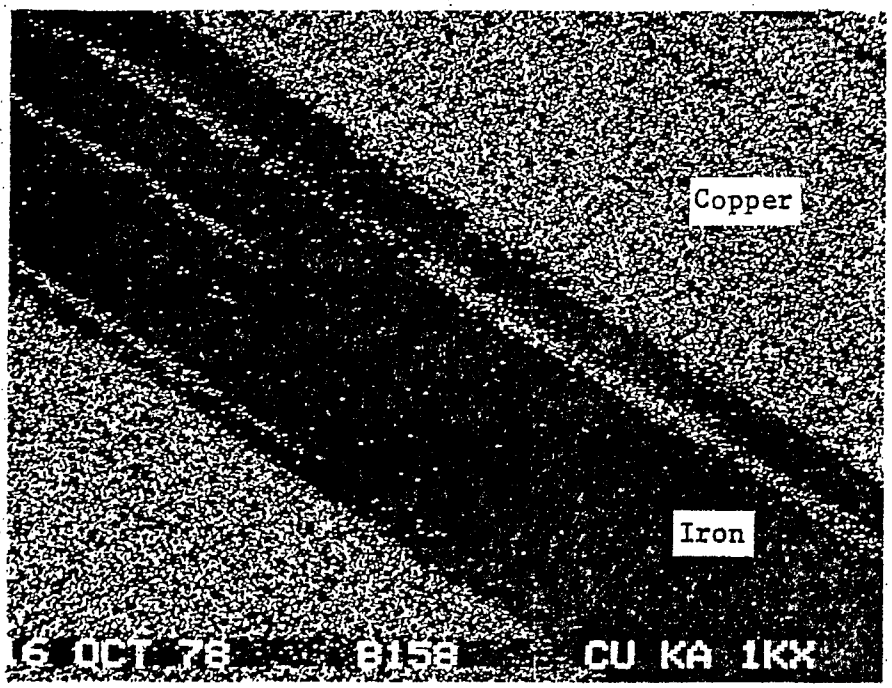

(ii)

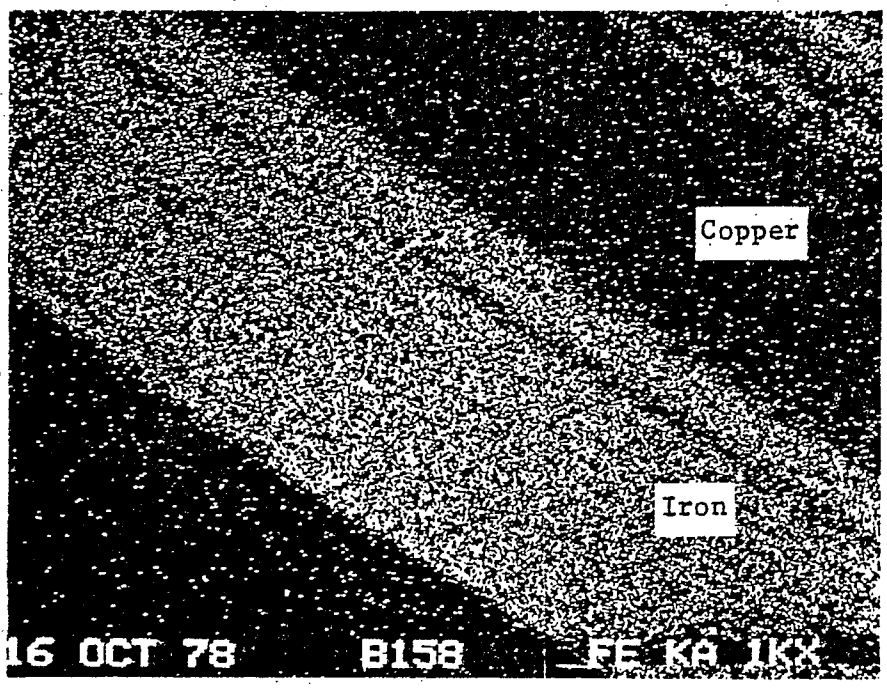

Fig. 4.3(b). X-ray photographs of a cross-section of the center conductor in 0.141" semi-rigid coaxial cable: (i) iron inclusion in darker center portion, copper surrounding, magnification = 1000X, (ii) iron inclusion in the lighter center portion, copper surrounding, magnification = 1000X.

The instability of IM product levels created by the movement of components can also be used as a diagnostic tool. Such instabilities would indicate that the IM is being generated at a junction, rather than by bulk properties of the materials in system components.

4.3.4 Methods for Locating the Source of IM Products in a Measurement System.

Variable attenuators [5] can be used in each transmit circuit of a measurement system to permit determination of the degree of influence on IM product levels asserted by transmit power at each frequency. Further, if strategically placed, the attenuators can be used to locate offending components by noting IM product amplitude response to changes in attenuation in various parts of the circuit. Due to the rapid increase in IM product levels resulting from an increase in RF drive, one can assume that if product level changes are on a 1:1 ratio with changes in the setting of a particular attenuator, the IM source is between that attenuator and the transmitter. Alternately, if there is a greater than 1:1 response, the nonlinearity is between the attenuator and the receiver.

An additional means of locating IM sources of the junction type is by twisting, tapping or shaking various components in the set up, and noting product response. Movement of a bad component should have a significant effect on product levels.

4.3.5 Cleaning

It is essential that connectors and components being tested as well as those which are part of the measurement set up be kept free

from corrosion and from contaminants such as metal filings which may introduce nonlinear characteristics.

Connectors should be cleaned after each time they are used. Cleaning by immersion in liquid baths should be avoided, as there is a possibility that this could wash contaminants into inaccessible parts of the component being cleaned.

Equipment and test samples should be stored in covered containers and closed cabinets remote from magnetic fields and workbench areas where dirt from fabrication and modification processes can be picked up.

Excessive handling of component pieces exposed to RF fields may also deposit salts and perspiration on the conductors. The effect of such contaminants on PIM generation is not known.

4.3.6 Preliminary Measurements

In order to identify component types and hardware configurations that would lead to the elimination of PIM from UHF communications systems, it was one of the objectives of the study to measure the amplitude of IM signals generated in typical UHF components and subsystems. Before planning detailed measurements, a series of preliminary PIM experiments with passive RF hardware was conducted to gain familiarity with the test facility and to observe some of the characteristics that are reported in the literature. All measurements were made using the reflected mode (Section 4.2.2) test set configuration.

(1) Silver plated and nickel plated brass type N adapters were compared in consecutive tests using a female/female adapter with each type of plating between the duplexer output of the measurement facility and a modified* male/male adapter mated with the bulkhead connector on the dummy load.

At an applied transmitter power of one hundred watts per carrier and reasonably snug hand tightened connections the 3rd order PIM signal powers generated with the silver plated adapter in the test position varied between -120 dBm and -130 dBm depending on how tight the connections were made. When connections were very loose PIM signal powers as high as -87 dBm were observed.

Identical tests with the nickel plated adapter in the test position resulted in displayed IM signal powers between -98 dBm when connections were snug and -82 dBm for very loose connections.

Measurements confirmed reports [9] that nickel plated components can generate much stronger IM signals than comparative silver plated components. The similarity of PIM levels generated in each case when the adapters were very loose indicates that under this condition contact nonlinearities rather than bulk material properties were the predominant PIM generators.

(2) The variation in IM level as a function of RF drive for both silver plated and nickel plated type N female/female adapters was observed at third and fifth orders by decreasing the transmitter powers in steps from the hundred watt level. Very minimal changes in IM power

---

* modification discussed in Appendix C.

were observed with the silver plated adapter in the test position, but it was noted that IM power increased by approximately 1 dB on several occasions after the transmitter power was dropped from one level to the next.

Measurements made with the nickel plated adapter in the system showed a general trend toward a 2.5 dB IM power increase in response to a 1 dB increase in drive level at third order. The fifth order measurements showed an almost linear 3 dB/dB IM power response to drive power changes.

In both silver plated and nickel plated adapter experiments the IM power level was more responsive to drive power changes at the transmit frequency closest to the IM frequency.

(3) The amplitudes of PIM signals generated by two short lengths (3" and 12") of RG/9B braided coaxial cable were measured. The cables were individually placed in the test position of the measurement facility and 3 rd order PIM measurements were made at 100 W/carrier with the cables in various different flexed positions. Both cables were fitted with nickel plated brass type N connectors.

The power of PIM signals generated in the 3 inch cable sample varied between -105 dBm and -114 dBm. The highest PIM powers were measured during and after periods of continuous cable motion. Various stationary positions resulted in the lowest PIM levels

PIM powers measured with the 12 inch cable in the test position were fairly constant near the -112 dBm level for all flexed and moving cable tests.

The measurements showed that the PIM signals generated in the

longer cable were the weakest. This could have been due to factors such as PIM signals generated at different positions along the cable adding vectorially, or a difference in solder jobs at the connectors. The relationship between cable length and PIM signal power is not clear.

(4) Third order PIM signals generated by ten foot lengths of quarter inch semi-rigid cables fitted with different connector types were measured when the cables were tapped along their lengths with a screwdriver handle and when the cables were stationary. PIM levels were also measured when the cables were supported on a dolly, and when left to hang under their own weight. Three different connector types were used. Cable #1 had "solder-on" silver plated brass type N connectors, cable #2 had solder-on gold plated brass type TNC connectors, and cable #3 had crimp-on silver plated brass type N connectors.

Measurements made when the cables were supported showed that the power of PIM signals generated with cable #1 in the measurement circuit was lower (by approx. 5 dB) than PIM signal powers generated with either of the other cables in the test position. Tapping the cables fitted with type N connectors produced a 5 to 6 decibel variation in PIM signal power. The power variation was 3 dB greater when the cable with the TNC connectors was tapped.

A significant (5 dB to 15 dB) increase in PIM levels was observed when support was removed from the cables, resulting in greater stress on the connectors. Tapping resulted in a wider PIM variation in tests with cable #1 when support was removed. No significant

difference in PIM level response to tapping was noted as a result of removing support from cables 2 or 3.

During the preliminary experiments a number of measurement difficulties were encountered. Generally PIM levels were erratic, and measurements were not repeatable. Fig. 4.4 shows a strip chart recording of the residual test set 3rd order PIM level measured when the facility was left running with transmitter output powers of 100 watts per channel applied directly to the dummy load. The PIM power spikes are typical of system performance on many different occasions. Cleanliness played an important role in eliminating such instabilities. Lower, more stable PIM levels were recorded in several instances when parts of the system in which more than one transmit frequency can be present were taken apart, cleaned, and re-assembled.

Strained or misalligned connector parts were also found to result in very high and erratic PIM levels. The spreading of contact fingers to restore original dimensions and ensure good contacts in pressure type connections after repetitive connector use was found to increase PIM level stability. During one measurement when PIM powers were very erratic, it was found that the center conductor of one of the type N female/female adapters was not concentric with the outer conductor. Micrometer measurements showed that the center conductor pin on one end of the adapter was off center by approximately 20 thousandths of an inch. Replacement of the faulty adapter with another immediately resulted in more stable IM product amplitudes.

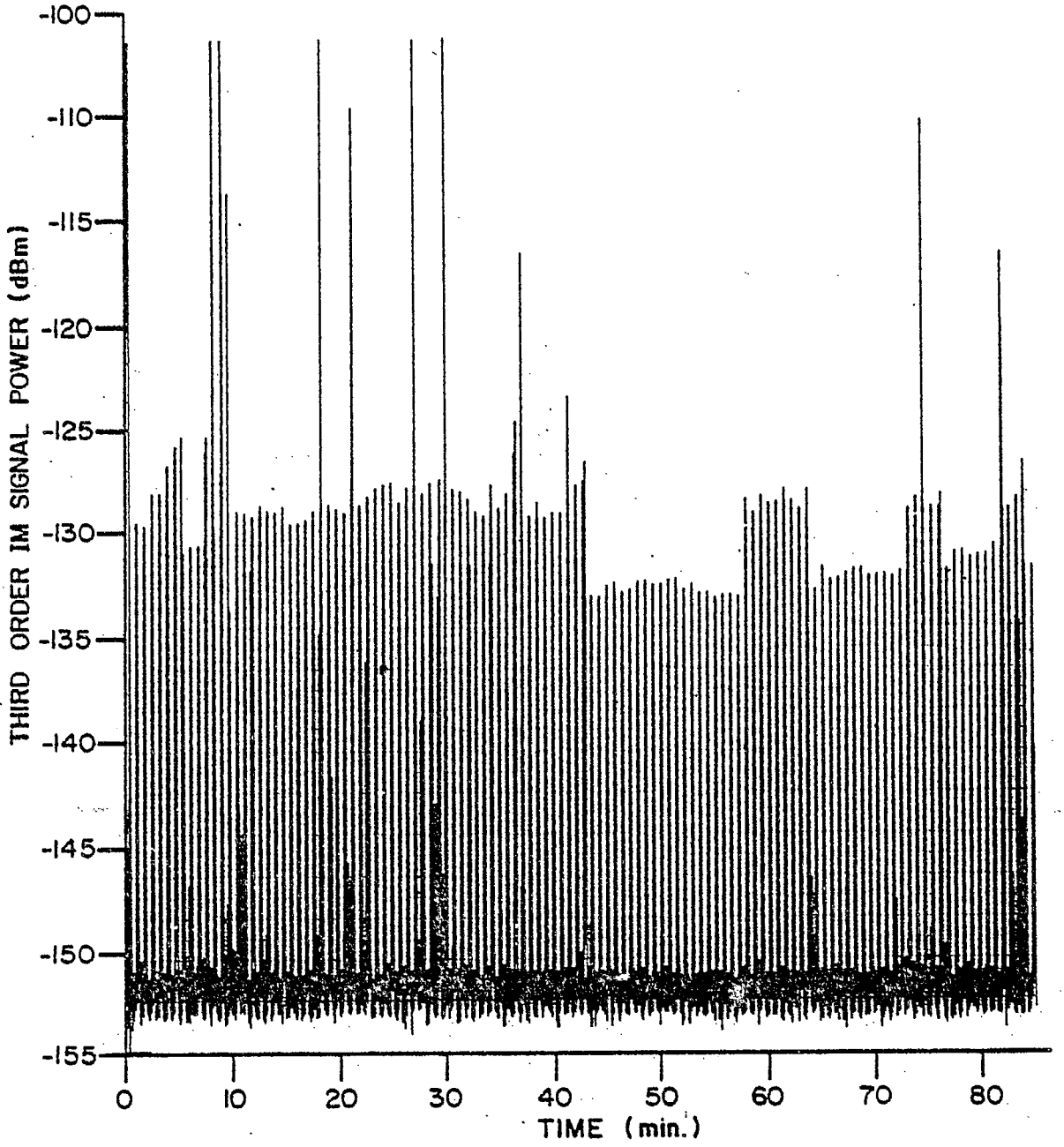

Fig. 4.4. Strip chart recording showing erratic 3rd order test facility residual PIM power spikes. Each vertical line represents the amplitude of the 3rd order PIM signal at the time of an individual spectrum analyser sweep.

In another case, the residual test set PIM level increased to 20 dB above normal and remained high. When the usual connector cleaning and maintenance procedures failed to lower the residual test set PIM to its normal level, the bulkhead connector and several centimeters of transmission line were removed from the dummy load. After soldering a modified* cable connector in place of the old bulkhead type, the residual PIM level of the system dropped to its original value and normal stability was again attained.

Examination of the old connector revealed the following:

(1) A solder sliver was lodged between the retaining nut and the teflon insert at the back of the connector. This fell out when the retaining nut was removed.

(2) Two silver plated brass washers were seated behind the retaining nut between which dirt had collected.

(3) A bulge was noted in the coaxial cable near the solder point. This was attributed to dielectric expansion with heat during soldering. No cracks in the exterior of the outer conductor surrounding the bulge were found. The interior side of the outer conductor was not examined.

(4) The contact surfaces of the connector were scraped and scored as a result of repeated use over a period of approximately one year.

It is possible that any of these conditions could have led

---

* Modifications are shown in Appendix C.

to an increase in the residual test set PIM level over a period of time. The wearing of the connector contact surfaces as a result of many mating cycles, however, is considered to be the major factor which contributed to the performance degradation.

It was also observed during preliminary experiments that the test set residual PIM level was higher immediately following a period of time (over night for example) during which the measurement facility had not been used.

After start-up, the residual 3rd order PIM signal power gradually decreased and could be consistently (when connectors were tight and clean) measured at a lower level at the end of approximately 3 hrs. of continuous operation. This gradual PIM level change could not be attributed to warm up thermal instabilities of the system electronics, as all portions of the system were left in the standby mode when not in use. It appeared instead that the PIM power decrease was related to the presence of RF in passive circuitry of the test facility.

Extensive "warm up" tests were performed during start-up periods to determine the cause for the higher PIM levels immediately following turn on. Simultaneous recording of the residual test set PIM level, transmitter powers, relative humidity in the laboratory, and load,receive filter, test port and room temperatures were made during 3 hr. periods following start-up on a number of different days. Fig. 4.5 shows the data from one three hour test. The objective in monitoring a number of different parameters was to correlate the PIM power patterns with one or several other of the recordings. No simple correlation between IM power and a single other parameter was evident, but the records show that the most consistent PIM levels resulted only after the temperature and transmitter powers had stabilized after initial

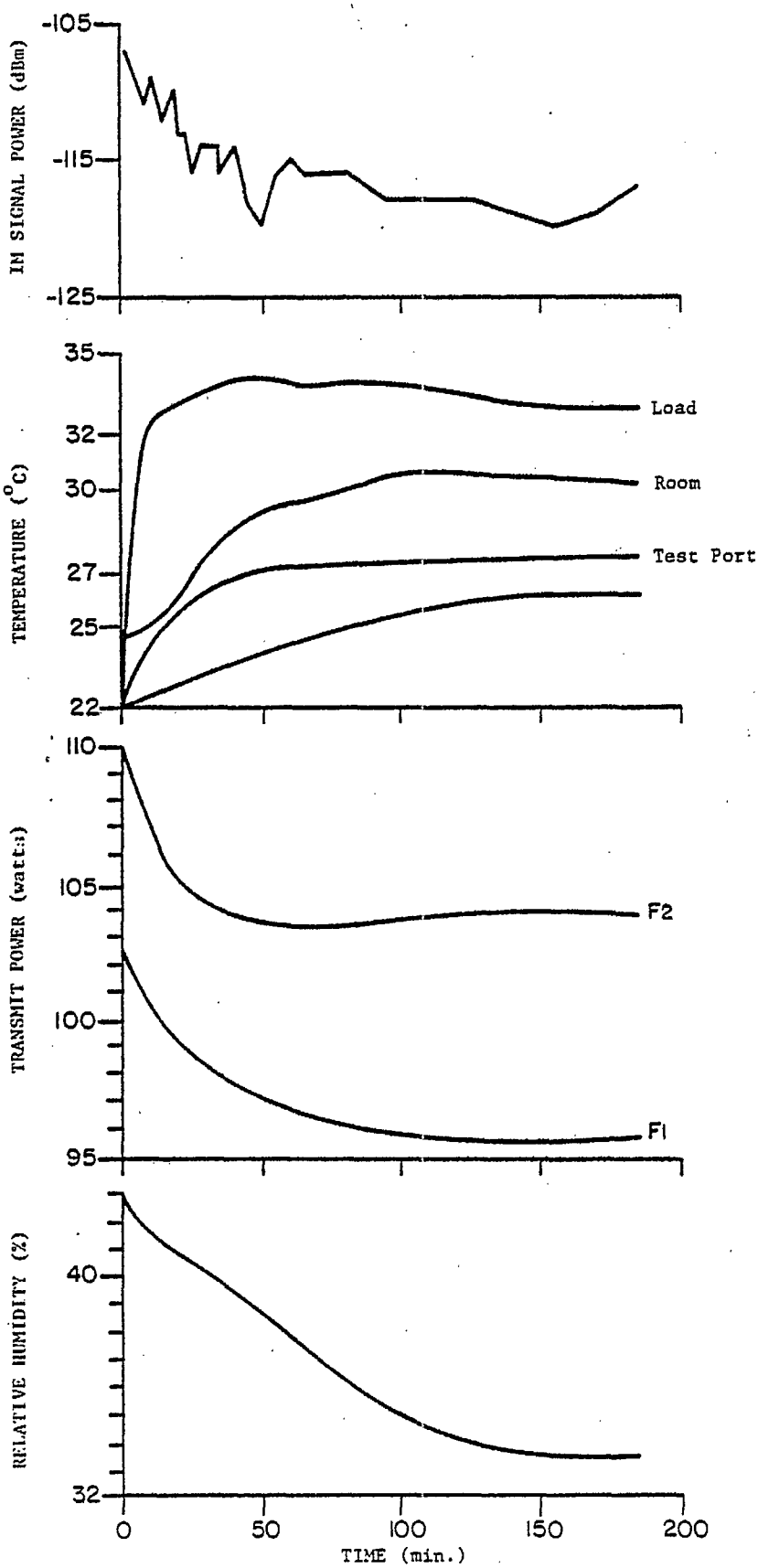

Fig. 4.5. Laboratory data collected during a 3 Hr. test facility "warm up" test.

slow transient behaviour. The least correlation was observed between PIM power level and laboratory humidity. This, however, did not rule out the possibility that humidity inside system components was responsible for the observed PIM power behaviour as suggested by others [1,6,30]. Additional warm up tests were conducted after shining a heat lamp on the test port prior to and during measurements in an attempt to burn off humidity faster. Results indicated no change in the warm up characteristics when the heat lamp was used.

In addition to showing some of the peculiarities of PIM measurements, the preliminary experiments revealed that some important characteristics of the test set such as the RF attenuation between different parts of the system, the linearities of the amplifiers and measurement accuracies were not known to the degree of accuracy that would be required for correlation of experimental results with theoretically based PIM calculations.

After consideration of the unknown equipment characteristics, and the problems encountered during the preliminary experiments, an equipment calibration was recommended and calibration tests were proposed, to be carried out by CRC personnel.

To determine the reason for displayed PIM signal amplitude instabilities, the tests included the measurement of:

(1) the dependence of dummy load VSWR on operating temperature

(2) transmitter frequency synthesizer frequency and output power stabilities

(3) the output power stability of the transmitter high power amplifiers

(4) the spurious response of the receiver low noise amplifier

(5) the receiver local oscillator frequency and output power stabilities, and output spectral purity

(6) the spectrum analyser display stability, amplitude response, and phase lock circuit characteristics.

In addition, RF interference in the laboratory and mechanical vibration at the test port were monitored simultaneously with a continuous recording of the test set residual PIM level so that IM amplitude spikes might be correlated with periods of high RFI, or increased vibration.

To determine measurement system characteristics so that the required degree of measurement accuracy could be attained, the following were measured:

(1) the linearity of the high power amplifiers

(2) the sensitivity and accuracy of the in-line power monitors

(3) the attenuation at applicable frequencies of all components in the receive and transmit paths

(4) the insertion loss, input and output VSWR, and frequency response of the transmit channel filters at various center frequencies within the transmit band

(5) transmit and receive filter characteristics including passband insertion loss, ripple and skirt slopes

(6) the receiver low noise amplifier frequency response

(7) the VSWR of the dummy load at various frequencies covering the transmit band.

A formal report of the calibration results was not available at the time of writing, and some of the proposed measurements had not been made. It was clear, however, from available results that equipment malfunctions were not the source of the measurement problems. The observed instabilities were concluded to be typical PIM characteristics caused by minute vibrations at metal-metal contacts, variable contact loads as a result of thermal stress, changing phase relationships between PIM signals generated by different mechanisms, microdischarges, and other similar hidden influences.

Since it was clear that measurement stability and repeatability were extremely difficult objectives to achieve, attention was turned from the measurement of absolute PIM amplitudes to the observation of general IM power trends. It was also concluded that the collection and analysis of data concerning the PIM production characteristics of low level generators should be conducted on a statistical basis.

CHAPTER V

ANALYTICAL AND EXPERIMENTAL INVESTIGATION OF INTERMODULATION PRODUCT CHARACTERISTICS

5.1 Introduction

In RF communication system design, as well as in PIM experiments, a knowledge of IM power level response to changes in input signal amplitudes is desirable.

In system design, it is necessary to predict how IM powers are affected by variations in transmit power, or changes in multi-frequency carrier power ratios. Conditions that may result in significant IM power levels in a normally quiet system can thus be avoided, and specifications can be written to adequately cover "worst case" conditions.

In PIM experiments, changes in IM power levels that can result from variations in transmit signal parameters should be understood so that specific IM characteristics can be distinguished from subsidiary effects resulting from peculiarities of a particular measurement procedure or equipment layout. There is also an interesting possibility that PIM sources can be identified in functioning RF systems by comparing measured IM signal response to variations in transmit signal powers with the known response of IM power levels generated by particular types of nonlinearity.

IM power characteristics are studied in this chapter. The nonlinear dc resistance characteristic of a semiconductor diode is used

in theoretical anaysis to compute IM powers delivered to the load in a RF system model operating with various assumed transmit signal combinations. Interest is in computing the general characteristics of IM signal response rather than in accurate IM signal power calculations. For this reason, the reactive nonlinearities of the diode junction are neglected, allowing the direct application of the analysis technique reported by Sea [3] (Section 3.3) in computer programs. Experimental investigations in which a diode was used as an IM source in the CRC test circuit are also reported. The diode was chosen as the IM generating nonlinearity in this study for two reasons. First, a knowledge of the diode parameters makes it possible to perform numerical calculations rather than purely algebraic manipulations. Secondly, the study results can aid in classification of PIM signals generated by semiconductor-type nonlinearities. Such a classification would be used in PIM source identification by IM signatures.

In the first section of the chapter a diode having a known I-V characteristic is placed in a RF system circuit model, and generalized circuit equations are developed. Two different methods for deriving a polynomial description of the diode nonlinearity are discussed. Section 5.3 describes computer exercises that were performed to simulate the application of various two frequency signal combinations to the diode, and presents computed results. Experiments using a commercially available hot carrier diode (minimal charge storage) as the device under test in the CRC measurement facility are described, and experimental results are summarized in Section 5.4. The chapter closes with a discussion and comparison of computed and measured IM characteristics.

5.2 The Generation of Intermodulation Product Signals by a Semiconductor Diode.

The nonlinear conduction characteristic of a semiconductor diode was chosen as the IM generating nonlinearity for the investigation of IM product power dependence upon input signal amplitudes. A physically existing nonlinearity rather than an arbitrary "mathematical" one was used as an IM source to avoid the possibility of assuming a nonlinear characteristic which would result in the computation of unrealistic IM signal properties. To further ensure that computations had a realistic basis, the dc I-V characteristic of a HP 5082-2800 Schottky diode was measured to obtain practical parameter values. Measured current and voltage data for every second voltage applied during the measurements are shown in Table 5-1.

5.2.1 Development of a RF System Circuit Model and Equations for the Calculation of IM Signal Powers.

The series circuit of Fig. 5.1 consisting of a two frequency transmitter, the diode IM source, and a load resistance was assumed as a circuit model for a typical RF system. Transmitter output and load impedances were assumed to be real and equal to 50 ohms. Based on the assumption that any nonlinearities such as that caused by a metal/metal-oxide/metal sandwich, or ferromagnetic inclusions in passive RF devices would be shunted by low impedance linear conduction paths, the linear resistance, R_{sh}, in parallel with the diode was included in the circuit model. The voltage developed across the shunted diode is designated

$$V_d = E_1 \cos \omega_1 t + E_2 \cos \omega_2 t$$

Table 5-1

The Conduction Characteristic of
a HP 5082-2800 Schottky Diode
Measured at dc

Voltage (mV)	Current (nA)
-100	-1.15
-80	-1.13
-60	-1.06
-40	-0.91
-20	-0.60
-10	-0.297
-9	-0.268
-8	-0.231
-7	-0.207
-6	-0.18
-5	-0.151
-4	-0.13
-3	-0.099
-2	-0.070
-1	-0.040
0	0
1	0.039
2	0.08
3	0.109
4	0.145
5	0.182
6	0.219
7	0.266
8	0.310
9	0.356
10	0.4
20	1.29
40	3.79
60	9.16
150	400.00
200	8000.00
230	10000.00

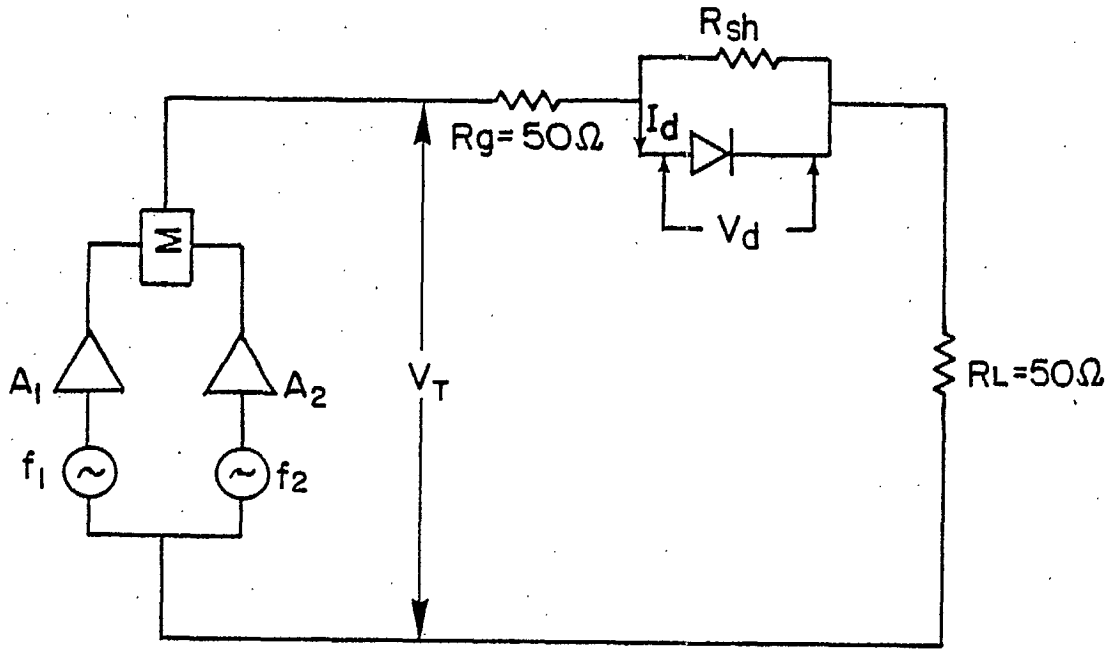

Fig. 5.1. RF system circuit model showing the diode IM source shunted by a linear resistance.

and the voltage at the transmitter output,

$$V_T = V_1 \cos \omega_1 t + V_2 \cos \omega_2 t$$

where ω_1 and ω_2 are radian frequencies.

At low diode currents R_{sh} provides an independent voltage source for the diode. In this range of operation the diode current, I_d, can be described by a polynomial in V from which IM currents of order N can be calculated using the equation

$$I_{IM_N} = \sum_{L=0}^{\infty} \frac{a_{N+2L}(N+2L)!}{2^{(N+2L-1)}} \sum_{q_1, q_2, \ldots q_M} \prod_{p=1}^{M} \frac{E_p^{2q_p+|\alpha_p|}}{(q_p+|\alpha_p|)!q_p!}, \quad (5.2\text{-}1)$$

developed by Sea [3] and re-derived in Section 3.3 of this report.

If the diode is assumed to be an IM current source having a much higher impedance than R_{sh} the IM current through the load is

$$I_{IML} = \frac{R_{sh}}{100 + R_{sh}} \times I_{IM} \quad (5.2\text{-}2)$$

and the voltage developed across the diode is given by

$$V_d = \frac{R_{sh}}{100 + R_{sh}} \times V_T = E_1 \cos\omega_1 t + E_2 \cos\omega_2 t. \quad (5.2\text{-}3)$$

Substituting (5.2-3) in (5.2-2) gives

$$I_{IML} = \frac{V_d}{V_T} \times I_{IM}.$$

The IM power delivered to the load resistance is therefore given by:

$$P_{IML} = I_{IML}^2 \times 50$$

$$= \frac{V_d^2}{V_T^2} \times I_{IM}^2 \times 50. \qquad (5.2\text{-}4)$$

Now, assume * R_{sh} has a value such that 14% of the voltage at the transmitter output appears across the shunted diode. Then from (5.2-4),

$$P_{IML} = 0.98\ I_{IM}^2 \approx I_{IM}^2 . \qquad (5.2\text{-}5)$$

5.2.2 Intermodulation Signal Current Calculations

Two different methods can be used to derive polynomial coefficients for use in eqn. 5.2-1 to calculate IM currents. These methods are described in the following paragraphs.

Method A: The Derivation of Describing Polynomial Coefficients from a Least Squares Approximation to the Measured Diode Conduction Characteristic

The coefficients of least squares or other polynomial approximations to measured conduction characteristics can be used for the calculation of IM signal amplitudes. Such coefficients, however, must be obtained from a single accurate polynomial fit to measured

* The value of 14% (R_{sh} = 8Ω) was chosen to be equal to the reactance of a wire shunt used in experiments described in Section 5.4.(see appendix D).

values covering the complete expected amplitude range of the input signal, extending from its maximum positive to its maximum negative value. For severe nonlinearities this limits the use of polynomial approximation techniques for IM signal calculations to cases in which power applied to the nonlinearity is low. Piecewise approximations covering different regions of the characteristic cannot be used, as difficulties are encountered with the vector addition of IM signals calculated from different polynomials which form parts of the complete approximation. Representation of the nonlinearity only in the region of expected peak input signal values also fails, as harmonic amplitudes cannot be accurately calculated unless the full range of operation is considered.

A CRC library computer program (LSQPOLY) was used to find a least squares polynomial approximation to the data in Table 5-1. The best agreement between measured and calculated current values resulted when a 12th degree polynomial was used to calculate currents corresponding to dc voltages in the -100 to +60 millivolt range. Outside this voltage range deviations of computed from measured currents increased rapidly due to the forward conduction breakpoint in the diode characteristic.

The coefficients of the "best fit" polynomial are listed in Table 5-2. Table 5-3 shows a comparison of calculated and measured currents for selected voltages in the -100 mV to 60 mV range.

Table 5-2

Coefficients from the "Best Fit" Least Squares Polynomial Approximation* to the dc Conduction Characteristic of a HP 5082-2800 Schottky Diode in the -100mV to 60mV Voltage Range

a_o	-9.352×10^{-12}
a_1	3.348×10^{-8}
a_2	8.473×10^{-7}
a_3	3.650×10^{-5}
a_4	7.480×10^{-5}
a_5	-2.380×10^{-2}
a_6	-1.087×10^{-1}
a_7	8.650
a_8	6.950×10^{1}
a_9	-1.103×10^{3}
a_{10}	-1.209×10^{4}
a_{11}	1.703×10^{4}
a_{12}	3.382×10^{5}

* $I = a_0 + a_1V + a_2V^2 + \ldots\ldots + a_nV^n$, where I has units of amps and V has units of volts.

Table 5-3

Comparison of Measured dc
Diode Currents and Currents Calculated
Using the Least Squares Polynomial Approximation

Voltage (mV)	Measured Current (nA)	Calculated Current (nA)	Percentage Difference
-100	-1.15	-1.786	55.3
-80	-1.13	-1.201	6.3
-60	-1.06	-1.047	-1.2
-40	-0.91	-0.945	3.8
-20	-0.100	-0.56	-6.7
-10	-0.287	-9.293	2.1
-9	-0.258	-0.266	3.1
-8	-0.231	-0.241	4.3
-7	-0.207	-0.214	3.4
-6	-0.18	-0.187	3.9
-5	-0.151	-0.160	4.0
-4	-0.13	-0.132	1.5
-3	-0.099	-0.103	4.0
-2	-0.070	-0.073	4.3
-1	-0.040	-0.042	5.0
0	0	0	0
1	0.039	0.025	-35.9
2	0.070	0.061	-12.9
3	0.109	0.099	-9.2
4	0.145	0.140	-3.4
5	0.182	0.184	1.1
6	0.219	0.230	5.0
7	0.266	0.279	4.9
8	0.310	0.331	6.8
9	0.350	0.386	8.4
10	0.4	0.445	11.2
20	1.29	1.232	-4.5
40	3.79	3.800	0.3
60	9.16	9.158	-0.2

A computer program, "IMPWR", based upon an algorithm reported by Sea and Vacroux [26] was written to calculate IM currents using eqn. 5.2-1. From calculated currents the program computes IM powers delivered to the load in the RF system model using eqn. 5.2-5. A complete description and statement listing for the program can be found in Appendix E.

Method B: The Calculation of IM Currents Using Coefficients Derived from a Taylor Series Expansion of the Exponential Term in the Shockley Equation

In PIM experiments IM products of very high order, (>75), have been observed at CRC during the exposure of semiconductor diodes to two frequency RF fields. It is shown in Chapter III that an IM product of order N can only be generated by nonlinearities of a degree greater than N. There is therefore an inconsistency between PIM observations and calculations which show the best fit to the diode transfer characteristic to be provided by only a 12th degree polynomial. It is uncertain, however, whether the characteristics of IM signals of order less than 12 should be considered inaccurate because of the discrepancy, or if the inability to calculate high order IM signal characteristics is the only disadvantage of using the curve fitting technique.

To enable the calculation of the characteristics of high order IM products, a Taylor series expansion of the exponential term in the Shockley Equation was used to obtain a polynomial representation containing very high index terms. This also provided a second

method for the computation of low order IM signal amplitudes for comparison with those calculated using method A.

The Shockley equation describes the diode I-V relationship as

$$I_d = I_s(e^{\frac{qV_d}{\eta kT}} - 1), \qquad (5.2\text{-}6)$$

where

I_d = total diode current (amps)

I_s = reverse saturation current (amps)

q = electronic charge (Coulombs)

k = Boltzmans' Constant (1.38×10^{-23} J/°K)

T = diode junction temperature (Kelvin)

η = a constant, $1 \leq \eta \leq 4$

V_d = voltage applied across the diode (volts)

(For the circuit of Fig. 5.1, $V_d = E_1 \cos\omega_1 t + E_2 \cos\omega_2 t$) (5.2-7)

The exponential in (5.2-6) can be expanded in a Taylor Series about $V_d = 0$ to give

$$I_d = I_s (a_1 V_d + a_2^2 V_d^2 + a_3^3 V_d^3 + \ldots + a_n^n V_d^n), \qquad (5.2\text{-}8)$$

where $a_i = \frac{q}{i!\eta kT}$

A simple modification to the program IMPWR was made to calculate

up to 82 coefficients of (5.2-8) and used in the program IMAMP (Appendix E) for computing IM currents (overflow problems were encountered for i > 82). Values for I_s and $q/\eta kT$ were found by repeated substitution of arbitrary numbers in (5.2-6) and calculation of currents until values close to those in Table 5-1 were obtained. The best agreement results when $q/\eta kT$ is set equal to 36, and I_s has a value of 1 nA. A comparison of measured currents and those calculated using these parameter values is shown in Table 5-4. The Table shows that the percentage difference between measured and calculated currents becomes larger as the diode voltage is increased.

5.3 Intermodulation Signal Power Calculations

With sets of coefficients calculated by each of the methods described in Section 5.2.2 a number of IM power characteristics were computed. This section explains how each characteristic was computed, and presents a summary of results.

5.3.1 The Dependence of IM Powers on Total RF Transmit Power

Without considering actual coefficient values, calculations based upon a limited number of terms in the polynomial

$$I = a_o + a_1 V_d + a_2 V_d^3 + a_3 V_d^3 + \ldots\ldots + a_n V_d^n \qquad (5.3\text{-}1)$$

indicate that the power of the Nth order IM product signal should change by N dB in response to each dB change in total power input to the generating nonlinearity. This characteristic was investigated

Table 5-4

Comparison of Measured dc Diode Currents and Currents Calculated using the Shockley Equation with $q/\eta kT = 36$ and $I_s = 1$ nA.

Voltage (mV)	Measured Current (nA)	Computed Current (nA)	Percentage Difference
-100	-1.15	-0.973	-15.4
-80	-1.13	-0.944	-16.5
-60	-1.06	-0.885	-16.5
-40	-0.91	-0.763	-16.2
-20	-0.60	-0.513	-14.5
-10	-0.287	-0.302	5.2
-9	-0.258	-0.277	7.4
-8	-0.231	-0.250	8.2
-7	-0.207	-0.223	7.7
-6	-0.180	-0.194	7.8
-5	-0.151	-0.165	9.3
-4	-0.130	-0.134	3.1
-3	-0.099	-0.086	13.1
-2	-0.070	-0.069	1.4
-1	-0.040	-0.035	12.5
0	0	0	0
1	0.39	0.037	-5.1
2	0.070	0.075	7.1
3	0.109	0.114	4.6
4	0.145	0.155	6.9
5	0.182	0.197	8.2
6	0.219	0.241	10.0
7	0.266	0.287	7.9
8	0.310	0.334	7.7
9	0.350	0.387	8.7
10	0.4	0.433	8.3
20	1.29	1.054	-18.3
40	3.79	3.220	-15.0
60	9.16	7.76	-15.3

numerically using coefficients derived by each of the methods explained in Section 5.2.2.

With equal carrier voltage inputs, E_1 and E_2, to the programs, a stepped increase in total RF power applied to the diode was simulated by increasing the values of E_1 and E_2 to represent 2 dB steps in total applied power from 0 to 30 dB above 6.3 mV per carrier (P_T= -8 dBm). The resulting changes in computed powers for different IM orders are plotted in figures 5.2 to 5.7. The values in figures 5.2 to 5.6 were calculated using polynomial coefficients derived by methods A and B. In each of these figures a straight line having a slope of N dB/dB has been drawn beside the power curve for the Nth order IM product for comparison. Figure 5.7 shows 3rd to 25th order IM power curves computed using the Taylor series coefficients of method B.

The power curves computed using method A have slopes close to the algebraically predicted N dB/dB over a larger input power range as IM order increases. For all orders, best alignment is at low input powers. The curves computed using method B all have slopes of approximately N dB/dB at low drive levels. For greater input powers, the slopes of the curves begin to increase, with the lower order curves being affected at lower powers. Results from the two calculation methods show the most similarity at low orders, and at low transmit powers, where the polynomial approximations are most accurate. Amplitudes calculated using the Taylor series coefficients are consistently lower than those calculated from the least squares coefficients.

Recall from Chapter III that contributions are made to the amplitude of the Nth order IM product signal by all terms in the describing

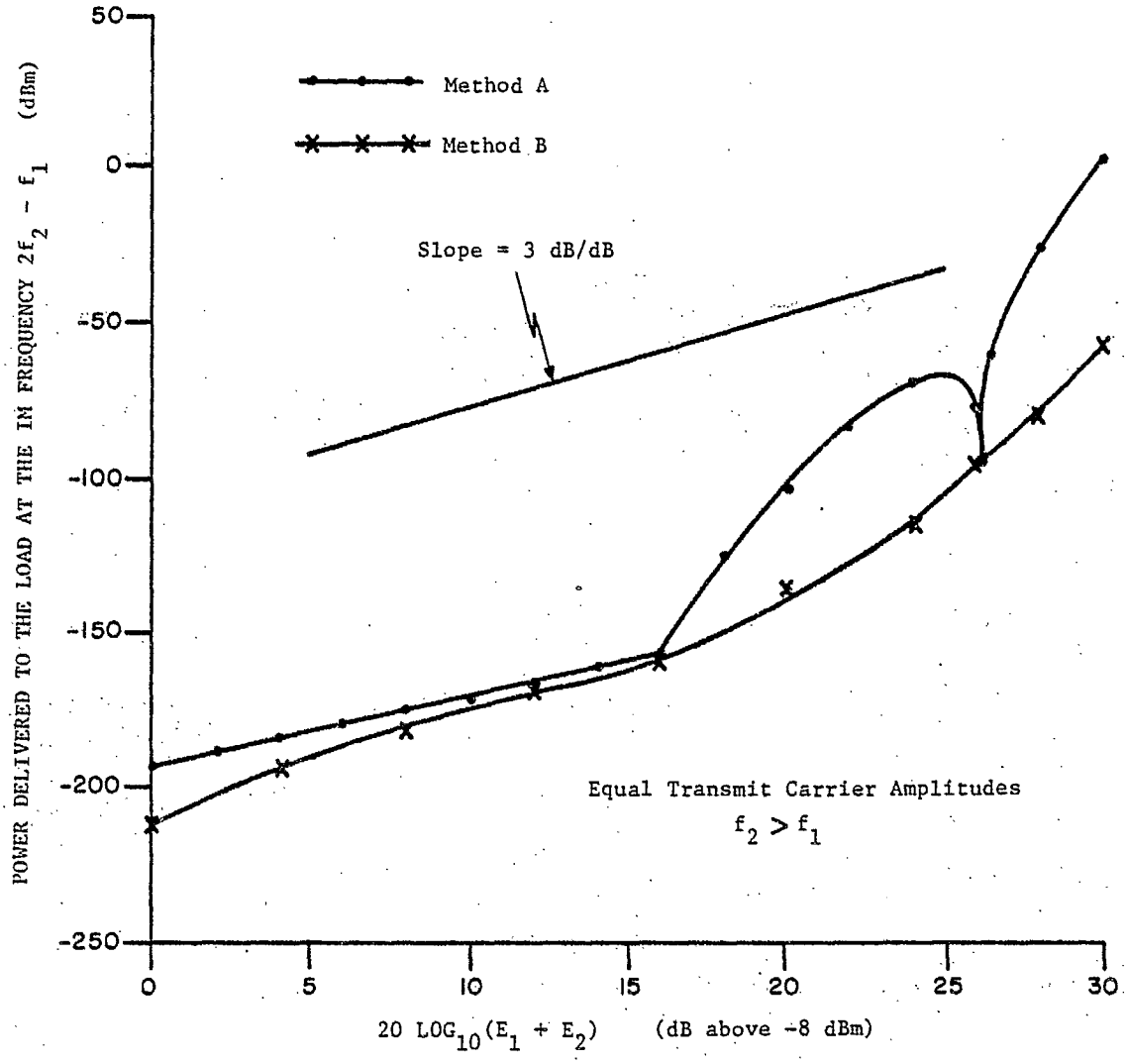

Fig. 5.2. Computed third order IM power dependence on total transmit power.

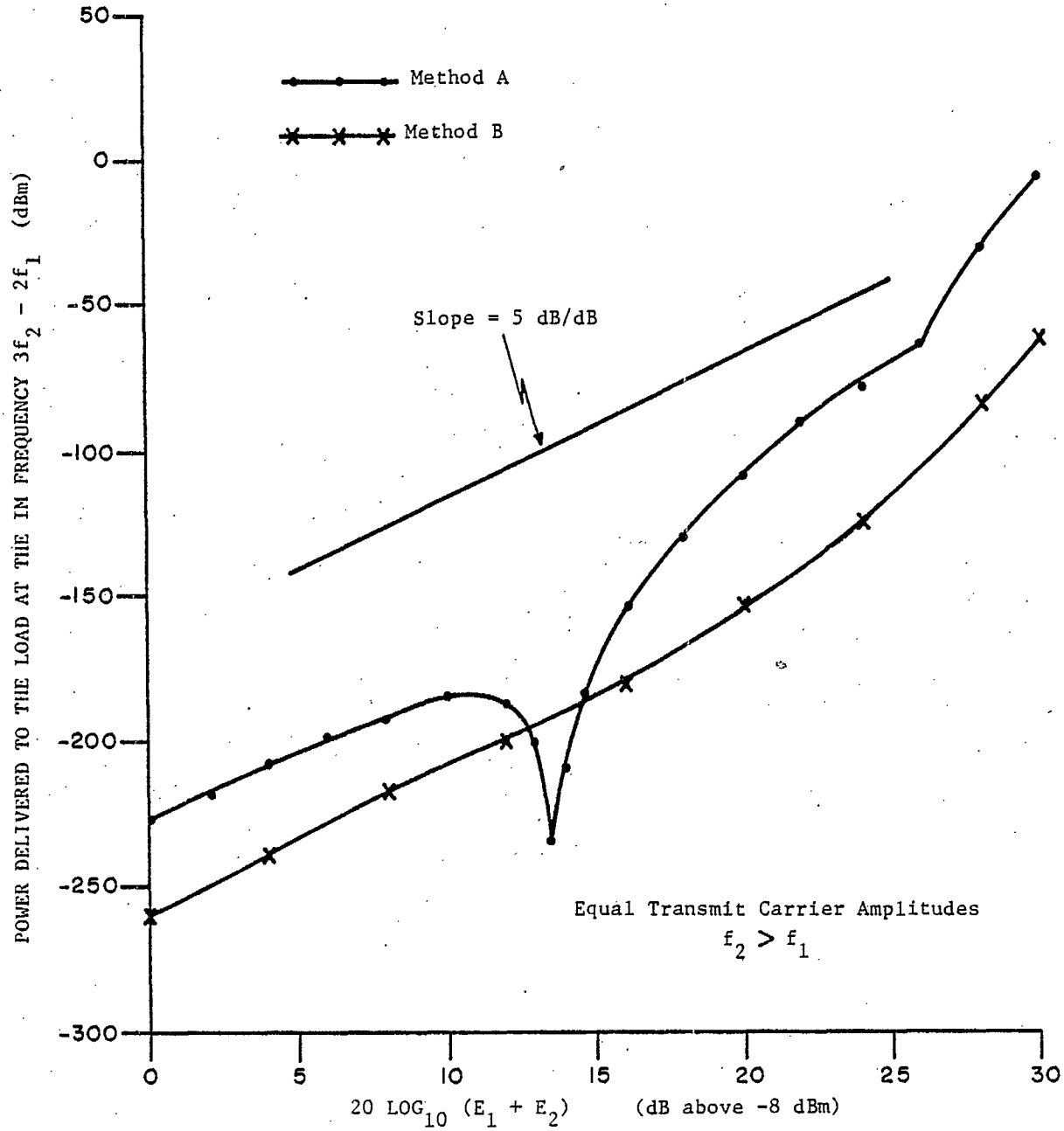

Fig. 5.3 Computed 5th order IM power dependence on total transmit power.

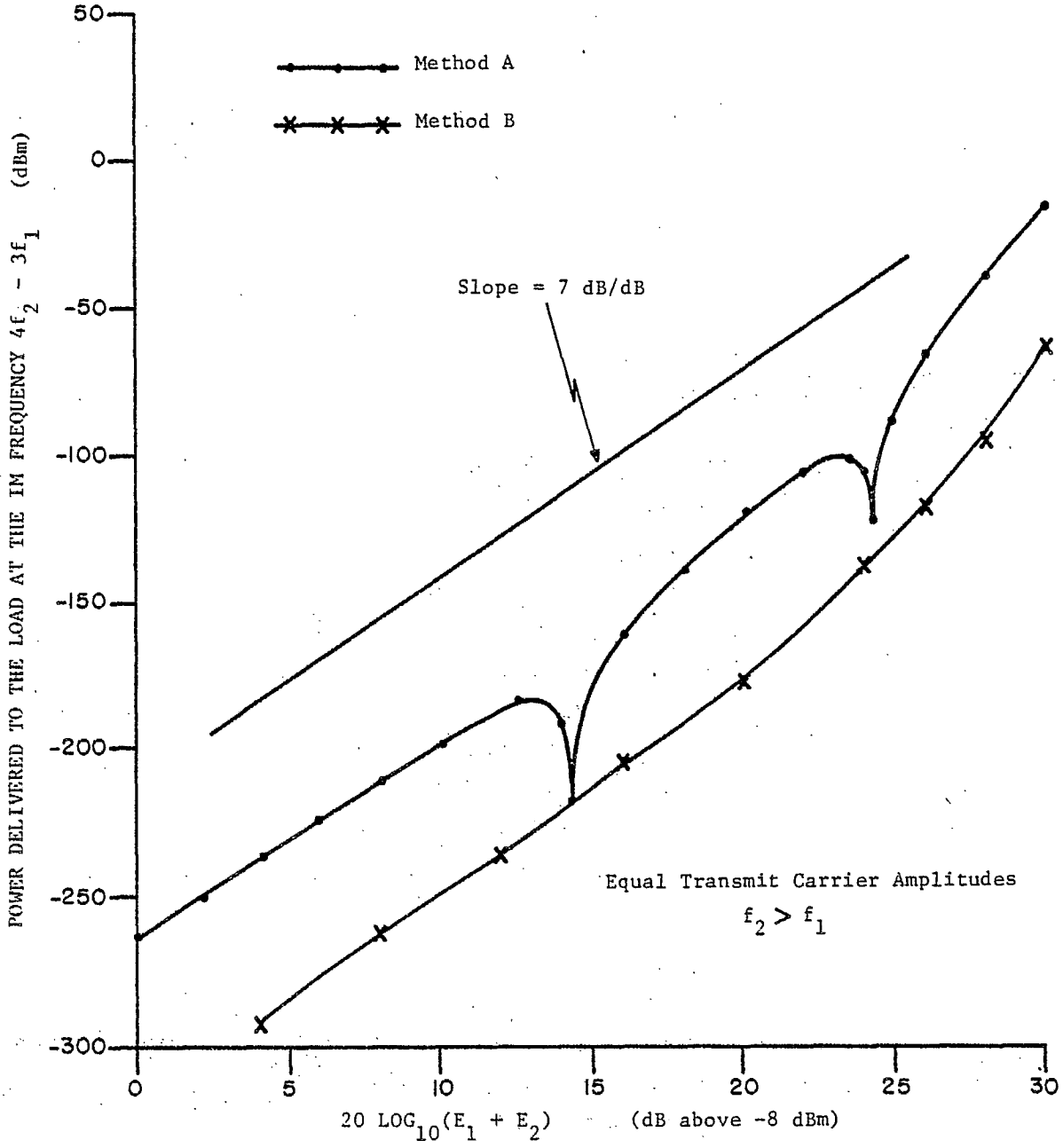

Fig. 5.4. Computed seventh order IM power dependence on total transmit power.

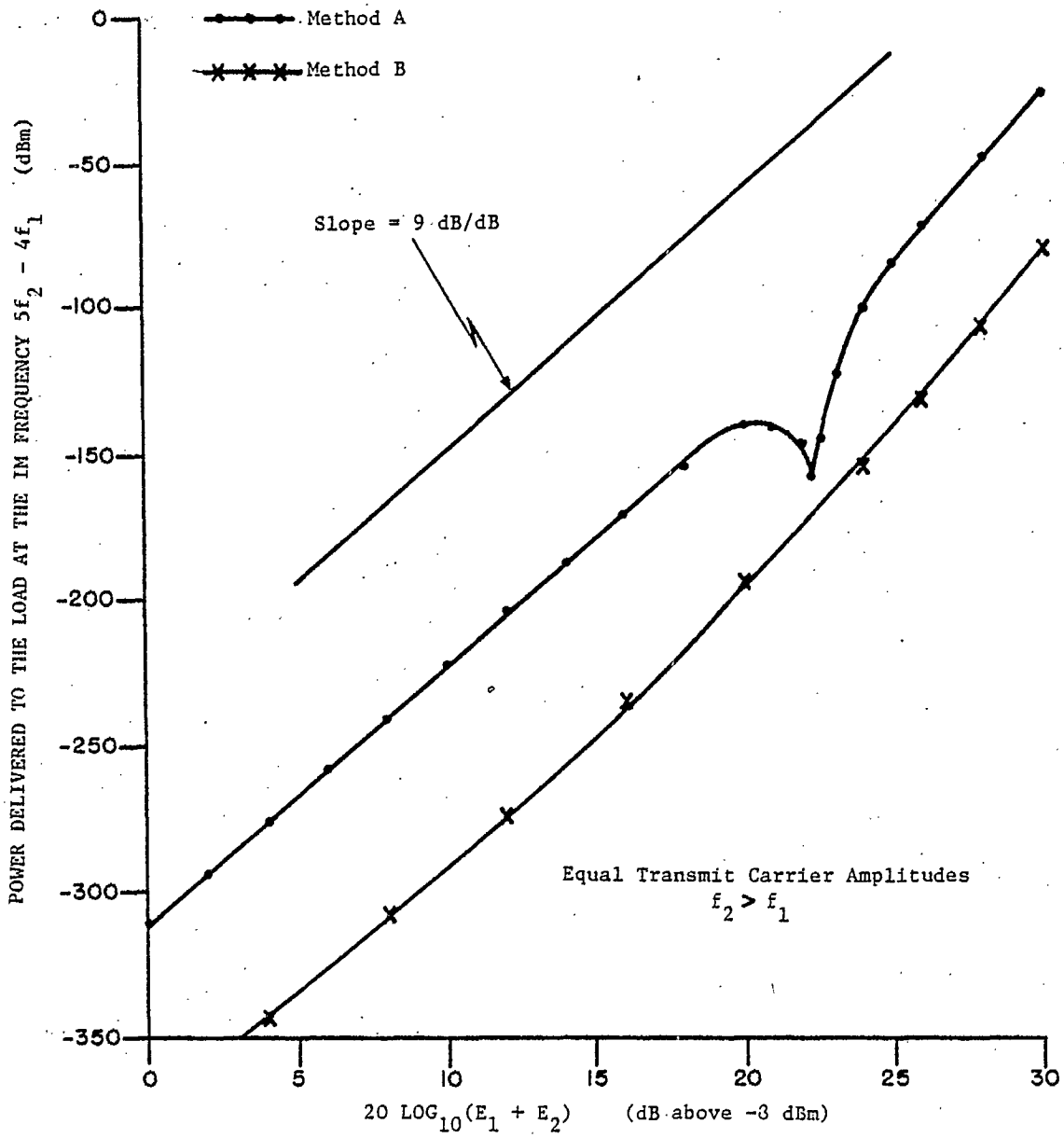

Fig. 5.5. Computed ninth order IM power dependence on total transmit power.

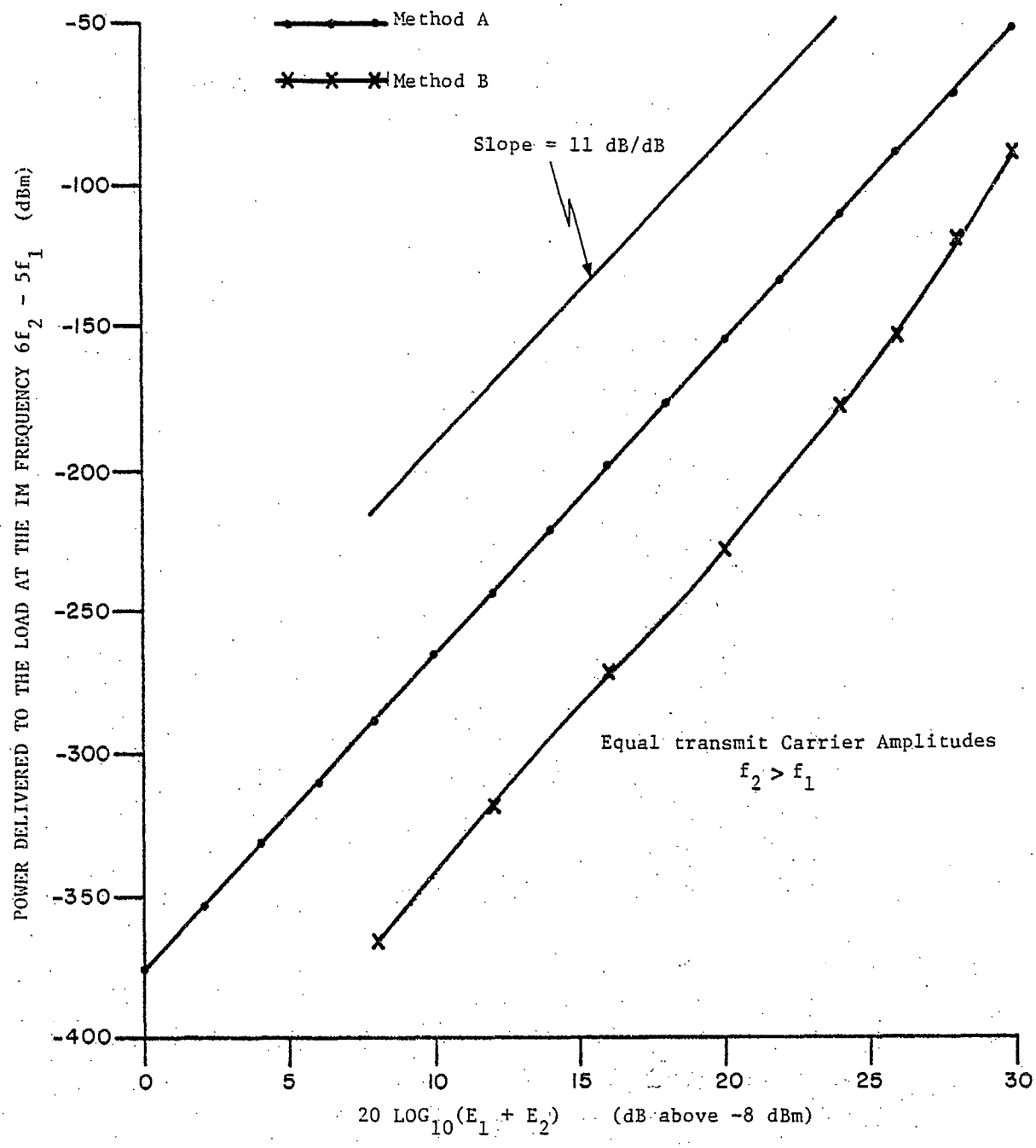

Fig. 5.6. Computed eleventh order IM power dependence on total transmit power.

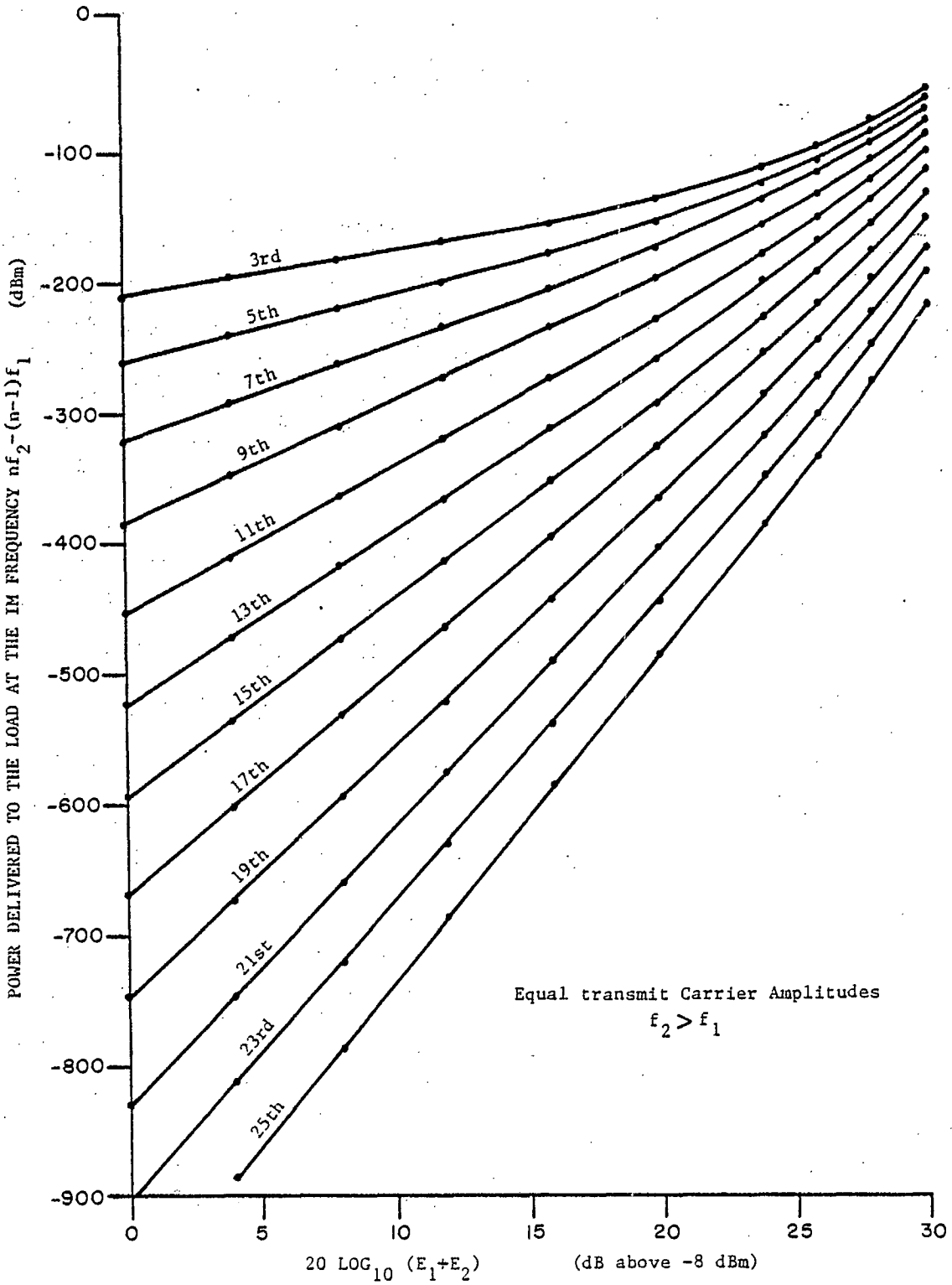

Fig. 5.7. IM Product power dependence on total transmit power, (data computed using method B).

polynomial which have a degree greater than N. It is the influence of the high index terms on low order IM signal levels that causes the greatest deviation from algebraically predicted power slopes to be associated with low order IM power curves. The coefficients, a_i, of the polynomial representing the diode nonlinearity increase in magnitude as the index, i, becomes larger, regardless of the method used for their derivation*. In addition, the relative magnitudes of the partial sums in eqn. 5.2-1 associated with each coefficient are dependent upon RF input power. Except at low powers, these factors result in a major contribution to low order IM signal amplitudes by high index terms in the describing polynomial. This means that the lower Nth order IM power levels vary in accordance with the $(N+\Delta)$th power of the input signal amplitudes, where Δ is a function of polynomial coefficient magnitudes and the input power level. As IM order increases, the Nth degree term of the describing polynomial becomes more dominant, and the IM power slopes follow the N dB/dB trend more closely.

The nulls in the characteristics computed using method A result from the changing influence of polynomial terms associated with negative coefficients as input power changes. Such nulls have also been observed experimentally (section 5.4-1), but are absent from the curves in Fig. 5.7, as the Taylor Series coefficients are all of the same sign.

5.3.2 The Relative Magnitude of IM Product Signals of Different Order.

Data were taken from Figures 5.2 to 5.7 and used to draw the curves of figures 5.8 and 5.9. These figures show the relative magni-

---

* The $q/\eta kTth$ term in the Taylor series has the largest coefficient. Coefficients associated with terms of higher index have progressively smaller values.

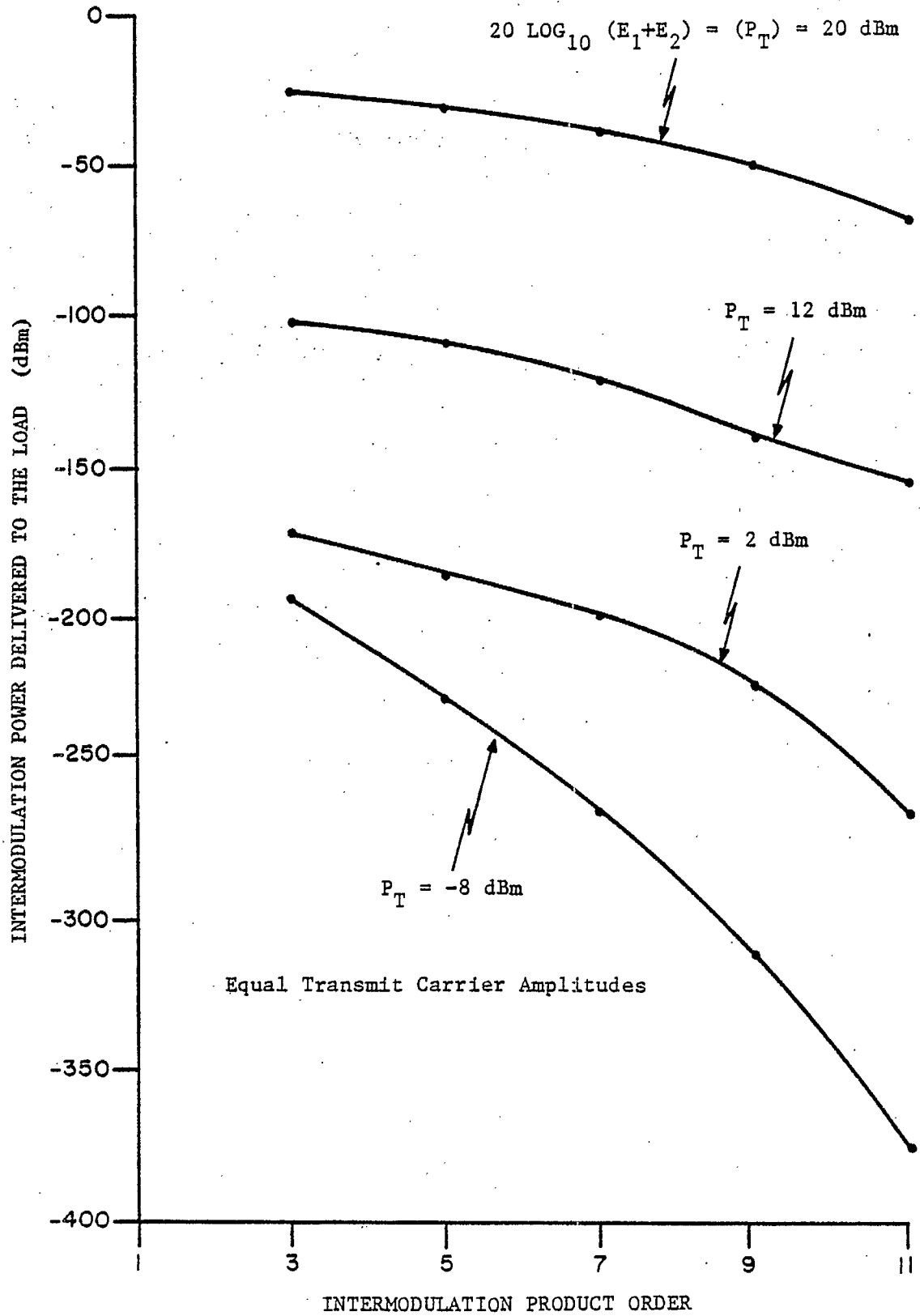

Fig. 5.8. The relative amplitude of IM products of different order (data computed using method A).

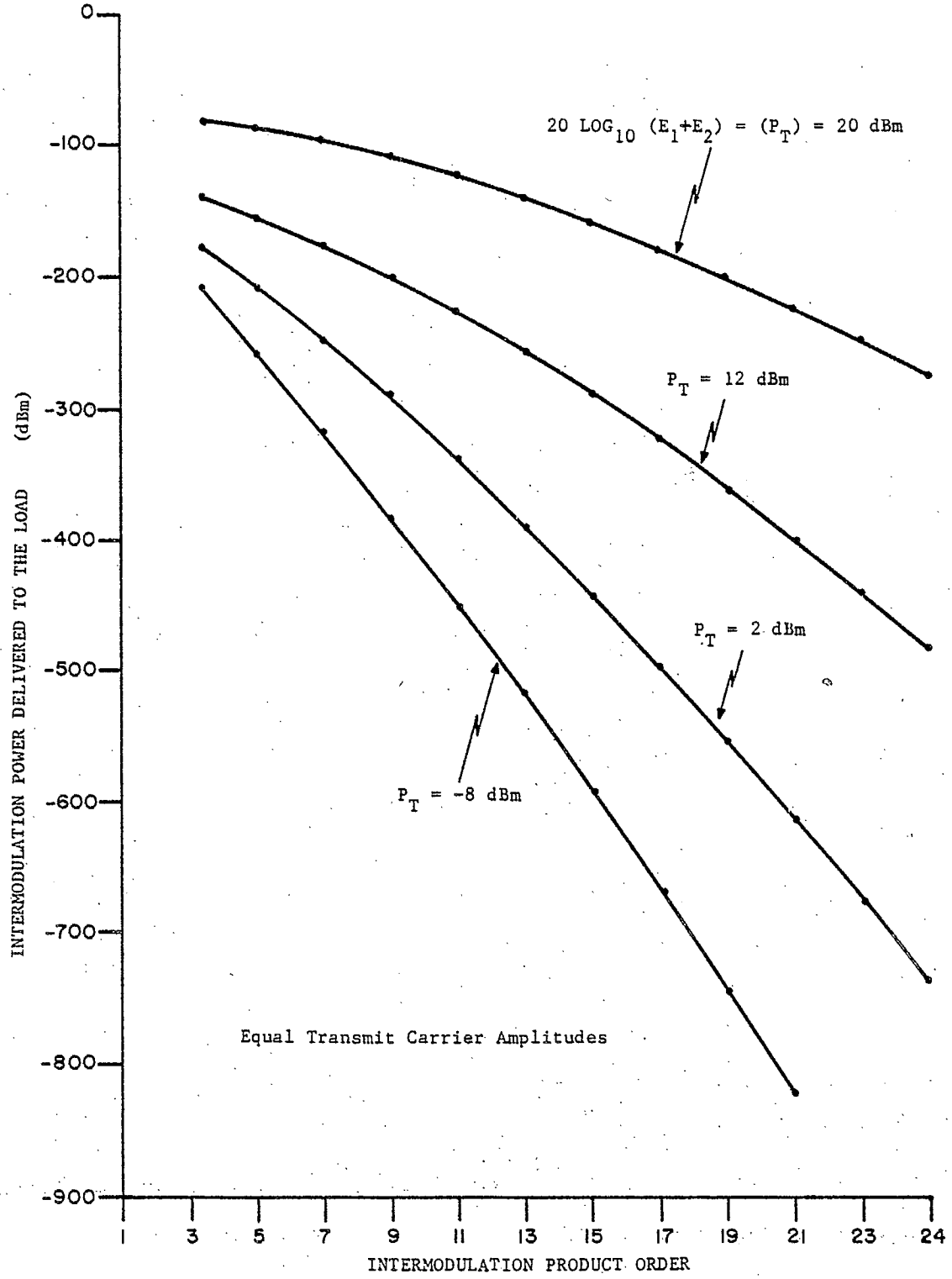

Fig. 5.9. The relative amplitude of IM products of different order, (data computed using method B).

tudes of IM products of different order computed at four different total input powers using methods A and B. Results show that the IM power/order relationship is dependent upon input power levels. The difference in power between IM signals of consecutive order is greatest at low input powers and decreases as input drive level is increased. The increasing slope of the curves also shows that there is generally a wider separation in power between high order IM signals than that between low order signals.

The trends discussed above are the result of the same factors that govern the characteristics discussed in Section 5.3.1. The changing influence of different terms in the describing polynomial as input power is varied accounts for the input power dependence, while contributions to low order IM signal amplitudes from high index polynomial terms results in the small separation in power between low order IM products. Slope changes in the characteristics computed using method A are due to contributions from polynomial terms with negative coefficients.

5.3.3 The Dependence of IM Signal Powers on the Ratio of Transmit Signal Amplitudes

In a similar computer exercise to that reported by Chapman et al [1], the sum of the carrier voltage inputs (E_1 and E_2), to the programs was held constant as their ratio, (E_1/E_2), was varied between -30 dB and +30 dB. This is analogous to a shift in power between channels in a two frequency RF communication system while maintaining the total input power to the system at a fixed level. Figures 5.10 (a) and (b) show IM signal power response to carrier power ratio changes for two different total transmit powers computed using method A.

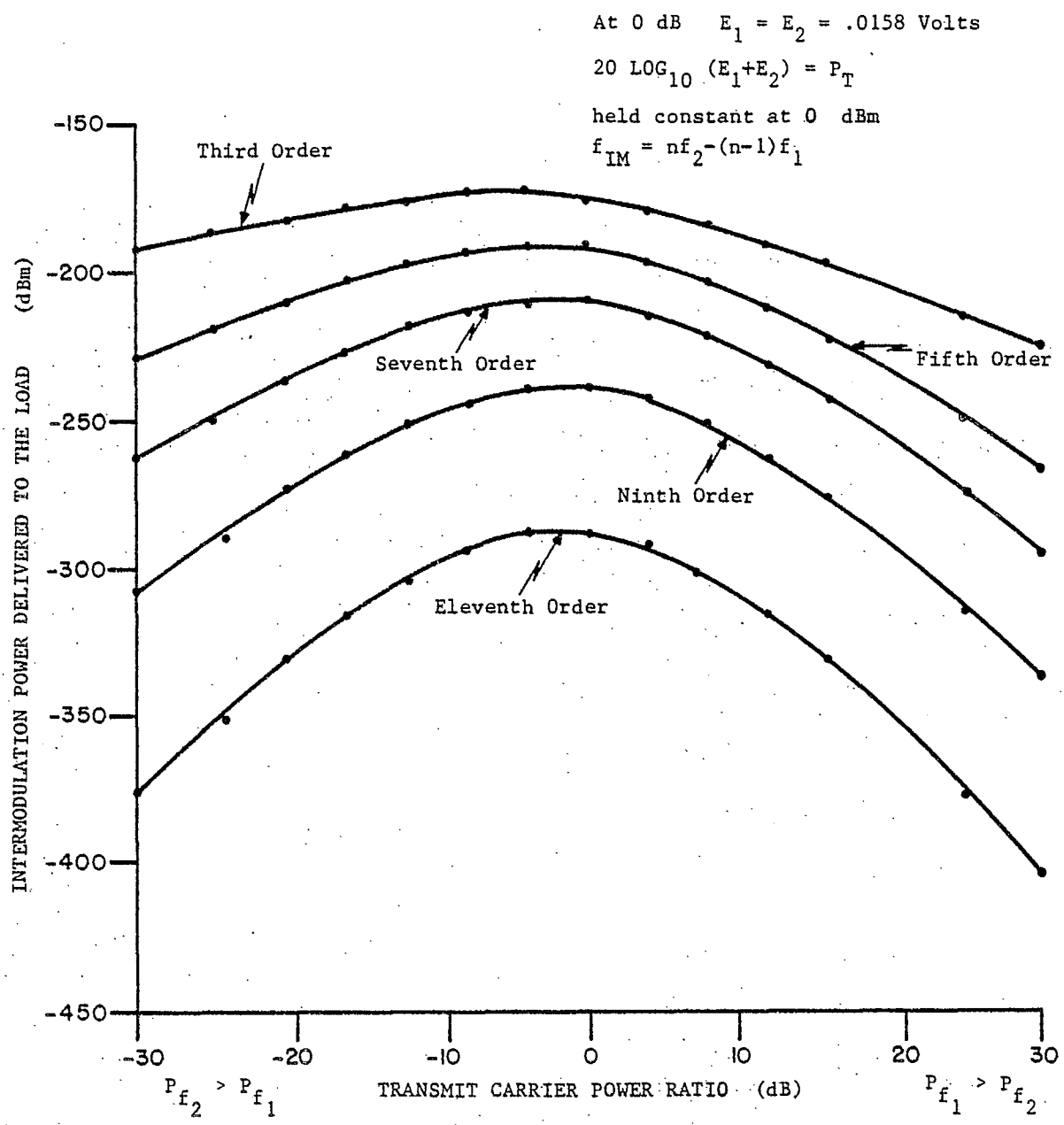

Fig. 5.10 (a). Intermodulation signal power dependence on the transmit carrier power ratio (P_{f_1}/P_{f_2}), (data computed using method A, P_T = 0 dBm).

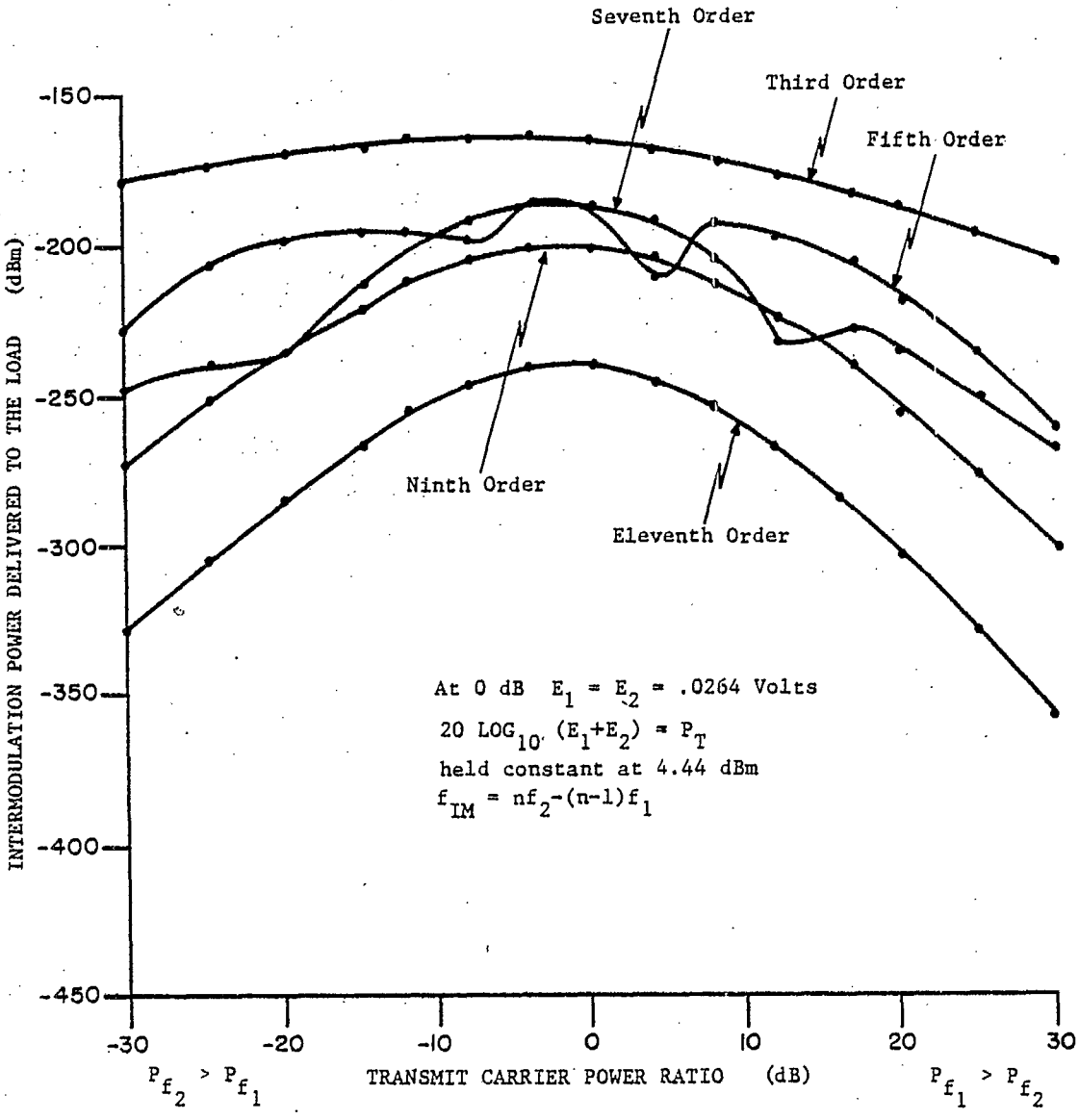

Fig. 5.10 (b). Intermodulation signal power dependence on the transmit carrier power ratio (P_{f_1}/P_{f_2}), (data computed using method A, $P_T = 4.44$ dBm).

Figures 5.11 (a) and (b) show corresponding data computed using method B.

The figures show that a wide variation in IM power at any particular order can result from carrier amplitude ratio changes even though the total input power to the IM generating nonlinearity is constant. A comparison of figures 5.10(a) and 5.10(b) shows that the characteristic computed using method A is altered by changing total input power. It is also clear from all figures that the IM power is most sensitive to power ratio changes when the carrier closest in frequency to the IM frequency is the weakest.

Maximum 3rd order IM signal power results when the power of the transmit carrier at the frequency closest to the IM frequency is 3 dB higher than the power of the other carrier. As order becomes higher, the maximum IM power point shifts toward a transmit carrier power ratio of unity. As the transmit carrier power ratio becomes large, IM signal powers decrease, and in the limiting case when the power of one carrier is essentially zero in comparison with that of the other, the IM signals vanish.

The shift in the power maximum from the unity ratio point, and the asymmetry of the power curves are both caused by the inequality of the exponents (n-1), and n, associated with E_1 and E_2 in the terms of the describing polynomial which contribute to the amplitude of a particular IM product (see Appendix A). The curves become more symmetrical as order increases since the difference between E^n and $E^{(n-1)}$ is small for large n and $E < 1$.

5.3.4 IM Power Sensitivity to Individual Transmit Carrier Powers

The characteristics of Section 5.3.3 show that IM power is

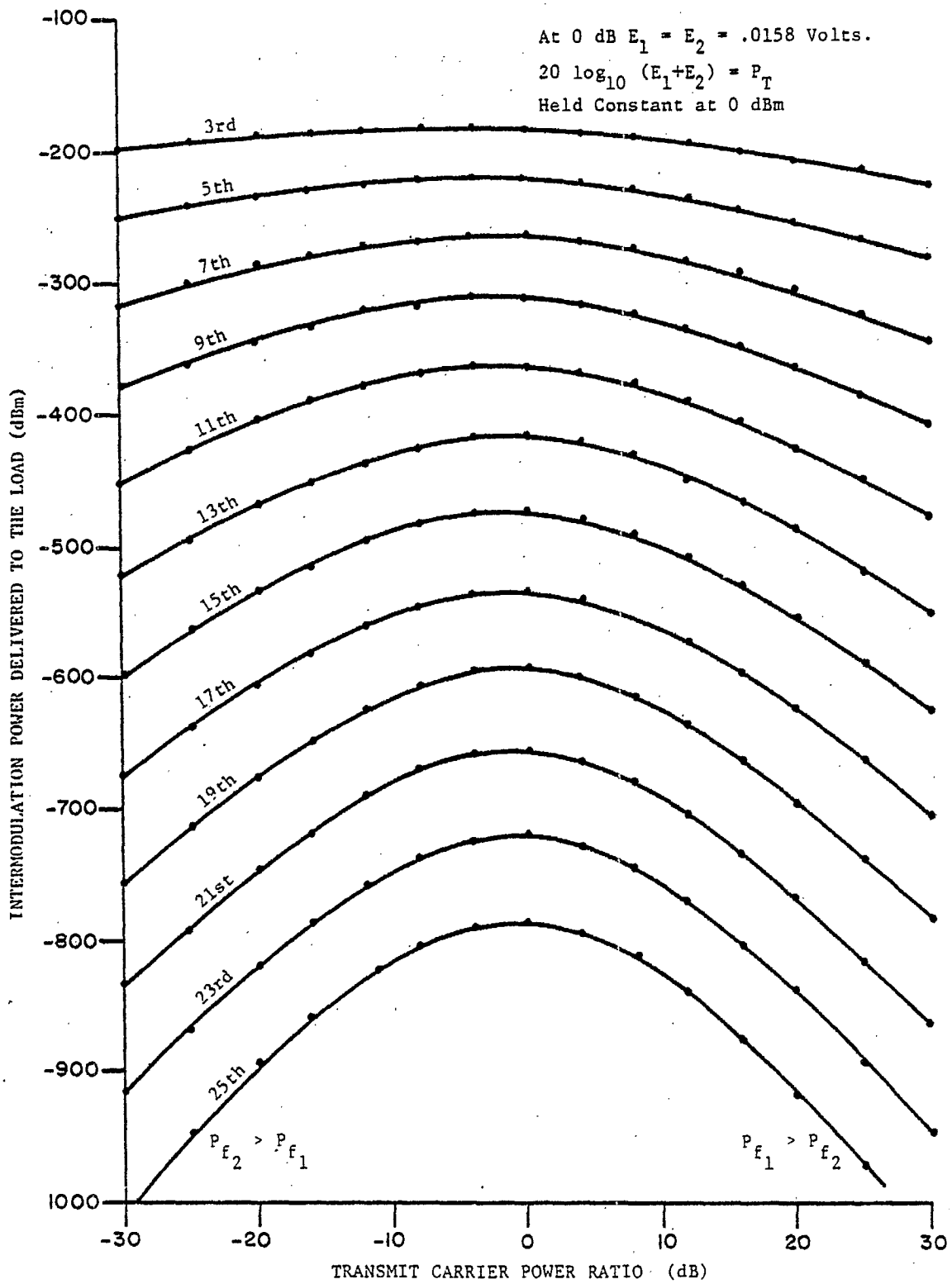

Fig. 5.11 (a). Intermodulation signal power dependence on the transmit carrier power ratio (P_{f_1}/P_{f_2}), (data computed using method B, P_T = 0 dBm).

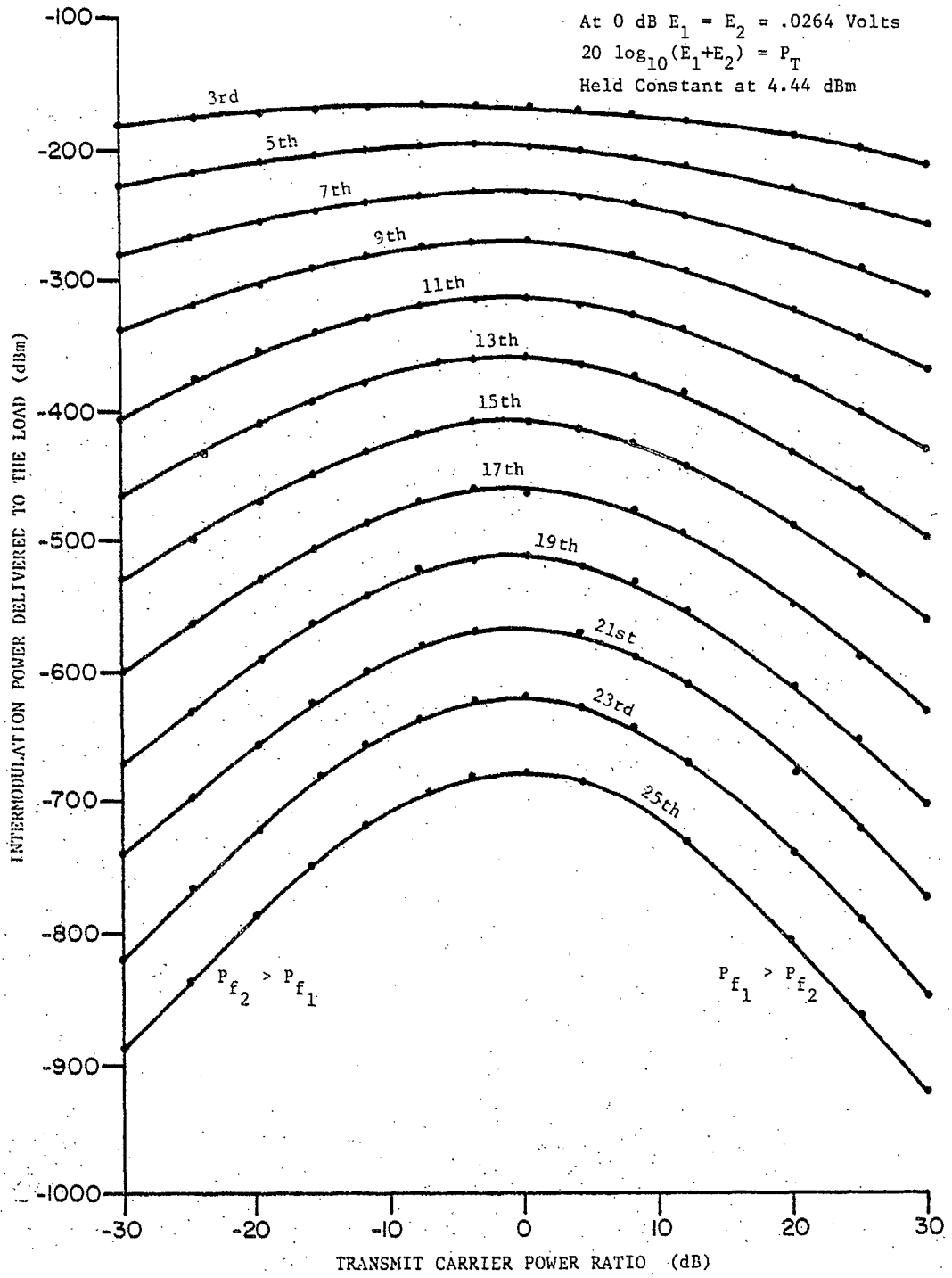

Fig. 5.11 (b). Intermodulation signal power dependence on the transmit carrier power ratio (P_{f_1}/P_{f_2}), (data computed using method B, $P_T = 4.44$ dBm).

most sensitive to transmit power variations at the carrier frequency closest to the IM frequency. Algebraic consideration of eqn. 5.3-1 leads to the following conclusions:

(i) At third order a n dB power change at the carrier frequency closest to the IM frequency should produce a 2 n dB change in IM power. A n dB change in power at the other carrier frequency should result in only a n dB change in IM power.

(ii) The IM power change should increase by n dB between consecutive orders if the initial input power change at either one of the transmit frequencies is n dB.

This characteristic was investigated numerically by first computing the IM powers generated by the diode when equal amplitude carrier voltages are applied at three different total power input levels. An increase in power delivered to the RF system at one of the carrier frequencies was then simulated by increasing one of the voltage inputs to the programs by a factor of $\sqrt{2}$ (3 dB power increase), and computed IM powers were compared with those corresponding to the equal carrier case. Next, the calculations were repeated with the previously incremented carrier voltage reduced to the voltage for which equal carrier IM powers were calculated and the other carrier voltage increased by a factor of $\sqrt{2}$.

Changes in IM powers from those computed for the equal carrier case are plotted in Figures 5.12 and 5.13. Figure 5.12 results from calculations using method A, and data for Fig. 5.13 were

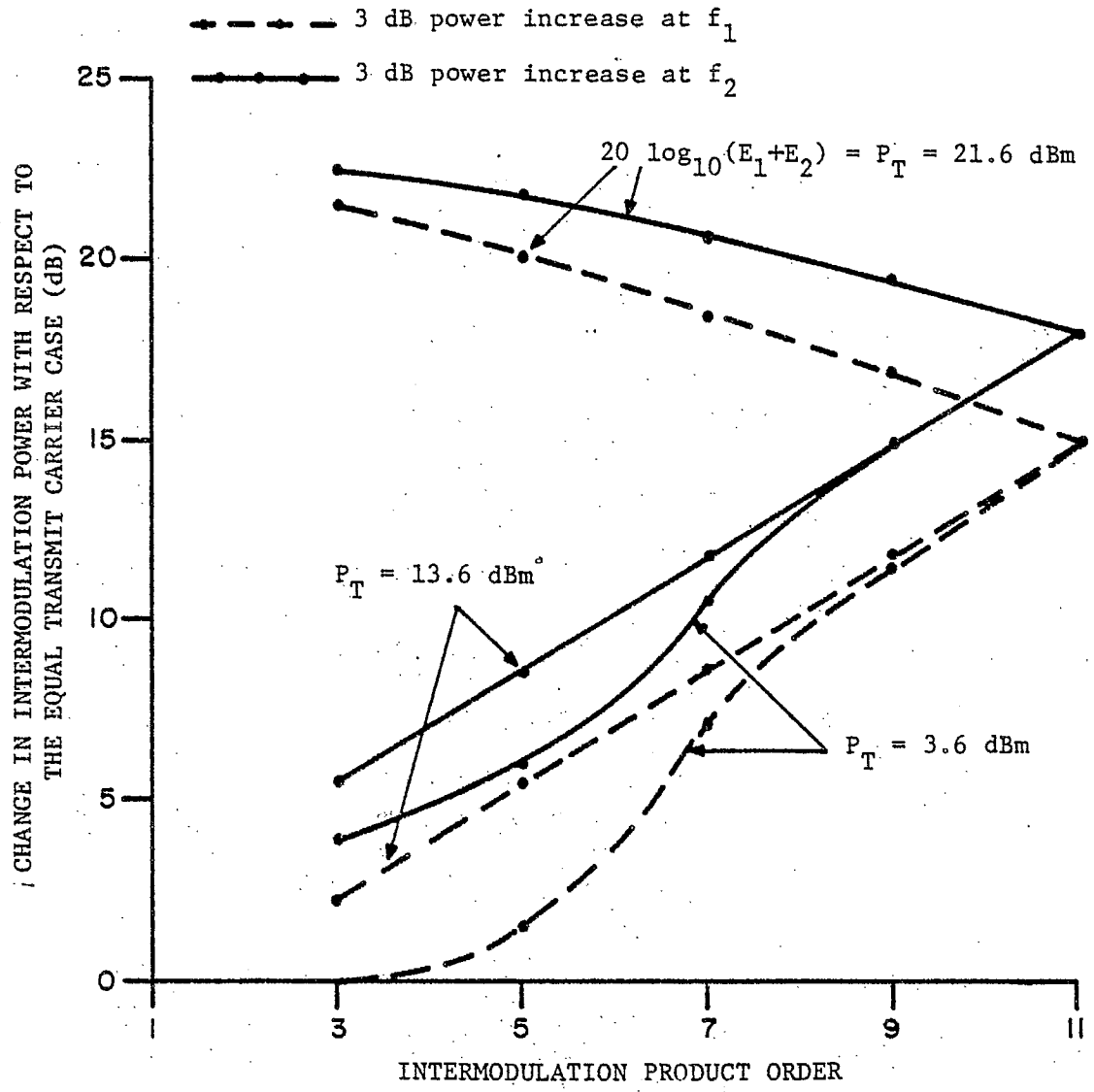

Fig. 5.12. Intermodulation signal power sensitivity to individual transmit carrier powers, (data computed using method A).

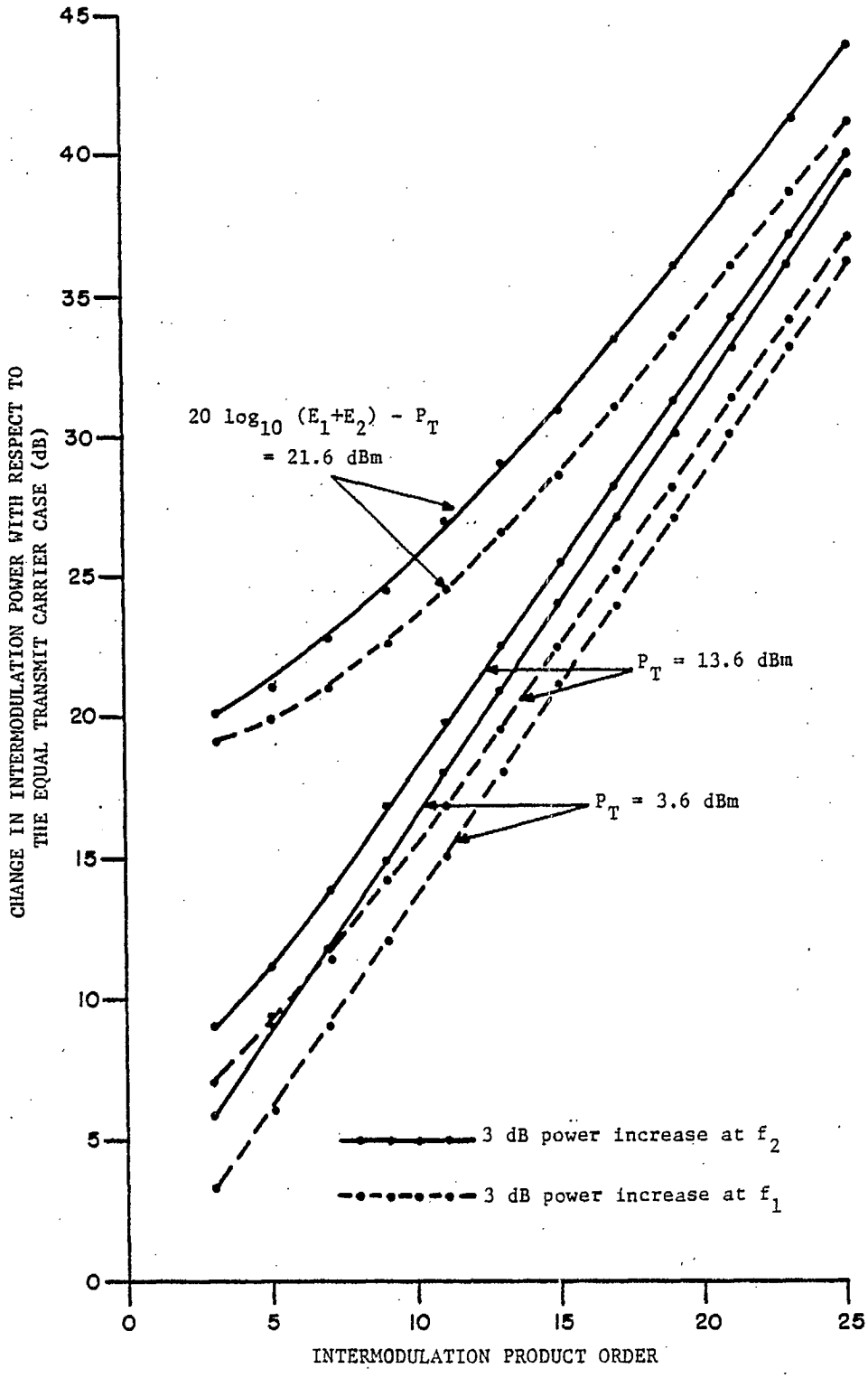

Fig. 5.13. Intermodulation signal power sensitivity to individual transmit carrier powers, (data computed using method B).

computed using method B. Reference to the figures shows that results are very dependent upon the total input power to the nonlinearity. At low input powers the algebraically predicted trend is followed closely. At higher input powers, substantial deviation from expected behaviour occurs. This, like several previously discussed trends, is the result of the changing influence of different terms in the describing polynomial in different regions of operation along the diode conduction characteristic. The curves of Fig. 5.12 show that in some regions of operation, the response to transmit power changes can actually be greater at low orders.

5.4 Experimental Investigations Concerning the Characteristics of IM Signals Generated by a Semiconductor Diode.

A series of experiments was conducted in which a semiconductor diode was used to generate IM signals in the CRC test circuit. The objective of experimentation was to observe actual IM signal response to changes in input signal parameters similar to those simulated in the computer exercises of Section 5.3. It was necessary during the experiments to apply higher transmit powers (see appendix D) to the diode than those represented in the simulations in order that IM signals could be measured above the noise floor of the measurement system. Without violating several assumptions, theoretical analyses could not be extended to cover transmit powers used in the experiments. This meant that it would not be possible to compare theoretical and experimental results corresponding to operation over the same transmit power range. It was considered, however, that

experiments in the higher power range could still provide useful information for determining the practicality of computed results.

A Hewlett Packard HP 5082-2800 Schottky diode was shunted with a tinned copper wire and soldered in place of the resistors in the body of a coaxial attenuator as shown in Fig. 5.14. This allowed connection of the diode assembly in the test circuit by means of the type N connector fittings on the attenuator housing. An equivalent circuit for the measurement system with the shunted diode in place is shown in Fig. 5.15.

The following subsections detail each of the experiments, and present measured results with describing annotations.

5.4.1 IM Power Dependence on Total Transmit Power

Starting with 43 mW of total transmit power at the test port of the measurement system, the equal carrier transmit power was increased in steps to 35 dB above the 43 mW level. The power of the IM signal displayed on the spectrum analyser was recorded after each step. This procedure was repeated sequentially with test frequencies such that 3rd to 11th order IM powers could be measured.

Figures 5.16 to 5.20 show the measured IM powers plotted as a function of the estimated* total transmit power at the test port. A straight line having a slope of N dB/dB has been drawn on each Nth order power curve for comparison.

The slopes of the measured IM power curves show a general trend toward the N dB/dB characteristic anticipated from algebraic

*Power at the test port was determined from calibration data showing total transmit power delivered to a 50 ohm load at the duplexer output as a function of high power amplifier drive level attenuator settings.

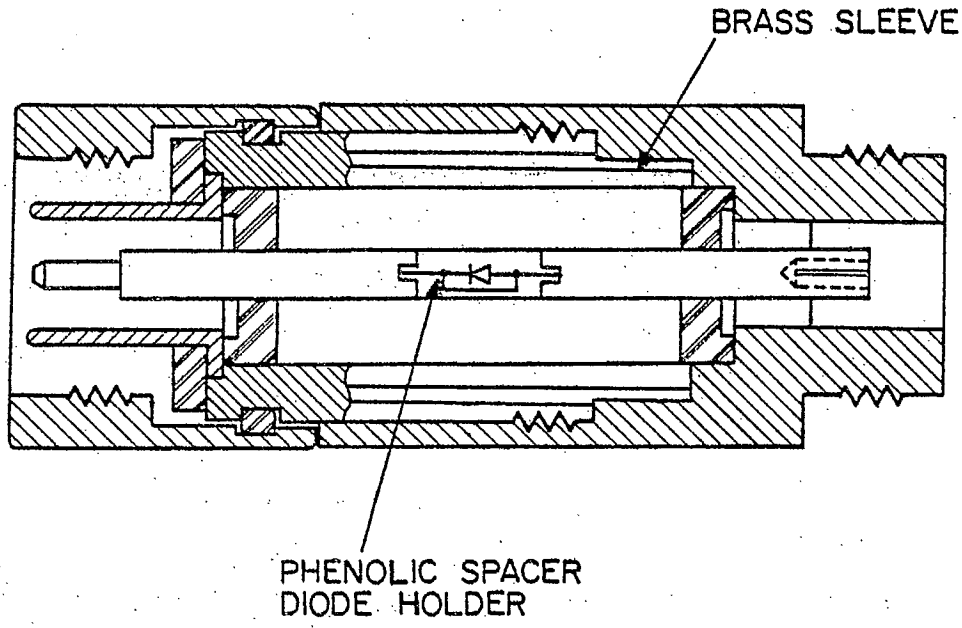

Fig. 5.14. Test jig assembly used for inserting the shunted diode in the CRC measurement circuit.

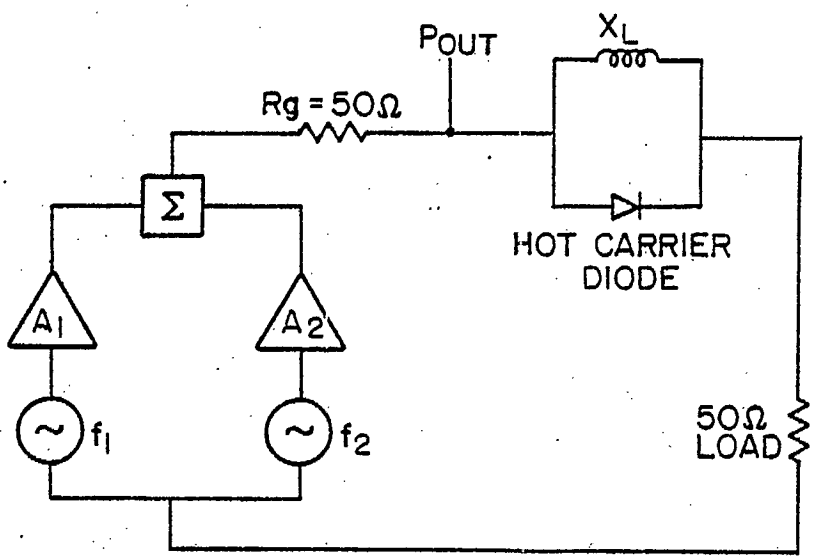

Fig. 5.15. Equivalent circuit for the CRC measurement set-up with the shunted diode IM generator in place.

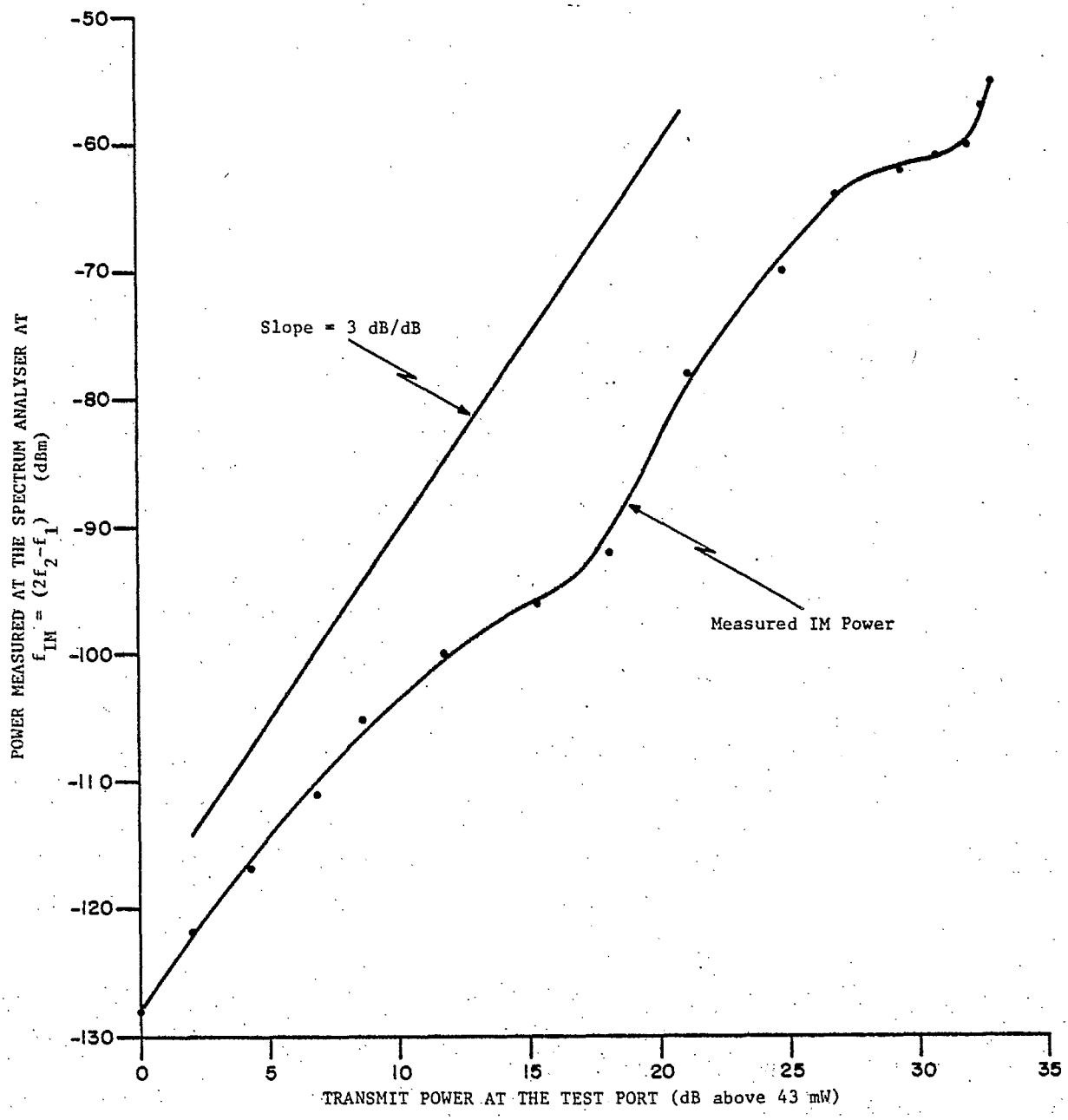

Fig. 5.16. Third order IM signal power dependence on total transmit power, (Diode #1).

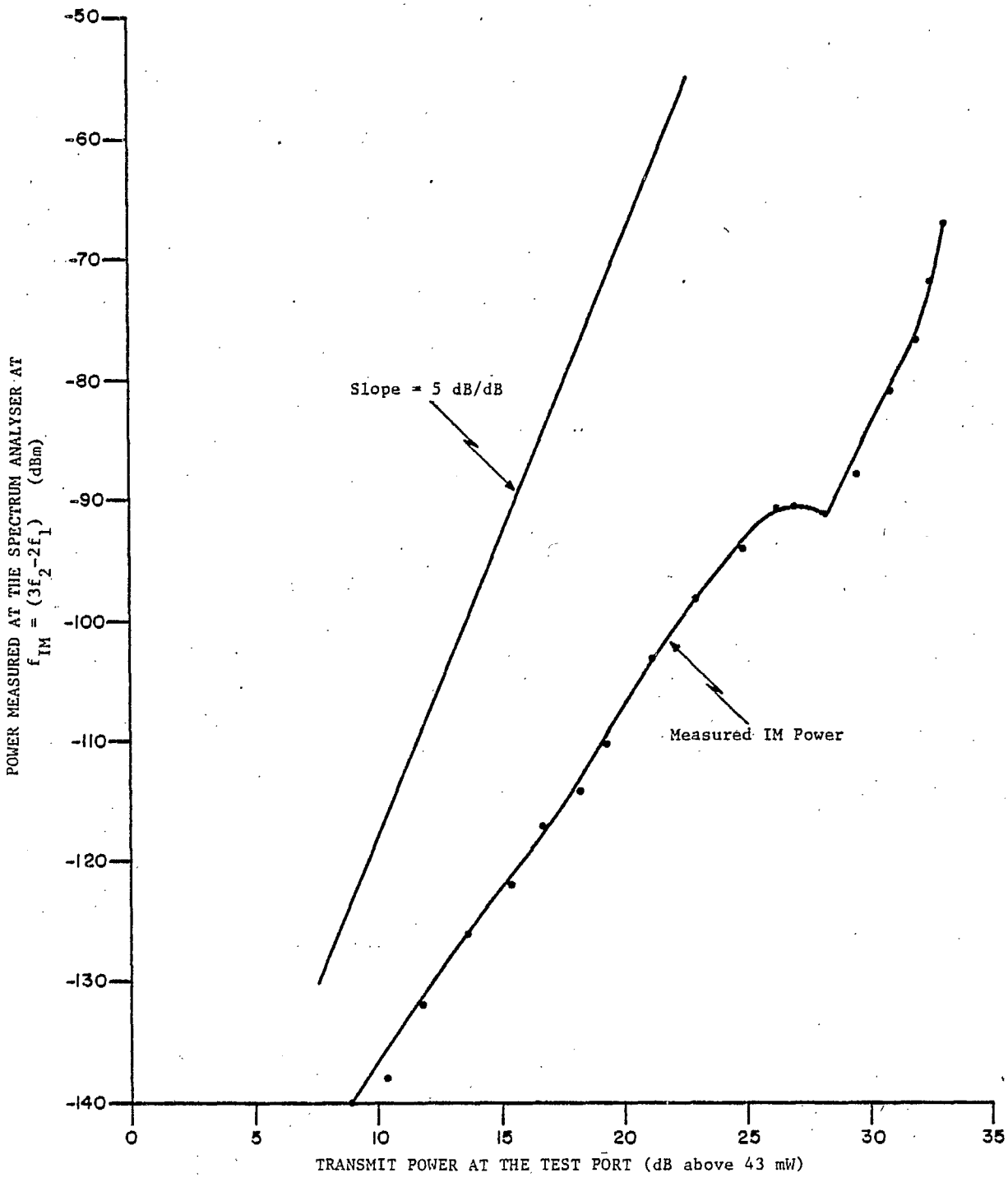

Fig. 5.17. Fifth order IM signal power dependence on total transmit power. (Diode #1).

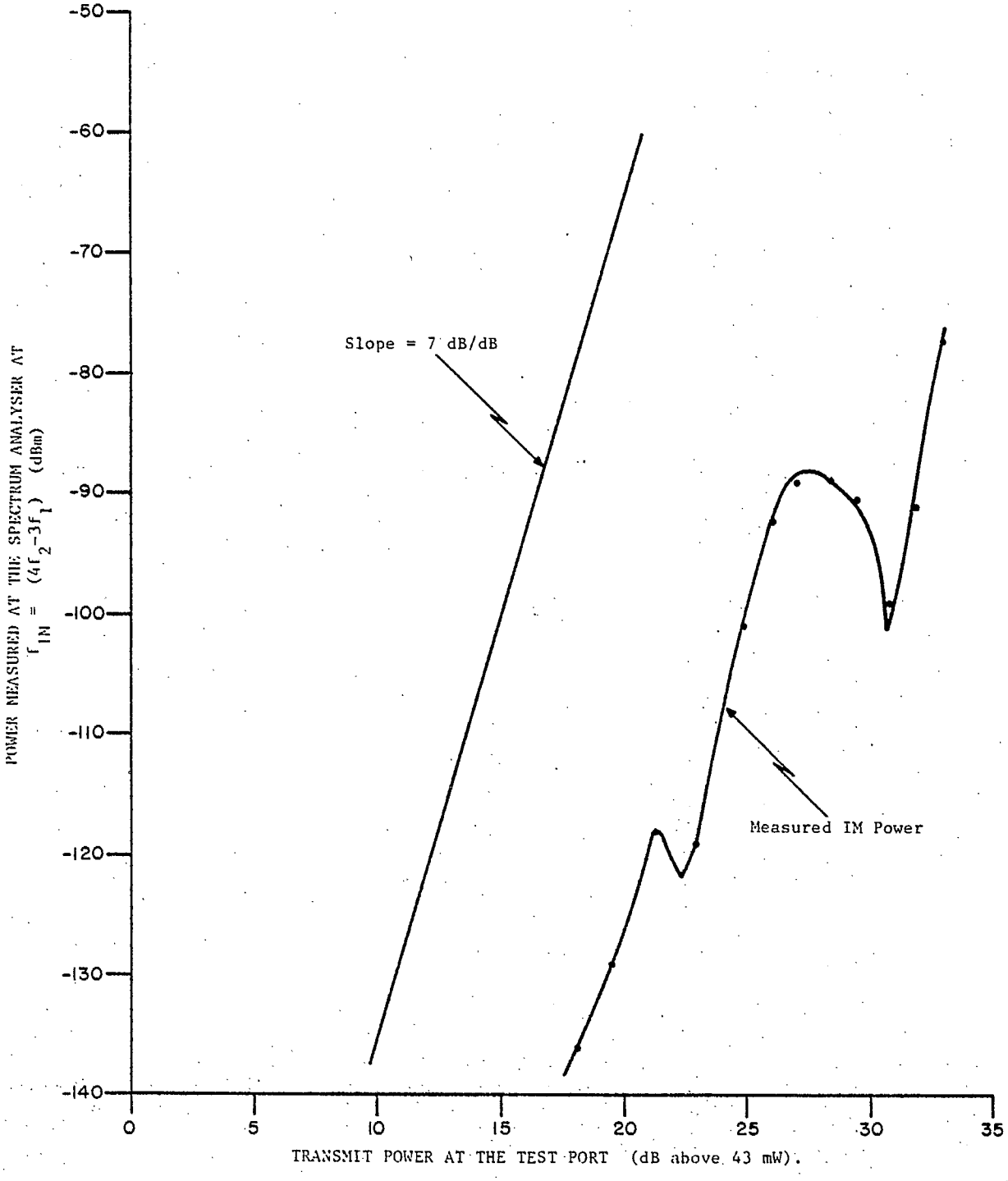

Fig. 5.18. Seventh order IM signal power dependence on total transmit power. (Diode #1).

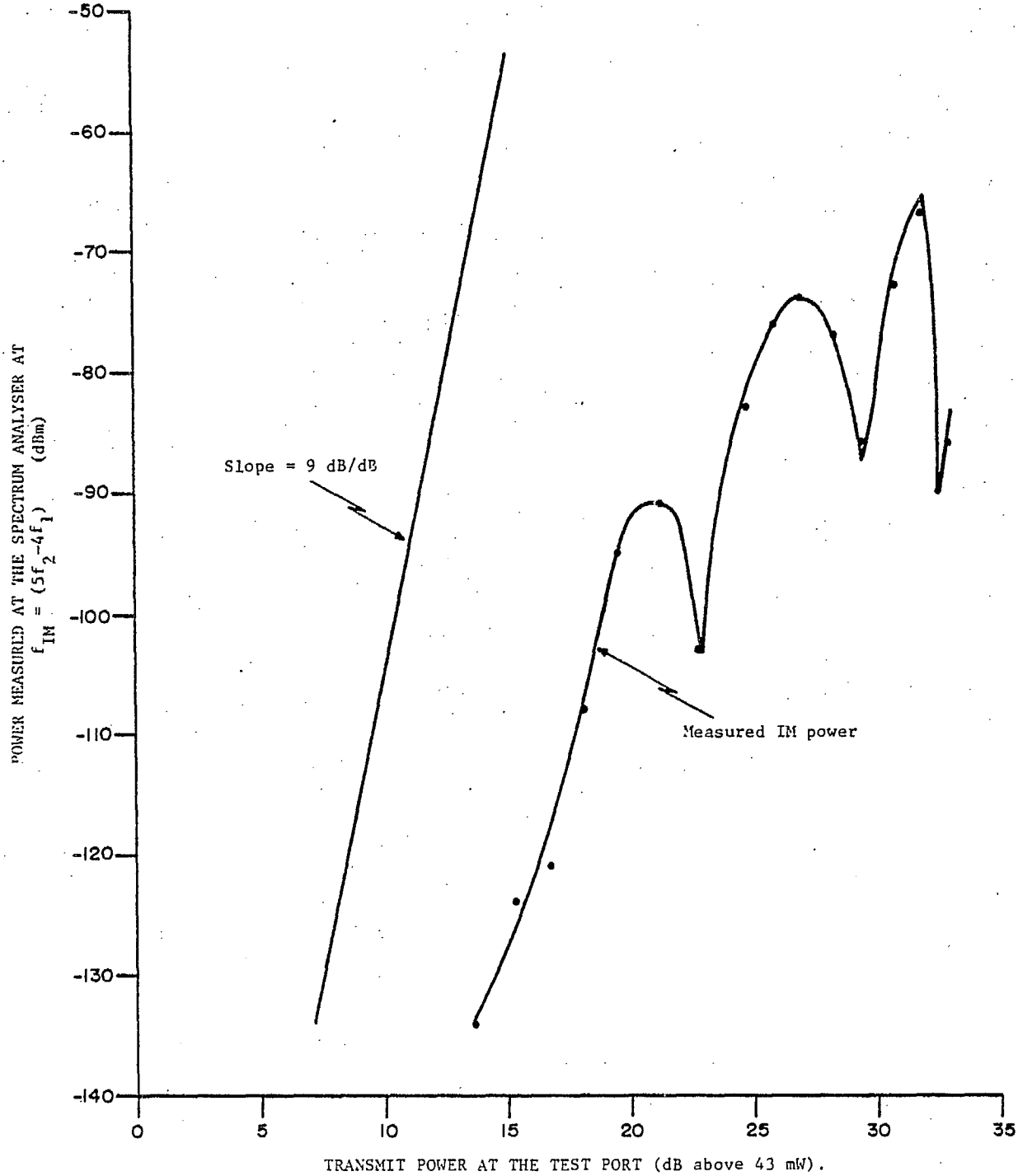

Fig. 5.19. Ninth order IM signal power dependence on total transmit power, (Diode #1).

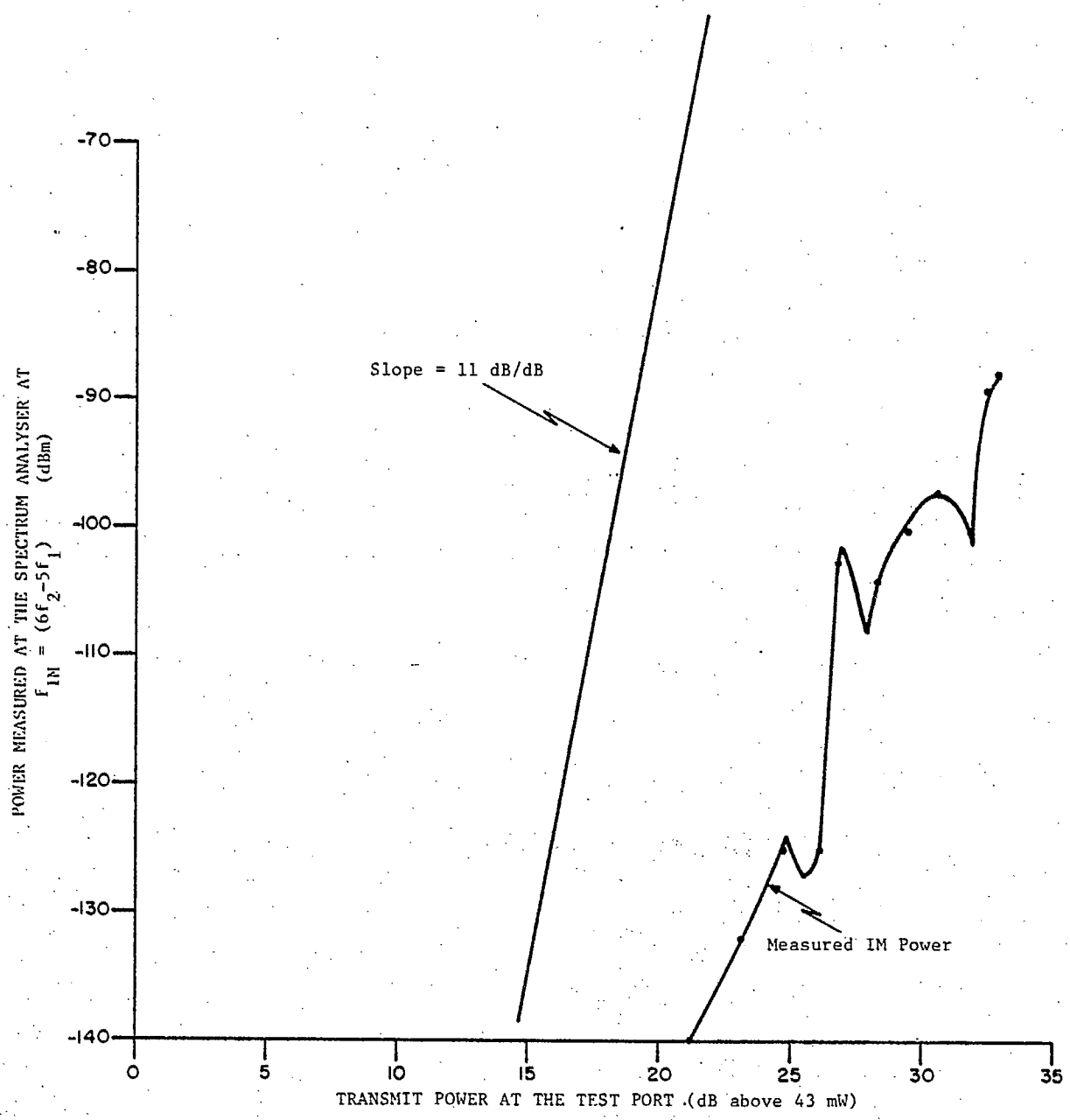

Fig. 5.20. Eleventh order IM signal power dependence on total transmit power, (Diode #1).

considerations, although there is a substantial deviation at higher transmit powers. The measured data also show minima similar to those in the curves drawn from IM powers calculated using the least squares approximation technique (method A). It is interesting to note that the separations between the nulls in the computed and measured curves (see Fig. 5.2 to 5.6) are similar, and that both sets of curves show that there are a greater number of nulls for higher order IM products.

5.4.2 The Relative Power of IM Signals of Different Order.

IM power values corresponding to three different total input power levels were taken from figures 5.16 to 5.20 and used to draw the histograms of Fig. 5.21.

The histograms show similar trends to those shown by the curves of Section 5.3.2 drawn from computed IM power data. Both computed and measured IM power/order relationships are dependent upon the total input power level. The greater difference in the power of IM signals of consecutive order at low transmit powers that was noted from the computed characteristics is also evident from the measured results.

It can be seen from Fig. 5.21 that the normally expected decrease in power for progressively higher order IM signal levels was not observed. Calculations using polynomial coefficients (Method A) derived from the least squares approximation technique can yield similar results. IM powers calculated using the Taylor series coefficients, however, always show a decrease in the power of consecutively higher order IM signals. It is believed that the departure from the expected monotonic decrease in signal powers results from direct phase cancella-

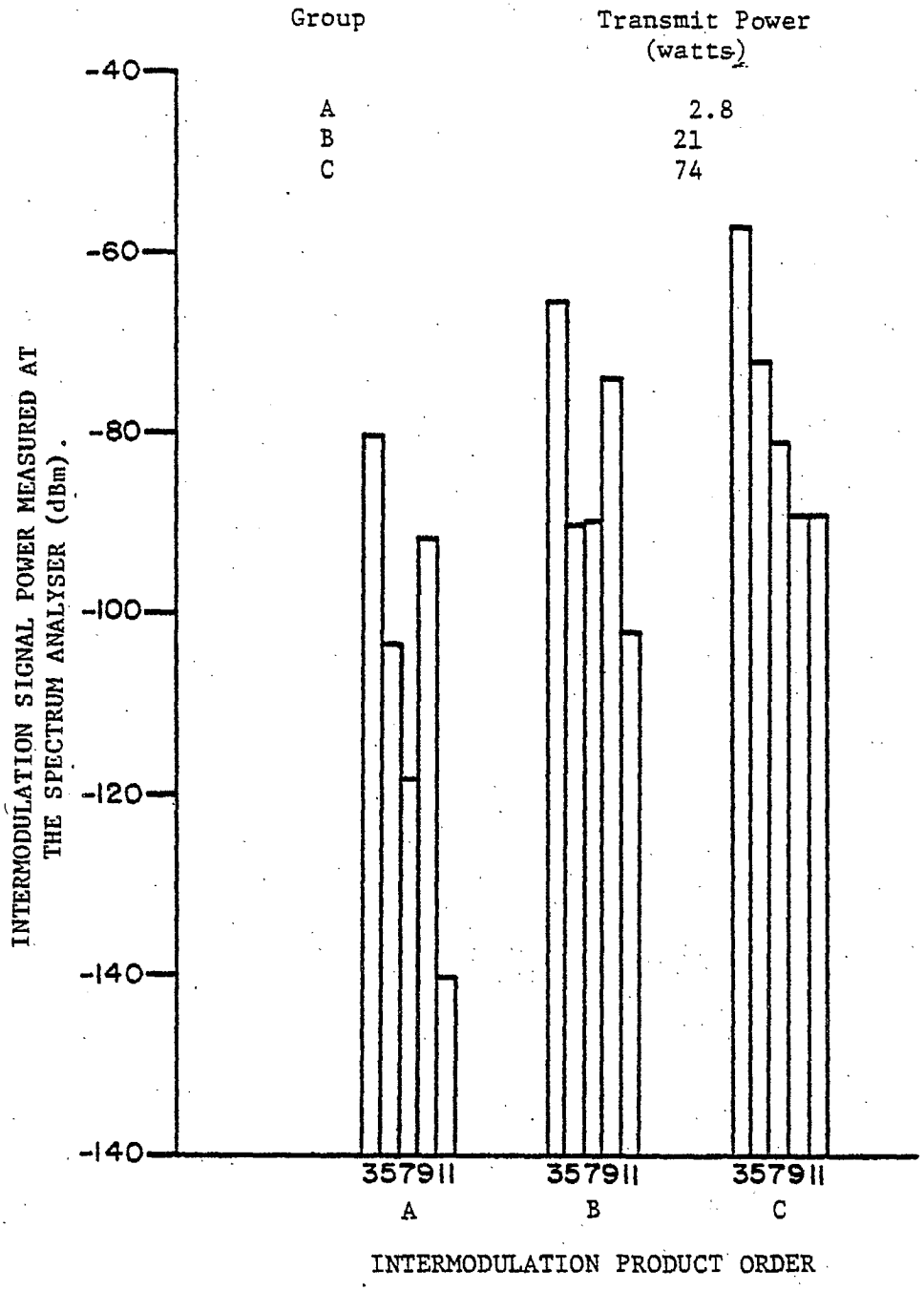

Fig. 5.21. The relative power of measured IM product signals of different order, (Diode #1).

tions, analogous to those which caused the nulls in the computed power curves of Section 5.3.1.

5.4.3 IM Power Sensitivity to Individual Transmit Carrier Powers

The input drive level to the high power amplifiers in the test facility could be adjusted only in steps of one dB. It was therefore not possible without equipment modifications to maintain a constant total transmit power while varying the transmit carrier power ratio as in the computer exercises of Section 5.3.3. A similar characteristic was, however, investigated as described below.

While maintaining the channel one carrier power fixed, the drive level to the channel two high power amplifier was varied by changing the input attenuator setting in 2 dB steps from 40 dB below to 20 dB above the channel one attenuator setting. The IM power level was recorded on the strip chart recorder after each change in attenuator setting. The channel two power was then fixed while the channel one drive level was varied and IM powers were recorded in a similar manner. It should be noted that transmit power increments in the varied channel were probably slightly less than the 2 dB drive power increments as a result of amplifier nonlinearity. No compensating corrections were made, however, as this small discrepancy was not considered to be important to the overall characteristic being studied. Experiments were conducted sequentially at three different fixed carrier power levels.

The third order characteristics were measured and the test set retuned for fifth order measurements. It was not possible to complete the experiment at fifth order, however, as the diode was destroyed during measurements at the highest fixed carrier power setting

(≈200 mW). The diode was removed from the test jig and a new shunted diode was soldered in its place.

With the second diode*, the higher order characteristics were measured first and care was taken to limit the time during which power was applied for each measurement to avoid overheating. Eleventh, thirteenth, fifteenth, and seventeenth order characteristics were measured. The test set was then retuned for low order measurements. The second diode was destroyed during measurements at third order. As time was limited, no further investigations of this characteristic were made.

The third order characteristics measured with the first diode (diode #1) are plotted in Fig. 5.22. Data from the higher order measurements using diode #2 are plotted in Figures 5.23 to 5.26. Fig. 5.22 shows the third order characteristic measured when the fixed carrier power was 2 mW, as saturation of the receiver low noise amplifier was observed over most of the measurement range in higher power tests. Figures 5.23 to 5.26 show characteristics measured with nominal fixed carrier power of 200 mW as saturation was not a problem. Lower power characteristics are not reported for experiments at the higher order as IM signal powers were above the measurement system noise level over only a limited portion of the varied channel transmit power range used in the experiment.

It is interesting to note for all orders, that in the region of positive carrier power ratios, the IM power decreases even though the total input power is continuously increased as the carrier ratios become larger. Attempts to realize this characteristic using the

* IM signals generated by different diodes vary by approximately ± 5 dB, but the slopes of their power response curves are identical.

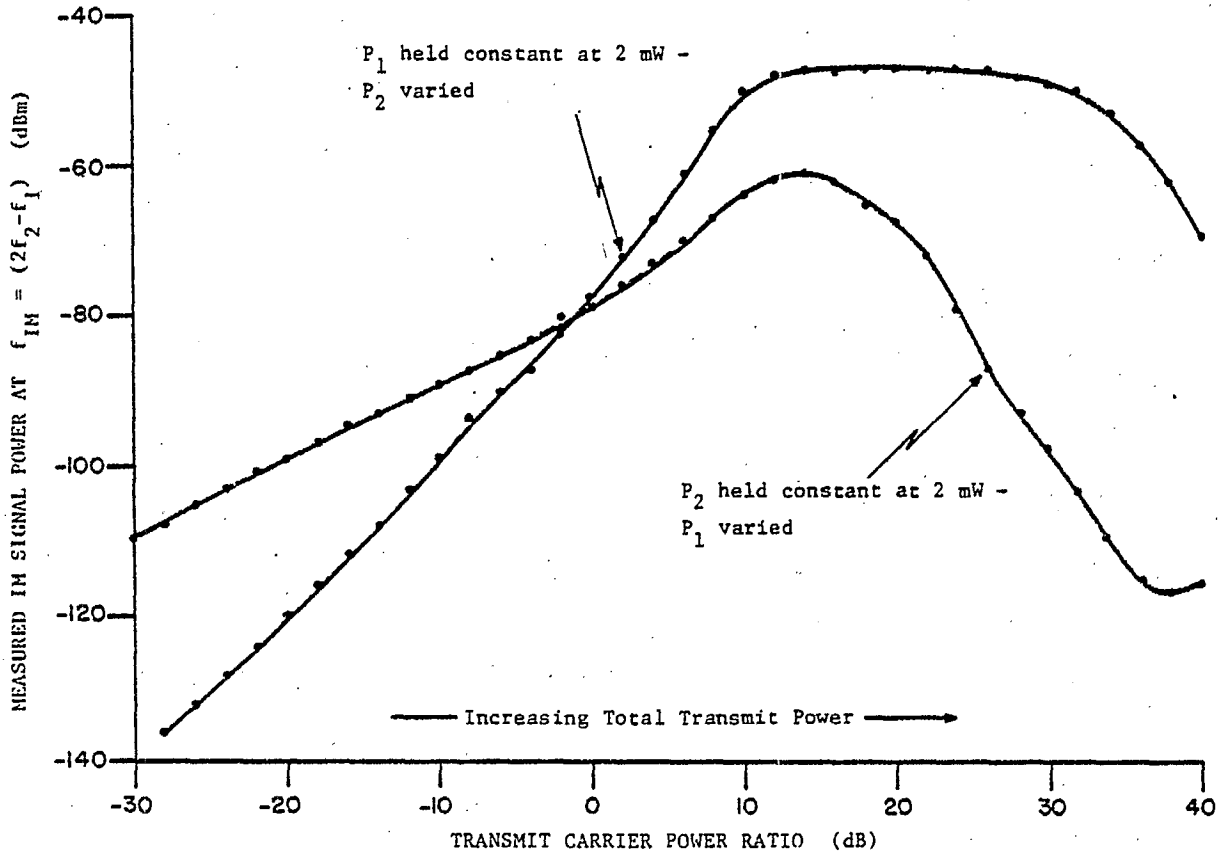

Fig. 5.22. Measured third order IM signal power sensitivity to individual transmit carrier powers, (Diode #1).

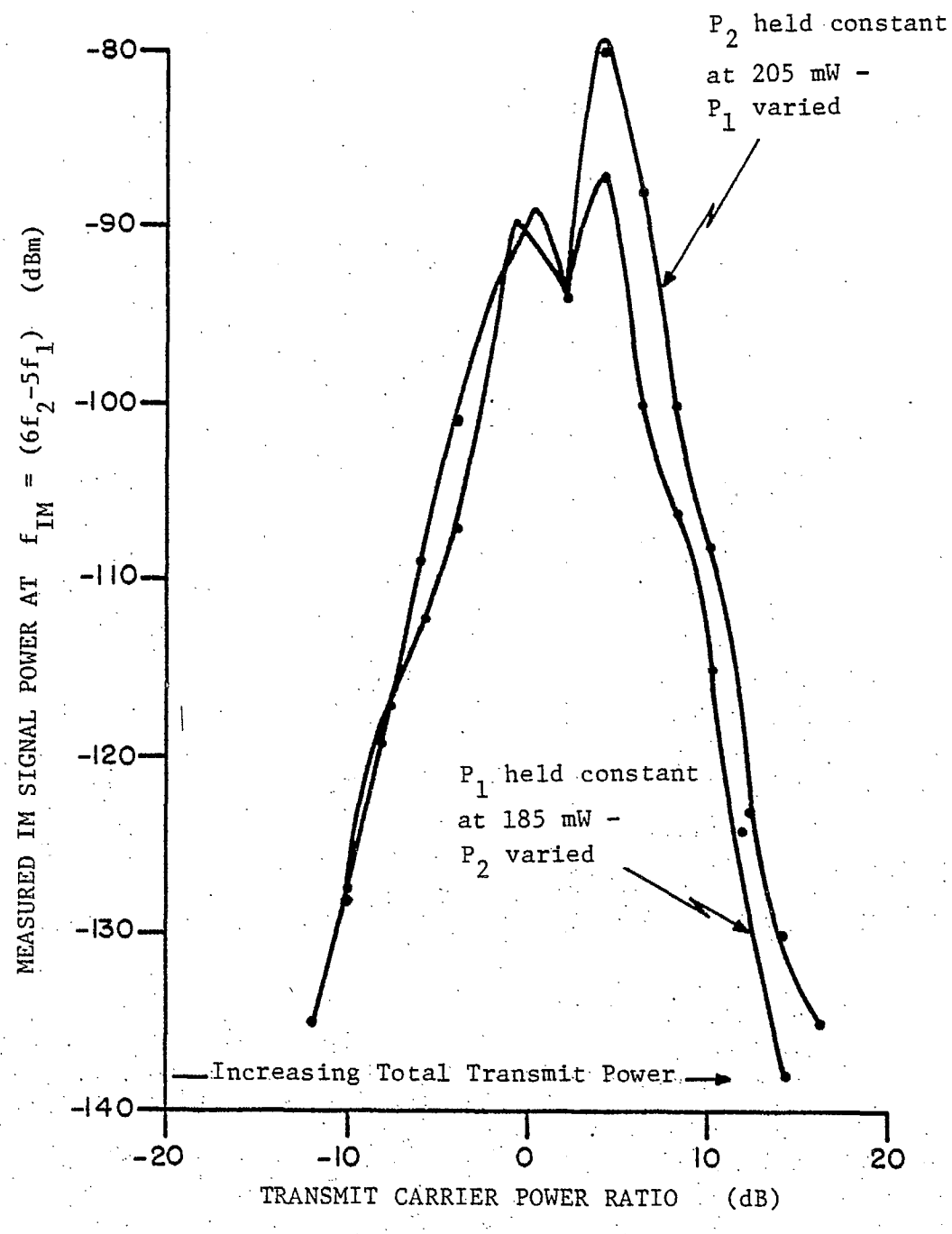

Fig. 5.23. Measured eleventh order IM signal power sensitivity to individual transmit carrier powers, (Diode #2).

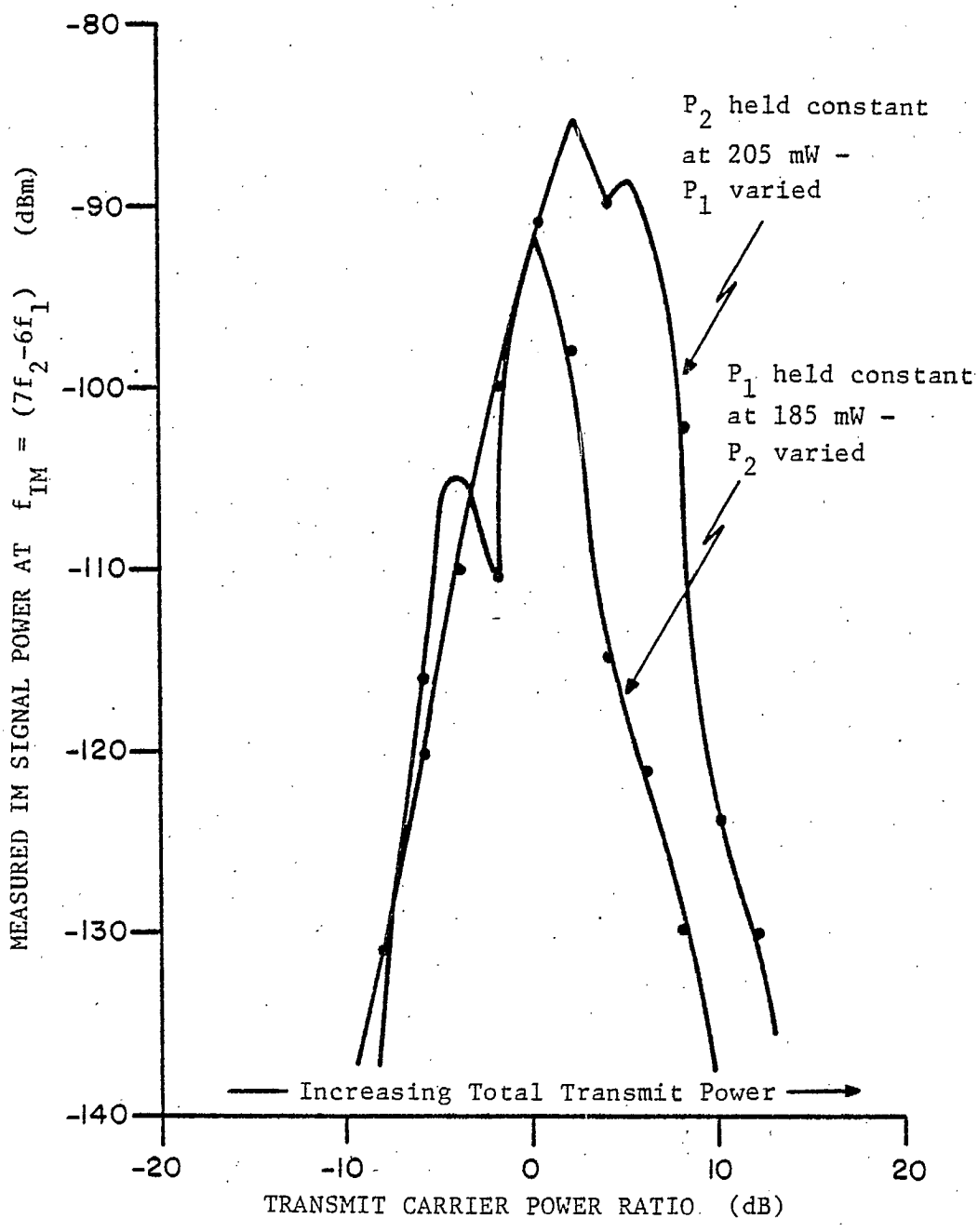

Fig. 5.24. Measured thirteenth order IM signal power sensitivity to individual transmit carrier powers, (Diode #2).

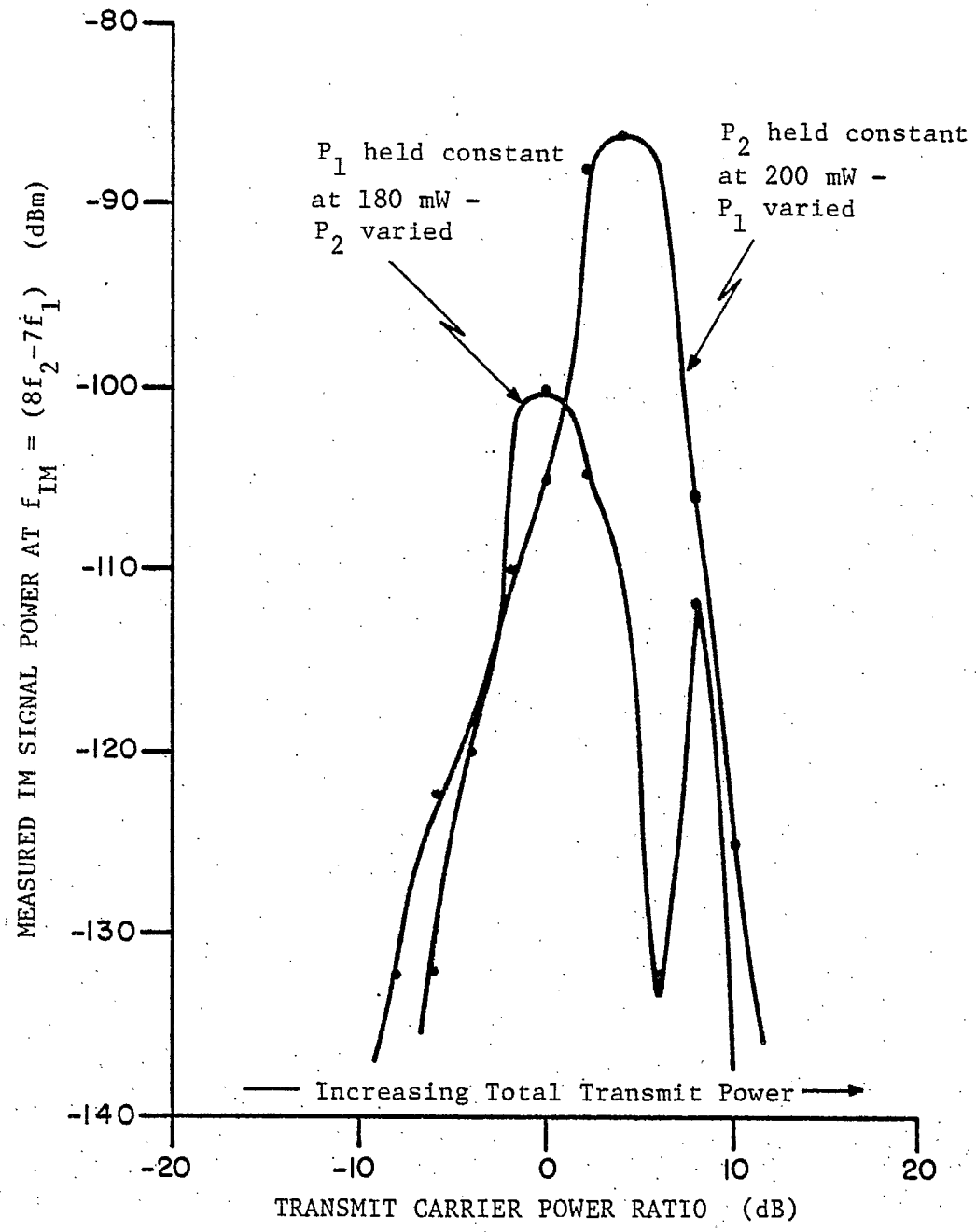

Fig. 5.25. Measured fifteenth order IM signal power sensitivity to individual transmit carrier powers, (Diode #2).

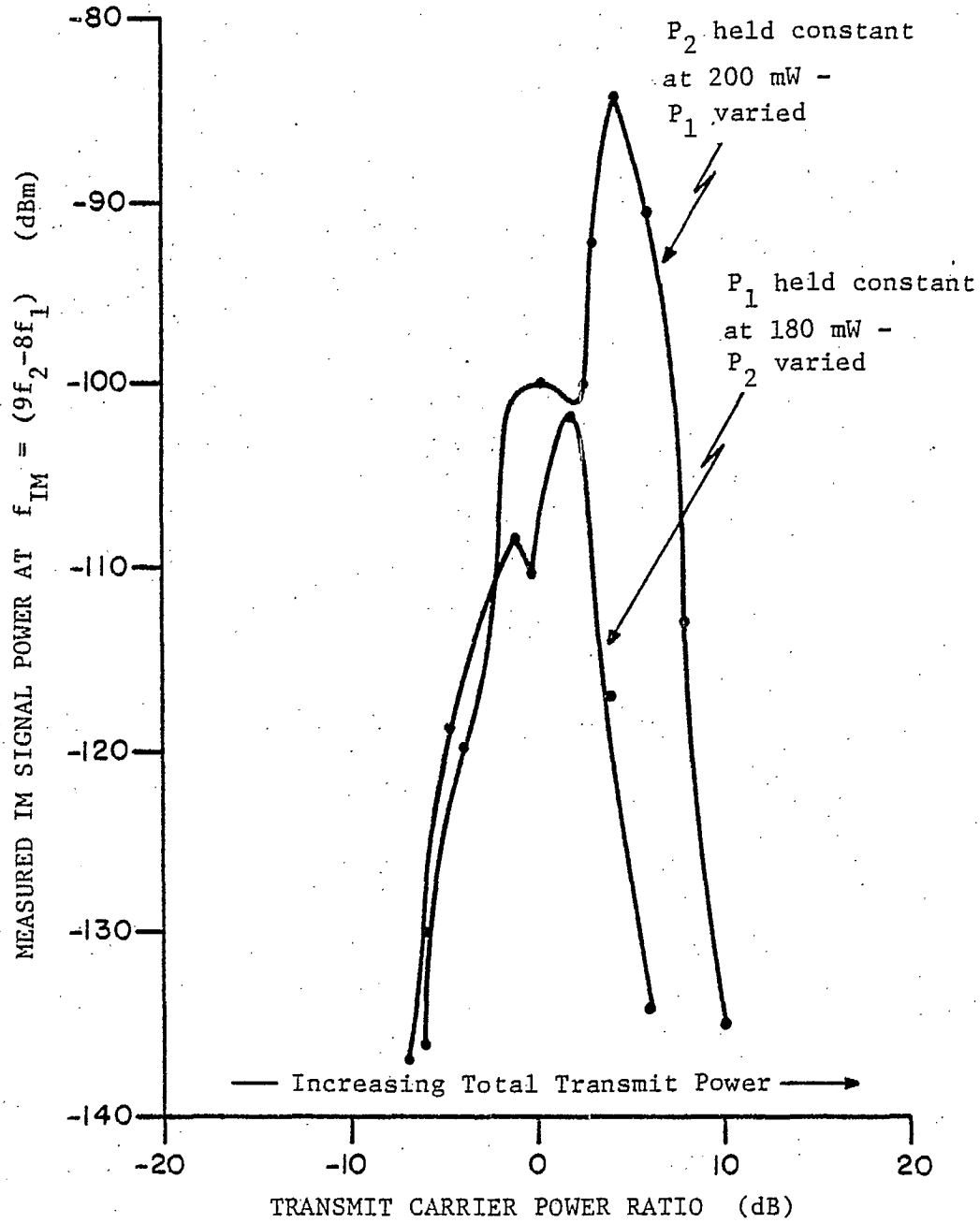

Fig. 5.26. Measured seventeenth order IM signal power sensitivity to individual transmit carrier powers, (Diode #2).

analysis techniques of Section 5.3 have repeatedly failed, showing instead, a general trend toward increasing IM powers as total power is increased, regardless of the carrier power ratio.

The third order characteristic of Fig. 5.22 shows clearly that IM powers decreases more rapidly when P_2, the power of the transmit carrier closest in frequency to the IM frequency is the weakest. At higher orders, the curves become more symmetrical. These characteristics are also true of the computed curves in Section 5.3.3. The measured data also show maximum IM power near unity transmit carrier power ratios as predicted by theory.

Tests at different fixed transmit powers showed that the general characteristics reported in the above paragraphs were true at all input power levels. For higher total input powers (fixed carrier power ≈ 2 W) it was noted that the peaks in some of the higher order characteristics interchanged positions. At lower powers, the double peaks shown in Figures 5.23 to 5.26 were not observed.

5.4.4 IM Power Sensitivity to Individual Transmit Carrier Power Increments

The second diode was replaced by a third, diode #3, and the test jig inserted in the measurement circuit. With equal transmit carriers, the powers of the 3rd to 11th order IM signals displayed on the spectrum analyser were recorded. The drive level to the channel one amplifier was then increased by 3 dB and IM power measurements were repeated. These measurements were repeated once more with the channel one power returned to its original value and the channel two drive

level increased by 3 dB. The difference between powers measured in equal and unequal carrier tests have been plotted against IM order in Fig. 5.27.

Results show a greater IM power response to carrier power changes at f_2, the frequency closest to the IM frequency. The algebraically predicted monotonic power dependence discussed in Section 5.3.4 was, however, not observed. Instead, the difference in IM power changes caused by power increments at f_1 and f_2 varied for different orders with no apparent relationship between order and IM signal power changes.

5.5 Discussion

The first sections of this chapter dealt with the development of a circuit model for a RF system containing a discrete IM signal generator, and the calculation of IM signal powers using two different methods. Although both calculation methods used the same technique for the manipulation of polynomial terms to compute IM amplitudes, results differed in some aspects. These differences were due in large part to the fact that the least squares approximation technique of method A contained both positive and negative coefficients, whereas all coefficients derived from the Taylor series expansion of the Shockley Equation (method B) were positive. The negative coefficients resulted in IM power minima and localized slope changes at particular values of transmit power peculiar to IM signals of a specific order. Such minima were absent from the power curves computed using the polynomial with only positive coefficients. Another factor which influenced the results was the number of terms in the polynomials. Accuracy considerations limited the least squares polynomial to only 12 terms. The polynomial derived

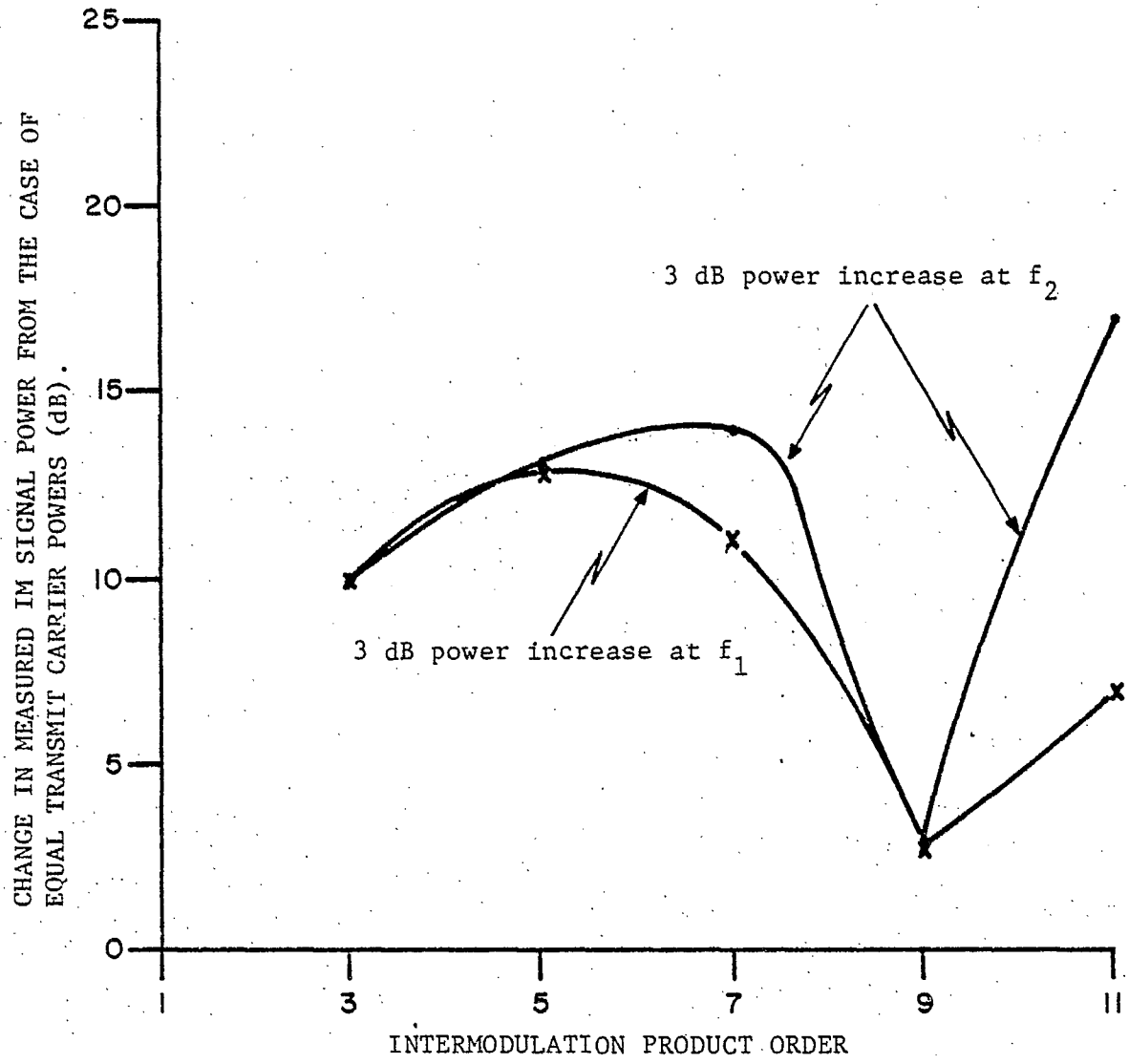

Fig. 5.27. Intermodulation signal power sensitivity to individual carrier power increments, (diode #3).

from the Shockley Equation had 82 terms, and was limited to that number only by programming difficulties. The coefficients of the least squares approximation technique were therefore forced to be larger than the first 12 coefficients of the Taylor Series in order to reflect the same nonlinearity. This resulted in the calculation of consistently higher IM powers when method A was used. Apart from the numerical differences, and the minima exhibited in the data computed from the least squares coefficients, the general trends of the power curves computed by the two methods were similar for low transmit powers, and low IM product orders. The progressive linearization of the higher order IM signal characteristics computed using method A should be noted. This indicates that caution is required when making Nth order IM signal calculations using a polynomial containing only a few more than N terms.

Results of Section 5.3 show that purely algebraic analysis of IM signal characteristics using a limited number of terms in a truncated polynomial such as that in equation 5.3-1 omits two important factors from consideration. These are the magnitudes, and the signs of the polynomial coefficients. Changes in either can have a marked effect on computed characteristics. This is shown by the difference in IM power trends computed using methods A and B.

Work reported in this chapter has revealed that computed IM characteristics are largely determined by the manner in which the terms of the polynomial describing a particular nonlinearity contribute to the amplitude of each IM product. The influence of each term in the polynomial is determined by the size of its associated coefficient, and the amplitude of the signals applied to the nonlinearity. For this reason, it is not possible to specify general rules based on algebraic manipula-

tions regarding the dependence of IM signal amplitudes on transmit signal parameters. Instead, each nonlinearity must be considered separately, and IM calculations must refer to a particular range of operation.

Though general rules cannot be specified, consideration of theoretical and experimental results of this chapter lead to conclusions concerning algebraically determined trends which are often assumed to be the characteristics of all IM signals.

(1) It is generally assumed that the power of an IM signal of order N changes by N dB in response to each dB change in transmit power. Experimental and computed results loosely follow the N dB/dB trend. However, there are two reasons why deviations might be observed in any practical measurement situation. First, local minima, or IM power nulls can occur at particular transmit powers. The measurement of IM power characteristics over a limited range of transmit powers near those which correspond to IM nulls could indicate a wide variety of transmit power/IM power relationships. Secondly, IM power response is very dependent upon the ratio of transmit carrier amplitudes. Measurements using unequal carriers or carriers with varying power ratios could yield results leading to incorrect conclusions.

(2) There is no fixed relationship between the amplitudes of IM product signals of different order. It is usually expected that higher order IM signals have smaller amplitudes. Over the range of transmit signal voltages for which IM powers were calculated, this trend was found to exist. The measured characteristics, however, show that higher order IM signals can have amplitudes significantly greater than those of IM signals of much lower order. The relationship between the amplitudes of different order products is dependent upon drive power. This is

important to consider when testing a system to determine if IM interference levels are below specified maximums. It is not sufficient to measure only low order signal levels, but the amplitudes of signals at all IM frequencies within the receive band must be measured.

(3) The greater sensitivity of IM powers to transmit power changes at one input frequency than to similar power changes at the other frequency is a well known characteristic. Computed and measured results indicate that IM power response to changes in the amplitude of the carrier at the frequency closest to the IM frequency is the greatest. There is no indication, however, that the response is predictable or well behaved. The identification of IM signal orders by observation of IM level changes in response to individual transmit signal power changes is therefore not reliable.

The wide range of IM powers resulting from different transmit carrier amplitude ratios at a fixed total transmit power is not often reported. This characteristic might be used to advantage in reducing IM levels by purposely specifying the use of unequal signal powers in multifrequency communications systems. Loo [31] has suggested this technique for the minimization of IM noise generated in a TWT amplifier.

Explanations cannot be offered for two of the characteristics reported. The nulls in the measured IM power curves are similar to those in the curves plotted from data calculated using the least squares polynomial coefficients. Nulls in the computed curves result from large contributions to a particular IM product amplitude by polynomial terms associated with negative coefficients. This is analagous to the vector addition of out of phase signals in a RF circuit. Practically, however,

multiple signals generated by different portions of the nonlinearity do not exist. Phase cancellation cannot therefore provide an adequate explanation for the nulls. An additional complication arises when one considers the larger number of nulls observed in the higher order characteristics. A possible explanation for this observation is the greater sensitivity of higher order IM signal powers to transmit carrier power ratios. During measurements, the carrier power ratio could have been different at different values of transmit power as a result of high power amplifier nonlinearities.

The other unexplained characteristic is the decrease in measured IM signal powers for positive carrier ratios even though total transmit power increased as the ratio became larger. This appears to be a result of the same factors which cause variations in IM signal amplitudes due to carrier power ratio changes when total input power is fixed. The inability to compute similar characteristics, however, requires further consideration.

A rough comparison of the slopes of the computed and measured IM characteristics shows the closest similarity to exist between measured data and the curves computed from the least squares coefficients. This is a surprising result, as before experiments were conducted, the least squares approximation technique was thought to be unacceptable because nulls, or decreases in IM power as transmit power is increased were thought to be unrealistic.

The value of the characteristics reported in this chapter for the identification of IM interference generated by semiconductor-type non-

linearities cannot be determined until similar studies of IM signals generated by other nonlinear types have been completed. The reported characteristics would be useful only if distinct differences can be found in the power response of IM signals generated by different nonlinearities exposed to the same range of transmit signal powers.

CHAPTER VI

MULTIPACTOR BREAKDOWN

6.1 Introduction

Multipactor breakdown was identified in Chapter II as a phenomenon that can result in the generation of very high levels of intermodulation interference in space satellite communication systems. In addition to generating very strong PIM signals [32], multipacting can lead to physical damage of RF system components. It is therefore imperative that this type of electrical breakdown be eliminated from space systems. This necessitates the understanding of the related physics, and a knowledge of the operating conditions under which multipactor can be expected.

The first five sections of this chapter are devoted to a thorough review of available literature on multipactor breakdown. The basic breakdown mechanism is explained, different types of multipactor are discussed, the effects of breakdown on RF circuitry are pointed out, and preventative measures are suggested.

Section 6.6 describes experiments that were conducted as part of this investigation to determine the effect of metal surface finishes on the conditions required for breakdown.

6.2 The Multipactor Breakdown Mechanism

6.2.1 Basic Breakdown Theory

In RF systems under conditions of high vacuum,[33,34,35,36,37] breakdown can take place between conducting or dielectric surfaces when certain relationships between the dimensions of the space between the surfaces, and the frequency of an applied RF voltage are satisfied. Breakdown occurs if the rate of production of electrons in the gap exceeds the rate of electron loss through diffusion or recombination.

In vacuum, the production of electrons by ionizing collisions is rare. This means [38] that the only mechanism by which free electrons can be produced in a gap between two surfaces is secondary emission due to electron impact at the gap walls if the mean free path for electrons is greater than the gap width. When a RF voltage is applied, a few electrons initially present are accelerated and collide with one wall, where secondary electrons are emitted on impact. The original impinging (primary) electrons are absorbed by the surface. The secondary electrons are then accelerated in the reverse direction during the next half RF cycle, and they too produce secondary electrons as they collide with the opposite gap wall. It is clear [38] that if the secondaries so produced are to be accelerated in a similar manner in the reverse direction before they recombine with the emitting surface, the transit time for an electron across the gap must equal one half cycle of the RF voltage. Also, if breakdown is to occur, the number of electrons in the gap must increase during each half cycle. An average of more than one secondary electron must then be produced upon impact of each of the accelerated electrons with the surfaces. That is, the secondary emission yield, or

secondary emission coefficient (δ) of the gap walls must be greater than unity at the energy with which the primary electrons impinge upon their surfaces.

The number of oscillating electrons in the gap can increase very rapidly to the point at which electrical breakdown occurs. This multiplication of electrons caused by electron impact has been given the name multipacting. The resulting electrical breakdown is thus called multipactor breakdown.

From the above description of Multipacting (MP) one might conclude that, for a given geometry, MP can occur only for a narrow band of applied signal frequencies. The MP frequency band, however, is quite broad [38] due to the fact that electrons cross the gap with widely varying transit times, depending upon the phase (ϕ) of the applied electric field at the time they are emitted from the wall. The MP process also is preferential [38] to certain ratios of initial to final (impact) velocity of the electrons. This ratio is commonly denoted K in the literature, [39] and is used as a constant in theoretical analysis. The most negative phase with which an electron can be emitted from a surface and still cross the gap in $\frac{1}{2}$ RF cycle with the required impact energy to produce secondary emission is a function of K.

There exists a cutoff frequency [38] below which breakdown cannot occur, no matter how large a RF voltage is applied. This has been explained [38] by the fact that as frequency decreases, the phase with which an electron must start at one wall in order to make the transit in

$\frac{1}{2}$ cycle becomes increasingly more negative. At the cutoff frequency, the phase is so negative with respect to the RF field that the electrons, in spite of their initial velocity, are driven back onto the wall by the field, and are lost.

6.2.2 Equations and Breakdown Prediction

A semi-empirical method has been developed [33] for calculating the conditions determined by gap geometry, frequency, and applied voltage under which multipacting can occur. If experimental RF breakdown voltages are plotted versus the product of frequency (f) and gap width (d), two breakdown voltage boundaries are traced, between which MP can occur. These boundaries are determined by the maximum positive and negative phases with which electrons can be emitted at one wall, so that they travel to the opposite wall during $\frac{1}{2}$ cycle of the applied field and produce secondary electrons on impact. These two phase boundaries can be joined at their lower and upper ends by curves corresponding to the minimum and maximum electron energies that are required to produce a secondary electron yield greater than unity. The four curves form a closed region within which MP can be initiated and sustained,* and outside of which MP cannot occur. The maximum energy boundary has never been reported as experimentally having been attained. The upper boundary is therefore not usually plotted in the literature. A typical experimental plot has the shape shown in Fig. 6.1.

Equations have been derived which can be fit to experimental data in order to determine the limiting phase and energy values. The

*Breakdown, once initiated, can be sustained at voltages less than $\frac{1}{3}$ that required for initiation [38].

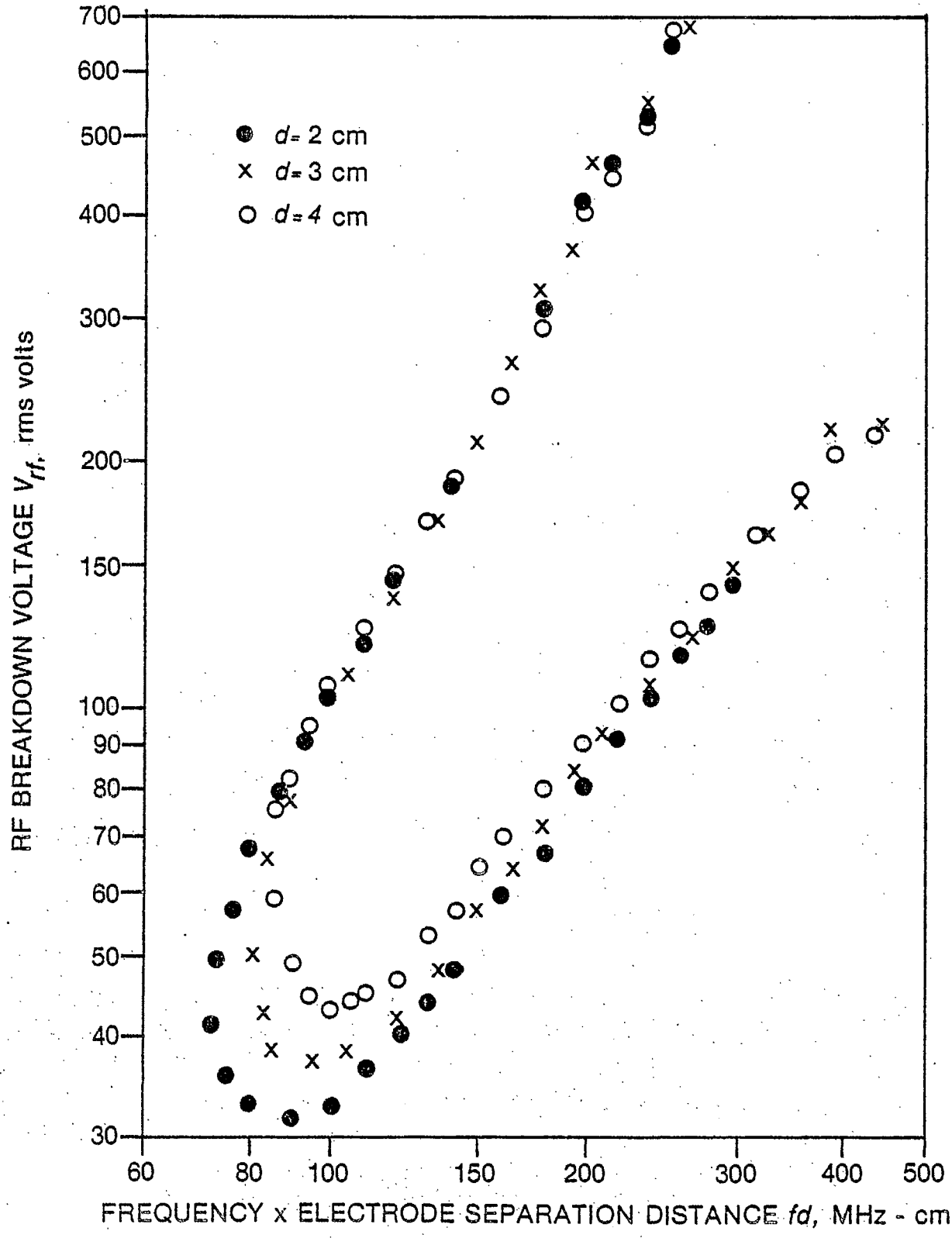

Fig. 6.1. Multipactor RF voltage breakdown boundary for coaxial electrodes with an inner to outer conductor diameter ratio of 2.3, (from Woo [42]).

theoretical development [33,35,40] is short, and can be reproduced here as follows.

Assuming the absence of a space charge, [41] in the gap, and that the applied field is spacially uniform, the equation describing electron motion is;

$$\frac{md^2x}{dt^2} = qE\sin(\omega t + \phi) , \qquad (6.2\text{-}1)$$

where, m is the mass of an electron

q is the electron charge

E is the peak value of the RF field

x represents distance

ϕ is the secondary emission time phase angle

and ω is the radian frequency of the applied voltage.

If one integrates (6.2-1) over the $\frac{1}{2}$ cycle transit time, the velocity of an electron on impact with a gap wall is found to be;

$$\frac{dx}{dt} = v_f = v_o + \frac{2qE\cos\phi}{m\,\omega} \qquad (6.2\text{-}2)$$

where, v_f = electron velocity on impact

v_o = initial electron velocity

A second integration over the same period and a gap width d yields;

$$x = d = \frac{v_o\pi}{\omega} + \frac{qE((2n-1)\pi\cos\phi+2\sin\phi)}{m\omega^2} , \qquad (6.2\text{-}3)$$

where n is the multipacting mode index to be discussed in the following section.

Rearranging, and using $V = \frac{E}{d}$ (6.2-3) gives the multipactor breakdown voltage as

$$V = \frac{4\pi^2(fd)^2}{\frac{q}{m}\Phi_n} \qquad (6.2\text{-}4)$$

where $$\Phi n = \frac{K+1}{K-1} \times [(2n-1)\pi\cos\phi + 2\sin\phi)] \qquad (6.2\text{-}5)$$

$$f = \frac{\omega}{2\pi}$$

and

$$K = v_f/v_o \quad .$$

The lowest RF voltages at which breakdown will occur can be calculated by maximizing Φ_n with respect to ϕ. This gives the emission phase angle value ϕ_L for the lower phase determined breakdown curve as;

$$\phi_L = \tan^{-1}\left[\frac{K-1}{K+1} \cdot \frac{2}{(2n-1)\pi}\right] \qquad (6.2\text{-}6)$$

If one fits (6.2-4) to a lower breakdown curve plotted from experimental data, Φ_n can be found. Simultaneous solution of (6.2-5) and (6.2-6) can then be used to calculate ϕ_L and K.

If K is held constant and ϕ is varied in (6.2-4) to plot a family of breakdown curves, the value of ϕ which traces the upper experimentally determined curve is denoted ϕ_U. This is the maximum secondary emission phase angle permissible if multipacting is to occur.

Finally, the expression $qW_f = \frac{1}{2}mv_f^2$ for the impact energy of an electron can be combined with eqn. 6.2-2 with $K = \frac{v_f}{v_o}$, and (6.2-4)

to give;

$$fd = \frac{(K - 1)\Phi_n}{K\cos\Phi} \cdot \left[\frac{qW_f}{8m}\right]^{\frac{1}{2}} \qquad (6.2\text{-}7)$$

The value of fd at each intersection of the experimentally determined minimum energy cutoff boundary with a member of the family of phase determined curves can be used in (6.2-7) to determine $W_{f\ell}$, the minimum electron impact energy such that $\delta = 1$.

The parameters resulting from the curve fitting procedures outlined above can be ascertained by testing various materials and geometries for their susceptibility to multipacting. These parameters can then be used in the equations for plotting theoretical breakdown curves for components or systems under development to enable the choice of designs such that multipactor breakdown is avoided.

6.2.3 Higher Order Modes

At higher frequencies, or in geometries where the gap width is too great for electrons to travel from wall-to-wall in one half [40] cycle of the RF, the conditions for MP can be met if the time of passage is any odd number(n) of half cycles.

If the appropriate mode index (n) is used in the equations of the previous section, along with the values of K, ϕ_U, ϕ_L and $W_{f\ell}$ obtained for the $\frac{1}{2}$ cycle mode, theoretical breakdown regions can be plotted for the higher order modes. The assumption that $\frac{1}{2}$ cycle mode values can be extended for use in higher order mode analysis is not completely warranted [40], but can be used as a first approximation in predicting higher order breakdown regions.

From plotting the theoretical breakdown boundaries for the higher order modes, one finds that these boundaries overlap and that the extent of overlap increases with mode index.

Experimental data show irregularities in breakdown curves at theoretically predicted points of cutoff for the higher order modes, although an experimentally completed breakdown curve for higher order modes has not yet been reported. The existence of higher order modes has been used to explain [40] the deviation at large values of fd of the lower phase determined boundary from a log-log slope of 2, as predicted by equation (6.2-5).

6.2.4 The Similarity Principle

It has been shown [36] experimentally that under certain conditions gaps with similar geometries exhibit identical breakdown characteristics.

Let V = RF voltage

B = magnetic flux density

f = frequency

v_f = electron velocity on impact

and define ℓ as the characteristic length for the system (any length that characterizes one of a family of configurations that differs only in scale).

Phase similar [41] solutions can be obtained to equations of motion for the electrons in the gap if $\frac{V}{(f\ell)^2}$, $\frac{B}{f}$, and $v_f/f\ell$ are invariant for configurations having different scales. Thus, if MP occurs for one such configuration, it will occur for all other configurations in the family. If $f\ell$ is also invariant under scaling, the energy solutions to the describing equations are similar, and breakdown voltages are identical for similar configurations of different scales.

This similarity principle is most useful when it is applied to geometries in which the electric field is nonuniform. For example, in the coaxial case the differential equations describing electron motion in the field are non-linear and solutions are very difficult. If calculations of electron trajectories are made for a particular configuration in which MP is known to occur, similarity can be used to identify other scaled configurations which are subject to MP, eliminating the need for detailed calculations for every design.

It should be noted that in coaxial geometries where fd is variant [42], the MP region shifts to higher values of RF breakdown voltage for greater values of the inner/outer conductor diameter ratio. This is due to increased nonlinearities of the field, which make it more difficult for MP to occur.

6.3 Multipactor Types

Multipactor breakdown can be classified according to the type and direction of the fields in the gap, and the number of electron emitting surfaces involved in the breakdown mechanism.

Classifications which have been made in the literature [43] are reported in this section.

6.3.1 Two Surface Multipactor

A. RF Electric Field Only, In A Direction Normal To The Gap Walls:

This is the type of MP that has been described in the previous sections. Typical characteristics are:

(i) The mechanism is phase focusing* and only synchronous electrons will multiply. The electrons involved in the breakdown process are therefore tightly bunched in time.

(ii) The discharge associated with breakdown has a relatively low impedance.

(iii) The discharge builds up rapidly and is self sustaining.

(iv) Nearly all the kinetic energy gained by the electrons from the RF field is given up in the form of heat at the gap surfaces upon impact.

The two surfaces involved in this type of multipacting may be conductors or insulators.

B. RF Electric Field and Static Magnetic Field - Both Fields Normal to The Gap Surfaces:

When a static magnetic field is superimposed on the RF electric field, the transit times of the electrons can be adjusted to produce a shift in the boundaries of MP region. This could be used as a means for avoiding MP in a gap of fixed dimensions.

* Phase focusing is defined and discussed in reference 45 and is beyond the scope of this report.

C. Crossed RF Electric and Static Magnetic Fields - Electric Field Normal To The Gap Surfaces:

If a static magnetic field is applied in a direction parallel to the gap surfaces and the RF electric field is applied normal to the surfaces such that the fields are crossed, electron trajectories can be altered by varying the magnetic field strength. The perpendicular magnetic field produces a helical motion of the electrons along an axis orthogonal to the plane of the fields. Thus, application of a transverse field can also be used to shift the MP region for a given configuration. Care must be taken however in this case to avoid the following situations.

(a) If the applied [43] electric field is near the cyclotron frequency, $f_c = \frac{eB}{2m\pi}$ the gyrating electrons in the gap resonate with the electric field and gain energy very rapidly. This causes a reduction in the RF voltage required for breakdown.

(b) If the frequency of the electric field is $\frac{1}{2}$ the cyclotron frequency electrons strike the gap surfaces at grazing incidence. This is a favourable condition for high secondary electron yields and aids in the MP process, again reducing the RF breakdown voltage.

6.3.2 Single Surface Multipactor

A. RF and dc Electric Field in a Direction Normal to the Gap Walls:

If a dc electric field is present in addition to the RF field,

one sided, or single surface multipacting can occur.

Assuming initially that the RF opposes the dc field, an electron emitted from the positively biased side of the gap is pulled away from the emitting surface against the dc field during the first half RF cycle. During the next half cycle, the motion of the electron is reversed, such that it is accelerated towards the emitting wall. Under proper conditions of frequency and field intensity, electrons so accelerated can return to the emitting wall at the end of one RF cycle with sufficient energy to cause secondary emission. This leads to one sided MP breakdown.

Plots of RF voltage versus dc bias voltage [34, 43] for one sided MP in a given geometry form a closed multipactor breakdown region which can be totally dissimilar to the region defined in the RF only case.

This type of MP can occur in geometries where the gap surfaces are dielectric materials when no external dc field is applied. The necessary static field is provided if the dielectric is positively charged. Where the gap walls are metallic, an external field must be applied as no static surface charge can exist.

It should be noted that one sided MP can be initiated at lower RF voltages than the two sided mode and can develop into two sided MP. This in effect lowers the two sided MP breakdown voltage boundary.

B. "Gliding" Single Surface Multipacting -RF Electric Field Only, Parallel to the Gap Surfaces:

For this class of MP to occur, the gap walls must be dielectric,

as the electric field is tangential to their surfaces.

Electrons are emitted at or near the times of zero field and accelerated parallel to the emitting surface. Their initial velocity always has a normal component which will carry them away from the wall. To cause MP they must be returned to the surface at the correct time by a unidirectional electric or static magnetic field which acts as a restoring force.

This type of breakdown can be very powerful and destructive since all kinetic energy derived from the electric field is transferred to the dielectric as heat. Also, since there is no requirement for a definite transit distance, MP can exist over a large range of electric field strengths, limited only by the upper and lower energy boundaries for $\delta=1$. The breakdown in this case is not self-starting unless the restoring force is present but once initiated, it can be sustained due to a static field caused by the space charge of electrons. The initiating force may result from a field due to an accumulation of positive charge on the dielectric surface.

C. Electric and Static Magnetic Fields -- Both Fields Parallel to the Gap Walls:

This is as described in section 3.2.2 above, but the restoring force is provided by a magnetic field acting in conjunction with the initial normal component of electron velocity.

The magnetic field strength may have values of $\frac{1}{2n+1}$ (n is an integer) of the value of magnetic field intensity required for cyclotron resonance at the frequency of the applied voltage.

6.4 Effects of Multipacting

Multipacting is always accompanied by a power loss [35] which is an inherent characteristic of the secondary emission process. An example cited is as follows:

In [35] a linear accelerator, typical input electron energy is approximately 200 eV (60-100 eV in a communications system). If $\delta=2$ the secondary emission energy of each electron has a value between 5 and 10 eV. The RF power loss corresponding to the 180-190 eV difference is dissipated as heat at the gap surface and can be very destructive. In addition, power may be lost as MP electrons ionize any of the few gas molecules which may be present in the gap (due to outgassing of the gap walls perhaps).

Multipactor breakdown has a loading effect on a RF system that can be complex, or purely reactive.

The resistive component of loading is clearly evidenced in the case of two-sided MP by the fact that energy is absorbed from the RF field. Typical electron emission angles which range between $+ 18^{\circ}$ and -60° with respect to the RF electric field suggest that there is also a reactive effect.

Where one-sided [34] MP occurs under conditions of uniform field, electrons are always in flight during an even number of RF half cycles. Net energy cannot, therefore, be gained from the RF field. This type of multipactor breakdown thus appears as a purely reactive load.

In a tuned circuit, the combination of loading [35] and detuning can result in an attenuation of several dB. Heating and mis-

matches caused by MP in transmission line sections can also severely impair a spacecraft communications system.

Of major concern is the nonlinear characteristic of passive components in which MP occurs. Application of a multifrequency RF signal to such a component would result in the generation of intermodulation products.

6.5 Prevention of Multipactor Breakdown

MP can have serious effects on the operation of any RF system, and steps must be taken towards its elimination. Methods that are commonly used to suppress MP in microwave vacuum tubes and linear accelerators along with the disadvantage in applying each method in spaceborne communication systems or satellites are discussed below.

6.5.1 Biasing with a dc Electric Field

As explained in section 6.3.2(A), application of a dc field can significantly modify the MP region and perhaps eliminate breakdown in a given set of circumstances.

Disadvantages, [32] are the possible requirement for high dc voltages, the no doubt complicated biasing circuit that would be required, and the possibility of one-sided MP.

6.5.2 Application of a Static Magnetic Field

Section 6.3.1(B) and 6.3.1(C) discuss the use of a static magnetic field to shift the MP region.

The high voltage requirement might be eliminated [32] by the use of permanent magnets. This would introduce additional weight.

6.5.3 "Conditioning" of the Gap Surfaces

By outgassing [33,38,42] the metal surfaces of an offending gap, it is possible to reduce the secondary emission coefficient, thereby increasing the RF voltage required for breakdown. Disadvantages of this procedure are not immediately apparent, and this may be a viable means for reducing MP in a space application. The extent of outgassing required would depend upon how much the breakdown boundaries must be moved, and the composition of the surfaces.

A possible result of burning could be an increased generation of intermodulation products, as scorched or burned surfaces [6] are very good generators.

6.5.4 Coating the Gap Surfaces

Coating the gap walls with a substance which has a low secondary emission coefficient has been used [43,45,46] effectively to reduce MP. Titanium, Tantalum carbide, Paladium black and Teflon [47] (P.T.F.E.) have all been used for this purpose. It has been found [43] that a film of between 50 and 100 Angstroms in thickness gives satisfactory results, depending upon the energies of electrons incident on the surface.

The drawback associated with the use of coatings is that they are generally more resistive than the covered surface, and therefore introduce increased attenuation. It should be noted that teflon coatings can be used to advantage also in reducing intermodulation [6] generation at metallic junctions where electrical continuity is not required. The possibility of eliminating PIM

from both MP and junction effects with one treatment has obvious advantages and is worth investigation.

6.5.5 Alteration of Gap Dimensions

This is an obvious solution that can be effected by designing components having fd products clear of theoretically predicted MP regions. Gap dimensions should be increased rather than decreased [32], since a decrease in dimensions would still leave field lines of appropriate length.

Prevention by design alteration fails in cases where existing or purchased equipment and components must be used. One must then resort to other means.

6.5.6 Subdivision of the Gap

Thin metallic or insulating baffles [35] can be used to subdivide a gap suspected of MP into smaller gaps narrower than that for MP cutoff. A system of such baffles can be designed to be effective in MP reduction as well as electrically nonperturbing. Partial suppression has been obtained with different numbers of smooth baffles at various spacings. It is interesting to note that only one baffle having a rough etched surface was needed to completely eliminate MP.

6.5.7 Potting the Gap

The potting of gaps [32] with silicon rubber or epoxy has been found effective in the elimination of MP. Care must be taken however, that thermal mismatches can be accommodated and electrical breakdown of air pockets in the potting material does not occur. Another disadvantage is the additional weight.

6.5.8 Making Gap Surfaces Irregular

In accordance with theory the electrons taking part in the MP process must move in a tightly bunched group and travel a definite fixed distance between the gap surfaces during n/2 RF cycles. If the gap surfaces were made irregular by an etching or knurling process, electron emission and impact angles would be widely dispersed, and the required bunching may not be obtained. This might be used for MP elimination and promise of its effectiveness is shown by the complete elimination of MP through using an etched aluminum baffle as reported in section 6.5.6. There is also [42] a tendency for rough surfaces to give low secondary electron yields.

On the negative side [42], it should be noted that when electrons are obliquely incident on the MP surfaces increased secondary emission yields can be obtained. When the angle between the primary "beam" and the normal is 60° or greater the secondary emission coefficient can be increased by more than 50%.

6.5.9 Changing Surface Geometry

The geometry of gap surfaces may play an important role in determining susceptibility to MP.

In the design of some microwave cavities [43], orifice sides are designed in cone shapes to maximize the radial electric field component and minimize the area of opposed (parallel gap surfaces. This has been found effective in eliminating MP due to the strongly curved field which by centrifugal force, throws the electrons outward causing them to lose synchronism with the field.

6.6 Multipactor Experiments

Experiments were performed to test the hypothesis (Section 6.5.8) that multipactor breakdown might be prevented by the use of rough finishes on the surfaces of conductors in vacuum spaced with the required dimensions for breakdown.

Figure 6.2 shows the equipment layout used in the experiments. A single frequency transmit signal is fed from the signal generator, through a directional coupler and into an adjustable gain wideband amplifier. The transmit frequency is monitored by a digital frequency meter connected at the branch arm of the directional coupler. From the wideband amplifier, the signal is applied through a circulator to the parallel plate test jig inside the vacuum chamber (bell jar). A 20 V dc bias is maintained on the fixed plate of the jig to attract electrons during multipactor. Breakdown is detected by monitoring the dc voltage drop across the 100kΩ resistor in the fixed plate electron collector circuit.

At applied powers lower than that required for breakdown, the test jig is an open circuit and has an input reflection coefficient of unity. This permits the convenience of monitoring the transmit power through the circulator as shown in the figure. When multipactor current is detected in the collector circuit the power meter reading is immediately recorded as the breakdown threshold.

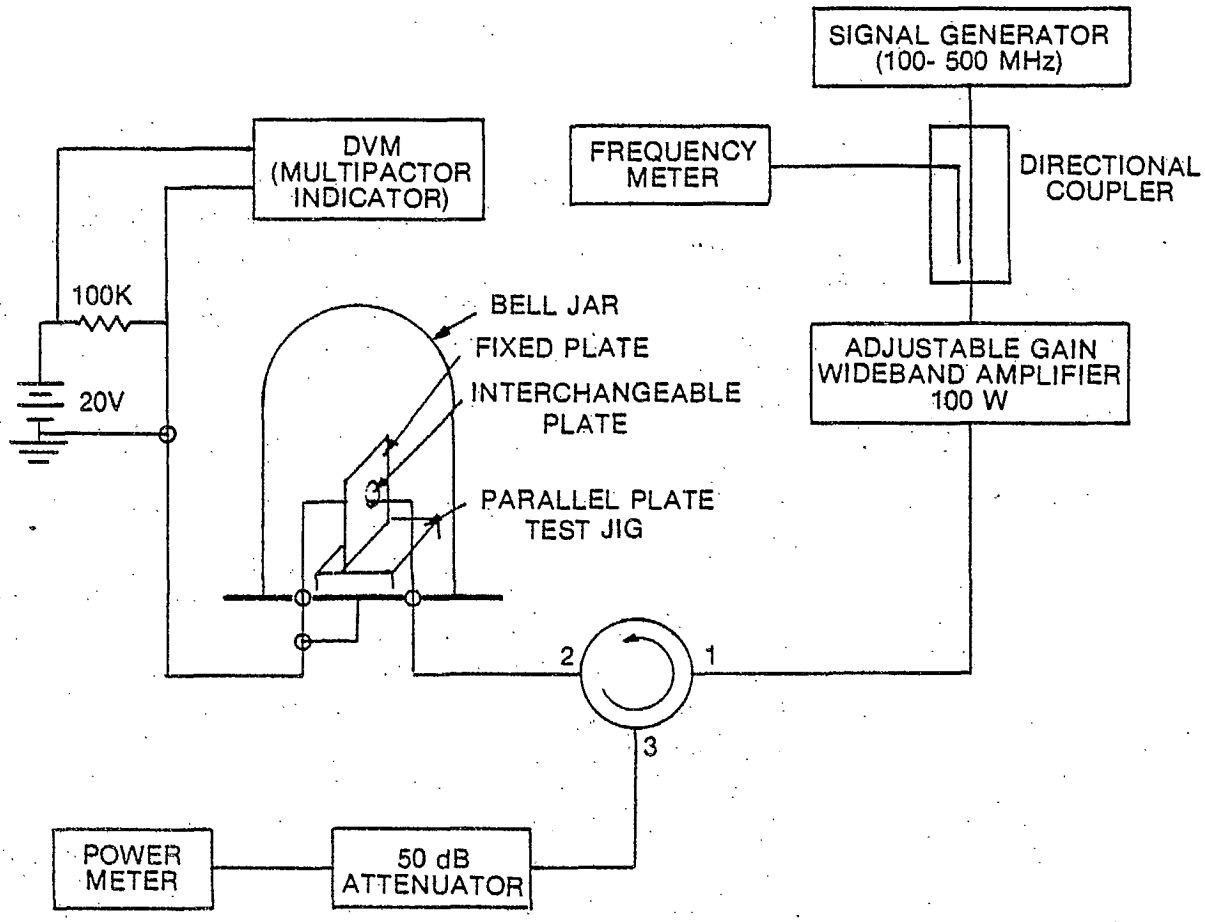

Fig. 6.2. Equipment layout for multipactor breakdown experiments.

Four identically sized interchangeable brass plates, each with a different surface finish, were tested consecutively to determine the effect of surface finish on the multipactor breakdown threshold. Table 6-1 gives a description of the finish on each plate. All tests were conducted using the same separation between fixed and interchangeable plates.*

With each of the interchangeable test plates in the circuit, the transmit power required for breakdown was recorded at 5 MHz frequency intervals (different values of the fd product) within the 100 to 300 megahertz band. After breakdown was detected the transmit power was quickly removed to avoid excessive burning or outgassing. It was therefore not considered necessary to clean the test plates between experiments with the same surface finish at different frequencies. The vacuum in the bell jar was broken only to interchange test plates after each set of threshold measurements.

Only very small differences in breakdown threshold were observed for the four surfaces tested. These differences were attributed to measurement inaccuracies, indicating that surface finish has no influence upon the transmit power required for breakdown. It is very difficult, however to draw conclusions from the limited experiments conducted during this study. A wider variety of experiments using test plates machined from a number of different metals are required to yield conclusive results. Time did not permit the additional investigations required.

*Difficulties were encountered in adjusting the test plates to be parallel. For this reason there may have been small differences in plate separation on consecutive runs with test plates having different surface finishes. The difference in separation between opposite sides of the interchangeable plate was of the order of 40 thousands of an inch.

TABLE 6-1

Brass Test Plates Used in the Multipactor

Breakdown Experiments

Plate #	Decription of Surface Finish
1	Polished surface - ≤maximum surface roughness of 2 μ"
2	Machined to 30 μ" then lapped to 12 μ"
3	Machined to 30 μ"
4	Hard polished to 30μ" then etched to 3μ" for 1 minute in Chromic Sulphuric (a solution of chromic and sulphuric acids)

CHAPTER VII

SUMMARY, CONCLUSIONS AND RECOMMENDATIONS

7.1 Summary

The objective of this investigation has been to gain sufficient knowledge of passive intermodulation phenomena to enable the establishment of guidelines for the design of MUSAT communication system components such that PIM interference can be maintained below the specified maximum level of -120 dBm.

The study began with a thorough review of available literature concerning known sources of PIM and research performed by others attempting to minimize IM interference in similar communications systems. Based upon information gained from the literature review, loose or stressed metallic joints, semiconductor junctions formed at metal/metal-oxide interfaces, electron tunneling through metal oxides, and multipactor breakdown were determined to be the most probable potential sources of PIM in the planned MUSAT system.

Next, a study of different techniques that can be used to calculate the amplitudes of spurious signals at the output from nonlinear circuit elements was conducted. Three methods of analysis were found to be applicable. These included; trigonometric expansion of the terms in a polynomial representation of the transfer characteristic of the IM source,

a more manageable algebraic equivalent, and analysis using a Volterra Functional Series representation of the generating nonlinearity. The difficulty in applying each of these techniques in PIM investigations was recognized to be the requirement for a precise knowledge of the IM producing nonlinearity. In most instances where PIM is encountered, this information is not available as nonlinearities in passive components are not easily detected, and several different phenomena may contribute to the total PIM generated by any single circuit element. Research to develop an analysis technique that would eliminate the requirement for a knowledge of the transfer characteristics of PIM generators was initiated. This resulted in the proposal of a technique based upon the decomposition and spectral analysis of the waveform at the output from a circuit element containing nonlinearities. Limitations of the technique in its present form were discussed and suggestions for additional development work were made.

To prepare for experimental work, a series of preliminary PIM measurements was conducted. This enabled the observation of some of the characteristics noted from the literature review and provided insight into the extreme difficulties in making PIM measurements. The preliminary tests also revealed factors that can influence the level of PIM interference. To determine if equipment malfunctions or laboratory environmental conditions were responsible for difficultities encountered during the preliminary experiments, a complete measurement facility calibration was performed. Results from the calibration showed that the measurement problems were not equipment related. The observed instability and apparently random variations of IM signal powers with time were therefore concluded to be typical PIM characteristics.Repetitive measurements, and

analysis of the results from PIM experiments on a statistical basis was recommended.

The investigation of analytical techniques showed that there are no accurate analytical methods that can be readily applied for calculating the amplitude of IM signals generated in passive circuitry. At the same time, the preliminary experiments showed that it was not possible to make repeatable measurements of IM signal powers. It was obvious therefore that attempts to calculate the power of IM signals generated in particular RF circuits and verify calculations with experimental results would be futile. It seemed possible, however, that the general characteristics of PIM signals generated by particular phenomena could be computed using available methods. It was also considered possible to measure the corresponding characteristics of isolated commercially available, or laboratory prepared test samples. Attention was thus turned to the classification of isolated nonlinear phenomena through combined theoretical and experimental investigation of IM signal trends. It was postulated that these IM signal "signatures" could be used in the identification of PIM generators in functioning RF systems. It was also considered that such investigations would lead to a better ability to anticipate which IM generating mechanisms would predominate in different device configurations or under different operating conditions.

To begin the study of IM signal characteristics, a semiconductor diode was chosen as an IM generator. This choice was in keeping with the earlier identification of semiconductor junctions in metal oxides as a potential source of PIM in the MUSAT system. In addition, the well known nonlinear characteristics of diodes and the immediate availability of test samples made the study of diode-generated PIM an

attractive starting point. The reactive nonlinearities of the diode junction and the package parasitics were neglected in theoretical analysis for simplicity. This allowed direct application of Sea's method for calculating IM signal amplitudes (Section 3.3), and programs were written to compute IM response to changes in transmit (drive) power. A Schottky diode was mounted in a test jig for experiments. It was found, however, that because of the measurement circuit receiver sensitivity threshold of -150 dBm and accuracy limitations which prevented the use of higher transmit power values in theoretical analyses, experimental and theoretical investigations corresponding to operation over the same range of transmit powers were not possible. Experiments were still considered worthwhile, and were conducted using the lowest transmit powers for which IM signals up to 17th order could be observed. Experimental data were used as a guideline to confirm that analytical results were realistic. Conclusions were drawn with regard to the prediction of the behavior of IM signals using purely algebraic, rather than numerical analysis. The use of IM signatures for the identification of IM generators was also discussed.

The problem of multipactor breakdown was addressed in a somewhat separate study from the PIM investigations. First, a literature review was conducted to gain information on the physics of multipactor breakdown, its effects on RF circuitry, and possible methods for its prevention. Since none of the preventative measures suggested in the literature appeared particularly well suited to the MUSAT application,

alternative solutions were sought. It was postulated that breakdown might be avoided if the surfaces of gaps having the required dimensions for multipacting were made irregular. Limited experiments were conducted with a planar gap configuration, and surfaces having a variety of finishes. All samples, regardless of surface finish were found to be susceptible to multipactor breakdown at approximately the same applied power levels. These results were considered inconclusive and it was noted that additional investigations are required.

7.2 Conclusions

At the risk of repetition, conclusions from this study have been divided into five parts. The first four parts contain information compiled from a combination of laboratory experience, and knowledge gained from the literature review. Included are a discussion of factors which influence PIM generation, comments concerning passive RF components, general guidelines for the minimization of PIM, and notes on laboratory and systems assembly procedures. References are given where recommendations are based upon results and conclusions reported by other investigators. Finally, conclusions from the theoretical investigations are presented.

7.2.1 Factors which Influence IM Generation

(1) Current Density

Reports [4,13] indicate that the power of IM signals generated at metal/metal-oxide interfaces and by ferromagnetic inclusions in conductors is proportional to current density. Precautions should be taken to minimize current density where PIM generation is anticipated. Such precautions include the use of conductors with large cross-sectional areas,

and the adjustment of VSWR and transmission line lengths so that standing wave current maximums are displaced from connectors, and other critical parts of the system.

(2) Contaminants

The influence of different conductor and contact surface contaminants (smoke, oil, perspiration, etc.) on PIM generation has not been fully established. It is certain that metal filings and oxidation at metal-metal contacts can enhance IM generation. Some cleaning agents are also suspected of aiding in the production of IM interference. It is best to ensure that system components are kept in sealed containers and handling is kept to a minimum before installation.

(3) Humidity

The ingress of moisture through the jackets and at connectors in coaxial transmission lines can lead to higher IM signal levels [8], as corrosion is accelerated by the presence of moisture. Where there are high potentials, microdischarges between water molecules can also [1] generate PIM.

(4) Thermal variations

Thermal variations can cause dimensional changes in conductors and dielectrics. One result is movement or increased stress at metallic contacts which could cause variations and a possible increase in IM levels.

7.2.2 RF Components in which IM Generation is Probable

(1) RF Connectors

Since metal/metal contacts are an inherent part of RF connectors

there is a high probability that IM signals can be generated at each point where non-permanent circuit connections (e.g. at RF connectors) are made. All the factors which influence IM generation at metal/metal contacts (Section 2.2) are important to consider when choosing (or designing) RF connectors. These include: contact pressure, the composition of the contact materials, contact geometry and surface finish, and corrosion. In addition, connectors for use in space must be designed so as to prevent multipactor breakdown.

Considerations concerning some of these design parameters are as outlined below.

(a) Materials

The use of hard metals at contacts permits the development of more pressure [8] between mating surfaces before deformation occurs. This is advantageous for penetrating surface oxides, but may result in lower contact area than that which can be attained using softer metals. Smaller total contact areas are forced to carry higher current densities leading to a possible increase in IM generation.

Contact materials which readily oxidize (e.g. copper, aluminum) should be avoided.* Gold, silver, rhodium, brass, and beryllium-copper have been found to be suitable materials for low-PIM contacts. [6,7,8]. The first three of these metals are very soft. To provide strength and resilience such metals

---

* Passivated materials have not been evaluated, but there is a chance that the passivation process could leave metal surfaces such that PIM would be enhanced due to mechanisms other than conduction through oxides.

would have to be used as platings on harder base metal connector parts. Ferromagnetic materials should, of course, be excluded from connector designs.

(b) Surface Geometry:

Point contacts permit the development of more pressure between mating surfaces. The larger surface area of spherical, or flat contacts, however, allows for lower current densities. This could lead to correspondingly lower PIM levels, or could preclude the possibility of reducing IM levels by the breakdown of semiconductor junctions that can be brought about by higher current densities.

(c) Multipactor Breakdown

Connectors must be designed so that when properly mated, multipactor breakdown cannot occur. This calls for care to avoid gaps of the required dimensions for breakdown between inner and outer conductors.

Laboratory experience* has shown that crimped joints between connector pieces can lead to high and erratic PIM levels. It is suggested that all connector parts should be soldered or welded together. Return to the previously used connector manufacturing technique of machining the outer conductor contact from one piece which includes the connector body has also been recommended by Young [54].

---

* An experimental evaluation of commercially available connector types was initiated [49,50], but proposed experiments were deferred in preference of conducting other investigations within the time limits set for the project.

Work with type N connectors has revealed that standard rather than precision types are preferable. This is a result of greater contact pressure exerted by the split (fingered) design of the outer conductor contact in standard male connectors. The outer conductor contact in precision male connectors is solid and allows no deformation, resulting in a poorer contact.

(2) Coaxial Cable Transmission Lines

To avoid the possibility of PIM generation by multiple inter-braidwire contacts in flexible cables, it is preferable to use semi-rigid coaxial cable for transmission lines. If, however, the operating environment is such that thermal cycling can occur due to variations in excitation* at high power or alternate periods of eclipse and direct exposure to solar radiation, serious problems can be encountered with semi-rigid cables. Since the thermal coefficient of expansion for normally used space approved dielectrics is greater than that of solid metallic outer conductors, dielectric expansion and contraction with thermal variations can lead to increased stress or movement of the center conductor contact at RF connectors. This could result in greater IM generation. In severe conditions, dielectric expansion can lead to total destruction of coaxial transmission lines by rupturing the outer conductor. These problems would not occur in flexible coaxial cables because of the elasticity afforded by the braided construction of the outer conductor.

---

*In vacuum appreciably greater temperature variations than would be expected in a non-vacuum environment can result from changes in RF excitation.

Investigations associated with work for this contract have resulted in suggested remedies to the dielectric expansion problems in semi-rigid cables [51,52]. These suggestions are listed below with cautionary notes indicating that further investigation is required.

(a) Aluminized teflon tape, white paint, or other surface finishes could be applied to the exterior of the outer conductor to alter its radiation (absorption) properties. The possibility of PIM generation by metallized taped or paints exposed to the antenna fields is a factor which could preclude such coverings as a solution.

(b) Electronically controlled substitute heaters might be used to limit the range of temperature variations. The drawback is that material properties (resistivity, ferromagnetic content, thermal conductivity, etc.) of heater elements could lead to PIM generation as a result of exposure to the transmit antenna fields. The complexity of heater control circuitry must also be considered from a viewpoint of system reliability.

(c) The insertion of expansion gaps and the design of connectors to permit longitudinal dielectric expansion is also a possible solution. It must be ensured, however, that such gaps do not allow multipactor breakdown. Figure 7.1 shows one possible configuration.

If further investigations shows that the difficulties with semi-rigid cables cannot be overcome, braided cables may be a necessity. In this event, the following information from a report on an experimental

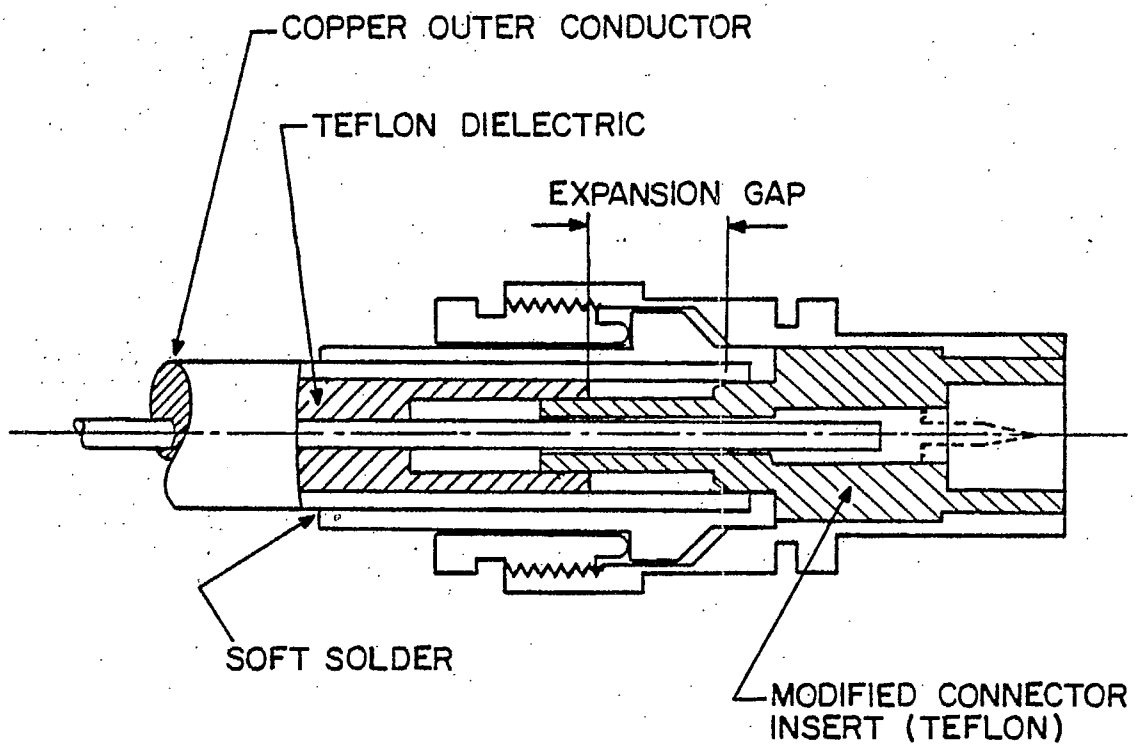

Fig. 7.1 Proposed anti-multipactor/PIM RF connector.

study by Amin and Benson [10] of braided coaxial cables at microwave frequencies should be considered.

(a) The composition of braidwires is of major importance. Braids with aluminium, stainless steel, or nickel-plated copper wires generate strong IM signals. Plain copper wire braids with a good filling factor and adequate inter-braidwire tension result in lower IM levels. Tin-plated, silver-plated, or enamelled copper braids were found to be best for low PIM.

(b) IM power levels increase as cable length increases.

(c) The release of inter-braidwire contact pressure (by the removal of the cable jacket for example) enhances IM generation.

(d) PIM levels generated by braided cables are affected by temperature variations. This results from changes in the volume of the dielectric which cause variations in inter-braidwire contact pressures.

Although electrostriction in dielectrics is a PIM generating mechanism that is considered to be of lesser importance, it should be noted that [13] related IM generation varies in inverse proportion with the square of the bulk modulus of the dielectric. Teflon is particularly bad in this respect, as it has a low bulk modulus.

(3) Antennas

The use of separate receive and transmit antennas for simultaneous two-way communications is preferable from PIM considerations. This mode of operation does not completely eliminate the PIM problem, but may

result in significantly lower IM levels than those generated in duplexed antenna configurations. There are two possibilities for IM generation when separate transmit and receive antennas are used.

(a) Electromagnetic fields at the transmit frequency which are radiated from the transmit antenna can impinge on the receive antenna and IM signals can be generated by nonlinearities in the receive system. The transmit signals captured by the receive antenna will be attenuated not only by the free space loss between antennas, but additional signal reduction will result from the directivities of the antennas at the transmit frequencies. Isolations greater than 50 dB can be provided with typical spacecraft configurations. Since transmit power/IM power characteristics generally (except in the case of localized minima) exhibit dB/dB slopes greater than unity, IM signal power depression should be many times greater than the inter-antenna isolation. For instance, at third order, IM signal depression with respect to the duplexed case might range between 100 dB and 150 dB if 50 dB of isolation between antennas is provided at the transmit frequencies.

(b) IM signals in the receive band can be generated by non-linear mechanisms in the transmit system and radiated toward the receive antenna. In this case, the IM signal depression would be less than in case (a) for two reasons. First, the advantage of the transmit power/IM power slope is lost since the transmit signals could be near full power at the generating nonlinearity.

Secondly, there is no reason to expect that the transmit antenna would be excited properly by IM fields generated in the transmit system at receive band frequencies. The advantage of the transmit antenna directivity might therefore be obliterated, depending upon the location of the IM generator. In a similar situation, PIM signals could be generated in or re-radiated from conducting structures (solar panels, feed supports, etc.) in the transmit antenna fields. IM signal depression would be expected to be greater in this case because of the losses incurred during each of the two radiation processes involved.

As in any other multifrequency RF sections of a communication sytems the choice of antenna and support construction materials is of major importance. Ferromagnetic materials should be avoided. As well, where corrosion at metallic contacts is possible, preventative action should be taken. Considerations which are peculiar to antenna systems are as follows.

(a) If wire meshes are used to form lightweight flexible portions of antenna reflectors, it may be necessary to solder each wire contact or to use punched sheet metal screens as an alternative.

(b) PIM generation has been traced [2] to riveted panel sections in reflectors. The use of metallized tapes over panel junctions (in parallel with the metal junction) to reduce current density at contact points is a possible

solution. Dielectric paints might also be used to capacitively shunt metal/metal contacts.

(c) Joints in deployment mechanisms could be problem areas. Nylon or plastic coverings with plastic rivets through metal members are suggested where adequate strength can be attained.

(d) Rotating joints or moveable feedlines such as those which might be required for mechanically steerable antennas or on despun antenna platforms would almost certainly lead to greater IM levels. Electronic phasing with fixed antennas is an alternative.

(e) Precautions should be taken to avoid multipactor breakdown in feed structures where high potentials can exist.

(4) Solar Panels

Reports [19,20] indicate that solar cells by themselves are not expected to generate strong IM interference as a result of exposure to radiated RF fields from transmit antennas. Solar panel support and attachment mechanisms are, however, a suspected IM source. In addition, associated electronic devices (e.g. steering diodes) can generate strong interference. RF screening and bypass capacitors for such devices are suggested preventative measures.

(5) High Q Structures

In high Q structures the threat of IM generation by conductor heating is enhanced by the presence of high intensity fields. If cavities are filled with solid dielectrics, electrostriction and non-linear dielectric mechanisms could also become significant sources of PIM.

7.2.3 General Guidelines for the Minimization of Passive Intermodulation

The following is a summary of guidelines for RF system and component design which would lead to the minimization of PIM. Trade-offs with other system parameters may preclude the use of suggested remedies under particular operating conditions. These considerations, however, have been discussed in other parts of the report. These guidelines have therefore been made as general as possible within the limitations of practical utility.

(1) Current densities should be kept low where IM generation is anticipated. Some suggestions are as follows.

(a) High pressures should be maintained at metallic contacts to ensure greater current-carrying contact area, and reduced current densities. Greater pressures at contacts also aid in the puncture of oxides in which nonlinear conduction can take place.

(b) Conductors with large cross-sectional areas can be used to effect a reduction in current density when the presence of ferromagnetic inclusions is suspected.

(c) Conducting metallic tapes can be applied over sheet metal seams (e.g. on antenna reflectors or the body of a spacecraft) to minimize the current flowing through intermetallic connection points. Dielectric coatings or non-conducting paints can also eliminate metallic contacts or provide shunt paths for RF currents where dc continuity is not required.

(d) VSWR should be kept low and line lengths should be adjusted to keep standing wave current maximums away from cable interconnections.

(2) In all stages of design, manufacture, and system assembly, extreme care should be taken to avoid the inclusion of ferromagnetic materials in multifrequency RF circuitry.

(a) System and circuit designs should exclude the use of components with ferromagnetic construction. Examples include many types of isolators, circulators, directional couplers, terminations, hermetic seals, paints and epoxies, and structural members. Screws, rivets, hinges and fasteners in all parts of the system should also be nonferromagnetic.

(b) Care should be exercised to avoid the inclusion of ferromagnetic materials in RF components during manufacture. This could necessitate the use of nonferromagnetic tools. All purchased components (e.g. transmission lines and RF connectors) should be scanned for ferromagnetic content before use.

(c) Workbenches should be kept clean and free from metal filings and magnetic dirt. Magnetic dust can be attracted toward regions of high field intensity and become lodged in RF components during system testing.

(3) Metal joints in support structures should be welded or soldered if movement is not required. Where sufficient strength can be attained,

non-metallic (plastic, teflon, nylon, etc.) materials could be used at fixed as well as moveable joints.

(4) The number of non-permanent circuit connections should be minimized. PIM generation is most probable at RF connectors.

(5) Solid jacketed (semi-rigid) transmission lines are preferable. Thermal cycling, however, can lead to problems stemming from the movement of dielectrics. These problems are accentuated when high powers are used in a space environment.

(6) Transmission lines should be fastened in fixed positions and their outer conductors electrically insulated from conducting support structures. Currents on the exterior of the outer conductor could lead to PIM if conducting contacts are permitted.

(7) Precautions must be taken to guard against corrosion in all exposed parts of a communication system. This includes portions of the system where electrical conductivity is not required. This applies particularly to metal/metal junctions formed by metals which oxidize easily (e.g. copper, aluminum).

(8) If diodes or other semiconductor devices are used for sensing and control (temperature sensors, steering diodes on solar panels [19,20], etc.) adequate RF shielding and bypass circuitry must be provided if exposure to RF fields is possible.

(9) It is desirable to use separate rather than duplexed antenna configurations.

(10) Multipactor breakdown must be prevented. Possible preventative measures are outlined below.

(a) Biasing with a dc Electric Field: Application of a dc electric field can significantly modify conditions of geometry and power necessary for multipactor breakdown. Biasing could prevent breakdown where multipacting could normally take place.

(b) Application of a Static Magnetic Field: The presence of a static magnetic field can also make fixed geometries less susceptible to breakdown.

(c) Conditioning of the Gap Surfaces: By outgassing the metal surfaces of a gap having the required dimensions for breakdown it is possible to reduce the secondary emission coefficient of the gap walls, thereby increasing the lower multipactor RF voltage breakdown threshold.

(d) Coating Gap Surfaces: Coating gap walls with a substance which has a low secondary emission coefficient can prevent multipacting.

(e) Alteration of the Gap Dimensions: This is an obvious solution that can be effected by designing components such that inter-conductor spacings lead to fd products which are outside the multipactor breakdown region.

(f) Subdivision of the Gap: Thin metallic or insulating

baffles can be used to subdivide gaps into smaller spaces where multipactor cannot take place.

(g) Potting the Gap: The potting of gaps with silicon rubber or epoxy can be effective in avoiding breakdown. Caution is required in the application of this remedy to ensure that thermal mismatches are accounted for, and that corona breakdown cannot occur in voids within the potting material.

(h) Alteration of Surface Geometries: The shape of gap walls can be designed so that electrons emitted from their surfaces cannot maintain synchronism with the RF fields. Under such circumstances, multipactor breakdown could not occur.

7.2.4 Laboratory and Assembly Procedures

The following recommendations are considered to be good laboratory practice and will result in the maximum use of experimental time, and aid in the reduction of PIM levels in systems under assembly. Several have been standard procedures in RF laboratories for considerable time, but are included for completeness.

(1) Cleanliness is of major importance in ensuring low PIM. All cutting, filing and manufacting processes should be separated from assembly and testing areas.

(2) The use of ferromagnetic tools (screwdrivers, wire cutters, etc.) should be avoided.

(3) Solder joints should be of good quality and made in

accordance with accepted soldering procedures for RF circuitry.

(4) Several inches should be trimmed from the end of coaxial cables before use, as higher moisture content, which could lead to accelerated corrosion is probable near cable ends.

(5) Connector contacts should be cleaned after each time they are used. Immersion in liquid cleaning solutions is not recommended, as contaminants could be washed into inaccessible areas.

(6) Connectors should be examined before use to ensure that proper mating can take place. Bent, or misaligned connector parts can result in very strong PIM.

(7) The identification of spurious signals by observing power response is not reliable. Changing transmitter frequencies and the observation of resulting spurious signal frequency movements is preferable.

(8) PIM generator locations can be traced by adding attenuation at various locations in a circuit. As a result of drive level IM power slopes which are normally greater than unity, PIM levels will be affected most by attenuation added between the transmitter and the IM source.

(9) PIM signals generated by ferromagnetic sources can be identified by noting the influence of externally applied magnetic fields. IM signals generated by other mechanisms should not be affected by magnetic fields.

7.2.5 Conclusions from Theoretical Investigations

Theoretical work began with the trigonometric and algebraic manipulation of terms in an arbitrary polynomial with algebraic coefficients. This analysis showed that:

(a) If the order (N) of an IM product is even, only even-powered terms in the polynomial representation of the generating nonlinearity contribute to the amplitude of the IM signal. Similarly, if N is odd, only odd-powered terms of the polynomial make contributions.

(b) If an IM product is of order N, no contribution is made to its amplitude from terms of a degree less than N. All even (or odd) terms of a degree greater than N contribute if N is even (or odd).

(c) When there are only two transmit frequencies, contributions to the amplitude of a particular IM product by all terms* in the describing polynomial with positive coefficients, have the same phase. The contribution from each term having a negative coefficient is exactly 180 degrees out of phase with the contributions from the positive terms. Direct subtraction is therefore the only type of phase cancellation that can take place. The phase angles of the transmit signals can therefore

---

*This assumes only real coefficients are contained in the polynomial. Polynomial representations with complex, coefficients were not considered (see Section 3.1).

be neglected in IM signal amplitude calculations. If there are more than two transmit frequencies, phase cancellation can arise from the vector addition of IM products of different order at the same frequency. Random phases should be assigned to transmit signals in all calculations (including the two frequency case) when only finite time intervals are considered such as in computer Fourier analysis.

Point (b) above shows that the observation of harmonics from a single frequency input to a circuit nonlinearity cannot be used to determine the coefficients for a polynomial representation of its transfer characteric.

Next, the method for the computation of IM signal amplitudes reported by Sea (Section 3.3) was used in numerical calculations. The objective was to compute the general characteristics of IM signals generated by a semiconductor diode using polynomial coefficients derived from approximations to the measured dc I-V transfer function for the diode. Results were shown to be realistic by comparison with experimentally determined IM power trends. Conclusions drawn from an examination of the computed characteristics are as listed below.

(a) IM characteristics are largely determined by the manner in which the terms of the polynomial describing the nonlinear mechanism contribute to the amplitude of each IM product. The influence of each term in the describing polynomial is determined by the magnitude of its associated coefficient and the applied transmit power. For this reason the response

of IM signals to drive level variations is often significantly different from the response anticipated as a result of non-numerical polynomial manipulations. For example, it is often anticipated that the power of third order IM signals should change by 3 dB in response to each dB change in transmit power. In practice, however, third order power curves can exhibit a wide variety of different slopes, depending upon the range of drive powers used in the measurements.

(b) There is no fixed relationship between the power of IM signals of consecutive order. The ratio of the power in IM signals of different order is dependent upon drive level. This is important to consider when a system is being tested to determine if IM interference specifications have been met. It is not sufficient to measure only the lowest order IM signals (which are normally assumed to be the largest), but measurements should be made at all IM frequencies within the bandwidth of the system receivers.

(c) IM signal powers are very sensitive to the ratio of the transmit signal powers. When there are only two transmit frequencies, third order IM products are largest when the power ratio is 3 dB, the transmit signal at the frequency nearest the IM frequency being the largest. As order becomes larger transmit power ratios corresponding to the peak IM power become closer to unity. For higher orders, the greater sensitivity to variations in power at the frequency closest

to the IM frequency disappears, and the characteristics become symmetrical about the unity power ratio point.

(d) Experimental and theoretical investigations concerning the response of IM signals generated by a semiconductor diode have shown a very great dependence upon transmit power. This is a result of differences in the slope of the diode I-V characteristic in different regions of operation and indicates a definite possibility that IM signals generated by different mechanisms respond with different slopes. No definite conclusions regarding the use of PIM signatures for generator identification can be drawn, however, until further investigations with other discrete generating mechanisms have been completed.

7.3 Topics for Further Investigation

(1) Much more effort is required in the development of a PIM-free RF connector for use at UHF. Emphasis should be placed on the experimental evaluation of different contact designs and manufacturing techniques.

(2) Additional theoretical and experimental work concerning the properties of different materials (dielectric and conducting) that lead to the generation of IM signals is needed.

(3) An investigation of the effect of contact surface contaminants such as smoke, perspiration and corrosion preventatives should be conducted.

(4) The sensitivity of IM power to VSWR at UHF should be measured. For example, the slope of the IM Power/VSWR characteristic for the case in which an RF connector is placed at the standing wave current maximum should be determined.

(5) Radiation experiments are needed to ascertain the PIM generating potential of materials and surfaces that could be exposed to RF fields radiated from transmit antennas. The influence of surface structure with different orientations in the fields, surface roughness, and protective coverings such as paint should be determined. PIM generated by frequency selective surfaces as well as other stripline and microstrip structures should also be investigated.

(6) A study of processes used for manufacturing system components could provide useful information. This might include a review of metal casting, joining, and forming techniques.

(7) Further research is recommended with regard to the possibility of PIM interference cancellation [13] by obtaining a sample of interference generated in a functioning system and adding it to the signal-plus-interference in receive channels with the phase and amplitude adjusted so as to cancel interference at the receiver input. The feasibility of such a scheme was demonstrated in the referenced report. Cancellation of PIM by inserting a diode at a fixed point in the test circuit has been observed in experiments at CRC.

(8) Experimental and theoretical work concerning the characteristics (signatures) of IM signals generated by different nonlinear phenomena should continue. This should include a study of PIM generated by

tunneling, space charge limited current flow, multipactor breakdown and ferromagnetic nonlinearities.

(9) Further development of analytical techniques for the prediction of IM signal levels is required. This effort should concentrate on the elimination of the requirement for a precise knowledge of the nonlinear mechanisms contributing to the total power of IM signals generated by RF components. In particular, the spectral analysis technique proposed in chapter 3 should be tested by experimentation and extended to the case of unequal transmit carriers.

(10) Passive intermodulation in systems with more than two transmit frequencies requires further investigation.

(11) The reduction of IM levels by the deliberate pre-setting of transmit power ratios should be studied.

(12) More work is required to find means for the prevention of multipactor breakdown. Experimentation with typical UHF system components is recommended.

REFERENCES

1. Chapman, R.C. and Darlington, J.C., "Intermodulation generation in normally passive linear components", USASCA Intermodulation Study, Final report on the analytical investigation of intermodulation product generation mechanisms, Report WDL-TR5242, Philco Ford Corporation, Palo Alto, CA, Aug. 1973.

2. Higa, Walter A., "Spurious signals generated by tunneling on large reflector antennas", Proc. IEEE, vol. 63, no. 2, pp. 306-313, Feb. 1975.

3. Sea, R.G., "An algebraic formula for amplitudes of intermodulation products involving an arbitrary number of frequencies", Proc. IEEE (Letters), vol. 56, no. 8, pp. 1514-1515, Aug. 1967.

4. Low, W., "Investigation concerning the development of combination frequencies in the operation of waveguide and coaxial components with several sending frequencies", English translation of article in Frequenz Bd. 17, no.3, pp. 94-102, March 1963, obtained in private communications with C.E. Young, Naval Research Laboratories, Washington, D.C., Nov. 1978.

5. Cox, R.D., "Measurement of waveguide component and joint mixing products in 6-Ghz frequency diversity systems", IEEE Trans. Commun. Technol., vol. COM-18, no.1, pp. 33-37, Feb. 1970.

6. Bayrak, M., and Benson, F.A., "Intermodulation products from nonlinearities in transmission lines and connectors at microwave frequencies", Proc. IEE, vol. 122, no. 4, pp. 361-367, April 1975.

7. Sanli, H., "Non-linear effects in contacts and coaxial cables at microwave frequencies", M. Eng. Thesis, Department of Electrical Engineering, Sheffield University, Sheffield, England, Nov. 1975.

8. Martin, R.H., "Intermodulation generation studies on materials, connectors, and structures", IRE Conference Proceedings, no. 39, Conference on Electromagn. Compat., University of Surrey, Guildford, England, April 1978.

9. Young, C.E., "An update on intermodulation product generation by RF connector hardware containing ferromagnetic materials", National Electronics Packaging Conference, (NEPCON), 1976, West Connector Symposium, Anaheim, CA, Feb. 24, 1976.

10. Amin, M.B., and Benson, F.A., "Nonlinear effects in coaxial cables at microwave frequencies", Electron. Lett., vol. 13, no. 25, pp. 230-231, Dec. 1977.

11. Betts, J.A., and Ebenezer, D.R., "Intermodulation interference in mobile multiple transmission communications systems operating at high frequencies (3-30 MHz)", Proc. IEE, vol. 120, no.11, pp. 1337-1344, Nov. 1973.

12. Wilcox, J.Z. and Molmud, P., "Thermal heating contribution to intermodulation fields in coaxial waveguides", IEEE Trans. Communications, vol. COM-24, no.2, pp. 238-243, Feb. 1976.

13. Royal, E. and Cushner, H., "Communications critical design review package (U) Appendix A", Parts 1 and 2, Report SAMSO-TR-No.-78-38, TRW Systems Group, Redondo Beach, CA, Nov. 1974.

14. Stauss, G.H., "Intrinsic sources of IM generation", Private communication, C.E. Young, Naval Research Laboratory, Washington, D.C., Nov. 1978.

15. Amin, M.B. and Benson, F.A., "Coaxial cables as sources of interference at microwave frequencies", IEEE Trans. Electromagn. Compat., vol. EMC-20, no. 3, Aug. 1978.

16. Bond, C.D., Guenzer, C.S. and Corosella, C.A., "Generation of intermodulation by electron tunneling through aluminum oxide films", Report 8170, Radiation Effects Branch, Radiation Technology Division, Naval Research Laboratory, Washington, D.C., Oct. 1977.

17. Rootsey, J.V., Gradisar, A.A. and Bordenave, J.R.P., "Intermodulation study - Final test report", "Intermodulation products - Satellite ground antennas", Report WDL-TR5243, Philco Ford Corporation, Palo Alto, CA, Aug. 1973.

18. Lindmayer, T. and Wrigley, C.Y., Semiconductor Devices, pp. 77-78, Toronto, New York: Van Nostrand, 1965.

19. Young, C.E., "FLTSATCOM solar panel IMG problem investigation at NRL", Naval Research Laboratory, Technical Memorandum 5430-200A, Washington, D.C., Nov. 1974.

20. Young, C.E., "Additional NRL data relating to solar cell IMG", Naval Research Laboratory, Technical Memorandum 5430-205A, Washington, D.C., Nov. 1974.

21. Bell Telephone Laboratories Inc., Transmission Systems for Communications, Chapter 10, Winston-Salem, North Carolina; Western Electric Co. Inc., Technical Publications, 1971.

22. Javed, A., Syrett, B.A. and Goud, P.A., "Intermodulation distortion analysis of reflection-type IMPATT amplifiers using Volterra series representation", IEEE Trans. Microwave Theory Tech., vol. MTT-25, no. 9, Sept. 1977.

23. Clarke, K.K. and Hess, D.T., Communication Circuits Analysis and Design, Chapter 4, Reading, Massachusetts, Don Mills, Ontario: Addison-Wesley, 1971.

24. West, J.C., Douce, J.L. and Livesley, R.K., "The dual input describing function and its use in the analysis of non-linear feedback systems", Proc. IEE, vol. 103B, pp. 463-474, 1956.

25. Zarkozy, Z.A., "Passive device intermodulation analysis in communications satellites", Paper 76-295, AIAA/CASI 6th Communications Satellite Systems Conference, Montreal, Canada, April 5-8, 1976.

26. Sea, R.G. and Vacroux, A.G., "On the computation of intermodulation products for a power series nonlinearity", Proc. IEEE (Letters), vol. 57, no. 3, pp. 337-338, March 1969.

27. Narayanan, S., "Transistor distortion analysis using Volterra series representation", Bell Syst. Tech. J., pp. 991-1024, May-June, 1967.

28. Bedrosian, E. and Rice, S.O., "The output properties of Volterra systems (Nonlinear systems with memory) driven by harmonic and Gaussian inputs", Proc. IEEE, vol. 59, no. 12, Dec. 1971.

29. Bussgang, J.J., Ehrman, L. and Graham, J.W., "Analysis of nonlinear systems with multiple inputs", Proc. IEEE, vol. 62, No. 8, Aug. 1974.

30. Young, C.E., Private communication, Naval Research Laboratory, Washington, D.C., Nov. 1978.

31. Loo, C., "Calculation of the suppression of signals and intermodulation noise when multiple unequal carriers are amplified by a TWT", Can. Elec. Eng. J., vol. 2, no. 4, pp. 29-32, 1977.

32. Clancy, P.F., "Multipactor control in microwave space systems", Microwave Journal, vol. 21, no. 3, p. 77, March 1978.

33. Hatch, A.J. and Williams, H.B., "The secondary electron resonance mechanism of low-pressure high-frequency gas breakdown", Jour. of Appl. Phys., vol. 25, no. 4, p.417, Apr. 1954.

34. Vance, E.F., "One sided multipactor discharge modes", Jour. of Appl. Phys., vol. 34, no. 11, p.3237, Nov. 1963.

35. Hatch, A.J., "Suppression of multipactor in particle accelerators", Nuclear Instruments and Methods, vol. 41, pp. 261-271, 1966.

36. Woo, R. and Ashimaru, A., "A similarity principle for multipacting discharges", Jour. of Appl. Phys., vol. 38, no. 11, p. 5240, Dec. 1967.

37. Howatson, A.M., An Introduction To Gas Discharges, Pergamon Press: 1965.

38. Gill, E.W.B. and Von Engel, A., "Starting potentials of high frequency gas discharges at low pressure", Proc. Royal Society of London, Vol. A 192, p. 446, 1948.

39. Miller, A., Williams, H.B. and Theimer, O., "Secondary-electron-emission phase angle distributions in high frequency multipacting discharges", Jour. of Appl. Phys., vol. 34, no. 6, p. 1673, June 1963.

40. Hatch, A.J. and Williams, H.B., "Multipacting modes of high frequency gaseous breakdown", The Physical Review, vol. 112, p. 681, Nov. 1958.

41. Francis, G. and Von Engel, A., "The growth of high frequency electrodeless discharge", Trans. Royal Society of London, vol. A 246, p. 19, 1953.

42. Woo, R. "Multipacting discharges between coaxial electrodes", Jour. of Appl. Phys., vol. 38, no. 11, p. 5240, Dec. 1967.

43. Priest, D.H., "Multipactor effects and their prevention in high power microwave tubes", Microwave Journal, p. 55, Oct. 1963.

44. Paschke, F., "Note on the mechanism of the multipactor effect", Jour. of Appl. Phys., vol. 32, p.747, 1961.

45. Talcott, R.C., "The effects of titanium films on secondary electron emission phenomena in resonant cavities and on dielectric surfaces", IRE Trans. Electron Dev., p. 405, Sept. 1962.

46. Zagar, B.A. and Tishin, V.G., "Multipactor discharge and ways of suppressing it", Soviet Physics-Technical Physics, vol. 9, no. 2, p. 234, Aug. 1964.

47. Willis, R.F. and Skinner, D.K., "Secondary electron emission yield behavior of polymers", Solid State Communications, vol. 13, p. 685, 1973.

48. Henney, K., The Radio Engineering Handbook, pp 90-91, New York, London,: McGraw Hill, 1941.

49. Bultitude, R.J.C., "Comparison of type N and type TNC connectors", Carleton University/CRC memorandum, Ottawa, Canada, Aug. 11, 1978.

50. Jaques, P., "TNC connector test # 01-s-c", CRC Space Mechanics Group Memorandum, Communications Research Centre, Ottawa, Canada, Aug. 18, 1978.

51. Wehrle, V., "Thermal expansion of semi rigid coax cable", CRC Memorandum, File # CRC 6656-8 (ST), Space Mechanics Groups, Communications Research Centre, Ottawa, Canada, July 7, 1978.

52. Wehrle, V., "Thermal expansion of coax cable under vacuum and free air laboratory test conditions", CRC Memorandum, File # CRC 6656-8 (ST), Space Mechanics Group, Communications Research Centre, Ottawa, Canada, July 14, 1978.

53. Bailey, G.C. and Ehrlich, A.C., "A study of RF nonlinearities in nickel", Private communications, G.C. Bailey, Naval Research Laboratory, Washington, D.C., Nov. 1978.

BIBLIOGRAPHY

P-1 Low, W., "Untersuchungen uber das Entstehen von Kombinationsfrequenzen beim Betrieb von Hohlleiter-und koaxialen Bautoilen mit mehreren Sendfefrequenzen", Frequenz Bd. 17, no. 3, pp. 94-102, March 1963.

P-2 Low, W., "Investigation concerning the development of combination frequencies in the operation of waveguide and coaxial components with several sending frequencies", English Translation of P-1, private communications with C.E. Young, Naval Research Laboratory, Washington, D.C., Nov. 1978.

P-3 Hallford, B.R. and Ratti, J.N., "Microwave receiver interference characteristic measurements", IEEE Trans. Commun. Technol., vol. COM-14, no.4, pp. 455-469, Aug. 1966.

P-4 Gretsch, W.R., "The spectrum of intermodulation generated in a semiconductor diode junction", Proc. IEEE, vol. 54, no. 11, pp. 1528-1535, Nov. 1966.

P-5 Ebstein, R., Huenemann, R. and Sea, R.G., "The correspondence of intermodulation and cross modulation in amplifiers and mixers", Proc. IEEE (Letters), vol. 55, no. 8, pp. 1514-1515, Aug. 1967.

P-6 Sea, R.G., "An algebraic formula for amplitudes of intermodulation products involving an arbitrary number of frequencies", Proc. IEEE (Letters), vol. 56, no. 8, pp. 1388-1389, Aug. 1968.

P-7 Sea, R.G. and Vacroux, A.G., "On the computation of intermodulation products for a power series nonlinearity", Proc. IEEE (Letters), vol. 57, no.3, pp. 337-338, March 1969.

P-8 Lotsch, Helmut K.V., "Theory of nonlinear distortion in a semiconductor diode", IEEE Trans. Electron Devices, vol. ED-15, no. 5, pp. 294-307, May 1968.

P-9 Cox, R.D., "Measurements of waveguide component and joint mixing products in 6-GHz frequency diversity systems", IEEE Trans. Commun. Technol., vol. COM-18, no. 1, pp. 33-37, Feb. 1970.

P-10 Chapman, R.C. and Darlington, J.C., "Intermodulation generation in normally passive linear components", USASCA Intermodulation Study, Final report on the analytical investigation of intermodulation product generation mechanisms, Report WDL-TR5242, Philco Ford Corporation, Palo Alto, CA, Aug. 1973.

P-11 Worontzoff, N., "Reduction of transmitter intermodulation product signals in airforce communications systems", Rome Air Development Center, Technical Report TR-72-312, Dec. 1972.

P-12 Rootsey, J.V., Gradisar, A.A. and Bordenave, J.R.P., "Intermodulation study - Final test report","Intermodulation products - Satellite ground antennas", Report WDL-TR5243, Philco Ford Corporation, Palo Alto, CA, Aug. 1973.

P-13 Betts, J.A. and Ebenezer, D.R., "Intermodulation interference in mobile multiple transmission communications systems operating at high frequencies (3-30 MHz)", Proc. IEE, vol. 120, no.11, pp. 1337-1344, Nov. 1973.

P-14 Heiter, G.L., "Characterization of nonlinearities in microwave devices and systems", IEEE Trans. Microwave Theory Tech., vol. MTT-21, no. 12, pp. 797-805, Dec. 1973.

P-15 Meyer, H.F., "Small signal suppression with two cascaded limiters separated by a filter", The Aerospace Corporation, Inter-office memo, March 1974.

P-16 Buckles, F.G. and Castrucci, P.E., "Intermodulation interference in multicoupled antenna systems", Sinclair Radio Laboratories Limited, Progress Report no. 512-1, May 1974.

P-17 Chase, W.M., "Ship RFI survey procedure for HF frequencies", Technical Document 336, Naval Electronics Laboratory Center, San Diego, California, June 1974.

P-18 Royal, E. and Cushner, H., "Communications critical design review package (U) Appendix A", Parts 1 and 2, Report SAMSO-TR-No. -78-38, TRW System Group, Redondo Beach, CA, Nov. 1974.

P-19 Young, C.E., "FLTSATCOM solar panel IMG problem investigation at NRL", Naval Research Laboratory, Technical Memorandum 5430-200A, Washington, D.C., Nov. 1974.

P-20 Young, C.E., "Additional NRL data relating to solar cell IMG", Naval Research Laboratory, Technical Memorandum 5430-205A, Washington, D.C., Nov. 1974.

P-21 Nuding, E., "Non-linearities of flange connections in transmission lines carrying high RF power", Proc. 4th European Microwave Conference, pp. 613-618, Sept. 1974.

P-22 Woodward, W.E., "Adjacent channel control techniques", Rome Air Development Center, Griffiss Air Force Base, New York 13440.

P-23 TTCP Subgroup "S" (Technical Panel) STP 1, "Intermodulation product survey", 1975.

P-24 Bailey, G.C., Kamm, G.N. and Ehrlich, A.C., "The generation of harmonic frequencies by nonlinear devices", Progress Report, Naval Research Laboratory , Washington, D.C., Feb. 1975.

P-25 Higa, Walter A., "Spurious signals generated by tunneling on large reflector antennas", Proc. IEEE, vol. 63, no. 2, pp. 306-313, Feb. 1975.

P-26 Guenzer, G.S., "Comment on "Spurious signals generated by tunneling on large reflector antennas" ", private communication, C.E. Young, Naval Research Laboratory, Washington, D.C., 1975.

P-27 Buckles, F.G. and Castrucci, P.E., "Intermodulation interference in multicoupled antenna systems", Sinclair Radio Laboratories Limited, Progress Report 512-2, Feb. 1975.

P-28 Engle, G.M., Conner, D.A. and Steen, W.J., "Determination of intermodulation product amplitudes", Space Systems Center, International Business Machines Corporation, Huntsville, Alabama.

P-29 Ehrlich, A.C., Kamm, G.M. and Bailey, G.C., "Intermodulation generation diagnosis by analytical and computer techniques", Private Communication, A.C. Ehrlich, Naval Research Laboratory, Washington, D.C., Nov. 1978.

P-30 Schelleng, J.H., "Ferromagnetic properties of RF components suspected of intermodulation generation", Technical Memorandum, Naval Research Laboratory, Washington, D.C., Feb. 1976.

P-31 Stauss, G.H., "Intrinsic sources of IM generation", Private communication, C.E. Young, Naval Research Laboratory, Washington, D.C., Nov. 1978.

P-32 Bayrak, M. and Benson, F.A., "Intermodulation products from nonlinearities in transmission lines and connectors at microwave frequencies", Proc. IEE, vol. 122, no. 4, pp. 361-367, April 1975.

P-33 Prochazka, A. and Neumann, R., "High frequency distortion analysis of a semiconductor diode for CATV applications", IEEE trans. Consumer Electronics, vol.,CE-21, no. 2, May 1975.

P-34 Young, C.E., "The danger of intermodulation generation by RF connector hardware containing ferromagnetic materials", Technical Memorandum 5430-180, Naval Research Laboratory, Washington, D.C., Sept. 1975.

P-35 Young, C.E., "An update on intermodulation product generation by RF connector hardware containing ferromagnetic materials", National Electronic Packaging Conference. (NEPCON), 1976, West Connector Symposium, Anaheim, CA, Feb. 24, 1976.

P-36 Wilcox, J.Z. and Molmud, P., "Thermal heating contribution to intermodulation fields in coaxial waveguides", IEEE Trans. Communications, vol. COM-24, no. 2, pp. 238-243, Feb. 1976.

P-37 Zarkozy, Z.A.,"Passive device intermodulation analysis in communications satellites",Paper 76-295,AIAA/CASI, 6th Communications Satellite Systems Conference, Montreal, Canada, April 5-8, 1976.

P-38 Chapman, R.C., Rootsey, J.V., Polidi I. and Davidson, W.W., "Hidden Threat: Multicarrier passive component IM generation", Paper 76-296, AIAA/CASI 6th Communications Satellite Systems Conference, Montreal, Canada, April 5-8, 1976.

P-39 Roscoe, O.S. and Vankoughnett, R., "Report on visit to Hughes Aircraft", Internal report, Communications Research Center, Ottawa, Canada, July, 1976.

P-40 Munzel, F., "Intermodulation products of sinewave carriers and noise in systems with strong nonlinearities", Seimens Forsch.-u. Entwickl.-Ber. Bd. 6, Nr. 3, pp. 125-131, 1977.

P-41 Loo, C., "Calculation of the suppression of signals and intermodulation noise when multiple unequal carriers are amplified by a TWT", Can. Elec. Eng. J., vol. 2, no. 4, pp. 29-32, 1977.

P-42 Matos, F., "A brief survey of intermodulation due to microwave transmission components", IEEE Trans. Electromagn. Compat. vol. EMC-19, no. 3, Aug. 1977.

P-43 Daniels, F., "Trip report: Visit to Naval Research Laboratory, Washington, D.C.", Internal Memorandum, Communications Research Ottawa, Canada, Feb. 1977.

P-44 Rees, G.J., "Signal distortion at a nonlinear element", IEEE Trans. Electromagn. Compat., vol. 19, no. 2, pp. 96-98, May 1977.

P-45 Amin, M.B. and Benson, F.A., "Nonlinear effects in coaxial cables at microwave frequencies", Electron. Lett., vol. 13, no. 25, pp. 230-231, Dec. 1977.

P-46 Ward, Alan A., "Equipment for the remote detection and location of nonlinear targets", IEEE International Conference and Exhibition, Toronto, Canada, pp. 230-231, 1977.

P-47 Bailey, G.C. and Ehrlich, A.C., "A study of RF nonlinearities in nickel", Private communications, G.C. Bailey, Naval Research Laboratory, Washington, D.C., Nov. 1978.

P-48 Martin, R.H., "Intermodulation generation studies on materials, connectors, and structures", IRE Conference Proceedings, no. 39, Conference on Electromagn. Compat., University of Surrey, Guildford, England, April 1978.

P-49 Bultitude, R.J.C., "Passive intermodulation in multifrequency radio communications systems", , Internal report, Dept. of Electronics Engineering, Carleton University, Ottawa, Canada, March 1978.

P-50 Bultitude, R.J.C., "Analysis of frequency combinations causing unwanted intermodulation products", Internal Memorandum, Carleton University/Communications Research Center, Ottawa, Canada, Oct. 1978.

P-51 Hahn, R.F., "MUSAT Passive intermodulation report (Interim)", Technical Memorandum, Serial #85/78, Communications Research Center, Ottawa, Canada, Oct. 1978.

P-52 Hahn, R.F., "MUSAT Multipactor report (Interim)", Technical Memorandum, Serial #84/78, Communications Research Center, Ottawa, Canada, Oct. 1978.

P-53 Bultitude, R.J.C., "Multipactor breakdown", Internal Memorandum, Carleton University/Communications Research Center, Ottawa, Canada, May 1978.

P-54 Bultitude, R.J.C., "Progress with theoretical work on the subject of passive intermodulation", Internal Memorandum, Carleton University/Communications Research Center, Ottawa, Canada, Oct. 1978.

P-55 Amin, M.B. and Benson, F.A., "Coaxial cables as sources of interference at microwave frequencies", IEEE Trans. Electromagn. Compat., vol. EMC-20, no. 3, Aug. 1978.

P-56 Young, C.E., "Connector design techniques to avoid RFI", Private communication, C.E. Young, Naval Research Laboratory, Washington, D.C., Nov. 1978.

P-57 Bond, C.D., Guenzer, C.S. and Carosella, C.A., "Generation of intermodulation by electron tunneling through aluminum oxide films", Report 8170, Radiation Effects Branch, Radiation Technology Division, Naval Research Laboratory, Washington, D.C., Oct. 1977.

P-58 Martin, R.H., "Non-linearity in RF cables and connectors", ERA Report 2885, under DCVD Research Project RP 34-11, Contract N/CP 541/73, Final Report, April 1976.

P-59 Martin, R.H. and Williams, A., "Measurement of intermodulation products at UHF in aircraft related situations", ERA Report 3082, under RAE Contract K/LR 236/376, Sept. 1976.

P-60 Martin, R.H. and Williams, A., "Non-linearity in RF cables and connectors-supplementary results at UHF", ERA Report 77-2022, DCVD Research Project RP 34-17, Oct. 1977.

P-61 Martin, R.H., "Predictions of IP levels over the frequency range 20 MHz-5 GHz", ERA Report 77-2021, DCVD Research Project RP 34-17, Sept. 1977.

P-62 Martin, R.H. and Williams, A., "Non-linearity in HF coaxial lines", ERA Report 77-2023, DCVD Research Project RP 34-17, Final Report, 1978.

P-63 Price, Gary B. and Khan, Peter J., "Large signal analysis of semiconductor circuits with multifrequency excitation", Proc. IEEE, vol. 67, no. 1, pp. 177-178, Jan. 1979.

P-64 Maseng, Torleiv, "On the characterization of a bandpass non-linearity by two-tone measurements", IEEE Trans. Communications, vol. COM-26, no. 6, June 1978.

P-65 Sanli, H., "Non-linear effects in contacts and coaxial cables at microwave frequencies", M. Eng. Thesis, Department of Electrical Engineering, Sheffield University, Sheffield, England, Nov. 1975.

P-66 Chapman, R.C., Polidi, I. and DeHaven, "METTRA Producibility investigation", Report WDL-TR-5880, Aeronutronic-Ford Corporation, Palo Alto, CA., June 1975.

P-67 Elsner, R.F., "Comments on "Coaxial cables as sources of intermodulation interference at microwave frequencies"", IEEE Trans. Electromagn. Compat., vol. EMC-21, no. 1, Feb. 1979.

APPENDIX A

TRIGONOMETRIC EXPANSION OF THE COSINE TERMS IN THE POWER SERIES OF EQUATION 3.2-2

Equation (3.2-2) relates output current from a given non-linear circuit element resulting from an applied voltage V as

$$I = a_o + a_1V + a_2V^2 + a_3V^3 + a_4V^4 + a_5V^5 \qquad \text{(A-1)}$$

where,

$$V = E_1\cos(\omega_1 t + \phi_1) + E_2\cos(\omega_2 t + \phi_2)$$

Using the appropriate trigonometric expansions of V, the spurious components generated by each term of (3.2-2) can be calculated to be as listed below.

I The a_o term results in only a d.c. component, "a_o"

II Components of the a_1 term are:

$$a_1E_1\cos(\omega_1 t + \phi_1) \quad + \quad a_1E_2\cos(\omega_2 t + \phi_2)$$

III Components of the a_2 term are:

$$a_2\left[\frac{E_1^2}{2} + \frac{E_2^2}{2}\right] + a_2\frac{E_1^2}{2}\cos(2\omega_1 t + 2\phi_1) + a_2\frac{E_2^2}{2}\cos(\omega_2 t + 2\phi_2)$$

$$a_2E_1E_2\cos[(\omega_1 + \omega_2)t + \phi_1 + \phi_2] + a_2E_1E_2\cos[(\omega_1 - \omega_2)t + \phi_1 - \phi_2]$$

IV Components of the a_3 term are:

$$a_3[\tfrac{3}{4}E_1^3 + \tfrac{3}{2}E_1E_2^2]\cos(\omega_1 t + \phi_1)$$

$$+ a_3[\tfrac{3}{4}E_2^3 + \tfrac{3}{2}E_1^2E_2]\cos(\omega_2 t + \phi_2)$$

$$+ \frac{E_1^3}{4} a_3\cos(3\omega_1 t + 3\phi_1) + a_3\frac{E_2^3}{4}\cos(3\omega_2 t + 3\phi_2)$$

$$+ \tfrac{3}{4}a_3E_1^2E_2\cos[(2\omega_1 - \omega_2)t + 2\phi_1 - \phi_2]$$

$$+ \tfrac{3}{4}a_3E_1^2E_2\cos[(2\omega_1 + \omega_2)t + 2\phi_1 + \phi_2]$$

$$+ \tfrac{3}{4}a_3E_1E_2^2\cos[(2\omega_2 + \omega_1)t + 2\phi_2 + \phi_1]$$

$$+ \tfrac{3}{4}a_3E_1E_2^2\cos[(2\omega_2 - \omega_1)t + 2\phi_2 - \phi_1]$$

V Components of the a_4 term are:

$$a_4[\tfrac{3}{8}E_1^4 + \tfrac{3}{8}E_2^4 + \tfrac{3}{2}E_1^2E_2^2]$$

$$+ a_4[\frac{E_1^4}{2} + \tfrac{3}{2}E_1^2E_2^2]\cos(2\omega_1 t + 2\phi_1)$$

$$+ a_4[\frac{E_2^4}{2} + \tfrac{3}{2}E_1^2E_3^2]\cos(2\omega_2 t + 2\phi_2)$$

$$+ a_4\frac{E_1^4}{8}\cos(4\omega_1 t + 4\phi_1) + a_4\frac{E_2^4}{8}\cos(4\omega_2 t + 4\phi_2)$$

$$+ a_4[\tfrac{3}{2}E_1^3E_2 + \tfrac{3}{2}E_1E_2^3]\cos[(\omega_1 + \omega_2)t + \phi_1 + \phi_2]$$

$$+ a_4[\tfrac{3}{2}E_1E_2^3 + \tfrac{3}{2}E_1^3E_2]\cos[(\omega_1 - \omega_2)t + \phi_1 - \phi_2]$$

$$+ \frac{3}{4}a_4E_1^2E_2^2\cos[(2\omega_1 - 2\omega_2)t + 2(\phi_1 - \phi_2)]$$

$$+ \frac{3}{4}a_4E_1^2E_2^2\cos[(2\omega_1 + 2\omega_2)t + 2(\phi_1 + \phi_2)]$$

$$+ \frac{a_4}{2}E_1^3E_2\cos[(3\omega_1 - \omega_2)t + 3\phi_1 - \phi_2]$$

$$+ \frac{a_4}{2}E_1^3E_2\cos[(3\omega_1 + \omega_2)t + 3\phi_1 + \phi_2]$$

$$+ \frac{a_4}{2}E_1E_2^3\cos[(3\omega_2 - \omega_1)t + 3\phi_2 - \phi_1]$$

$$+ \frac{a_4}{2}E_1E_2^3\cos[(3\omega_2 + \omega_1)t + 3\phi_2 + \phi_1]$$

VI Components of the a_5 term are:

$$a_5[\frac{5}{8}E_1^5 + \frac{15}{4}E_1^3E_2^2 + \frac{5}{8}E_1E_2^4]\cos(\omega_1t + \phi_1)$$

$$+ a_5[\frac{5}{8}E_2^5 + \frac{15}{4}E_1^2E_2^3 + \frac{5}{8}E_1^4E_2]\cos(\omega_2t + \phi_2)$$

$$+ a_5[\frac{5}{16}E_1^5 + \frac{5}{4}E_1^3E_2^2]\cos(3\omega_1t + 3\phi_1)$$

$$+ a_5[\frac{5}{16}E_2^5 + \frac{5}{4}E_1^2E_2^3]\cos(3\omega_2t + 3\phi_2)$$

$$+ \frac{a_5}{16}E_1^5\cos(5\omega_1t + 5\phi_1) + \frac{a_5}{16}E_2^5\cos(5\omega_2 + 5\phi_2)$$

$$+ a_5[\frac{15}{8}E_1^2E_2^3 + \frac{5}{4}E_1^4E_2]\cos[(2\omega_1 + \omega_2)t + 2\phi_1 + \phi_2]$$

$$+ a_5\left[\frac{15}{8}E_1^2E_2^3 + \frac{5}{4}E_1^4E_2\right]\cos[(2\omega_1 - \omega_2)t + 2\phi_1 - \phi_2]$$

$$+ a_5\left[\frac{15}{8}E_1^3E_2^2 + \frac{5}{4}E_1E_2^4\right]\cos[(2\omega_2 + \omega_1)t + 2\phi_2 + \phi_1]$$

$$+ a_5\left[\frac{15}{8}E_1^3E_2^2 + \frac{5}{4}E_1E_2^4\right]\cos[(2\omega_2 - \omega_1)t + 2\phi_2 - \phi_1]$$

$$+ \frac{5}{8}a_5E_1^3E_2^2\cos[(3\omega_1 + 2\omega_2)t + 3\phi_1 + 2\phi_2]$$

$$+ \frac{5}{8}a_5E_1^3E_2^2\cos[(3\omega_1 - 2\omega_2)t + 3\phi_1 - 2\phi_2]$$

$$+ \frac{5}{8}a_5E_1^2E_2^3\cos(3\omega_2 + 2\omega_1)t + 3\phi_2 + 2\phi_1]$$

$$+ \frac{5}{8}a_5E_1^2E_2^3\cos[(3\omega_2 - 2\omega_1)t + 3\phi_2 - 2\phi_1]$$

$$+ \frac{5}{16}a_5E_1^4E_2\cos[(4\omega_1 + \omega_2)t + 4\phi_1 + \phi_2]$$

$$+ \frac{5}{16}a_5E_1^4E_2\cos[(4\omega_1 - \omega_2)t + 4\phi_1 - \phi_2]$$

$$+ \frac{5}{16}a_5E_1E_2^4\cos[(4\omega_2 + \omega_1)t + 4\phi_2 + \phi_1]$$

$$+ \frac{5}{16}a_5E_1E_2^4\cos[(4\omega_2 - \omega_1)t + 4\phi_2 - \phi_1]$$

APPENDIX B

DERIVATION OF A CLOSED FORM EXPRESSION FOR THE SUM OF TWO COSINUSOIDAL CARRIERS HAVING DIFFERENT AMPLITUDES

Let

$$V = E_1 \cos\omega_1 t + E_2 \cos\omega_2 t, \; E_1 \neq E_2 \qquad \text{(B-1)}$$

To obtain a single frequency time domain expression for (B-1), consider the representative phasor diagram shown in Fig. B.1.

Let

$$\omega_2 = \omega_1 + \Delta\omega \quad .$$

Then,

$$R = E_1 \cos\omega_1 t + E_2 \cos(\omega_1 + \Delta\omega t)$$

$$= \text{Re}\{E_1 e^{j\omega_1 t} + E_2 e^{j(\omega_1 + \Delta\omega)t}\} = \text{Re}\{\hat{R}\}$$

Splitting up the second exponential, and division by E_1 gives

$$\hat{R} = E_1 e^{j\omega_1 t}[1 + \frac{E_2}{E_1} e^{j\Delta\omega t}]$$

$$= E_1[1 + \frac{E_2}{E_1}(\cos\Delta\omega t + j\sin\Delta\omega t)]e^{j\omega_1 t}$$

$$= E_1[1 + \frac{E_2}{E_1}\cos\Delta\omega t + j\frac{E_2}{E_1}\sin\Delta\omega t]e^{j\omega_1 t}$$

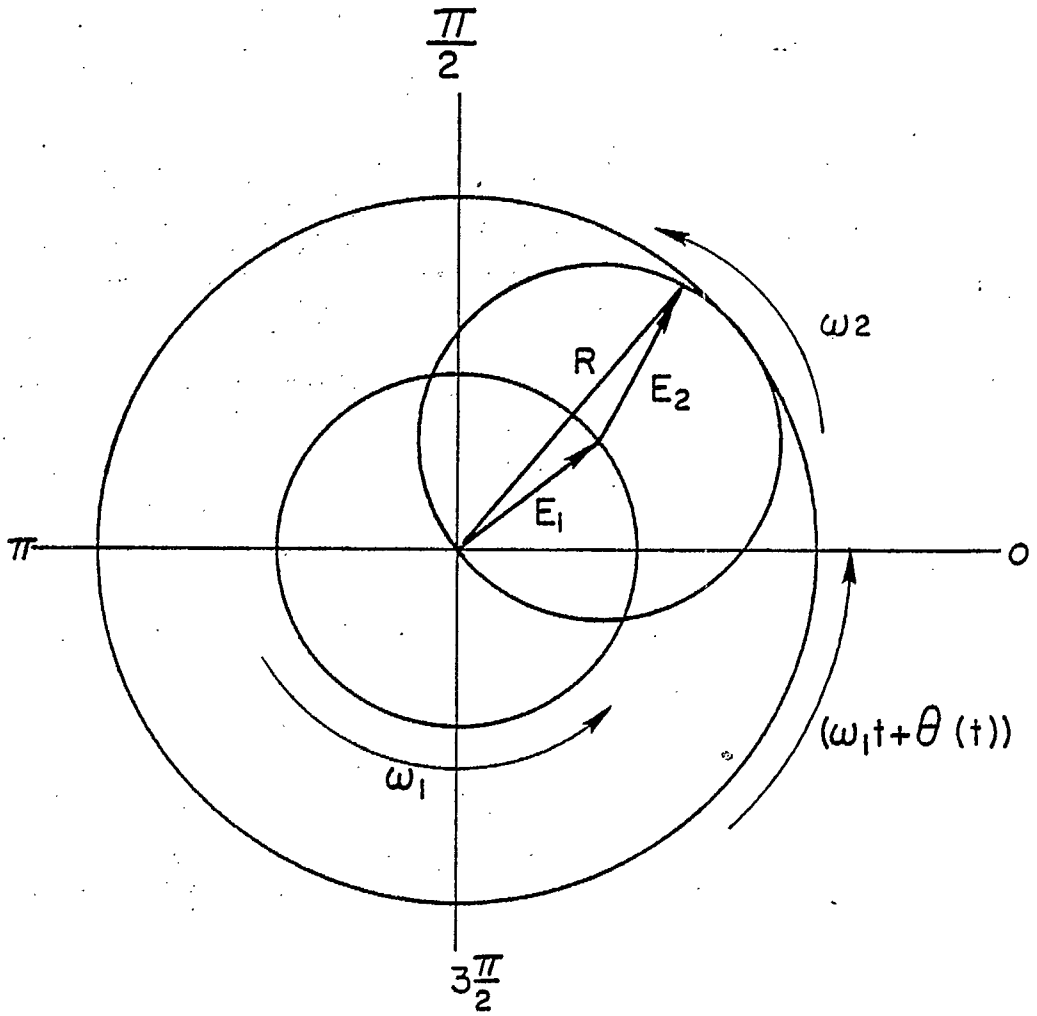

Fig. B.1 Phasor diagram representing the sum of two cosine waves.

In phasor form

$$\hat{R} = |R|e^{j\underline{/R}}$$

where,

$$|R| = E_1\sqrt{\left(1 + \frac{E_2}{E_1}\cos\Delta\omega t\right)^2 + \left(\frac{E_2}{E_1}\sin\Delta\omega t\right)^2}$$

$$= E_1\sqrt{1 + 2\frac{E_2}{E_1}\cos\Delta\omega t + \left(\frac{E_2}{E_1}\right)^2}$$

and

$$\underline{/R} = \omega_1 t + \theta(t)$$

where

$$\theta = \tan^{-1}\left[\frac{\frac{E_2}{E_1}\sin\Delta\omega t}{1 + \frac{E_2}{E_1}\cos\Delta\omega t}\right]$$

Then

$$R = \mathrm{Re}\{\hat{R}\}$$

$$= E_1\sqrt{1 + \frac{2E_2}{E_1}\cos\Delta\omega t + \left(\frac{E_2}{E_1}\right)^2}\cos(\omega_1 t + \theta(t)) \qquad \text{(B-2)}$$

This equation represents a time dependent waveform having amplitude modulation and phase jitter.

If $E_1 = E_2$, equation B-2 becomes

$$R = E_1\sqrt{2(1 + \cos\Delta\omega t)}\cos\left[\omega_1 t + \tan^{-1}\left[\frac{\sin\Delta\omega t}{1 + \cos\Delta\omega t}\right]\right]. \qquad \text{(B-3)}$$

Now, from mathematical tables,

$$\frac{\sin\Delta\omega t}{1 + \cos\Delta\omega t} = \tan\left(\frac{\Delta\omega t}{2}\right)$$

and

$$\sqrt{\frac{1 + \cos \Delta\omega t}{2}} = \cos \frac{\Delta\omega t}{2}$$

Substitution of these identities in eqn. B-3 gives

$$R = 2E \cos \frac{\Delta\omega t}{2} \cos(\omega_1 t + \frac{\Delta\omega t}{2})$$

and using $\Delta\omega = \omega_2 - \omega_1$ yields

$$R = 2E \cos[\frac{\omega_2 - \omega_1}{2}]t \cos [\frac{\omega_2 + \omega_1}{2}]t$$

for the sum of two cosine waves of equal amplitude, E.

APPENDIX C

MODIFICATIONS TO TYPE N MALE/MALE RF ADAPTORS AND TYPE N BULKHEAD CONNECTORS WHICH HAVE BEEN FOUND TO RESULT IN LOWER, MORE STABLE PIM LEVELS

Figures C.1 and C.2 on the following pages show modifications that were made to standard commercially available RF connectors to reduce PIM powers and maintain better PIM stability.

Figure C.1 shows a modification that was made to type N male connectors to reduce PIM levels. The silicon rubber washers were removed from the connectors and the underlying compression joint was soldered. It was thought best not to replace the rubber washer after the modification to permit easier connector cleaning. It was found, however, that the washer is necessary to prevent overtightening and deformation of the connector threads which results in higher PIM signal levels.

Fig. C.2 shows how a standard female/female type N adapter was modified for use in place of the bulkhead connector on the test facility dummy load. This arrangement proved to result in a more stable "residual" test set PIM power level.

These modifications were proposed and prepared by Hahn at CRC.

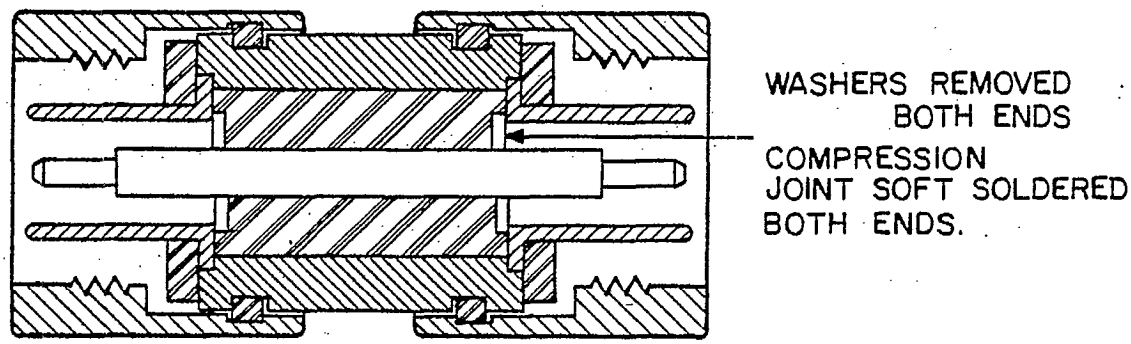

Fig. C.1 Modification to type N male/male RF adapter.

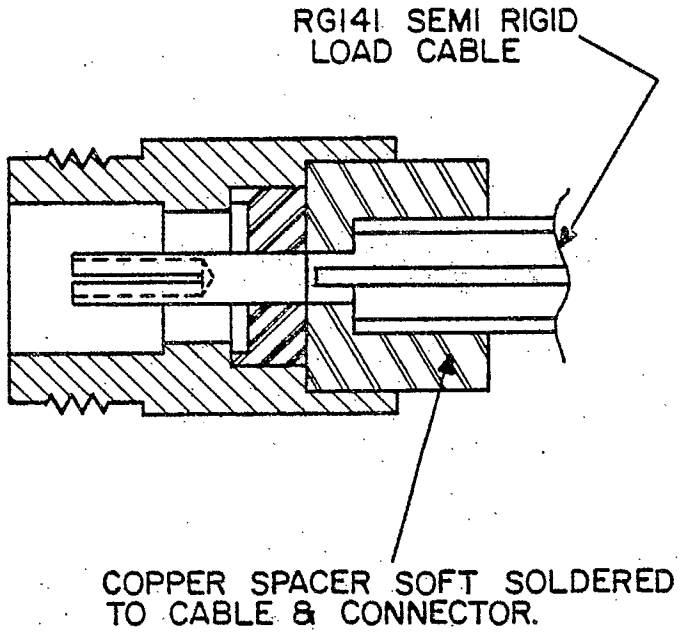

Fig. C.2 Modified type N female/female adapter used to replace the bulkhead connector on the PIM test facility dummy load.

APPENDIX D

ESTIMATION OF THE MINIMUM VOLTAGE DEVELOPED ACROSS THE DIODE DURING PIM EXPERIMENTS

In the experiments of Section 5.4, it was necessary to use sufficient transmit powers to generate IM signals that could be measured above the -150 dBm noise floor of the measurement system.

To define a suitable minimum total transmit power for use in all experiments, a preliminary test was performed with the diode* in the test circuit. The transmitter drive levels were adjusted to produce two equal amplitude RF signals at the test port such that the displayed third order IM signal level was approximately 10 dB above the system noise level. The driver attenuator settings were recorded before turning the transmitters off. The diode was then removed from the circuit and replaced by a 30 dB directional coupler with the standard 50 ohm test facility load connected at the through port, and a power meter connected at the branch arm. With the transmitter drive levels that produced the IM signal 10 dB above noise, the power (P_{out}) at the test port was found to be 43 mW. Although it is recognized that a small change in power would result from mismatches with the diode connected in the circuit, this value was used to calculate the voltage applied to the diode at the defined minimum transmit power of 43 mW. Calculations are as follows.

Reference to The Radio Engineering Handbook [48] shows that the inductance of a straight round copper wire at 300 MHz - 400 MHz

---

*This test was performed using diode #1.

can be estimated using the equation

$$L = 0.002\,\ell\,(2.303 \log_{10} \frac{4\ell}{d} - 0.988)$$

where

L = inductance in μH

ℓ = wire length in cm

d = wire diameter in cm.

For the 5mm length of #28 (d = 0.032 cm) copper wire used to shunt the diode, this equation gives L = 0.0032 μH.

The reactance (X_L) of the shunt is therefore 6 ohms at 300 MHz (transmit band) or 8 ohms at 400 MHz (receive band).

Now, if it is assumed that the diode current is low in comparison with that carried by the shunt at 43 mW of transmit power, the diode impedance can be omitted from voltage calculations. Under these conditions the voltage applied across the diode (see Fig. 5.15) can be calculated from

$$V_d = \frac{X_L}{(X_L+50)} \sqrt{P_{out} \times 50}$$

$$= \frac{6}{56} \times 1.47$$

$$= 157 \text{ mV.}$$

From Table 5-1, the diode current corresponding to a voltage of 150 mV is 0.4 μA. For 157 mV across the 6 ohm wire shunt, the current is 26 mA. The initial assumption of low diode current in comparison with the shunt current has therefore been verified, and 157 mV is a reasonable estimation for the diode voltage at 43mW of transmit power.

For higher transmit powers the diode voltage is markedly non-sinusoidal and is very difficult to calculate. In this range of operation the diode current becomes the independent variable and the voltage developed across the diode can be calculated from a known diode current using Bessel Function techniques [23]. Consideration of the fact that curve fitting techniques cannot be extended to accurately cover operation above 60 mV, however, shows that it would be futile to pursue reported techniques for calculating diode voltages above the calculated minimum of 157 mV.

APPENDIX E

COMPUTER PROGRAMS "IMPWR" AND "IMAMP"

E.1. Program IMPWR

Program IMPWR calculates the power of specified IM products resulting from a two frequency input to the IM generating nonlinearity using the method derived by Sea (Section 3.3). The program is based upon an algorithm reported by Sea and Vacroux [26].

E.1.1 Program Inputs

The following are the program inputs in the sequence in which they are requested.

(1) The number of coefficients in the polynomial representation;

$$Y = a_0 + a_1X + a_2X^2 + a_3X^3 + \ldots\ldots\ldots + a_nX^n \qquad \text{(E.1.1)}$$

(2) The coefficients (a_0 to a_n) of the polynomial.

The maximum number of coefficients permissible is 100.

(3) Program Options:

(a) OPTION:

i) If OPTION = "1", the power of a single specified IM product at the frequency (A2F2 - A1FA1) is calculated, where A1 and A2 are inputs to the program.

ii) If OPTION = "2", the power of all odd order IM products between a specified minimum (MINORD $\geq$ 1 and odd) and a specified maximum (MAXORD) are calculated. In this case IM frequencies are fixed at f_{IM} = (A2F2-A1F1), where A2 is incremented in steps of "1" from A2=(MINORD + 1)/2. The maximum value for MAXORD is dependent upon the coefficients and the power of the transmit signals.

(b) PARTSUM:

i) If PARTSUM = "1", the program outputs the partial sums (Appendix A) associated with each coefficient in the describing polynomial. This permits determination of the relative influence of each term on the computed IM signal amplitudes.

ii) IF PARTSUM = "2" the partial sums are not printed. This is the normal mode of operation.

(4) EN:

EN may have the values:

"1" if it is desired to calculate the dc component in the output from the nonlinearity. This must be used in conjunction with OPTION = 1 and A1 = A2 = 0. (See Eqn. 3.3-20-a).

or "2" if it is desired to compute IM product amplitudes.

(5) The fifth set of input variables requested by the program is dependent upon OPTION.

(a) If OPTION = "1" (for the power of a single IM product) the program will request values for:

ORDER - the IM order of interest

A1 - the f_1 multiplier

A2 - the f_2 multiplier

E1 - the amplitude of the transmit signal (V or I) at f_1.

E2 - the amplitude of the transmit signal at f_2.

(b) If OPTION = "2" (for the amplitudes of IM products of consecutive odd orders between MINORD and MAXORD) the program will request values for:

MAXORD - the highest IM order of interest.

MINORD - the lowest IM order of interest.

E1 - the amplitude of the transmit signal at f_1.

E2 - the amplitude of the transmit signal at f_2.

It should be noted that IMPWR is an interactive program and will request each input from the operator at the appropriate time after the "RUN IMPWR" command has been entered. Instructions and parameter definitions are given each time the program requests an input.

E.1.2 Program Outputs

The program outputs the polynomial coefficients in a list immediately after the last coefficient has been read in. This allows time to check for errors before proceeding. Thereafter, the form of the output from the program is dependent upon the options chosen.

(a) If OPTION = "1", the program outputs the following data in sequence.

ORDER

A1

A2

E1

E2

IMO - the order of the computed IM product (IMO should equal ORDER)

AMP - the absolute amplitude of the computed IM product

PWR - the relative amplitude of the computed IM product (PWR = 10 $\log_{10}$ (AMP^2)+30)

(b) If OPTION = "2", the program outputs the following data in sequence.

MAXORD

MINORD

E1

E2

IMO - the order of the <u>first</u> computed IM product

AMP - the absolute amplitude of the first computed IM product

PWR - the relative amplitude of the first compute IM product (PWR = 10 $\log_{10}(AMP^2)+30$)

IMO - the order of the second computed IM product

.

.

.

etc. (information repeated for each IM order)

.

.

.

(c) If PARTSUM = "1" with OPTION = "1" or "2", the program will print the input data as in (a) and (b) above, then the partial sums will be printed as follows.

J = the IMOth index of the coefficient A(J)

F1 = $(A(J) \times J!)/2^J$

PHI(2,I) = $\Phi(2,I)$
see program explanation (Section E.1.3)

F2 = F1 x PHI(2,I)

J - the index of the (IMO + 1) th coefficient

.

.

.

etc. (information repeated for each coefficient)

.

.

.

The program then outputs:

IMO

AMP

PWR

in the normal fashion.

When the program is finished the operator is requested to enter "1" if another run is desired. This eliminates the necessity to enter the polynomial coefficients each time the input parameters are changed.

E.1.3 Program Explanation (IMPWR)

Program IMPWR is based upon an algorithm reported by Sea and Vacroux [26].

First, the magnitude of the IM product wave represented by eqn. 3.3-20 is written for the case of two transmit signals in the form:

$$Y_{IM_N} = \varepsilon_N \prod_{i=1}^{2} A_p^{|\alpha_p|} \sum_{L=0}^{\infty} \frac{a_{N+2L}(N+2L)!}{2^{N+1}} \Phi(2,L) \qquad (E.1\text{-}2)$$

*

where $$\Phi(2,L) = \sum_{q_1} \cdots \sum_{q_M} \prod_{p=1}^{2} \frac{A_i^{2q_i}}{(q_p+|\alpha_p|)!q_p!}$$

$$q_1 + \cdots + q_M = L$$

It can be shown [26] that

$$\Phi(1,q) = \frac{A_1^{2q}}{(q+|\alpha_1|)q!} \qquad (E.1\text{-}3)$$

and, $$\Phi(2,q) = \sum_{q_2=0} \frac{A_2^{2q_2}}{(q_2+|\alpha_2|)!q_p!} \Phi(1,q-q_2) \qquad (E.1\text{-}4)$$

Thus [26] if it is desired to compute Y_{IM_N} by eqn. E.1-2 truncated at $L = L_0$, it is necessary to compute $\Phi(2,L)$ for $L = 0,1,\ldots,L_0$. Program IMPWR computes $\Phi(2,L)$ iteratively by first computing $\Phi(1,q)$ for $q = 0,1,\ldots L_0$ using eqn. E.1-3, then computing $\Phi(2,q)$ for $q = 0,1,2\ldots L_0$ using eqn. E.1-4. Values for Y_{IM_N} are then computed by substitution in eqn. E.1-2.

---

* $\varepsilon_N = 1$ for dc calculations, or 2 for IM calculations (see eqn. 3.3-20)

E.1.4. Program Flow Chart (IMPWR)

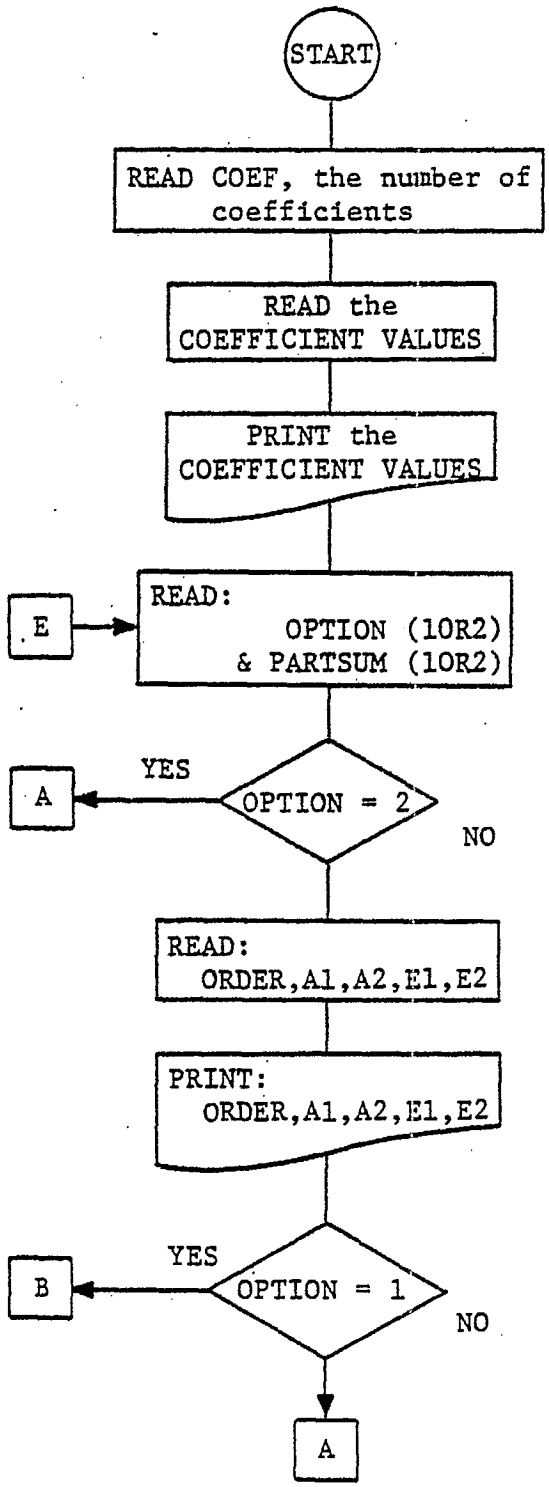

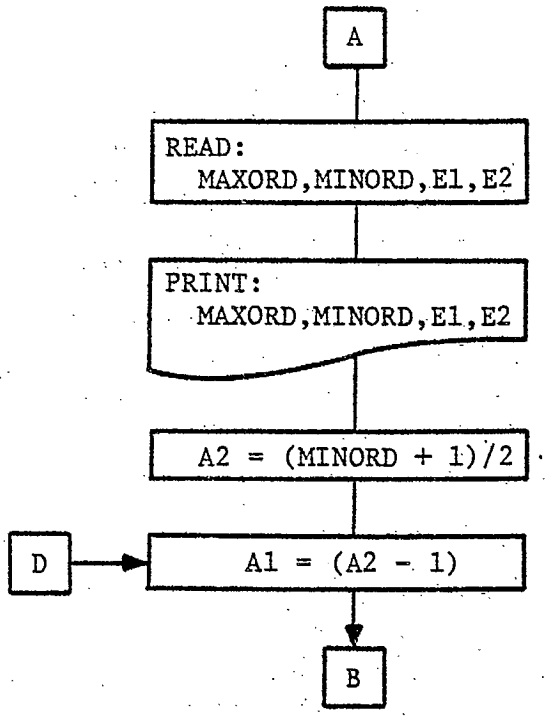
A
READ:
MAXORD,MINORD,E1,E2
PRINT:
MAXORD,MINORD,E1,E2
A2 = (MINORD + 1)/2
D
A1 = (A2 - 1)
B

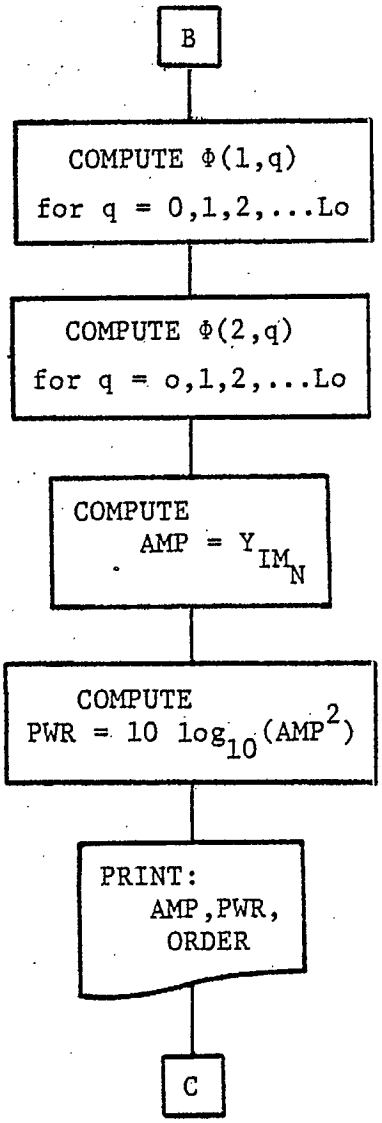
B
COMPUTE Φ(1,q)
for q = 0,1,2,...Lo
COMPUTE Φ(2,q)
for q = o,1,2,...Lo
COMPUTE
AMP = Y_{IM_N}
COMPUTE
PWR = 10 $\log_{10}(AMP^2)$
PRINT:
AMP,PWR,
ORDER
C

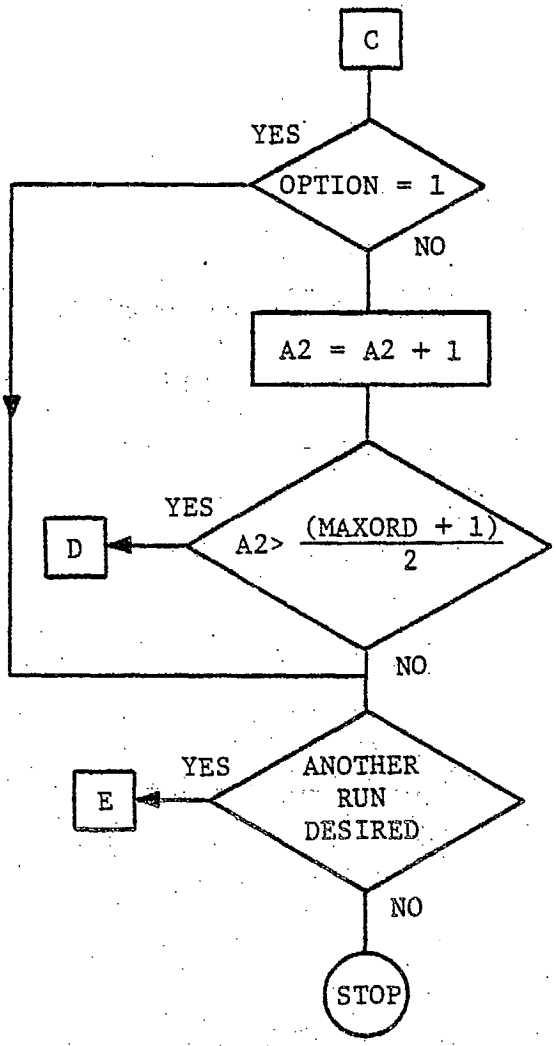
C
YES
OPTION = 1
NO
A2 = A2 + 1
YES
D
A2> (MAXORD + 1) / 2
NO
YES
E
ANOTHER RUN DESIRED
NO
STOP

E.1.5 Program Statement Listing (IMPWR)

```
 1.000 C      THIS PROGRAM COMPUTES IM AMPLITUDES 3RD-65TH ORDER
 2.000 C      IMO=MAXORD=ORDER,(A1+A2)=ORDER
 3.000 C      E1 AND E2 ARE CARRIER AMPLITUDES
 4.000        INTEGER A2
 5.000        DIMENSION A(0:100)
 6.000        DO 200 I=0,100
 7.000  200   A(I)=0
 8.000        WRITE(108,202)
 9.000  202   FORMAT(/'INPUT NUMBER OF COEFFICIENTS',/)
10.000        INPUT COEF
11.000        WRITE(108,700)
12.000  700   FORMAT(/,'INPUT THE COEFFICIENTS',/)
13.000        DO 561 I=0,COEF
14.000        INPUT A(I)
15.000  561   CONTINUE
16.000   10   FORMAT(6X,E.4)
17.000        DO 11 I=0,COEF
18.000   11   OUTPUT A(I)
19.000 C
20.000  100   WRITE(108,80)
21.000   80   FORMAT(/,'INPUT OPTION(1OR2),PARTSUM(1OR2)',
22.000      X'EN(1OR2)',/,
23.000      X'OPTION=1 FOR AMPLITUDE OF A SINGLE ORDER',
24.000      X/,'PARTSUM=1 OUTPUTS PARTIAL SUMS',/
25.000      X,'EN=1 FOR DC COMPONENT  2 FOR IM PWRS',/)
26.000        INPUT OPT,PARTSUM,EN
27.000        IF(OPT.EQ.2) GO TO 7
28.000        WRITE(108,1)
29.000     1 FORMAT(/,'INPUT ORDER,A1,A2,E1,E2',/
30.000      X,'FIM=(A2F2-A1F1)',/,
31.000      X'E1&E2 ARE TRANSMIT SIGNAL AMPLITUDES')
32.000        INPUT MAXORD,A1,A2,E1,E2
33.000        OUTPUT MAXORD,A1,A2,E1,E2
34.000        WRITE(108,701)
35.000  701   FORMAT(//)
36.000        IMO=MAXORD
37.000     7  CONTINUE
38.000        INTEGER C,D
39.000        COMMON Q
40.000        COMMON N,I,C,J,D,L
*
```

```
41.000          DIMENSION PHI(2,100)
42.000          IF(OPT.EQ.1) GO TO 13
43.000          WRITE(108,6)
44.000        6 FORMAT(/,'INPUT MAXORD,MINORD,E1,E2',/,
45.000         X'MAXORD & MINORD ARE MAX AND MIN ORDERS',/,
46.000         X'E1&E2 ARE TRANSMIT SIGNAL AMPLITUDES')
47.000          INPUT MAXORD,MINORD ,E1,E2
48.000          OUTPUT MAXORD,MINORD,E1,E2
49.000          WRITE(108,703)
50.000  703     FORMAT(//)
51.000 C
52.000          S=(MAXORD+1)/2
53.000          A2=(MINORD+1)/2
54.000     20   A1=(A2-1)
55.000          IMO=((2*A2)-1)
56.000 C
57.000 C        GENERATE PHI(M,L)
58.000 C
59.000 C
60.000       13 L=IFIX(((COEF+2)-IMO)/2)
61.000          DO 2 I=1,(L+1)
62.000          PHI(1,I)=0
63.000          PHI(2,I)=0
64.000       2  CONTINUE
65.000          DO 3 I=1,(L+1)
66.000          K=2*(I-1)
67.000          C=A1+(I-1)
68.000       3  PHI(1,I)=(E1**K)/(FACT(I-1)*FACT(C))
69.000          DO 4 I=1,(L+1)
70.000          J=0
71.000          TRM=0
72.000       5  K=2*J
73.000          D=A2+J
74.000          E=(I-J)
75.000          TRM1=PHI(1,E)
76.000          TRM2=(E2**K)/(FACT(J)*FACT(D))
77.000          TRM=TRM1*TRM2
78.000          PHI(2,I)=PHI(2,I)+TRM
79.000          J=J+1
80.000          IF(J.GT.(I-1))GO TO 4
```

```
 81.000          GO TO 5
 82.000      4   CONTINUE
 83.000  C
 84.000  C       CALCULATE IMP AMPLITUDES
 85.000  C
 86.000          T=(E1**A1)*(E2**A2)
 87.000          F3=0
 88.000          DO 8 I=1,(L+1)
 89.000          K=(I-1)
 90.000          J=(IMO+(2*K))
 91.000          F1=(A(J)*FACT(J))/(2**J)
 92.000          F2=F1*PHI(2,I)
 93.000          IF(PARTSUM.EQ.2) GO TO 8
 94.000          WRITE(108,45)
 95.000     45   FORMAT(//)
 96.000          OUTPUT J,F1,PHI(2,I),F2
 97.000      8   F3=F3+F2
 98.000          AMP=ABS(T*F3*EN)
 99.000          PWR=10*(LOG10((AMP)**2))+30
100.000          WRITE(108,701)
101.000    702   FORMAT(//)
102.000          OUTPUT IMO,AMP,PWR
103.000          IF(OPT.EQ.1)GO TO 25
104.000          A2=(A2+1)
105.000          IF(A2.GT.S)GO TO 25
106.000          GO TO 20
107.000     25   CONTINUE
108.000          WRITE(108,33)
109.000     33   FORMAT(/,'INPUT (1) IF ANOTHER RUN DESIRED',/,
110.000         X'(2) OTHERWISE')
111.000          INPUT AGN
112.000          IF(AGN.EQ.1) GO TO 100
113.000          STOP
114.000          END
115.000  C
116.000  C       FACTORIAL GENERATION
117.000  C
118.000          FUNCTION FACT(N)
119.000          L=0
120.000          FACT=1
```

```
121.000          L=N
122.000      1   IF(L)2,3,4
123.000      4   FACT=FACT*L
124.000          L=L-1
125.000          GO TO 1
126.000      2   FACT=0
127.000      3   RETURN
128.000          END
```

E.2 Program IMAMP

Program IMAMP is identical to IMPWR except that the polynomial coefficients used in this program are computed from a Taylor Series expansion of the exponential term in the Shockley Equation for the I-V transfer characteristic of a semiconductor diode.

E.2.1 Program Inputs:

(1) Program options

(a) OPTION

(b) PARTSUM

as for IMPWR

(2) EN:

as for IMPWR

(3) The third set of inputs depend upon OPTION.

(a) If OPTION = "1" inputs are as follows:

IS - Reverse diode saturation current

Q/KT - q/kT

ORDER

A1

A2 as for IMPWR

V1

V2

(b) If OPTION = "2" inputs are as follows:

IS

Q/KT

MAXORD

MINORD — as for IMPWR

V1

V2

E.2.2 Program Outputs

Program outputs are the same as for IMPWR, except that no coefficient values are printed.

E.2.3 Program Explanation

IMAMP calculates the power of IM products using the same algorithm as IMPWR.

The polynomial used in the IM calculations is

$$I = I_s\left[1 + (q/kT)V + \frac{(q/kT)^2V^2}{2} + \ldots + \frac{(q/kT)^nV^n}{n!}\right]$$

The coefficients used in IMAMP are therefore computed from

$$a_i = \frac{(q/kT)^i}{i!}$$

E.2.4 Program Statement Listing (IMAMP)

```
C      THIS PROGRAM COMPUTES 3RD TO 65TH
C      IM ORDERS PROVIDING Q/KT<41 AND E1+E2<1
C      M=Q/KT,IMO=MAXORD=ORDER,(A1+A2)=ORDER
C      E1 AND E2 ARE CARRIER AMPLITUDES
       INTEGER A2
C
 100   WRITE(108,80)
  80   FORMAT(/,'INPUT OPTION(1OR2),PARTSUM(1OR2)',
     X',EN(1OR2)',/,
     X'OPTION=1 FOR AMPLITUDE OF A SINGLE ORDER',
     X/,'PARTSUM = 1 OUTPUTS PARTIAL SUMS',/,
     X'EN=1 FOR DC COMPONENT OR 2 FOR IM PWRS',/)
       INPUT OPT,PARTSUM,EN
       IF(OPT.EQ.2) GO TO 7
       WRITE(108,1)
   1   FORMAT(/,'INPUT IS,Q/KT,ORDER,A1,A2,E1,E2',/
     X,'IS=REVERSE SATURATION CURRENT',/
     X,'FIM=(A2F2-A1F1)',/,
     X'E1&E2 ARE TRANSMIT SIGNAL AMPLITUDES',/)
       INPUT SATC,M,MAXORD,A1,A2,E1,E2
       WRITE(108,101)
 101   FORMAT(//)
       OUTPUT SATC,M,MAXORD,A1,A2,E1,E2
       IMO=MAXORD
   7   CONTINUE
C
C
       INTEGER C,D
       COMMON Q
       COMMON N,I,C,J,D,M,L
       DIMENSION PHI(2,100)
       IF(OPT.EQ.1) GO TO 13
       WRITE(108,6)
   6   FORMAT(/,'INPUT IS,Q/KT,MAXORD,MINORD,E1,E2',/,
     X'IS=REVERSE SATURATION CURRENT',/,
     X'MXORD & MNORD = MAX AND MIN ORDERS',/,
     X'E1 & E2 ARE TRANSMIT SIGNAL AMPLITUDES')
       INPUT SATC,M,MAXORD,MINORD,E1,E2
       WRITE(108,102)
 102   FORMAT(//)
```

```
41.000          OUTPUT SATC,M,MAXORD,MINORD,E1,E2
42.000 C
43.000          S=(MAXORD+1)/2
44.000          A2=(MINORD+1)/2
45.000    20    A1=(A2-1)
46.000          IMO=((2*A2)-1)
47.000 C
48.000 C        GENERATE PHI(M,L)
49.000 C        L IS THE # OF TERMS AFTER A(M,IMO)
50.000 C        THE LOWEST ORDERS REQUIRE THE LARGEST VALUES OF L
51.000 C
52.000 C
53.000    13    L=(81-IMO)/2
54.000          DO 2 I=1,(L+1)
55.000          PHI(1,I)=0
56.000          PHI(2,I)=0
57.000     2    CONTINUE
58.000          DO 3 I=1,(L+1)
59.000          K=2*(I-1)
60.000          C=A1+(I-1)
61.000     3    PHI(1,I)=(E1**K)/(FACT(I-1)*FACT(C))
62.000          DO 4 I=1,(L+1)
63.000          J=0
64.000          TRM=0
65.000     5    K=2*J
66.000          D=A2+J
67.000          E=(I-J)
68.000          TRM1=PHI(1,E)
69.000          TRM2=(E2**K)/(FACT(J)*FACT(D))
70.000          TRM=TRM1*TRM2
71.000          PHI(2,I)=PHI(2,I)+TRM
72.000          J=J+1
73.000          IF(J.GT.(I-1))GO TO 4
74.000          GO TO 5
75.000     4    CONTINUE
76.000 C
77.000 C        CALCULATE IMP AMPLITUDES
78.000 C
79.000          T=(E1**A1)*(E2**A2)
80.000          F3=0
```

```
      DO 8 I=1,(L+1)
      K=(I-1)
      J=(IMO+(2*K))
      F1=(A(J,M)*SATC*FACT(J))/(2**J)
      F2=F1*PHI(2,I)
      IF(PARTSUM.EQ.2) GO TO 8
      WRITE(108,104)
  104 FORMAT(//)
      OUTPUT J,F1,PHI(2,I),F2
    8 F3=F3+F2
      AMP=T*F3*EN
      PWR=(10*LOG10(AMP**2)+30)
      WRITE(108,103)
  103 FORMAT(//)
      OUTPUT IMO,AMP,PWR
      IF(OPT.EQ.1)GO TO 25
      A2=(A2+1)
      IF(A2.GT.S)GO TO 25
      GO TO 20
   25 CONTINUE
      WRITE(108,33)
   33 FORMAT(/,'INPUT (1) IF ANOTHER RUN DESIRED',/,
     X'(2) OTHERWISE')
      INPUT AGN
      IF(AGN.EQ.1) GO TO 100
      STOP
      END
C
C     FACTORIAL GENERATION
C
      FUNCTION FACT(N)
      L=0
      FACT=1
      L=N
    1 IF(L)2,3,4
    4 FACT=FACT*L
      L=L-1
      GO TO 1
    2 FACT=0
    3 RETURN
```

```
      END
C
C     GENERATE COEFFICIENTS FOR THE DIODE EQN.
C     PROGRAM CAN COMPUTE 81 TERMS CORRECTLY IF
C     Q/KT=40
C     NMAX=(IMO+54) IS MAX # OF TERMS
C
      FUNCTION A(N,M)
      INTEGER Q
C     TEST FOR EVEN INTEGERS SO THAT FACTORIALS CAN
C     BE BROKEN UP TO AVOID OVERFLOW
      IF(N.GT.0) GO TO 51
      A=1
      GO TO 5
   51 S=N
      P=S/2
      Q=IFIX(P)
      R=(P-Q)
      IF(R.EQ.0) GO TO 2
C     BREAK UP MULTIPLICATION TO AVOID OVERFLOW
      F6=(Q+1)
      TRMA=(M**F6)
      TRMB=TRMA/FACT(Q)
      TRMD=1
      DO 10 I=1,(Q+1)
   10 TRMD=TRMD*(N-(I-1))
      TRMC=(M**Q)/TRMD
      A=TRMB*TRMC
      GO TO 5
    2 TRMA=(M**P)
      TRMB=TRMA/FACT(Q)
      TRMD=1
      DO 11 I=1,Q
   11 TRMD=TRMD*(N-(I-1))
      TRMC=(M**P)/TRMD
      A=TRMB*TRMC
    5 CONTINUE
      RETURN
      END
```